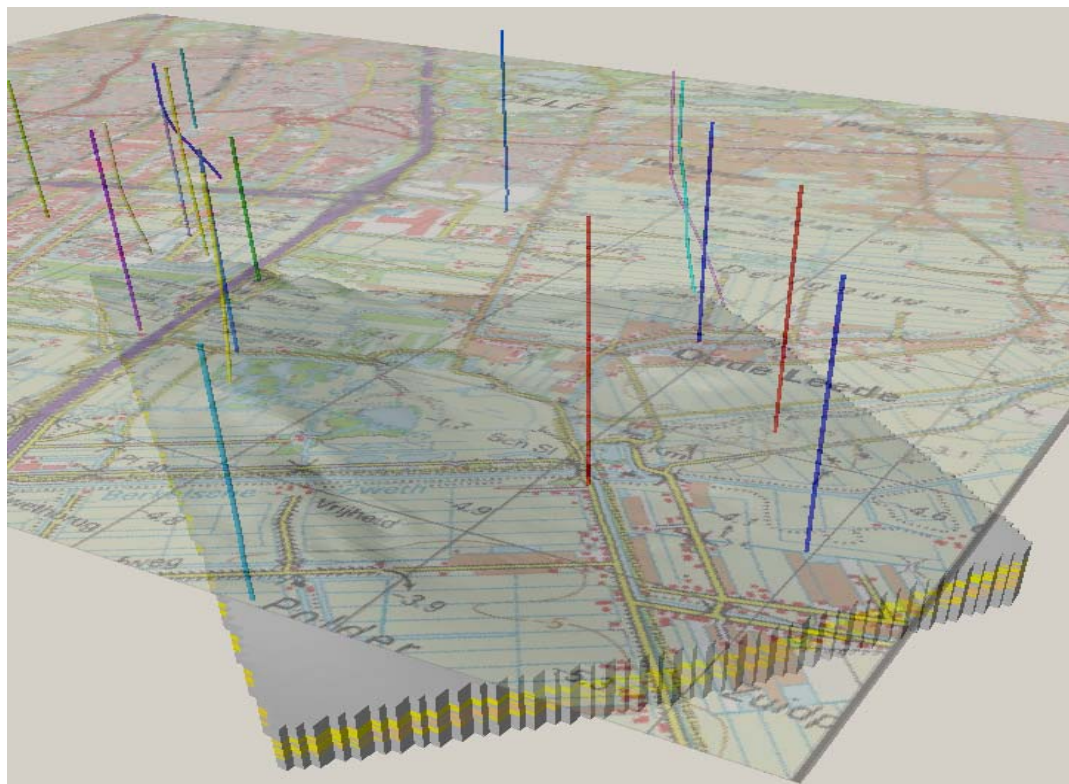


AES/PE/10-04 Heterogeneity determination of the Delft subsurface for heat flow modelling

18-June-2010 D.T. Gilding



Disclaimer

The results and maps in this report are based on local and regional geological mapping of the West Netherlands Basin. The results and maps in this report have been carefully compiled. Nonetheless the presented results may contain incomplete, incorrect information. The results and maps were generated by a modelling study of geological parameters of the studied aquifers. Therefore, the results and maps of this report should only be used for regional geological evaluations and optimization discussion. The results and maps in this report should not be used for local geothermal studies and commercial purposes. Furthermore, advances in knowledge and new data may cause some results and maps to become out of date. TU Delft and DAP claim to be not responsible for any eventual errors or other consequences resulting from the use of the results, model and maps in this report.

Title : Heterogeneity determination of the Delft
subsurface for heat flow modelling.

Author(s) : D.T. Gilding

Date : 18th of June 2010

Supervisor(s) : Prof. Dr. J. Bruining

Dr. M.E. Donselaar

Dr. K.H.A.A. Wolf

TA Report number : AES/PE/10-04

Postal Address : Department of Applied Earth Sciences
Delft University of Technology
P.O. Box 5028
The Netherlands

Telephone : (31) 15 2781328 (secretary)

Telefax : (31) 15 2781189

Copyright ©2010 Section for Applied Geology

All rights reserved.

No parts of this publication may be reproduced,
Stored in a retrieval system, or transmitted,
In any form or by any means, electronic,
Mechanical, photocopying, recording, or otherwise,
Without the prior written permission of the
Department of Applied Earth Sciences

Abstract

Geothermal energy is hot and sustainable. A recent run for licences has sparked questions on the optimisation and recovery of geothermal energy from the subsurface of the Netherlands through optimal project placement.

The effect of heterogeneities on interference of geothermal projects in the West Netherlands Basin and the target Early Cretaceous Delft Sandstone Member has not been sufficiently studied. The objectives of this study are: (1) to gain a better understanding of the geological setting, the depositional setting and the heterogeneities of the primary target Delft Sandstone Member; (2) to show the effect of heterogeneities in the subsurface on interaction and interference of flow on closely placed geothermal systems; and (3) to build a subsurface dynamic reservoir model with which optimal well performance and placement can be assessed.

The basin evolution, depositional setting and depositional processes of the Delft Sandstone Member are determined by combining the available data. The seismic, well, core and cutting data are combined to build a static 3D reservoir architectural model of the Delft subsurface. The static model is incorporated with the flow characteristics from petrophysical log data and used for temperature and fluid flow behaviour simulations. By modelling flow and temperature behaviour, the flow rates and production temperatures of a single geothermal system and the interference of the different geothermal systems were determined and quantified.

This study gives new insights and a better understanding of the reservoir architecture of the Delft Sandstone Member. The Vrijenban Syncline is the predominant structure in the Delft subsurface and the sediments of the Delft Sandstone Member are deposited by a meandering fluvial system in three different depositional settings, controlled by tectonic movement. The depositional characteristics related to subsidence and accommodation space increase can have a large impact on the reservoir behaviour of the Delft Sandstone Member. It has therefore been chosen to include this effect in the model.

From the flow simulations in the Delft Sandstone Member it shows that different geothermal systems closely placed within one reservoir will have pressure interference. From this study it is concluded that multiple geothermal systems can be placed in one reservoir and sustain economic production temperature for over 30 years. Different geothermal systems in one reservoir will however communicate in the reservoir creating both positive and negative effects on flow that are large enough to respectively improve or badly affect the economics of a project.

The results of this study will be a base case for further research as it will form a benchmark for future local and regional geothermal studies. Simulations of multiple well configurations to determine optimal well placement can now be performed. This will ensure and provide the foundation for a true roll out of geothermal systems through the western parts of the Netherlands.

Acknowledgements

I would like to thank my supervisors, Professor Hans Bruining, Karl-Heinz Wolf, Rick Donselaar and Remo Groenenberg for their unlimited support during this master thesis project. Without their passionate devotion to this project it would not have been possible. I would also like to thank Pieter Jongerius for his membership in my graduation committee.

The Delft Geothermal Project (DAP) was started in 2007 by students, alumni and staff of the Department of Applied Earth Sciences. Basic idea is to develop an innovative geothermal system, with the objectives to provide for sustainable heating of Delft University of Technology, to demonstrate novel technologies reducing the cost of geothermal systems, to investigate options for co-injection of CO₂, and to generate new research opportunities. Contributing to this project was a great honour and I would like to thank everybody for the pleasant cooperation.

DAP is under performance with the financial support of the Ministry of Economic Affairs, Energiebeheer Nederland (EBN), Eneco Energy, Dutch State Mines (DSM), Wintershall Noordzee, Nederlandse Aardolie Maatschappij (NAM), PGMI, WEP, Acquit, IF Technology, Panterra, the Province of Zuid-Holland and TNO, and is hosted and supported by Delft University of Technology. Ammerlaan Hydocultuur BV supported this project and gave the opportunity to witness the drilling operations in Pijnacker. The Nederlandse Aardolie Maatschappij (NAM) is particularly acknowledged for the kind provision of subsurface data of the West Netherlands Basin especially Daan Den Hartog-Jager who made the core analysis possible. Panterra, thank you for letting me use your lab facilities. Thanks to Schlumberger is granted for the use of the software Petrel and Eclipse. I would also like to acknowledge Midland Valley for the use of 3D Move and Jan-Kees and Michael for their guidance in the use of this software. Of course I would like to thank all the students I worked with within this project, Andrina, Ko, Mark, Claartje, Nathalie, Chris, Jeroen, Roeland-Jan, Gregory and most of all Peter Smits. The people of TU Delft have been very helpful during my studies. All mentioned and unmentioned parties involved are acknowledged for their input into the project and this study; and appreciated for granted permission to publish.

Special thanks goes to Andries Wever for more then I can put to words. The results are evident with the first well that spudded on the 9th of March 2010!

I owe my appreciation to my brothers and parents who have supported and encouraged me over the years.

And finally I would like to extend sincere gratitude to my girlfriend Claartje Wigger for all her support during this thesis project and my studies over the years.

Table of Contents

Abstract	6
Acknowledgements	8
Table of Contents	9
List of Figures.....	12
List of Tables.....	17
List of Equations	17
1. Introduction.....	19
2. Regional geology and climate.....	23
2.1. Introduction	23
2.2. Pre-rift Stage	24
2.3. Syn-rift Stage.....	24
2.4. Post-rift Stage	25
2.5. Stratigraphy.....	25
2.6. Basin movement, global climate and eustatic sea level	28
3. Data and Methods.....	29
3.1. Methods	30
3.2. Well data	31
Available Cores	32
Cuttings and thin sections	33
Formation fluid samples.....	34
Well log correlation panels,.....	34
3.3. Available Seismic data.....	37
4. Analysis of the relation tectonics and sedimentation.....	38
4.1. Introduction	38
4.2. Seismic interpretation.....	38
Horizon and fault interpretation	39
4.3. Reservoir architecture	40
Pijnacker High.....	41
Delft High (Delft Pop-up structure)	42
4.4. Accommodation space evolution	43
4.5. New insights	46
5. Formations	48
5.1. Introduction	48
9 Heterogeneity determination of the Delft subsurface for heat flow modelling.	
MSc Thesis Douglas Gilding	

5.2.	Alblasserdam Member (SLDNA).....	49
	Depositional environment of the Alblasserdam Member	51
5.3.	Delft Sandstone Member (SLDND)	52
	Depositional environment of the Delft Sandstone Member	53
	Unit one, the Lower Delft Sandstone Member	54
	Unit two, the Middle Delft Sandstone Member.....	55
	Unit three, the Upper Delft Sandstone Member	55
5.4.	Rodenrijs Claystone Member (SLDNR).....	57
	Depositional environment of the Rodenrijs Claystone Member.	58
6.	Petrophysics	60
6.1.	Introduction	60
6.2.	Discrete well log.....	60
6.3.	Porosity permeability relationship.....	61
6.4.	Log analyse.....	62
	Porosity.....	62
	Horizontal Permeability.....	63
	Vertical permeability	63
6.5.	Temperature	65
	Temperature Equation and maps.....	65
6.6.	Formation fluid properties.....	67
7.	Constructing a static model of the Delft Sandstone Member.	68
7.1.	Work flow.....	68
7.2.	Building a structural framework	69
	Determining the top and base of the model.....	69
	Modelling area boundaries	70
	Building the grid	71
	Zones	71
	Layers.....	74
	3D grid model discussion.....	75
7.3.	Facies modelling, populating the grid.....	76
	Facies Modelling.....	76
	Modelling the Alblasserdam- and Rodenrijs Claystone Member.	76
	Modelling the Lower Delft Sandstone Member zone,	77
	Modelling the Middle Delft Sandstone Member zone.....	78

Modelling the Upper Delft Sandstone Member zone	79
Facies Discussion	80
7.4. Adding the petrophysical properties to the static model.....	81
Upscaling the wells.....	81
Property based modelling,.....	82
8. Dynamic flow and temperature modelling	88
8.1. Work flow.....	88
8.2. Volume calculation	89
8.3. Fluid flow modelling.....	90
Development strategy, a geothermal doublet, the wells	90
Flow behaviour simulations	93
8.4. Flow behaviour simulation results.....	94
8.5. Heat flow modelling.....	97
The temperature of the injection water	98
Rock specific heat.....	98
Fluid specific heat data.....	98
Temperature modelling.....	99
Results of temperature modelling	100
8.6. Homogeneous versus Heterogeneous static model.....	103
The temperature results of homogeneous simulation case	107
8.7. Effect of thermal conductivity	110
New insight.....	113
9. Conclusion and recommendations.....	114
9.1. Conclusions	114
9.2. Recommendations	116
10. References,.....	119
A. Appendix Formation and group abbreviations.	122
B. Appendix Nomenclature and abbreviations	122
C. Appendix Moerkapelle core log	122
D. Appendix List of wells.....	122
E. Appendix Palinspastic reconstruction	122
F. Appendix 3D static architectural reservoir modelling processes.....	122
G. Appendix Temperature and flow simulation processes.....	122
H. Appendix Additional Equations	122

List of Figures

Figure 1-1 (Left) Map of the Netherlands with exploration licence applications for geothermal energy in May 2010 (Modified after TNO, 2010); (Right) Map of the West Netherlands Basin with applied licenses, oilfields and wells (Modified after Vis et al., 2010).	19
Figure 1-2 Side view of a geothermal doublet with a production- (red) and an injection-well (blue).	20
Figure 1-3 First geothermal well drilled in the Netherlands at Asten in 1986 (Heederik, 2009).	20
Figure 1-4 (Left) Map of the Netherlands with target area Vrijenban; (Right) Map of Delft and the target area Vrijenban. Large black square is the exploration licence Delft. Three circles show the three doublet top hole locations, scale 1:50.000.....	22
Figure 2-1 Map of the Netherlands with the West Netherlands Basin during the Late Jurassic to Early Cretaceous (Van Adrichem Boogaert & Kouwe, 1993-1997).	23
Figure 2-2 The table shows the succession of groups, formations and target members around the target formation. The formations are placed top to bottom from young to old. The Delft Sandstone Member is the target sandstone.....	25
Figure 2-3 Stratigraphy of target Area Vrijenban.....	26
Figure 2-4 The position of western Europe on the globe at different moments in geological history. Modified after Berendsen (2004).	28
Figure 3-1 The fieldwork area, with the map of Delft. The black polygon indicates the study area.	29
Figure 3-2 Oil (red) and gas (green) fields in the West Netherlands Basin. Black stars: location of wells (DEL-03 and MKP-11) used in this study. Blue stars: location of geothermal wells started in 2010, Box: study area. Modified after NLOG (2010).	30
Figure 3-3 On the left the Spontaneous Potential log of the Delft-03 well with the formation tops and the available thin sections of the cuttings as described in Drost & Korenromp (2010) in true vertical depth. The right top figure shows the cutting sample nr; "5" from 1806-1808 m depth of the Delft-03 well. The right bottom figure, shows the thin section of cemented grains made from the cutting sample "5" of the Delft-03 well.....	33
Figure 3-4 The west of the Netherlands with wells, map of Delft and the well correlation cross panel lines through the wells. Blue is the northwest-southeast well correlation line (Figure 3-5), Red is the southwest-northeast correlation line (Figure 3-6).	34
Figure 3-5 Well correlation panel from northwest to southeast showing the wells KDZ-2A, HAG-02, HAG-01, RWK-17, -04, -18A, Del-02, -03, -08 and OLE-01 with correlated well top markers in true vertical depth in meters. The scale is 1:2000.....	35
Figure 3-6 Well correlation panel from southwest to northeast showing the Lir-45, Delft-03, PNA-13, LED-1 and MKP-11 wells with correlated well top markers in true vertical depth in meters, scale 1:2000.....	36
Figure 3-7 Map of Delft with available seismic data sets. The black cube represents the PSDM seismic data, the blue cube represents the regional time migrated seismic data. The arrows point to seismic inline 2640 used in Figure 4-1.	37
Figure 4-1 3D Side view of all interpreted faults in the seismic data with the surface of the top Delft Sandstone Member, PSDM Seismic inline 2640 (Figure 3-7), and well Delft-03.	38
Figure 4-2 Depth-converted seismic cross section through the study area shows that the Delft Sandstone Member is situated in a gentle, broad syncline bounded by two pop-up structures (inversed normal faults). For location see line SW-NE in Figure 4-3.....	39
Figure 4-3 The interpreted top of the Delft Sandstone Member, including major faults and the names of the structures. The southwest-northeast seismic section (SW-NE) is shown in Figure 4-2.	40

Figure 4-4 Cross-section of the predominant pop-up structure in the West Netherlands Basin (Van Balen et al, 2000).....	41
Figure 4-5 The Pijnacker High predominant pop-up structure from inline SW-NE, with major faults (dotted lines), group names, fault numbers and names of the structural elements.....	41
Figure 4-6 Delft High predominant pop-up structure with major faults with numbers and group names.....	42
Figure 4-7 Cross section of the Vrijenban area based on a 2D reconstruction of the Late Triassic. The structural setting of the target area Vrijenban, major surfaces and faults are shown.....	43
Figure 4-8 Cross section of the Vrijenban area based on a 2D reconstruction. The structural setting of the target area Vrijenban is shown during the Late Jurassic. Major surfaces and faults PA and DA show the differential faulting and the synsedimentary growth along the faults.	44
Figure 4-9 Cross section of the Vrijenban area based on a 2D reconstruction. The structural setting of the target area Vrijenban is shown during the Early Cretaceous. Major surfaces, faults PA and DA and fault movements are shown.	45
Figure 4-10 Cross section of the Vrijenban area after 2D reconstruction. The structural setting of the target area Vrijenban is shown at the start of the Tertiary. Major surfaces and faults PA, DA, DB2 and PB1 are indicated.	45
Figure 4-11 Cross section of the Vrijenban area after a 2D reconstruction. The structural setting of the target area Vrijenban is shown as today it can be found on seismics. Major surfaces and fault PA, DA, PB and DB2 are indicated.	46
Figure 4-12 Smeared or mineralized sealing fault found in core section 889.25-889.70 of the Well MKP-11. The throw of the fault is 6 cm and the change in oil staining clearly shows the sealing capacity of the small fault.	47
Figure 5-1 Representative pictures of the three facies from the MKP-11 well, from left to right; the Alblasserdam Member, the Delft Sandstone Member and the Rodenrijs Claystone Member. The Alblasserdam Member is a laminated interbedded oil-stained sand- and claystone with lignite bands. The Delft Sandstone Member shows an oil saturated friable sandstone (No oil found in the Delft-03 well). The Rodenrijs Claystone Member is organic rich laminated claystone with siderite modules. .	49
Figure 5-2 The contact between the Alblasserdam Member and the Delft Sandstone Member in the core of the MKP 11 well section (909.50 – 909.95m). The colour change is sharp, in the core above the contact surface clayclasts and lignite shards can be seen in the oil saturated sandstone. The black dotted line shows the lamination. The contact surface can clearly be interpreted as a cutting surface (Light blue dashed line).	50
Figure 5-3 The Alblasserdam Member signature in the SP-log of the Delft-03 and on the gamma ray log MKP 11 well. Scale is 1:1000. Wells are in depth along the borehole in meters.	51
Figure 5-4 Delft Sandstone Member on well logs of the Delft-03 (SP), MKP- 12A, - 12 and MKP-11 with the Upper, Middle, and Lower Delft Sandstone Member. Scale 1:1000 in true vertical depth. ..	52
Figure 5-5 The Delft Sandstone Member is divided into three units in the Lower-, Middle- and Upper Delft Sandstone Member on wells Delft-03 and MKP 16, 13, 12A, 12, 11 10, 9A and 2 with the SP or Gamma Ray well log. Scale 1:1000 in true vertical depth.....	53
Figure 5-6 The depositional setting of the Delft Sandstone Member with its varying thickness towards the growth fault. It also shows the deposition of sand and floodplain deposits and the isolation or amalgamation of fluvial deposits.	56
Figure 5-7 The contact between the Rodenrijs Claystone Member and the Rijswijk Member in the MKP 11 and Delft 3 wells. The transitional change from interbedded silt- to claystone to a thick	

sandstone body marks the contact, the SLDNR_T line. Also is shown the clear serrate like pattern of the Rodenrijs Claystone Member on SP log of the Delft-03. The MKP-11 is given with a scale of 1:200 with true depth in meters with the gamma ray, zone log and mirrored gamma ray. The Delft-03 well is given in scale 1:1000 depth with in meters with the SP log, zone log and mirrored SP log.....	58
Figure 6-1 The Delft-03 and the MKP-11 wells: mirrored SP-log and discrete facies log for the Delft-03 well and mirrored GR-log, discrete facies log for MKP-11. MKP-11 scale is 1:250, Delft-03 scale is 1:750. Scale is in meters true vertical depth.....	61
Figure 6-2 Porosity graph of the Delft Sandstone Member from all available well log porosity data points. The horizontal axis shows the porosity and the vertical axis gives the percentage of the total data points.....	63
Figure 6-3 Porosity(left) and horizontal Permeability(perm) (centre) and Vertical permeability(Kv Perm Z) (right) Log of the MKP-11 over the Delft Sandstone Member. Depth is in true vertical depth in meters.	64
Figure 6-4 Temperature map of the Top Rodenrijs Claystone Member.....	66
Figure 6-5 Temperature map of the Top Delft Sandstone Member.	66
Figure 6-6 Temperature profile of the Delft Sandstone Member with the Delft-03 on seismic inline 2760 (figure 3-7), depth to length ratio to 2:1.....	67
Figure 7-1 Workflow used in this study to build a defined static model for dynamic flow modelling.	68
Figure 7-2 3D view showing the top Rodenrijs Claystone Member, the Delft Sandstone Member and the proposed base of the model, the Inter Alblasserdam Member. Depth is in meters, XY to Z ratio is 1:2. Also shown is the Delft-08 Well and seismic inline 2814 of the PSDM data, the location of this inline is shown in Figure 7-3.....	69
Figure 7-3 Map of the target area with the trapezium shaped polygon used to create the dimensions of the model. The black line is the seismic inline 2814 in PSDM as shown in Figure 7-2.	70
Figure 7-4 A) Map of Delft with the outline of the structure in black. B) Side view of the created coloured grid. C) View from the south of the created grid surfaces. D) View from below on the created model.	71
Figure 7-5 The SP log of the Delft-03 well and the Gamma ray log of the MKP-11 well with well tops of the formation and zones used in the model.	72
Figure 7-6 A 3D side view from the east of the created model with the zones and the Delft wells. X,Y,Z ratio is 1:1:1 and the scale and depth is in meters. The arrows point to the thickness variation in the zones.....	73
Figure 7-7 A 2D Seismic inline 2765 with the created zones and the Delft-03 well, depth in meters. On the right is the map of Delft showing the inline 2765(black line) and the modelled area (blue).	74
Figure 7-8 Side view from the west of the created layers in the zones of the model.	74
Figure 7-9 Side view from the east of the total created 3D grid structure with the Delft-03 well.	75
Figure 7-10 Facies model of the Lower Delft Sandstone Member, the single meandering fluvial channels on a background of floodplain deposits with the Delft-03 well. Z is the depth in meters.	77
Figure 7-11 Top view of the object based modelled Lower Delft Sandstone Member facies in Petrel. Arrows show the predominant trend line.....	77
Figure 7-12 Facies model of the Middle Delft Sandstone Member, mostly siltstone deposits with isolated channels and the Delft-03 well. Z is depth in meters.	78
Figure 7-13 Top view of the object based modelled Middle Delft Sandstone Member facies.....	78
Figure 7-14 Facies model of the Upper Delft Sandstone Member, the multi stacked fluvial channels with the Delft-03 well. Z is depth meters.....	79

Figure 7-15 Top view of the object based modelled Upper Delft Sandstone Member facies in Petrel.....	79
Figure 7-16 3D Side view from the east of the total created facies model with Delft-03 well. The Z to XY ratio is 2:1. So the model is stretched over the Z axis two times.....	80
Figure 7-17 The Delft-03 well with the Middle and Lower Delft Sandstone Member with from left to right the Mirrored SP log, the zones, porosity log (line), upscaled porosity log (blocks), facies log, layers of the model, upscaled facies log, horizontal permeability log (line), and the upscaled permeability log (blocks) respectively.....	81
Figure 7-18 The created porosity model with the Delft-03 well. Z is depth in meters.....	82
Figure 7-19 The 3D Horizontal permeability with the Delft-03 well. Z is depth in meters.....	83
Figure 7-20 The 3D vertical permeability assigned static model with the Delft-03 well. Z depth (m) ..	83
Figure 7-21 An internal layer of the Lower Delft Sandstone Member with A) facies B) porosity C) Horizontal Permeability D) vertical Permeability.....	84
Figure 7-22 Graph showing the distribution in % of the porosity assigned static model (POR), upscaled well logs and the porosity in the well logs.....	85
Figure 7-23 Graph showing the distribution in % of the derived horizontal permeability in the assigned static model, upscaled well logs and the permeability derived well logs (Perm). (the mDarcy scale is logarithmic.)	86
Figure 7-24 Graph showing the distribution in % of the derived vertical permeability in the assigned static model, upscaled well logs and the permeability derived well logs (Perm). (the mDarcy scale is logarithmic.)	87
Figure 8-1 Workflow used in this study to build 3D property models for dynamic flow modelling....	88
Figure 8-2 Visualised 3D model of the pore volume, the colours represent the pore volume in m ³ ...	89
Figure 8-3 Cross panel showing the A,B and C injection and production wells with the model facies found in the well and the zones representing the formation members. The black lines are a schematic representation of the well.....	91
Figure 8-4 Map of Delft and the well locations in the model scale 1:50000.	92
Figure 8-5 A 3D view from the southeast of the facies model with the 6 vertical wells.	92
Figure 8-6 3D view from east of the pressure in the Middle and Lower Delft Sandstone Member and Alblasserdam Member at the start of simulation, T = 01-01-2010.....	93
Figure 8-7 3D view from east of the pressure in the Middle and Lower Delft Sandstone Member and Alblasserdam Member. After 5 years of running the simulation case with 3 doublets at full production, T = 01-01-2015.....	93
Figure 8-8 Bottom Hole Pressures of the A, B, and C I=Injection and P=production wells.....	94
Figure 8-9 Injection in the A, B and C injection wells. The high peaks at the start represent the flow rates before the pressure constraints are reached.....	95
Figure 8-10 Production from A, B and C production wells.....	96
Figure 8-11 3D side view of the static temperature model at the start of the simulation. The temperature of each cell is the calculated by the thermal gradient times the average depth of the cell block.	97
Figure 8-12 3D View showing temperature flow from production wells to injection wells after 30 years viewing the Top Delft Sandstone Member.....	99
Figure 8-13 The production and injection temperature in degrees Celsius of fluids produced and injected by wells A, B, and C over time in years.....	100

Figure 8-14 The production temperature in degrees Celsius of fluids produced by wells A, B, and C over time in years. Y scale starts at 72 degrees Celsius.....	101
Figure 8-15 Overview showing the temperature flow from injections well to the production wells after 30 years in the Upper Delft Sandstone Member.....	102
Figure 8-16 Top view showing temperature flow from production well BI blue to injection well BP (red) after 30 years in the Upper Delft Sandstone Member.....	102
Figure 8-17 Top view showing temperature flow from injection to production (Den Boer, 2008)....	102
Figure 8-18 Cross section showing temperature flow from injection well PI (Blue well) to production well BP (Red Well) after 30 years, Z:X ratio 2:1. (see also Figure 8-16)	103
Figure 8-19 Top view of the Delft Sandstone Member in the 3D homogeneous model, A) Porosity, B) Horizontal Permeability, C) Vertical Permeability, D) 3D side view of the homogeneous static model with the Rodenrijs Claystone Member and the Alblasserdam Member.....	104
Figure 8-20 Production from A, B and C production wells in simulation case called “homogenous1”.	105
Figure 8-21 Production from A, B and C production wells in both the heterogeneous static model called “Vrijenban”(Green) and the homogeneous static model called “Homogenous1” (Purple)....	106
Figure 8-22 Overview showing temperature flow from production wells to the injections well after 30 years in a homogeneous reservoir in the Upper Delft Sandstone Member.	107
Figure 8-23 Top view showing temperature flow from injection well PI blue to production well BP red after 30 years in a homogeneous reservoir. Model is flattened and shows the Upper Delft Sandstone Member.....	108
Figure 8-24 Cross section showing temperature flow from injection well PI (Blue well) to production well BP (Red Well) after 30 years, model is flattened.....	108
Figure 8-25 The production temperature in degrees Celsius of fluids produced by wells A, B, and C over time in years in both the heterogeneous static model called “V=Vrijenban”(Green) and the homogeneous static model called “H=Homogenous1” (Purple). Y scale starts at 68 degrees Celsius.	109
Figure 8-26 Cross section showing temperature flow from injection well CI (blue well) to production well CP (red well) after 30 years.....	110
Figure 8-27 Overview showing temperature flow from the injections well to the production wells after 30 years in a heterogeneous reservoir simulation case with no thermal conductivity at the top of the Lower Delft Sandstone Member. Arrows show cold water breakthrough.....	111
Figure 8-28 Overview showing temperature flow from the injections wells to production wells after 30 years in a heterogeneous reservoir simulation case with thermal conductivity at the top of the Lower Delft Sandstone Member.	111
Figure 8-29 The production temperature in degrees Celsius of fluids produced by wells A, B, and C over time in years in a heterogeneous static model both with thermal conductivity called “V=Vrijenban”(Green) as without thermal conductivity called “nT=Vrijenban no ThCon” (Purple). Y scale starts at 74 degrees Celsius.....	112
Figure 8-30 Cross section showing temperature flow from injection well PI (Blue well) to production well BP (Red Well) after 30 years. The Rodenrijs Claystone Member is cooled done in both cases. A is in heterogeneous static reservoir model and has Z:X ratio 1:2. Figure B is homogeneous static reservoir model and has been flattened.....	113

List of Tables

Table 3-1 Wells that hit the top of the target formations Rodenrijs Claystone Member (SLDNR), the Delft Sandstone Member (SLDND) in yellow and the Alblasserdam Member (SLDNA).	31
Table 3-2 Table of the available log data per well used in the Petrophysical analyse and evaluation of the Delft Sandstone Member. The full names can be found in the nomenclature (Appendix B).....	31
Table 3-3 Available core data of the Delft Sandstone Member, the Rodenrijs Claystone Member, and the Alblasserdam Member and their recovery rates.	32
Table 5-1 The three formations of the Schieland Group with their zone nomenclature, depth, descriptions and depositional environment.	48
Table 5-2 Gamma-ray log signature, facies description and interpreted depositional architecture of the three units in the Delft Sandstone Member.....	54
Table 6-1 the four discrete facies with code, name, colour and description.....	60
Table 6-2 Table of the available log data per well used in the Petrophysical analyze and evaluation of the Delft Sandstone Member. The full names can be found in the nomenclature (Appendix B), the porosity logs are indicated in green.	62
Table 6-3 Temperature equations and gradients from different studies in the West Netherlands Basin. Left to right: author, equation and target study area. Equation parameters: T is the temperature in degrees Celsius, depth Z is in 100 meters based on True Vertical Depth from NAP... ..	65
Table 7-1 Zones used to build the model. Each zone represents a stratigraphic unit.	72
Table 7-2 Layers used to build the model. Each zone is divided into multiple layers.....	74
Table 7-3 Average, minimum and maximum thickness of layers in the Delft Sandstone Member....	75
Table 8-1 The calculated bulk, net and pore volume of one modelled realisation of the Delft Sandstone Member.....	89
Table 8-2 Doublet names, the well names, the type of well, locations, the start and end date and the simulated rate of production and injection of all 6 wells in the Vrijenban area.....	91
Table 8-3 Injection temperatures for well A, B, and C.	98
Table 8-4 Thermal conductivity of the formation rock input in Eclipse.	98
Table 8-5 Thermal conductivity formation fluid input in Eclipse.	98
Table 8-6 Porosity, horizontal and vertical permeability input for the static homogeneous model..	103

List of Equations

Equation 6-1 Permeability porosity equation, “DAP trendline” (Smits, 2008).	61
Equation 6-2 Vertical permeability (Kv) equation based on the horizontal permeability (Kh).....	64
Equation 6-3 Temperature to depth relationship based on empirical data taken from corrected well bore hole measurements. T in degrees Celsius and Z depth is in 100 meters in the true vertical depth from NAP	65
Equation 8-1 The equations used to calculate the Net Volume and the Pore Volume.	89

1. Introduction

Geothermal energy is hot. Recently a gold rush for geothermal exploration licenses started in the Netherlands by glasshouse farmers and energy companies. From 2008 to 2010, 400 square kilometres of exploration license applications were received by the Dutch Ministry of Economic Affairs for areas in the Netherlands with a goal to drill for geothermal energy (Vis et al., 2010). By utilising the geothermal heat from the subsurface it is possible to sustainably heat buildings and businesses. Glasshouse businesses and energy companies see geothermal energy as the sustainable CO₂-emission free solution for heat production. The run for licences has sparked questions on the optimisation and recovery of geothermal energy from the subsurface of the Netherlands through optimal project placement.

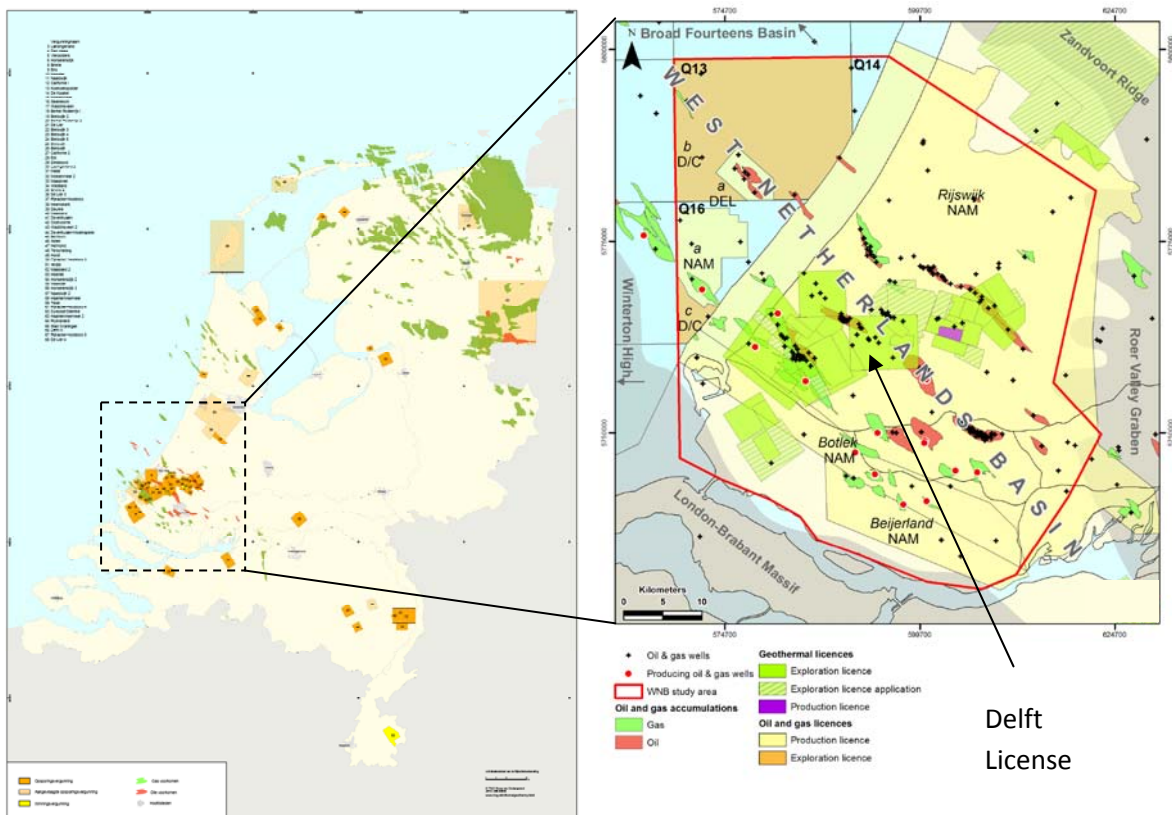


Figure 1-1 (Left) Map of the Netherlands with exploration licence applications for geothermal energy in May 2010 (Modified after TNO, 2010); **(Right)** Map of the West Netherlands Basin with applied licenses, oilfields and wells (Modified after Vis et al., 2010).

Because of the low geothermal gradient, 3 degrees per 100 meters (Smits, 2008), only two types of geothermal systems are present in the Netherlands: 1) Shallow geothermal systems targeting shallow groundwater for seasonal heat and cold storage of a single building; and 2) A deep geothermal system producing heat from aquifers 500 up to 5000 meters deep for large glasshouses and district heating networks. No enhanced geothermal system (EGS) or ultra deep geothermal systems, system to 5000 meters deep or more, have been realised in the Netherlands. This study targets deep geothermal systems from 500 meter to 3000 km that utilise aquifer water for heat production from 30 to 150 degrees hot, high permeable porous reservoirs.

A deep geothermal system consists of two wells, a so-called geothermal doublet. One deviated well is used to produce hot water from a target subsurface aquifer at two kilometres depth. The heat is then extracted by a heat exchanger to a local heating grid to sustainably heat buildings and local glasshouses. A second well re-injects the cooled down produced aquifer water into the same reservoir rock two kilometres away from the production point (Figure 1-2).

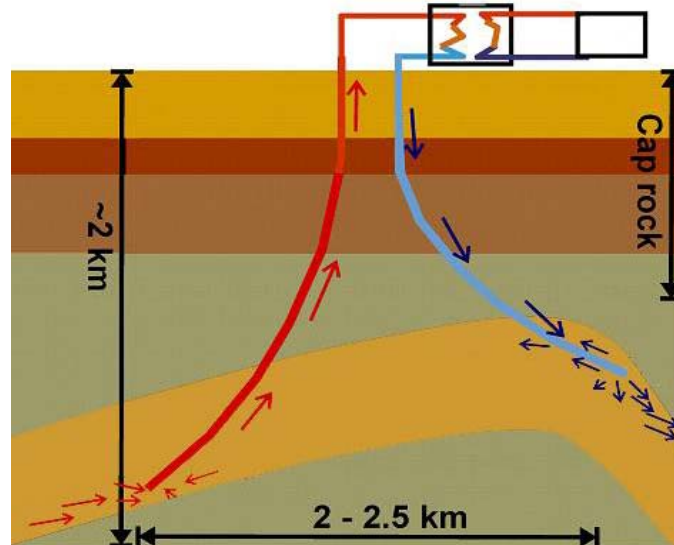


Figure 1-2 Side view of a geothermal doublet with a production- (red) and an injection-well (blue).

From the start of the 1940s several oil and gas fields were discovered in the area by the Nederlandse Aardolie Maatschappij (NAM) which provided the available data for this study. The search for deep geothermal energy in the Netherlands started in the late 1970s during the first oil crisis (Dufour, 2009). Initial studies by Visser and Boomer in 1970's and 1980's targeted feasibility studies for single deep geothermal systems and regional geothermal potential (Dufour, 2009; Heederik, 2009). Apart from a test well drilled at Asten in 1986-1987, no geothermal systems were realised until the period of 2006-2007 when both the "Heerlen Mijnwater" project and the "Blijswijk" project were successfully completed (Figure 1-3) (Heederik, 2009; Gilding, 2009).



Figure 1-3 First geothermal well drilled in the Netherlands at Asten in 1986 (Heederik, 2009).

During the realisation of the “Blijswijk” project no thermal or flow effect studies were performed on fluid or thermal breakthrough time (Ramaekers et al., 2006). The first geothermal energy breakthrough studies for the “Bleiswijk” geothermal project were performed by Den Boer (2008). The study by Den Boer (2008) is based on a homogenous reservoir model and studied the breakthrough time, the effect of viscosity changes caused by cold water injection. The first study into optimal geothermal heat recovery and well placement was performed by Mijnlief et al. (2009) and concluded that well placement in homogeneous modelled reservoirs for deep geothermal can contribute to a large increase in geothermal heat recovery. The first study into the effect of pressure and heat flow in the Delft subsurface was performed by Smits (2008) with a homogeneous thermal model. The effect of heterogeneities on geothermal projects and interference of different projects in the subsurface of the Netherlands have not been sufficiently studied. Multiple studies into the geology of the Netherlands (Van Adrichem Boogaert & Kouwe, 1993-1997) and into the West Netherlands Basin have been conducted by for example, Den Hartog Jager (1996), and DeVault & Jeremiah (2002). More recently detailed studies of the Delft Sandstone Member and the target area have been performed by Smits (2008), Wiggers (2009), and Drost & Korenromp (2010).

The target area of this study lies near the city of Delft where three projects will commence drilling a total of 6 wells, by the start of 2010 (Figure 1-4 Left). The three projects will place the three doublets in close proximity to each other (Figure 1-4 Right). To gain maximum hot water and reduce the hydrocarbon hazard the lower and synclinal structures are targeted for geothermal purposes. The target synclinal structure of this study is called the target area Vrijenban. Target area Vrijenban is situated between the Delft structural high containing the Delft Oil field and the structural high containing the Pijnacker Oil Field to the north east. To achieve global optimization on heat recovery and economic parameters, the production and injection rate of the doublets should be at least 100 m³ per hour and be upheld for 30 years for each system, while keeping the distance between the systems minimal. Surface locations planned for these doublets are on the premises of the Delft University of Technology (TU Delft) and its immediate vicinity; the target is the Early Cretaceous aged Delft Sandstone Member.

The Netherlands and target area Vrijenban

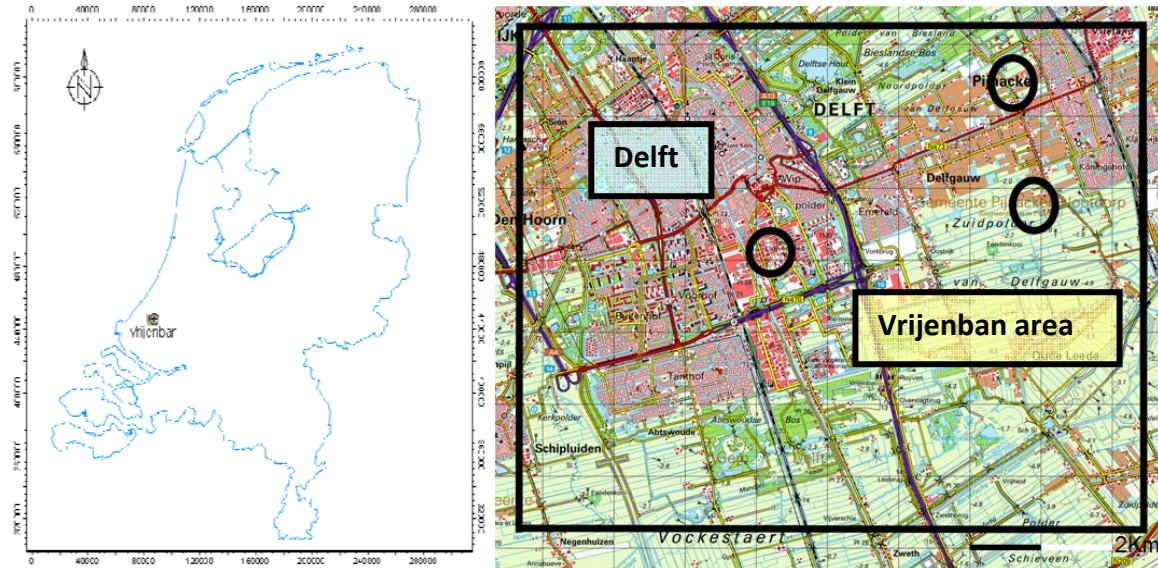


Figure 1-4 (Left) Map of the Netherlands with target area Vrijenban; **(Right)** Map of Delft and the target area Vrijenban. Large black square is the exploration licence Delft. Three circles show the three doublet top hole locations, scale 1:50.000.

The objectives of this study are: (1) to show the effect of heterogeneities in the subsurface on interaction and interference of flow on closely placed geothermal systems; (2) to gain a better understanding of the geological setting and the heterogeneities and the depositional setting of the primary target Delft Sandstone Member; and (3) to build a subsurface dynamic reservoir model with which optimal well performance and placement can be assessed. From a dynamic temperature heat flow reservoir model it is possible to determine the effects of heterogeneities on heat and fluid flow in the reservoir. Simulations can be run of multiple well configurations determining the effect of interference and field performance. This can then be used to find the optimal well placement and determine the positive and negative effect on pressure performance per well. The results of this study will be a base case for further research as it will form a benchmark for future local and regional geothermal studies.

This study results in new insights and a better and detailed understanding of the reservoir architecture of the Delft Sandstone Member. Results of the dynamic flow model are compared with prior work by Smits (2008), and Mijnlief & Van Wees (2009). Also several recommendations are made to ensure and provide the foundation for a true roll out of geothermal systems through the western parts of the Netherlands.

This report describes the results of the study performed and the model that has been built. First, in Chapter 2 the regional geology is described. In the third chapter the data and used methods are described, followed by a description of the analysis of the relation of syn-tectonic movement and sedimentation in the fourth chapter. Chapter 5 shows an overview of the studied formations. Chapter 6 is dedicated to petrophysical properties used in this study followed by the model building process and the dynamic flow modelling in chapter 7 and chapter 8 respectively. Finally, in the last chapter, the conclusions and recommendations are given.

2. Regional geology and climate

2.1. Introduction

The Delft Sandstone Member forms part of the infill of the West Netherlands Basin (WNB) and is situated in the Rijswijk Oil Province in the western part of the Netherlands. The main axis of the West Netherlands Basin is in the southeast to northwest direction and is connected to the north-west to the Broad Fourteens Basin and to south-east to the Roer Valley Graben. The Zandvoort ridge formed a prominent high block to the northeast and the London Brabant Massif was situated to the southwest (Van Balen et al., 1999) (Figure 2-1). The West Netherlands Basin is situated on top of a tectonic active area where deformation has played a role from the Late Carboniferous onwards (Wiggers, 2009).

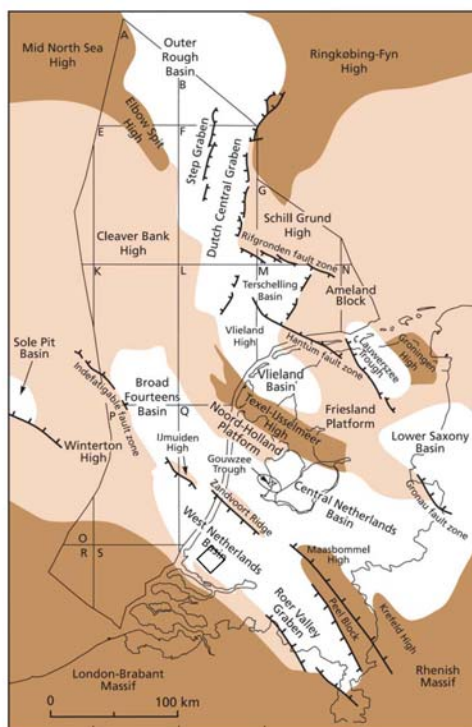


Figure 2-1 Map of the Netherlands with the West Netherlands Basin during the Late Jurassic to Early Cretaceous (Van Adrichem Boogaert & Kouwe, 1993-1997).

The West Netherlands Basin is created by the continuing regional thermal subsidence during Middle Triassic to Middle Jurassic on top of the older Campine basin (Wiggers, 2009). This first stage of the formation of the West Netherlands Basin was during the first extensional Early Kimmerian pulse movement at the break up of Pangea (Geluk, 1999). This was followed by a second stage in the West Netherlands Basin of stronger rifting of the basin by the first Late Kimmerian rifting pulse caused by Middle Jurassic crustal separation in the Central Atlantic and Tethys domains. The crustal separation accelerated rifting in the North Sea rift system, comprising crustal-extension strain that affected the whole NW Europe (Kabel, 1986; De Jager, 2007). The first Late Kimmerian rifting pulse movement forms an integral part of Late Jurassic and Early Cretaceous rift and wrench tectonics and became the main tectonic element in the subsurface of the West Netherlands Basin (De Jager, 2007). Rifting gradually stopped during the later part of the Early Cretaceous but the subsidence continued (Van Wijhe, 1987).

Tectonic compression occurred during the middle of the Late Cretaceous by collision of the European and African plates and active spreading of Atlantic and Arctic mid-oceanic ridges, resulted in N-S regional compression and caused inversion throughout the West Netherlands Basin (Vis et al., 2010; Van Wijhe, 1987). This third tectonic stage in the West Netherlands Basin is referred to as the Sub-Hercynian tectonic stage (Van Adrichem Boogaert & Kouwe, 1993-1997). At the end of the Cretaceous after the compression of the Early Alpine movement, regional subsidence set in and continued to today. The development of the West Netherlands Basin can therefore be divided into three stages, 1) a pre-rift section from Middle Triassic to Middle Jurassic, 2) a syn-rift stage during the Late Jurassic and Early Cretaceous and 3) a post-rift stage during the Late Cretaceous and Cenozoic (Van Balen et al., 2000).

2.2. Pre-rift Stage

The first Early Kimmerian tectonic movement formed a structurally rather simple large-scale half-graben, bounded to the northeast by a major fault zone. The West Netherlands Basin is first filled in with Upper Germanic Triassic Group lacustrine and shallow marine claystones, carbonates and evaporates (Verweij & Simmelink, 2001). This followed by a large intra Triassic hiatus (Van Adrichem Boogaert & Kouwe, 1993-1997). Differential faulting and subsidence formed various sub-units in the basin from the Late Triassic onwards. During the Early Jurassic a wide sea had developed in which locally more than 1800m of fine-grained clastics of the Altena Group accumulated throughout the West Netherlands Basin (De Jager, 2007). The marine environment in which the Altena Group is deposited retreated completely from the Netherlands after the first pulse of the Mid Kimmerian phase during the Middle Jurassic resulted in erosion and the formation of an unconformity (Herngreen & Wong, 2007; Smits, 2008; Van Balen et al., 2000).

2.3. Syn-rift Stage

The Syn-rift period from Late Jurassic to Early Cretaceous started with the Late Kimmerian first rifting pulse (Van Balen et al., 2000). Strong rifting by extensional movement induced rapid subsidence of the West Netherlands Basin, causing large differential subsidence and faulting (Simmelink et al., 2007). The differential subsidence caused oblique movement of the long NW-SE trending faults and the breaking up of the West Netherlands Basin into further subunits (Van Wijhe, 1987).

A differentiation is caused between rapidly subsiding basins accumulating very thick syn-rift sediment packages and more quiescent platform areas where thin layers of sediment were deposited or erosion took place (De Jager, 2007). During the Late Jurassic continental sediments like the Schieland Group started to unconformably overly the Altena Group deposits with the floodplain deposits of the Nieuwekerk Formation (Wong, 2007). The extensional basins were filled with locally more than 2500m of sands and clays which belong to the continental Schieland Group containing the Alblasserdam-, Delft Sandstone- and Rodenrijs Claystone Member. First the floodplain deposits of the Alblasserdam Member unconformably overly the Altena Group followed by the fluvial sediments of the Delft Sandstone Member. As subsidence increased and sea level rise occurred the lower coastal sand and silts of the Rodenrijs Claystone Member were deposited. This continued throughout the Early Cretaceous as the Schieland Group is conformably or mild unconformably overlain by the marine deposits of the Rijnland Group (Van Adrichem Boogaert & Kouwe, 1993-1997). In the large formed open-marine basin the Rijnland Group then deposited up to 1400 m of mainly fine-grained clastics with coastal sandstones of the Vlieland- and Holland Formation.

2.4. Post-rift Stage

During the Middle to Late Cretaceous compressive movement caused the inversion of previous depositional centres by reactivation of faults. The oblique movement along existing faults created flower structures, which form the basin highs (De Jager, et al., 1996). Only in marginal troughs that formed to the north and south of the basin sedimentation still took place (Wiggers, 2009).

Regional subsidence after the Late Cretaceous in combination with a major eustatic rise in sea level inundated the remaining highs. The Rijnland Group in the target area was completely capped by the Chalk Group. After the Chalk Group was deposited the compressive forces stopped at the end of the Cretaceous, this prevented further inversion of the structures. Regional subsidence and sedimentation continued in the Early Tertiary resulting in a sequence of marine fine-grained clastics (predominantly clays) belonging to the Lower North Sea Group, deposited on top of the Chalk Group (Van Adrichem Boogaert & Kouwe, 1993-1997).

2.5. Stratigraphy

Based on nearby local wells in the target area Vrijenban and available core and log data the following stratigraphy build up is made. The names represent the most commonly used names in the stratigraphy of the Netherlands; the formations have been placed in groups which each containing several members (Adrichem Boogaert & Kouwe, 1993). From the oldest to youngest; group, formation and members as found in the Rijswijk, Delft and Pijnacker oil wells can be found in Figure 2-2 and Figure 2-3. The target of this study is the Delft Sandstone Member, a part of the Nieuwekerk Formation and the Schieland Group. Below the Delft Sandstone Member lies the Alblasserdam Member and above the target Delft Sandstone Member is the Rodenrijs Claystone Member.



Figure 2-2 The table shows the succession of groups, formations and target members around the target formation. The formations are placed top to bottom from young to old. The Delft Sandstone Member is the target sandstone.

Stratigraphy of the Target Area Vrijenban.

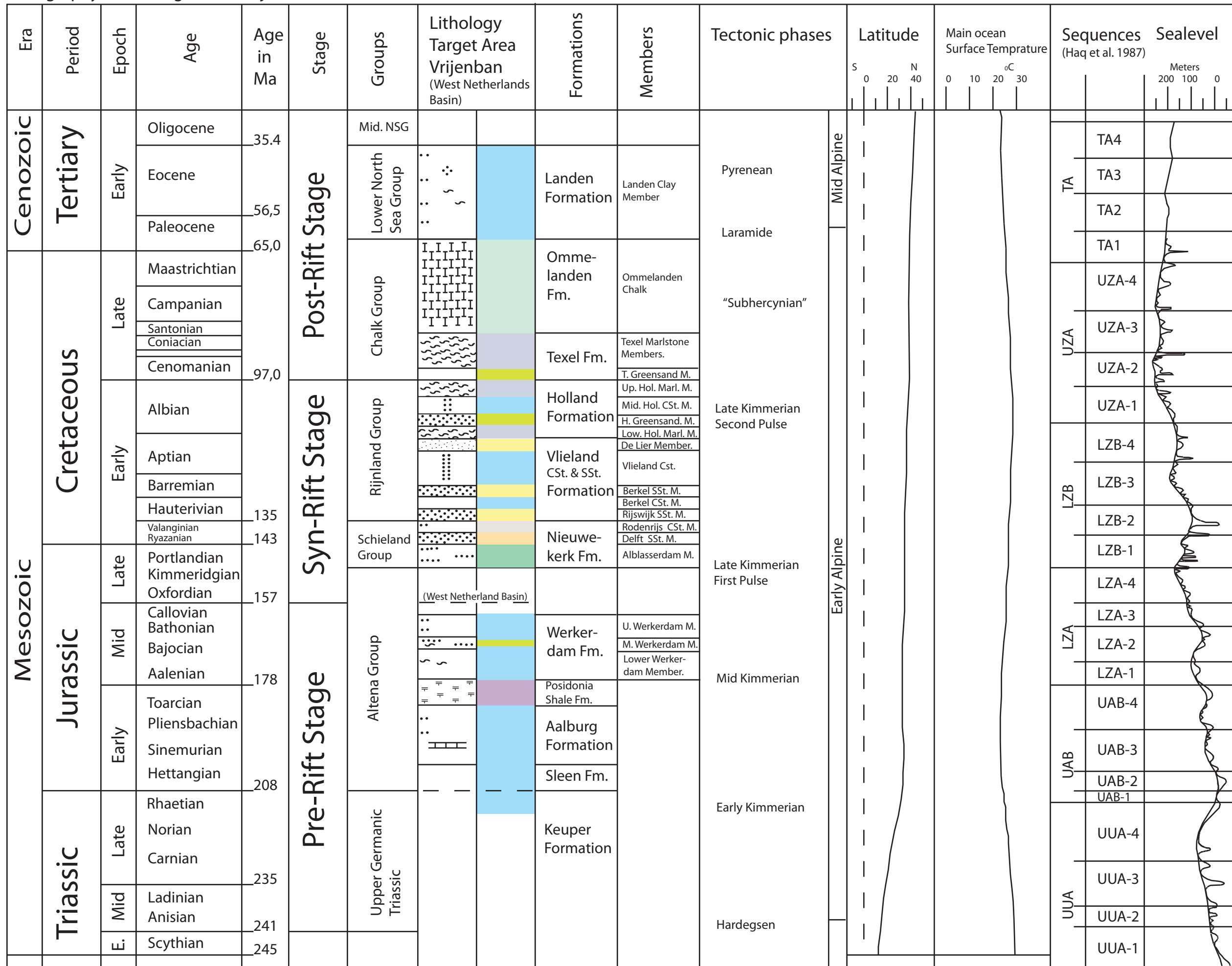


Fig 2.3 Stratigraphy of target Area Vrijenban.; Time and age after Van Adrichem Boogaert & Kouwe, (1993-1997), Lithology Vrijenban based on wells Del-, 3,8 and PNA-, 13-15 and the West Netherlands Basin based on RWK-1, Group, Formation & Member names, Colours & Lithology legend based on Van Adrichem Boogaert & Kouwe (1993-1997), Latitude and Temperature after Verweij & Simmelink (2001), and Sequence and Eustatic Sea level after Haq et al., (1987).

2.6. Basin movement, global climate and eustatic sea level

During the Triassic to Early Cretaceous continental break-up, the area of the Netherlands moved from the arid climate zone to sub-tropical climates of the northern hemisphere (De Jager, 2007). During the period from Early Jurassic to the end of the Early Cretaceous the area moved over the 40 degrees latitude from 20 to 0 degrees longitude as can be seen in Figure 2-3 (Scotsese et al., 1987). This movement combined with eustatic sea level fluctuations affected the sedimentation, depositional environment, and erosion in the West Netherlands Basin (Berendsen, 2004).

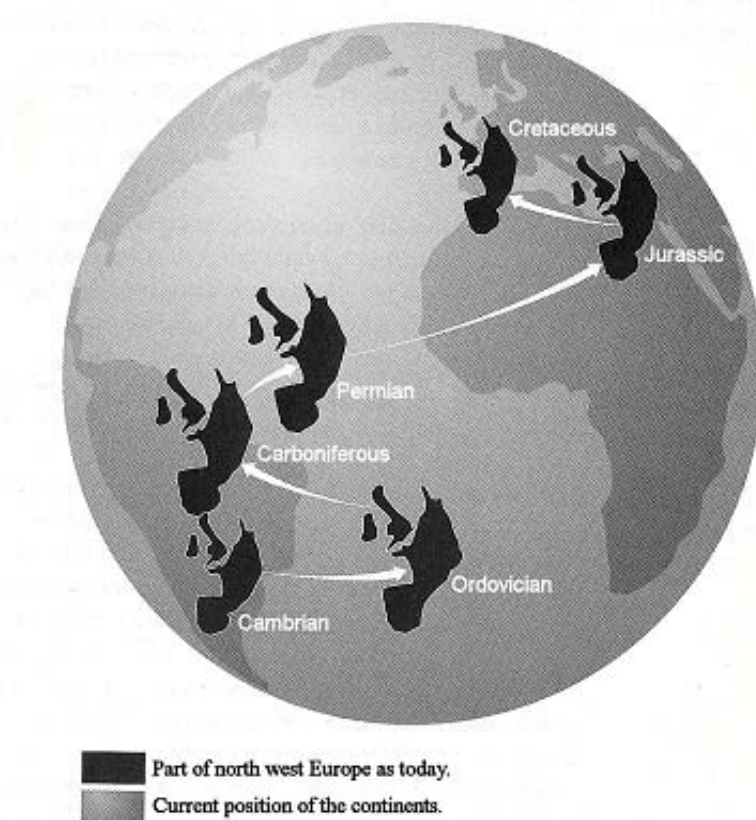


Figure 2-4 The position of western Europe on the globe at different moments in geological history.
Modified after Berendsen (2004).

As the climate in the area changed from an arid climate to a sub-tropical climate, the basin average temperature changed. The average temperature was high at the start of the pre-rift stage and cooled down throughout the Triassic from 25 to 15 degrees Celsius. During the syn-rift stage it slowly heated up from 15 to 25 degrees until at the start of the post rift stage it started to cool down again (Verweij & Simmelink, 2001). The average surface temperature can be found in the stratigraphy chart (Figure 2-3).

The sea-level is relatively low in the north-west of Europe during the Late Jurassic, and the entire West Netherlands Basin is above sea level (Hancock, 1984). Through eustatic sea level oscillation during the Late Jurassic and the start of the Early Cretaceous, the trend of sea level is transgressive. During this syn-rift stage the facies in the West Netherlands Basin are controlled by the tectonic setting, base level fall and availability of source materials. The eustatic global sea level is studied by Haq et al., (1987). In the stratigraphy chart the eustatic sea level curve and sequences can be found (Figure, 2-3).

3. Data and Methods.

The study is based on the interpretations of the available data of the Vrijenban area in the West Netherlands Basin. A static 3D reservoir architecture model was made through the analysis and correlation of the interpreted data. The available data consists of 3D seismic sections of the area, local well data, petrophysical log data and cores- and cutting-samples. Furthermore, thin sections from the "MKP 11" core and the cuttings of the "Delft 03" well were studied. From the "VDB 01" well formation fluid was taken and analysed by Chun (2009). The available data was provided digitally and forms the basis for the interpretation of faults and folds, the tectonic setting, formations descriptions and the modelling of the target formations. The quality of the data was checked by comparing it to the original recorded data. First the methods and software used in this study are described. Then the available well log and core data is presented, followed by the formation fluid analyses and the well correlation panels. Finally the available seismic data is described and discussed in the last paragraph.

The study area lies between the city of Delft and the village of Pijnacker in the western part of the Netherlands (Figure 3-1). From the start of the 1940s several wells were drilled, finding large amounts of oil and gas in the West Netherlands Basin. All data used in this study is provided by the Nederlandse Aardolie Maatschappij (NAM) apart from the formation fluid samples which are from the VDB-1 Well. All data is loaded into the "Rijksdriehoek" coordinate system which is the national coordinate system used in the Netherlands.

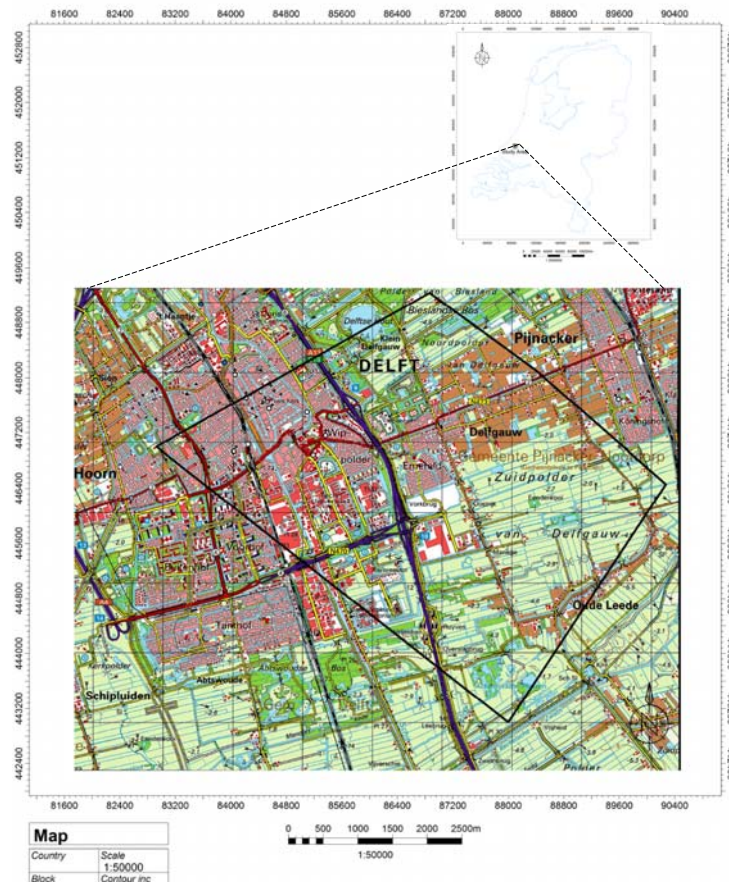


Figure 3-1 The fieldwork area, with the map of Delft. The black polygon indicates the study area.

3.1. Methods

To interpret and process the available seismic and well log data Petrel software is used. The formation markers found in the well log data were reinterpreted and improved. The seismic data is interpreted and horizons and faults are mapped. On multiple 2D sections a palinspastic reconstruction is performed using the program 3D MOVE. Core and cuttings data are studied and interpreted. From the combined interpretation of data, the depositional setting and depositional process of the formation are determined. The available data is combined to build a static 3D reservoir architecture model of the target formations using Petrel 2009.1, Schlumberger's modelling package. Petrophysical data from well log and plug measurements are combined with the results of previous work by Smits (2008) and Van Eldert (2008). The Petrel 2009.1 petrophysical modelling pack is used to interpret the petrophysical data and to create the property maps. The static 3D reservoir architecture model is incorporated with the created property maps and the formation fluid data into a dynamic flow and temperature model. This modelling process is performed using the Eclipse 100 2007.1 Schlumbergers Office software and the results are visualised in Petrel 2009.1.

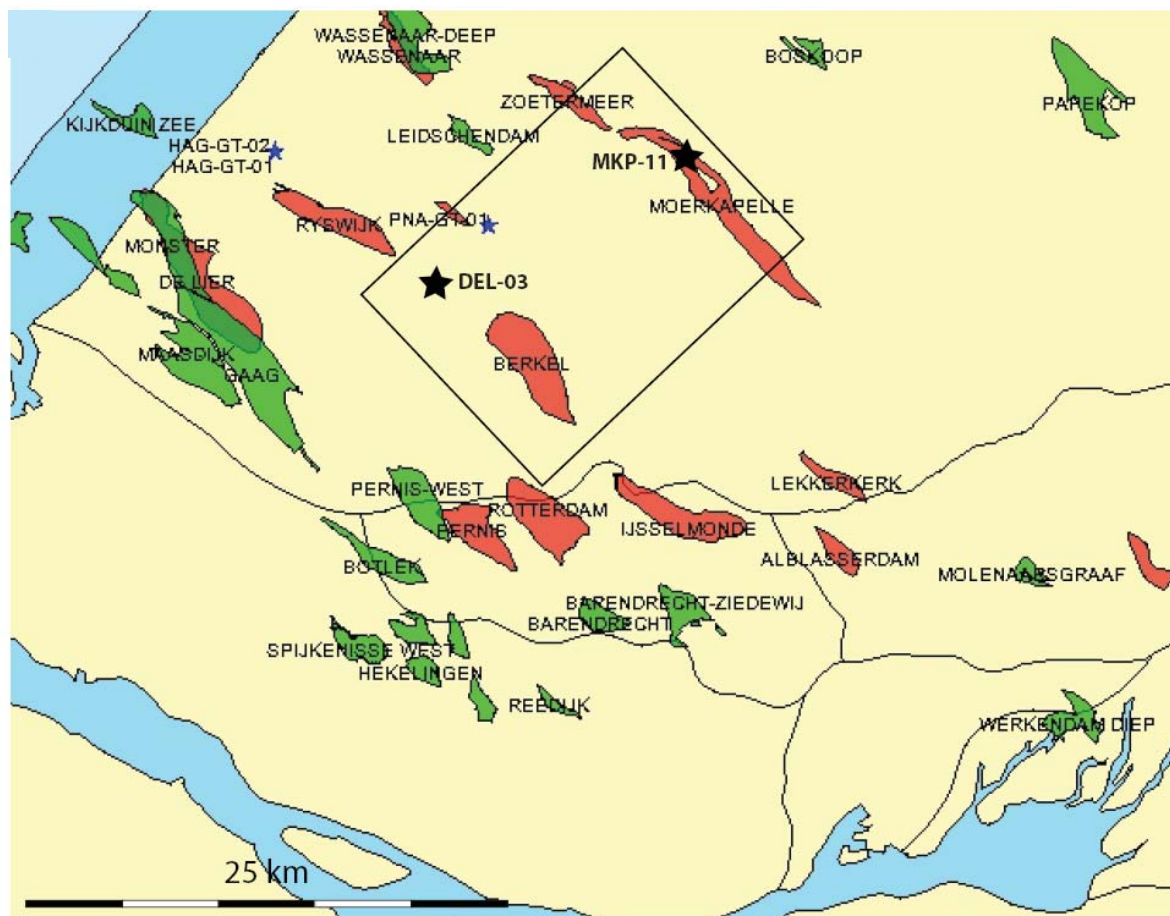


Figure 3-2 Oil (red) and gas (green) fields in the West Netherlands Basin. Black stars: location of wells (DEL-03 and MKP-11) used in this study. Blue stars: location of geothermal wells started in 2010, Box: study area. Modified after NLOG (2010).

3.2. Well data

Over a hundred wells and sidetracks are drilled in the West Netherlands Basin which mostly target shallow oil fields. In and around the target area Vrijenban there are 50 wells of which the data are available for this study (Figure 3-2)(Appendix D). Not all wells in and around the target area Vrijenban area drilled beyond the Cretaceous and hit the target Delft Sandstone Member (SLDND). Table 3-1 shows the wells that hit the target Delft Sandstone Member in and around the target area Vrijenban. The range and quality of the data varies and depends on the amount of logs run and the age of the well. A full list of all available log data used in this study can be found in Table 3-2.

Well	Formation Name Abbreviation			MKP-9A	SLDNR	SLDND	SLDNA
DEL- 2	SLDNR	SLDND		MKP- 10	SLDNR	SLDND	SLDNA
DEL- 3	SLDNR	SLDND	SLDNA	MKP- 11	SLDNR	SLDND	SLDNA
DEL- 5	SLDNR			MKP- 12	SLDNR	SLDND	SLDNA
DEL- 8	SLDNR			MKP- 12A	SLDNR	SLDND	SLDNA
HAG- 1	SLDNR	SLDND	SLDNA	MKP- 13	SLDNR	SLDND	SLDNA
HAG- 2	SLDNR	SLDND	SLDNA	MKP- 14	(Fault)	SLDND	SLDNA
KDZ- 2	SLDNR	SLDND	SLDNA	MKP- 15	(Fault)	SLDND	SLDNA
KDZ- 2A	SLDNR	SLDND	SLDNA	MKP- 16	SLDNR	SLDND	SLDNA
LED- 1	SLDNR	SLDND	SLDNA	OLE- 1	SLDNR		
LIR- 45	SLDNR	SLDND	SLDNA	PNA- 13	SLDNR	SLDND	SLDNA
MKP-1	(Fault)	SLDND	SLDNA	PNA- 14	SLDNR		
MKP-2	SLDNR	SLDND	SLDNA	PNA- 15	SLDNR		
MKP-3	SLDNR	SLDND	SLDNA	RWK- 1	SLDNR	SLDND	
MKP-9	SLDNR	SLDND		RWK- 18A	SLDNR	SLDND	SLDNA

Table 3-1 Wells that hit the top of the target formations Rodenrijs Claystone Member (SLDNR), the Delft Sandstone Member (SLDND) in yellow and the Alblasserdam Member (SLDNA).

Well name	Available Well Logs
DEL-02	RESD, SP
DEL-03	RESM, SP, RESD
PNA-15	DENS, GR, RESD, SH, RESM, NEUT, SON, POR, FLGR, CAL
OLE-01	RESD, RESM, FLGR, SP, CAL, GR
MKP-16	RESM, SZ40, SH, SZ50, NEUT, CAL, POR, SZ70, SZ30, GR, DENS, FLGR, RESD, SON
MKP-14	POR, SH, SZ40, SZ30, RESM, DENS, GR, CAL, NEUT, SON, SZ70, FLGR, SZ50
MKP-13	NEUT, CAL, RESM, POR, GR, SON, DENS, SH, FLGR
MKP-12A	RESM, FLGR, NEUT, POR, RESD, SON, SH, DENS, GR, CAL
MKP-12	RESM, FLGR, NEUT, POR, RESD, SON, SH, DENS, GR, CAL
MKP-11	FLGR, GR, RESM, DENS, SH, CAL, SON, NEUT, RESD, POR
MKP-10	SH, SON, RESM, GR, DENS, NEUT, SZ40, SZ30, SZ70, FLGR, POR, RESD, CAL, SZ50
MKP-9A	CAL, DENS, RESD, SON, SZ40, SZ30, SZ70, SZ50
MKP-2	CAL, RESD, SP

Table 3-2 Table of the available log data per well used in the Petrophysical analyse and evaluation of the Delft Sandstone Member. The full names can be found in the nomenclature (Appendix B).

Available Cores

Several wells were cored in the West Netherlands Basin. During the study, presented in this report, the cores from 5 wells were available (Table 3-3). All cores studied were taken, stored, and made available by the NAM. Core data used in this study concentrated on the target formation Delft Sandstone Member and the overlying Rodenrijs Claystone Member. Of the Alblasserdam Member almost no core data is available. Of all the wells that hit the target Delft Sandstone Member only 3 have cores containing the target sandstone but the recovery is low. For this study a new core description is made of the “MKP 11” well which can be found in appendix C (Loerakker, 2009). Apart from the slabs of the “MKP 11” well, also the original core rock is available. Plugs for further research and thin sections were obtained and studied. From the MKP-11 well core, samples and plugs were taken and further analyzed at PanTerra geoconsultancy Drost & Korenromp (2010).

Well	Well NR	Top MD	Bottom MD	Recovery	Member
MOERKAPELLE- 1	MKP- 1	721.00	727.00	33.3 %	SLDND
MOERKAPELLE- 1	MKP- 1	727.00	733.00	75 %	SLDND
MOERKAPELLE- 5	MKP- 5	1054.00	1060.00	50 %	SLDNA
MOERKAPELLE- 5	MKP- 5	985.00	991.00	0 %	SLDND
MOERKAPELLE- 5	MKP- 5	735.00	735.40	100 %	SLDNR
MOERKAPELLE- 5	MKP- 5	752.00	758.00	63.3 %	SLDNR
MOERKAPELLE- 9	MKP- 9	859.50	875.50	75 %	SLDND
MOERKAPELLE- 9	MKP- 9	841.00	850.00	100 %	SLDNR
MOERKAPELLE- 9	MKP- 9	850.00	859.50	95.7 %	SLDNR
MOERKAPELLE- 9	MKP- 9	859.50	875.50	75 %	SLDNR
MOERKAPELLE-11	MKP- 11	906.50	912.00	78.2 %	SLDNA
MOERKAPELLE-11	MKP- 11	853.00	859.00	53.3 %	SLDND
MOERKAPELLE-11	MKP- 11	859.00	860.50	53.3 %	SLDND
MOERKAPELLE-11	MKP- 11	860.50	866.50	45 %	SLDND
MOERKAPELLE-11	MKP- 11	866.50	872.50	76.7 %	SLDND
MOERKAPELLE-11	MKP- 11	872.50	877.50	28 %	SLDND
MOERKAPELLE-11	MKP- 11	878.50	885.90	73 %	SLDND
MOERKAPELLE-11	MKP- 11	887.00	893.00	98.3 %	SLDND
MOERKAPELLE-11	MKP- 11	893.00	899.50	54.6 %	SLDND
MOERKAPELLE-11	MKP- 11	899.50	904.90	87 %	SLDND
MOERKAPELLE-11	MKP- 11	906.50	912.00	78.2 %	SLDND
MOERKAPELLE-11	MKP- 11	837.00	843.00	95.8 %	SLDNR
MOERKAPELLE-11	MKP- 11	843.00	847.00	90 %	SLDNR
MOERKAPELLE-11	MKP- 11	847.00	853.00	88.3 %	SLDNR
MOERKAPELLE-11	MKP- 11	853.00	859.00	53.3 %	SLDNR
MOERKAPELLE-15	MKP- 15	962.00	970.00	94.7 %	SLDNA
MOERKAPELLE-15	MKP- 15	970.00	979.00	95 %	SLDNA

Table 3-3 Available core data of the Delft Sandstone Member, the Rodenrijs Claystone Member, and the Alblasserdam Member and their recovery rates.

Cuttings and thin sections

Because of lack of quality of well logs from the Delft Sandstone Member in the target area Vrijenban, a cutting study is performed on the Delft-03 Well. The Delft-03 well was drilled in 1953 to a true vertical depth of 2200 going through the entire Rodenrijs Claystone Member, the Delft Sandstone Member and parts of the Alblasserdam Member. Apart from studying the cuttings, thin sections were made. The thin sections were studied to further understand the cementation and type of mineral content found in the well. Thin sections were made of both the core of the MKP-11 well and from the cuttings of the Delft-03 well. The thin sections that are made from the core of MKP-11 well were taken from samples as found in core log (Appendix C). The location of the thin sections as made from the Delft-03 cutting study, can be found in Figure 3-3. A full description of the thin sections can be found in Drost & Korenromp (2010).

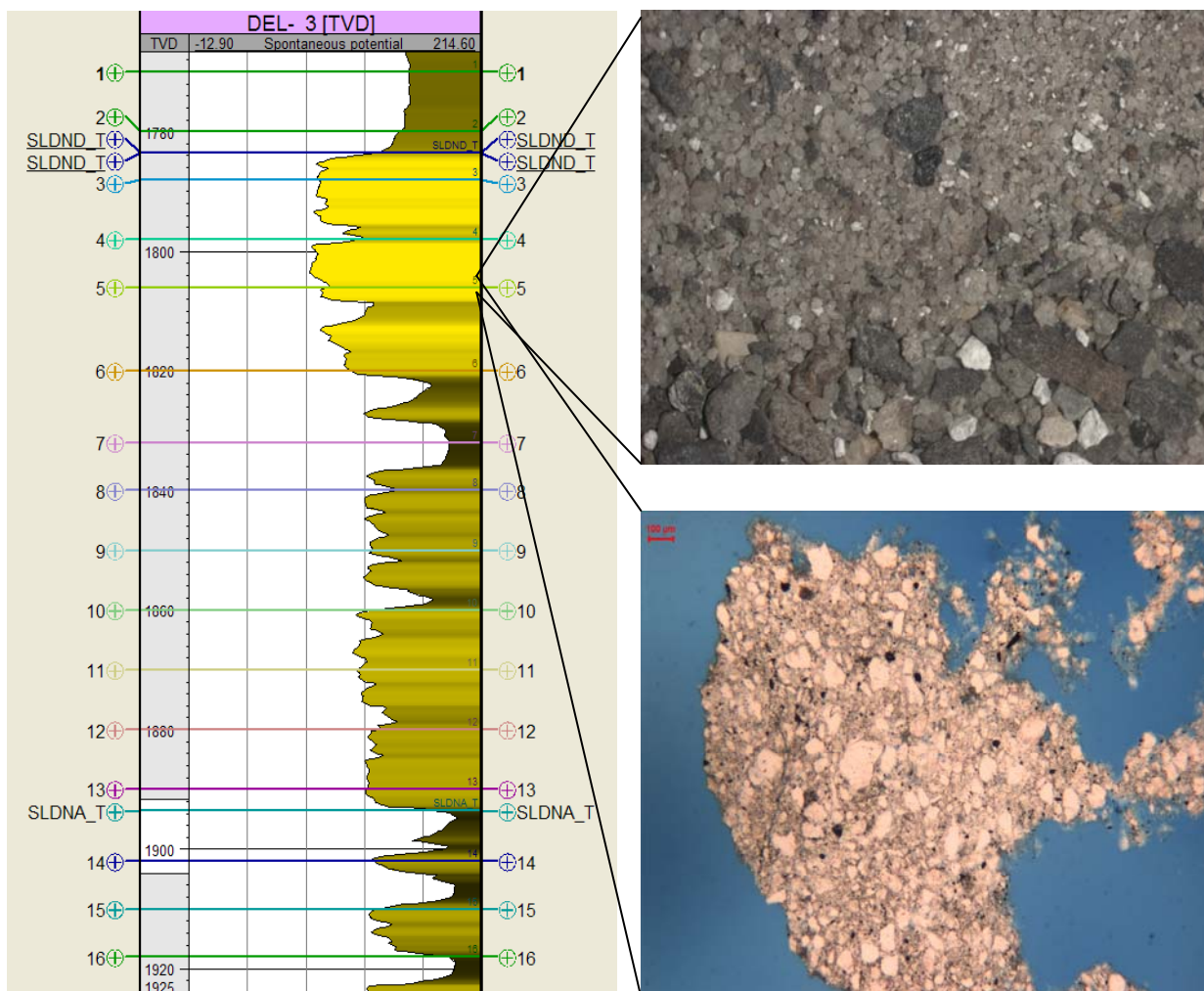


Figure 3-3 On the left the Spontaneous Potential log of the Delft-03 well with the formation tops and the available thin sections of the cuttings as described in Drost & Korenromp (2010) in true vertical depth. The right top figure shows the cutting sample nr; "5" from 1806-1808 m depth of the Delft-03 well. The right bottom figure, shows the thin section of cemented grains made from the cutting sample "5" of the Delft-03 well.

Formation fluid samples

Formation fluid samples or fluid data from wells in the target area Vrijenban are unavailable. Therefore fluid samples of other nearby wells are studied to determine the fluid properties. A study was conducted by (Chun, 2009) to determine the content and properties of the formation fluid. The total number of dissolved substances in the formation fluid gives an average salinity of 98,4 mg/L (Chun, 2009). The salinity, the calculated density, and derived thermal conductivity of the formation fluid are used in the dynamical modelling of the reservoir flow and temperature (paragraph 8.3).

Well log correlation panels,

Well correlation panels were created across the West Netherlands Basin in the target area Vrijenban (Figure 3-4). The panels show that the formations can be correlated over long distances in two perpendicular directions, northwest-southeast and southwest-northeast respectively. Hence the Delft Sandstone Member, member of the Schieland Group, can be found over large distances and is not a local anomaly (Figure 3-5, Figure 3-6).

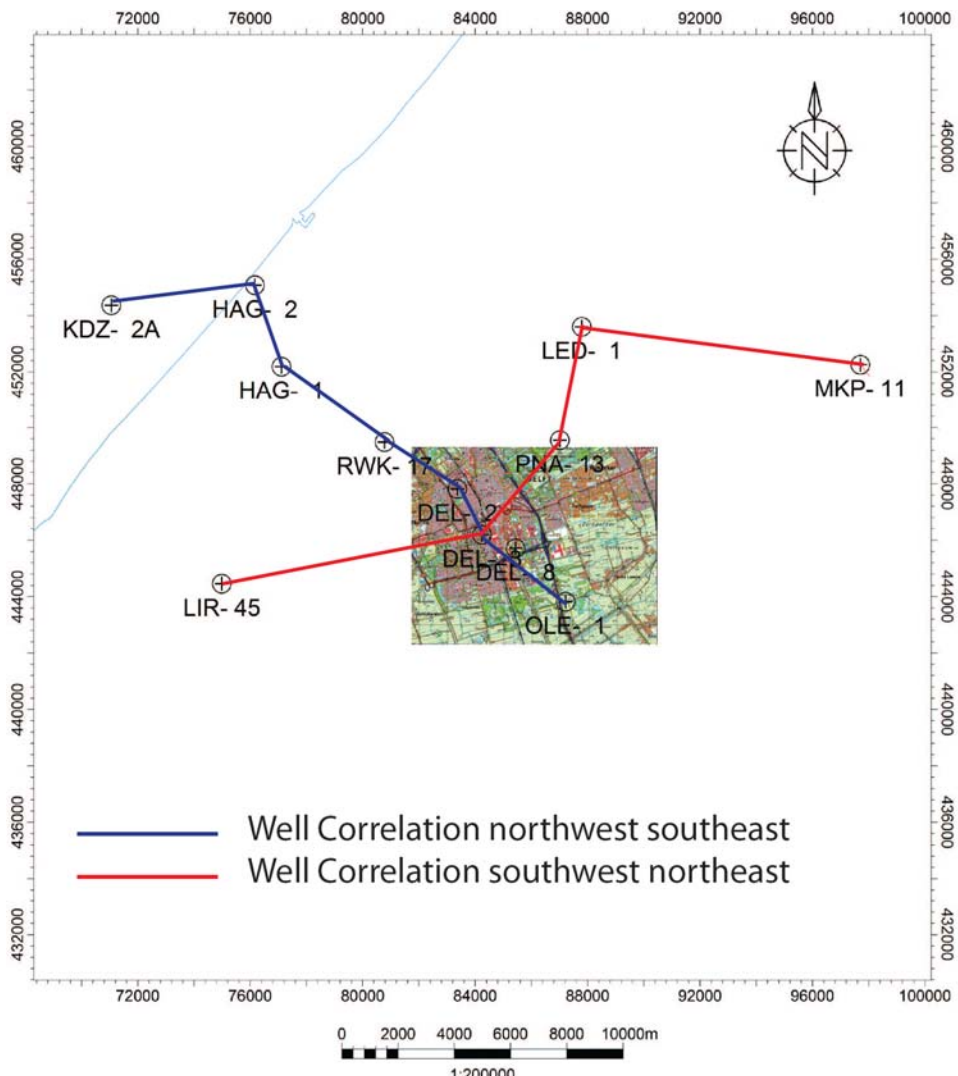


Figure 3-4 The west of the Netherlands with wells, map of Delft and the well correlation cross panel lines through the wells. Blue is the northwest-southeast well correlation line (Figure 3-5), Red is the southwest-northeast correlation line (Figure 3-6).

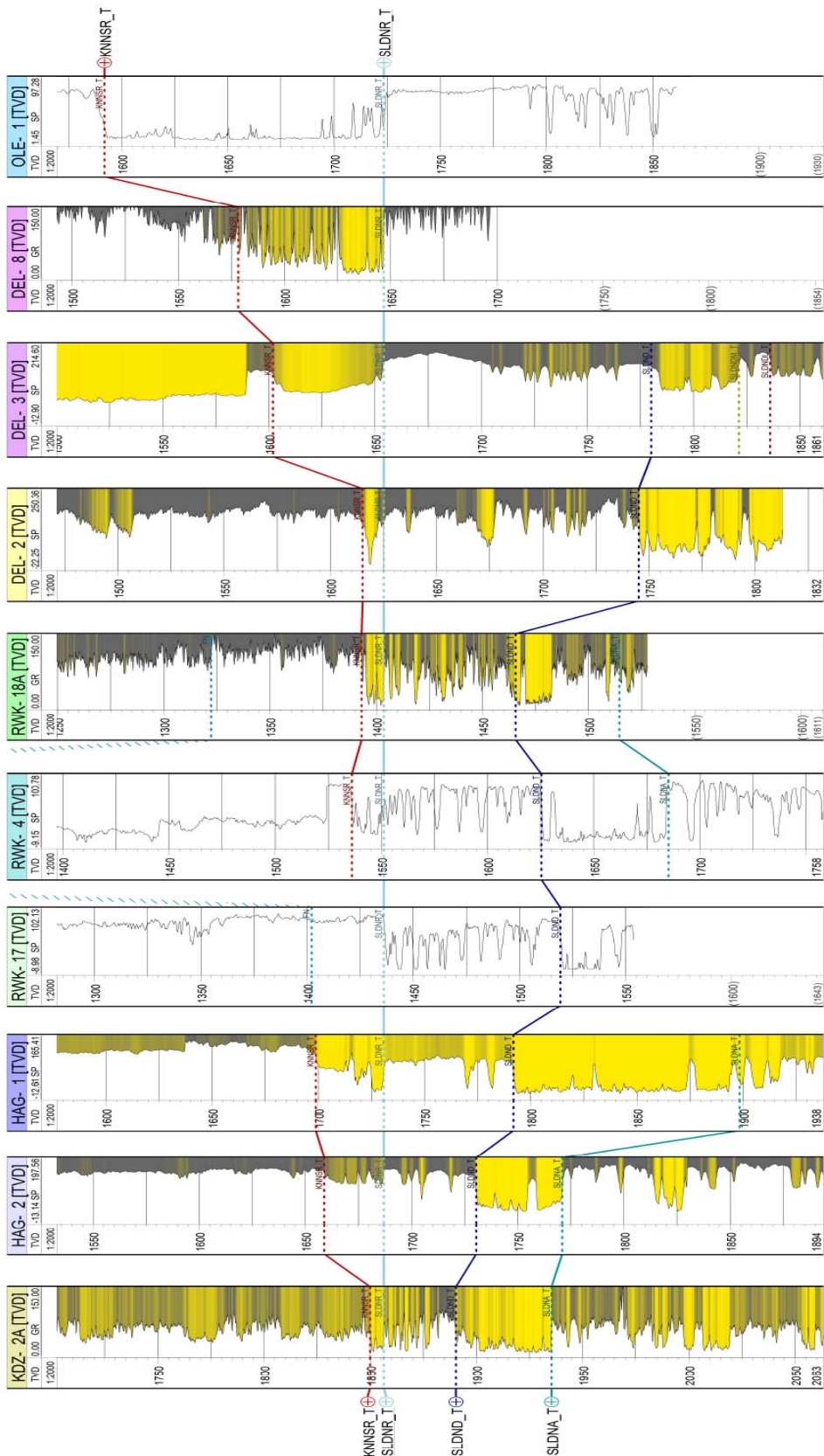


Figure 3-5 Well correlation panel from northwest to southeast showing the wells KDZ-2A, HAG-02, HAG-01, RWK-17, -04, -18A, Del-02, -03, -08 and OLE-01 with correlated well top markers in true vertical depth in meters. The scale is 1:2000.

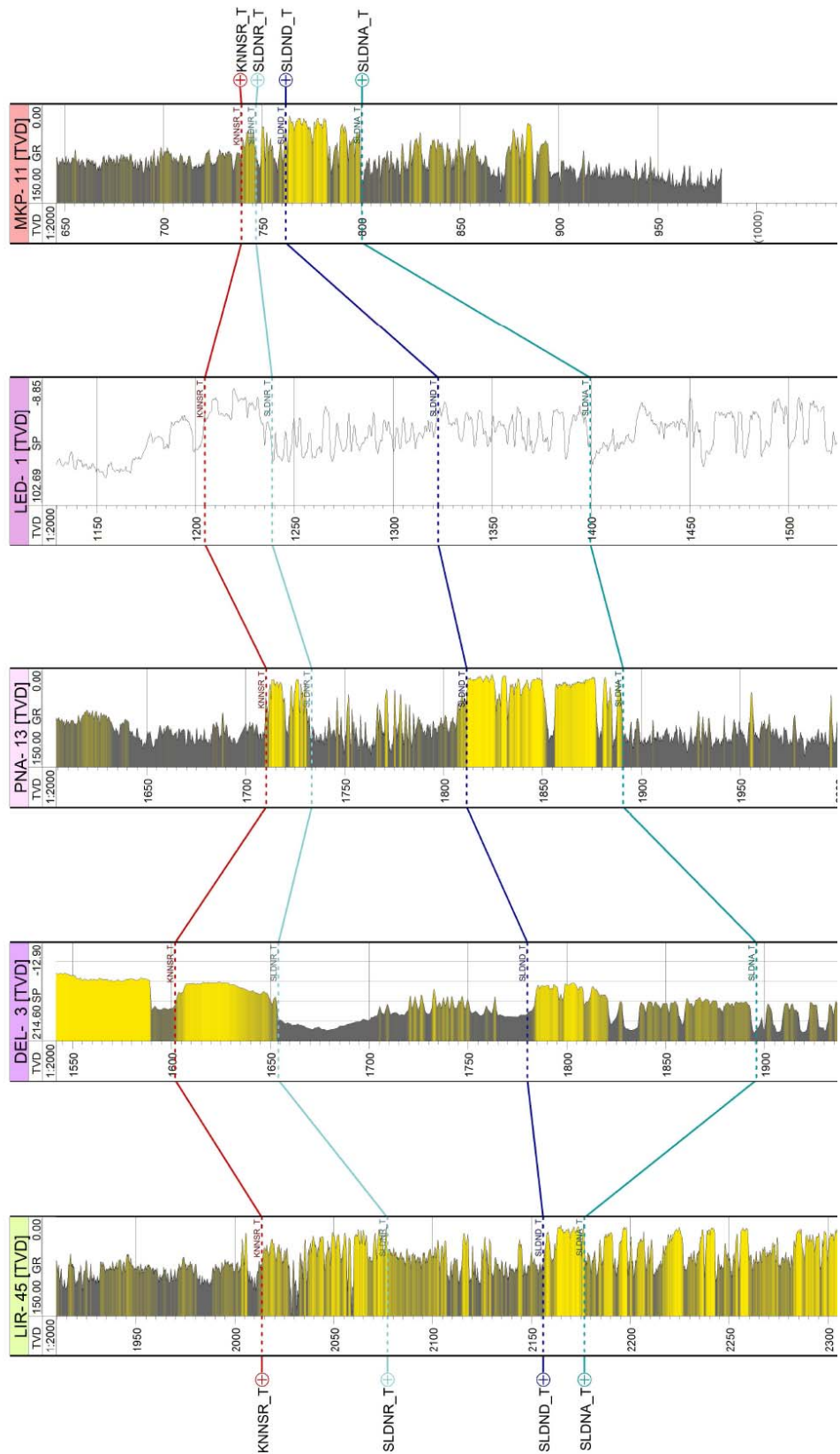


Figure 3-6 Well correlation panel from southwest to northeast showing the Lir-45, Delft-03, PNA-13, LED-1 and MKP-11 wells with correlated well top markers in true vertical depth in meters, scale 1:2000.

3.3. Available Seismic data

For the seismic interpretation of the subsurface of the target area Vrijenban a seismic study is performed on data provided by the Nederlandse Aardolie Maatschappij (NAM). The acquisition of the data took place in 1986 from January until June. The quality of the original 1986 data is good enough to interpret fault and folds but resolution at target depth is beyond the size of smaller formations. The prestack depth-migrated (PSDM) seismic data used in this study is data that was reprocessed in 2003 from the original shot seismic from 1986. Next to the PSDM seismic data, a regional depth converted time migrated seismic dataset is also available. A surface map of the target area Vrijenban with the available 3D seismic surveys is shown in Figure 3-7.

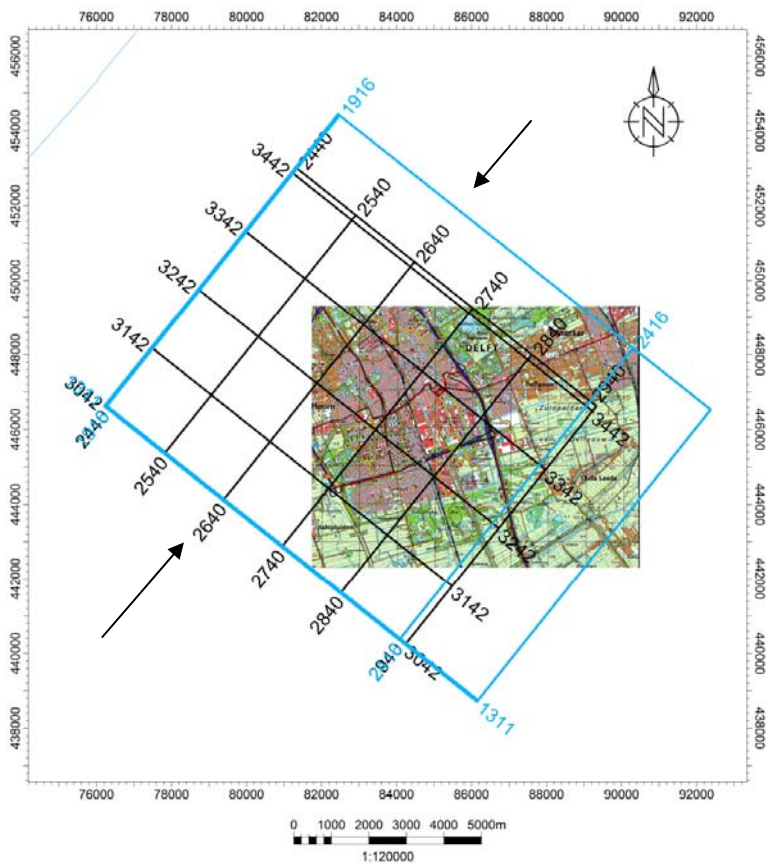


Figure 3-7 Map of Delft with available seismic data sets. The black cube represents the PSDM seismic data, the blue cube represents the regional time migrated seismic data. The arrows point to seismic inline 2640 used in Figure 4-1.

The seismic area is called the L3NAM1985. The sources used during the acquisition is vibroseis and dynamite and the data was recorded on tape, with 18 receivers per group with each a 40 meter spacing. The bin size of the data collection is 50 meters, making the vertical error 2 bin sizes or 100 meter. No information about the reprocessing or the used velocity model was released by the NAM. The seismic section was cut off beyond the 3000 meters line so the maximum depth that can be interpreted is around 3 km. The depth conversion is reliable as the well markers of the wells match the surfaces in the seismic data. As there is no insight into the resolution or error it is determined from the data that the error is 1% of the depth. For example at 2000 meters depth the seismic error is found to be around 20 meters. All figures presented in this study are of a volume for which the showrights are granted by the NAM.

4. Analysis of the relation tectonics and sedimentation.

4.1. Introduction

The goal of this study is to better understand the subsurface geology and determine the heterogeneities of the Delft subsurface. By better understanding the relation between the tectonics, the subsurface structures and the evolution of the Vrijenban area with the deposition of sediments, a better understanding of the heterogeneities in the subsurface can be obtained. For this reason an analysis of the relation between the syn-tectonic movement in the area and the sediments deposition was performed. First the available data is interpreted. The fault, folds and key surfaces of the subsurface below the Vrijenban area are mapped. The reservoir architecture is interpreted and key structures, faults and folds are described. From this the accommodation space evolution can be derived and the relation between the tectonics and sediments can be determined, presented and discussed. The new insights will form a base for the static architectural reservoir model and the understanding of the depositional setting of the area.

4.2. Seismic interpretation

To determine the reservoir architecture and the accommodation space development, the subsurface needs to be interpreted from seismics. The available 3D seismic surveys are loaded and interpreted using Petrel[®]. The seismic interpretation was performed on both the NAM provided prestack depth-migrated seismic data (PSDM) and the regional time-depth migrated seismics. The data was combined with well data in the integrated seismics interpretation platform Petrel[®]. Overall quality of the seismic data is good as structures and layers can be interpreted although parts of the seismic data have a low resolution and interpretation is not possible. The resolution at target depth of 2 km is beyond that of a single formation or sandstone body; for example the top Alblasserdam Member could not be confidently interpreted. The polarity of the seismic data is reversed SEG and all figures in this study are in depth (m). The identification of the reflections is tied back to the stratigraphy as found in the well. Major structures and layers could be interpreted and are presented below.

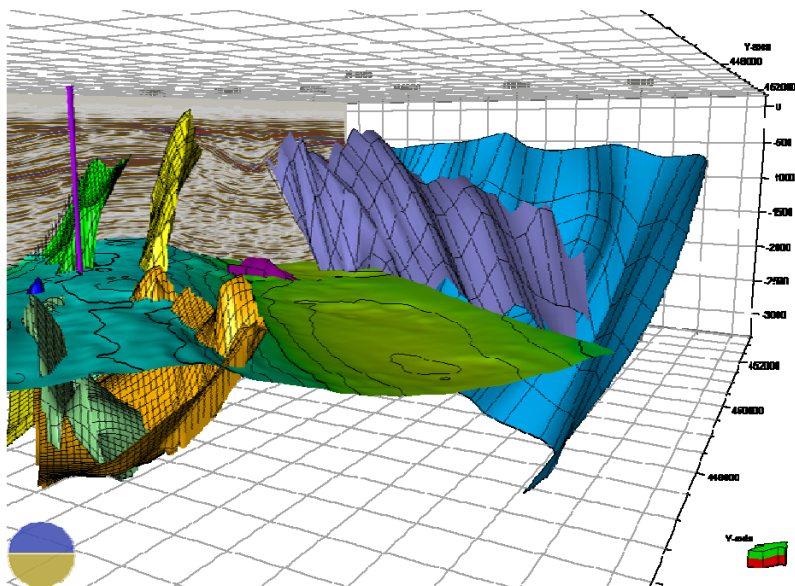


Figure 4-1 3D Side view of all interpreted faults in the seismic data with the surface of the top Delft Sandstone Member, PSDM Seismic inline 2640 (Figure 3-7), and well Delft-03.

Horizon and fault interpretation

Multiple horizons are interpreted in the PSDM seismic data and tied back to well locations. The horizon interpretation is based on the stratigraphy as given in paragraph 2.5. The top of the Alblasserdam Member could not be interpreted because of the lack of resolution at target depth. Therefore, an internal Alblasserdam surface that is clearly seen on seismics, the “Inter-Alblasserdam Member” is interpreted. Multiple faults were found in seismic data and are interpreted and mapped on both the PSDM seismics and in regional time depth migrated seismics (Figure 4-1). The following reflections were interpreted in the seismic data;

- The Base Tertiary, the Base of the North Sea Group.
- The Texel Marlstone Member., the Top of the Texel Formation.
- Top Rodenrijs Claystone Member, the Top of the Schieland Group.
- Top Delft Sandstone Member.
- And a clear surface within the Alblasserdam Member, the “Inter-Alblasserdam Member surface”.

A 2D seismic line across the target area is used additional to the two available 3D seismic volumes. The southwest-northeast seismic inline (Figure 4-2) is used to gain a better understanding of the structural framework of the target area Vrijenban. The 2D line is from a larger regional time migrated seismic 3D volume and was provided by Panterra (Grobbelen, 2009) (Figure 4-2).

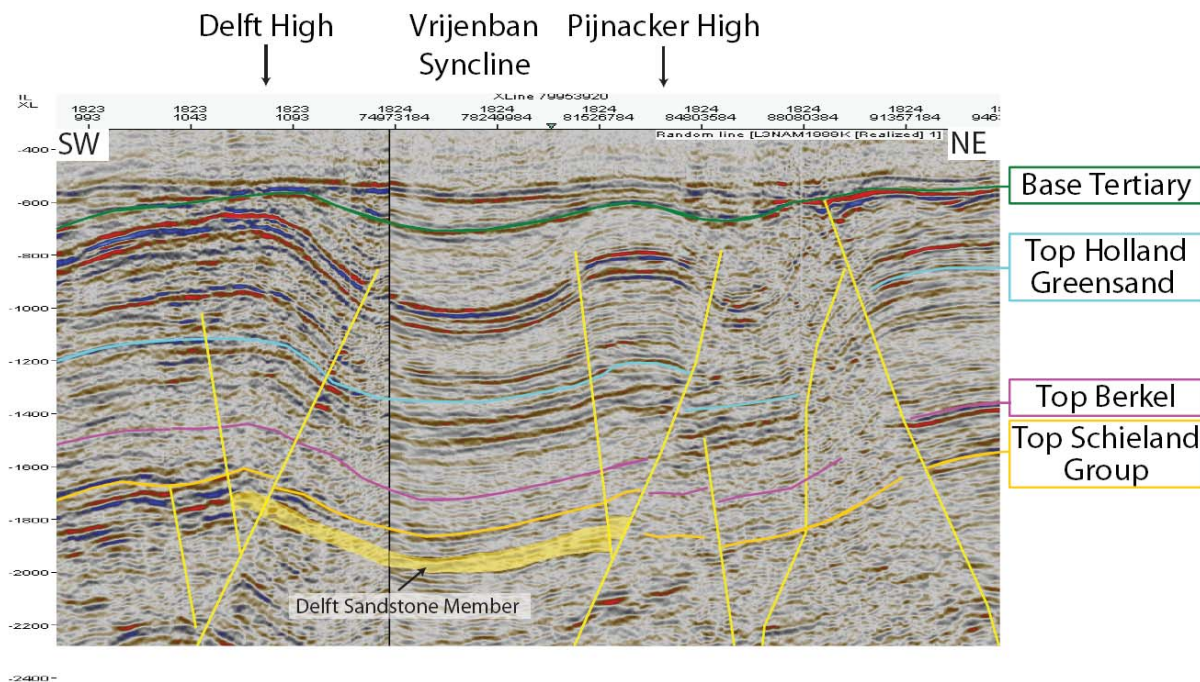


Figure 4-2 Depth-converted seismic cross section through the study area shows that the Delft Sandstone Member is situated in a gentle, broad syncline bounded by two pop-up structures (inversed normal faults). For location see line SW-NE in Figure 4-3

4.3. Reservoir architecture

The description of the reservoir architecture is based on described fault and fold interpretations. Figure 4-3 shows a plan view of the numbered faults and the names of dominant anticlinal and synclinal structures. The Vrijenban syncline lies between the Delft High and the Pijnacker High and is at least 7 km long and approximately 3 km wide at the top of the Delft Sandstone Member (Figure 4-3). The deepest part of the structure at the top of the Delft Sandstone Member is at 2200 m true vertical depth. The highest part of the syncline in the southwest near the Delft High is observed at 1900 meters. The Vrijenban syncline is bounded on the southeast by the Delft main boundary fault (DA) and on the northwest by the Pijnacker main boundary fault (PA) (Figure 4-3). To the northwest the Vrijenban syncline is bounded at the Delft Sandstone Member level by a southwest to northeast trending normal fault 'V' (Figure 4-3). The normal fault V is a 45° degree south south east dipping fault and terminates at the base of the Vlieland Formation. From the seismic data a thickness difference could be observed in the members of the Schieland Group across the fault, indicating synsedimentary growth. The synsedimentary growth is not as extensive as across the main boundary faults PA and DA. The termination of the fault at the Base of the Vlieland Formation indicates no lateral movements after the deposition of the Schieland Group.

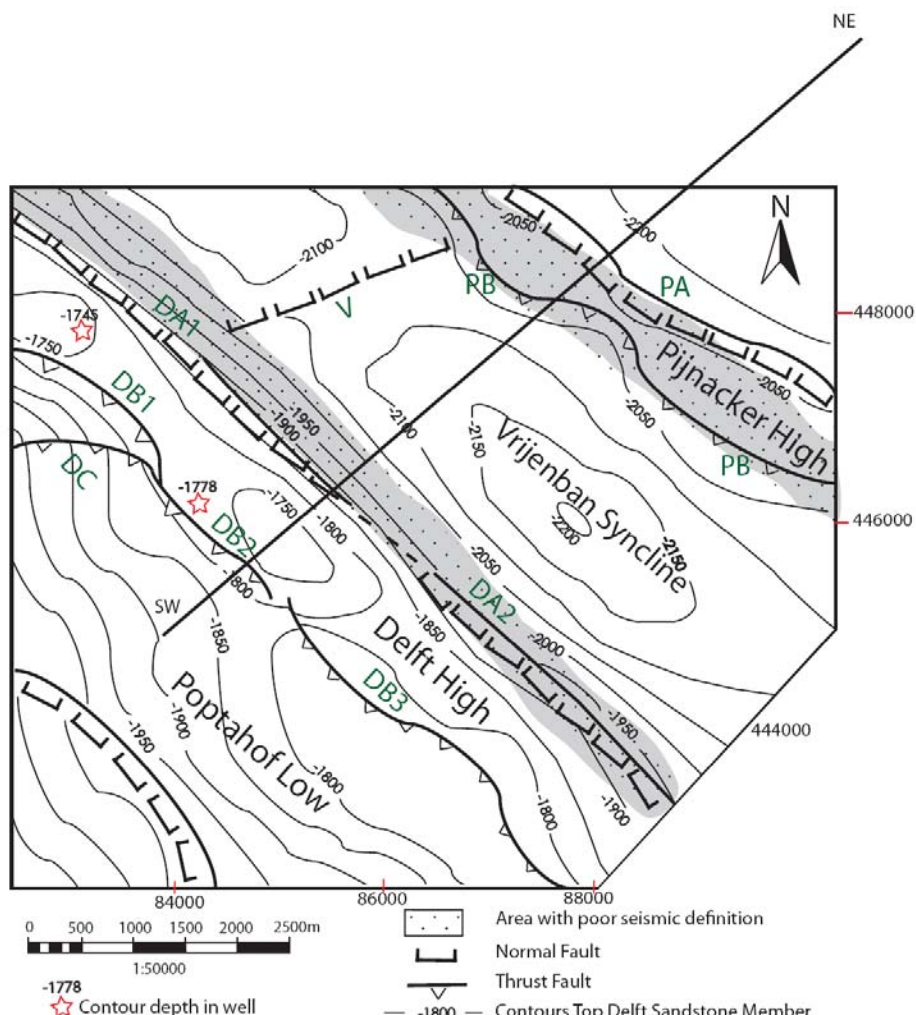


Figure 4-3 The interpreted top of the Delft Sandstone Member, including major faults and the names of the structures. The southwest-northeast seismic section (SW-NE) is shown in Figure 4-2.

Pijnacker High

The Vrijenban syncline is bounded in the northeast by the Pijnacker High. The interpretation of both the Pijnacker High and the Delft High show a large similarity to the predominant pop-up structures found throughout the West Netherlands Basin as described by De Jager (1996). Figure 4-4 shows a simple flower structure, characterised by the anticlinal structure with a main boundary fault (Fault type A) on one side of the axis of the pop-up and a parallel secondary fault (Fault type B) on the other side of the axis coning to a single fault at the base of the structure.

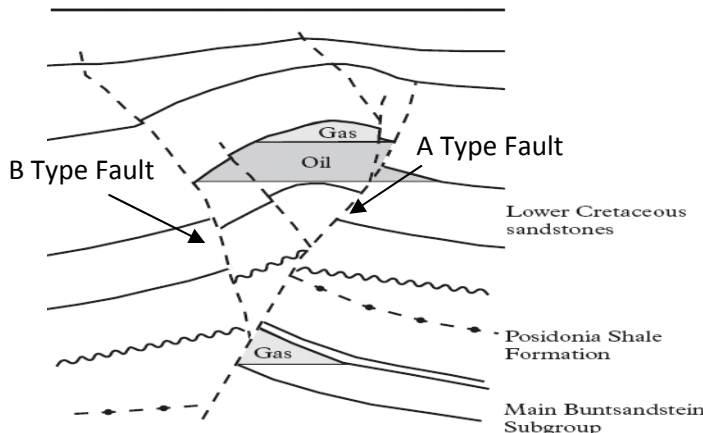


Figure 4-4 Cross-section of the predominant pop-up structure in the West Netherlands Basin (Van Balen et al, 2000).

The Pijnacker High is a contained northwest-southeast trending, complex asymmetrical pop-up structure on the side of a large horst block. The Pijnacker High is at least 10 km long and at least 0.5 km wide at the top of the Delft Sandstone Member (Figure 4-3). The Pijnacker High consists of two structural elements, a pop-up structure and a horst structure (Figure 4-5). The pop-up structure, is a typical flower structure and is formed by an intersecting reverse fault system with an inverted normal fault. The Pijnacker pop-up holds the Pijnacker oil field but only partly contains the target members of the Schieland Group (Figure 4-5).

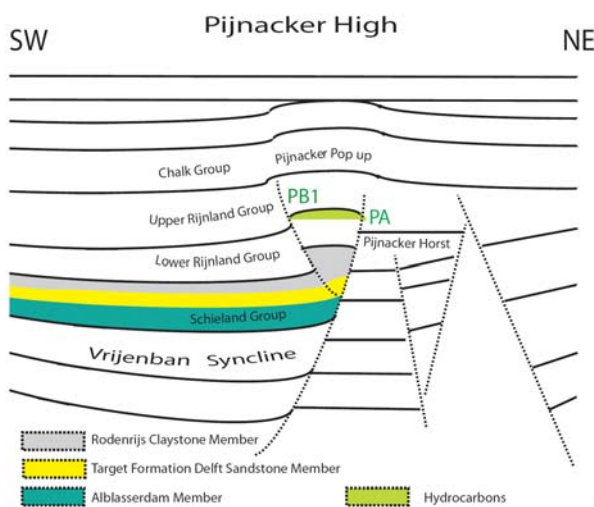


Figure 4-5 The Pijnacker High predominant pop-up structure from inline SW-NE, with major faults (dotted lines), group names, fault numbers and names of the structural elements.

The 70° SW dipping Pijnacker main boundary fault (number PA) is the dominant fault in the Vrijenban area. The PA fault is a major synsedimentary fault which divides the downthrown block containing the Vrijenban syncline with the Pijnacker Horst. The throw at the top of the Delft Sandstone Member varies laterally along the fault from 50 meters up to 200 meters and is 80 meters near the well Pijnacker 13. The “PA fault” normal growth movement created natural depositional thickness difference between the thick Schieland sequence in the Vrijenban Syncline and the Pijnacker Horst that contains a thin condensed Schieland sequence as found in the Pijnacker 14 well. Movement along the Pijnacker main boundary fault continued after the deposition of the members of the Schieland Group and was later reactivated and inverted. During this inversion the reversed normal PB1 fault was created. The PB1 fault partly faults, folds and throws the target members of the Schieland Group on the south-western side of the pop-up structure (Figure 4-5). The PB1 fault dips 30° to the southwest and terminates against the PA Fault through the members of the Schieland Group. In a plan view the PB fault planes curve along the direction of the PA fault (Figure 4-4). The fault is essentially a reverse fault with throws up to 50 meters of Delft Sandstone Member. As there is no evidence of synsedimentary growth along the fault it was most likely created during the inverted reactivation of the Pijnacker main boundary fault. An important feature of the PB1 fault is its possible sealing capacity as demonstrated in the Pijnacker oilfield.

Delft High (Delft Pop-up structure)

The Vrijenban syncline is bounded in the southwest by the Delft High that is contained within a northwest-southeast trending complex asymmetrical pop-up structure. The Delft High pop-up structure is at least 10 km long and approximately 1 to 2 km wide at the top of the Delft Sandstone Member. The structure grows from below the members of the Schieland Group by a 60° degree SW dipping inverted normal fault (DA1) and an 80° degree NE dipping reverse fault (DB2, Figure 4-6). These faults diverge upwards into two concave shaped faults in the Delft High, faulting the members of the Schieland Group. The Delft High including the crest area contains the Delft oil field above the target members of the Schieland Group. The high can be divided into three sections. The sections are named the Poptahof Low, the Delft Pop-up and the Vrijenban syncline respectively in the southwest, centre and northeast (Figure 4-4, Figure 4-6).

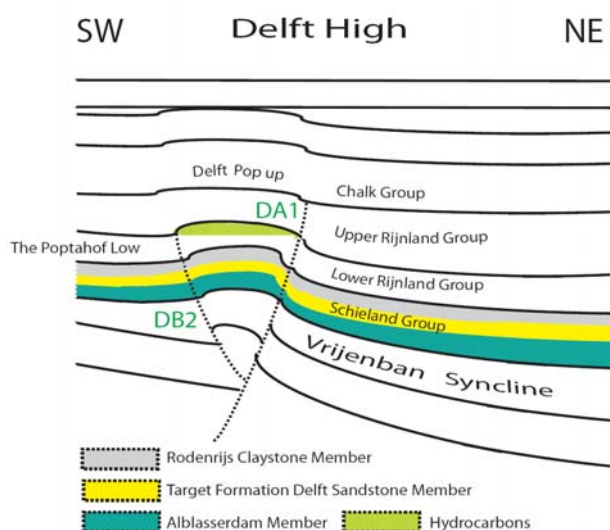


Figure 4-6 Delft High predominant pop-up structure with major faults with numbers and group names.

The faults that belong to the Delft High system are numbered DA for SW dipping faults and DB for NE dipping faults. The Delft main boundary fault consists of two connected echelon shaped faults (DA1 and DA2), both are a 60° SW dipping reversed synsedimentary growth fault and are similar to the PA Pijnacker main boundary fault. The faults have throws that vary laterally along the fault from 75 m in the southwest up to 150 m in the northwest at the Top Schieland Group level. The seismic data shows thickness changes of the members in the Schieland Group across the faults DA1 and DA2 indicating synsedimentary growth and movement after the deposition of the members of the Schieland Group, before reactivation and inverse movement. Movements along the Delft main boundary fault continued after the deposition of the Members of the Schieland Group and were later reactivated and inversed. The three faults DB1, DB2 and DB3 also belong to the Delft High but are less important with respect to the target area Vrijenban. The faults generally follow the descriptions of the reversed normal fault PB of the Pijnacker High.

A similar fault to the V fault exists in the Poptahof Low to the southwest of the Delft High, the fault DC1. The DC1 fault is a 45° S dipping normal fault and trends from southwest to northeast. It is important to recognise the angle with which it terminates against the DA fault in the Delft High pop-up structure. The trending southwest to northeast angle is similar to the 45° SE dipping and southwest to northeast trending fault V. A major difference is that the DC1 fault continuous through the Vlieland Formation while the fault V terminates at the base of the Vlieland Formation.

In the Vrijenban syncline three inversed synsedimentary growth faults interacted through differential faulting and created a complex subsurface with local strong varying depositional centres.

4.4. Accommodation space evolution

The description of the accommodation space evolution is based on the seismic interpretation, the 2D structural palinspastic reconstruction and available literature. A complete workflow and the results of the 2D structural palinspastic reconstruction can be found in appendix E.

The Vrijenban area formed as a structurally rather simple large scale half graben against the Pijnacker Horst along the Pijnacker main boundary fault (PA) during the Late Triassic (Figure 4-7). This matches the extensional Kimmerian structural style of the first movement during the Early Kimmerian as it is characterised by rotated fault blocks, horsts and simple large grabens (Kabel, 1986).

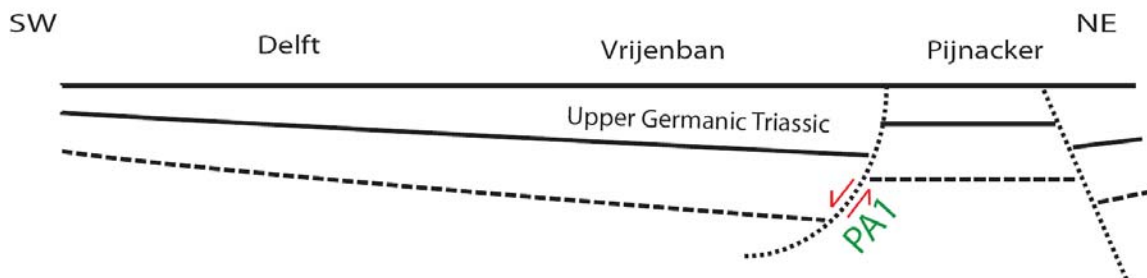


Figure 4-7 Cross section of the Vrijenban area based on a 2D reconstruction of the Late Triassic. The structural setting of the target area Vrijenban, major surfaces and faults are shown.

From the Late Triassic onwards differential faulting and subsidence caused various subunits of the basin to be formed, creating the Delft main boundary syn-sedimentary fault (Figure 4-8). The normal fault DA1 is less visible at Triassic level and is expected to be the result of the extensional Kimmerian block faulting in the Oxfordian based on an interpretation of the palinspastic reconstruction. This movement split the basin into two depositional centres creating accommodation space for the influx of sediment. The Syn-Rift stage from the Late Jurassic to Early Cretaceous started by the later Kimmerian pulse which induced rapid subsidence of the Vrijenban area, causing strong rifting by extensional movement and creating large differential subsidence and faulting (Van Balen et., 2000). It is most likely that fault V was also created during the differential subsidence. The differential subsidence created, combined with regional subsidence, large basins for the sedimentation of the Altena and later the Schieland Group. Highs or topographic relief would rarely have been present as there is no evidence to support their existence (DeVault & Jeremiah, 2002).

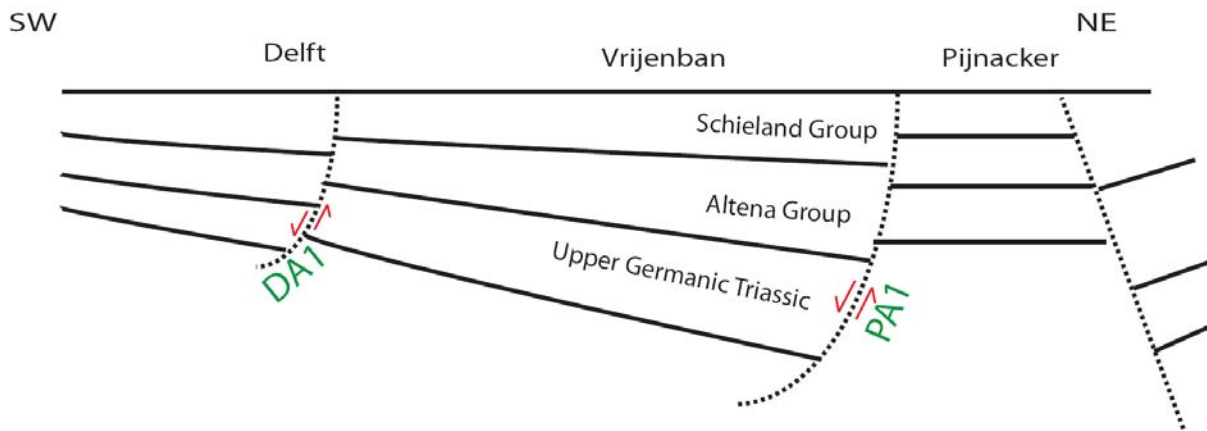


Figure 4-8 Cross section of the Vrijenban area based on a 2D reconstruction. The structural setting of the target area Vrijenban is shown during the Late Jurassic. Major surfaces and faults PA and DA show the differential faulting and the synsedimentary growth along the faults.

The differential subsidence caused breaking up of the Vrijenban area into more subunits and the formation of faults V and DC1 by movement along the PA and DA. A difference in deposition was caused as rapidly subsiding basins accumulated very thick syn-rift sediment packages along synsedimentary faults like the PA, DA, DC1 and V as can be seen in Figure 4-8. Less sediments were deposited on quiescent platform areas like the Pijnacker High where thin layers of sediment were deposited. The northeast boundary fault PA and to a lesser extent the southwest DA fault remained active during the Portlandian to Hauterivian deposition of the continental Schieland Group in the Late Jurassic to Early Cretaceous. This resulted in the deposition of a very thick Schieland Group sequence of 800 m in the depocentres of the Vrijenban area and only a thin condensed Schieland sequence on top of the Pijnacker Horst block. Downward movement continued during the deposition of the marine Vlieland Formation in the Early Cretaceous along the fault PA and to a lesser extent along the fault DA (Figure 4-9). Movement along fault V came to a halt during the Aptian, as the accommodation space increase across fault V became uniform during the deposition of the Rijnland Group. In the downthrown area and less on the horst area, the Rijswijk Sandstone Member was deposited followed by a complete Vlieland Shale sequence.

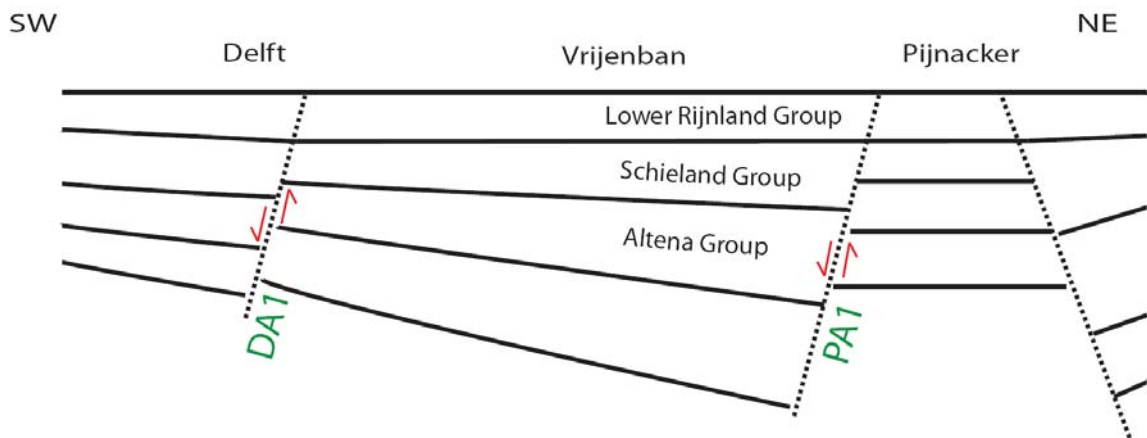


Figure 4-9 Cross section of the Vrijenban area based on a 2D reconstruction. The structural setting of the target area Vrijenban is shown during the Early Cretaceous. Major surfaces, faults PA and DA and fault movements are shown.

During the Mid Cretaceous to Quaternary the Sub-Hercynian tectonic phase created compressive forces in the West Netherlands Basin causing inversion of the structures during the Santonian to Campanian interval (Cacace, 2008). Compressive post-rift stage movement caused the inversion of previous depocentres by reactivation of faults creating complex inverted structures. Typical for the Sub-Hercynian structural styles are reverse faults and the strike-slip faults along the pre-existing Kimmerian faults, creating flower structures (De Jager et al., 1996). It is however difficult to recognize these strike slip elements in the fault styles in the Vrijenban target area. Synchronously with the inversion of fault systems PA and DA, the PB and DB faults developed. The oblique movement along existing faults created the PB and DB faults and the related pop-up structures in the new formed basin highs. Regional subsidence continued as the Chalk Group and younger sediments were deposited across the Vrijenban basin (Figure 4-10).

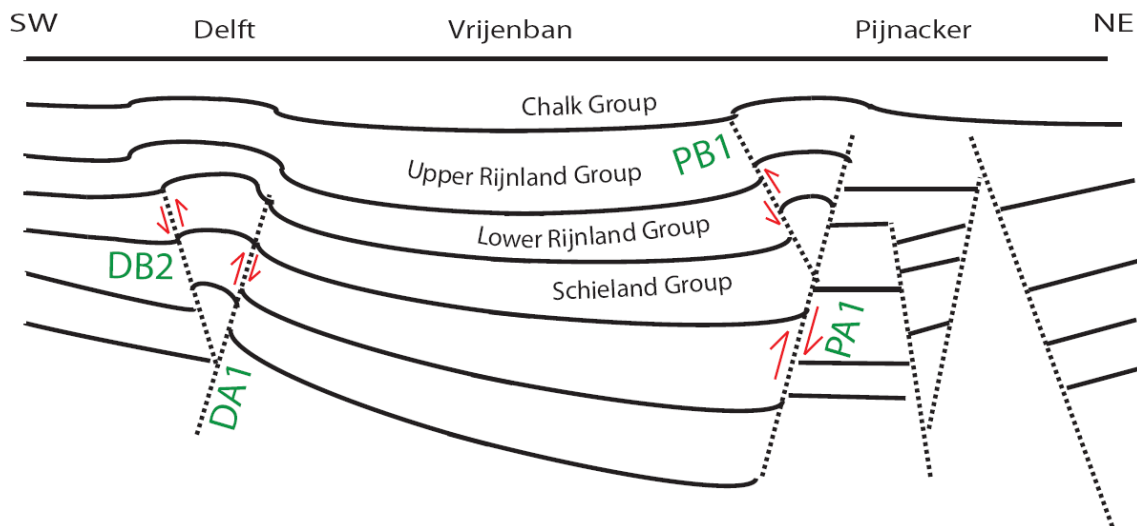


Figure 4-10 Cross section of the Vrijenban area after 2D reconstruction. The structural setting of the target area Vrijenban is shown at the start of the Tertiary. Major surfaces and faults PA, DA, DB2 and PB1 are indicated.

The DA and DB faults intersect each other in the horst block resulting in an interplay of movements along these faults. During the reactivation of the faults PA and DA gentle anticlinal structures developed in the overburden above the inversed areas as can be seen in Figure 4-10.

Structuration did not occur in discrete events; it was in most cases a more or less continuous process in response to ongoing convergence or divergence of lithospheric plates (De Jager, 2007). The inversion of the two main structural elements along existing faults caused the normal wedge shaped structure to be deformed to a large simple syncline form. This large synclinal form is the Vrijenban Syncline as seen in the subsurface today (Figure 4-11).

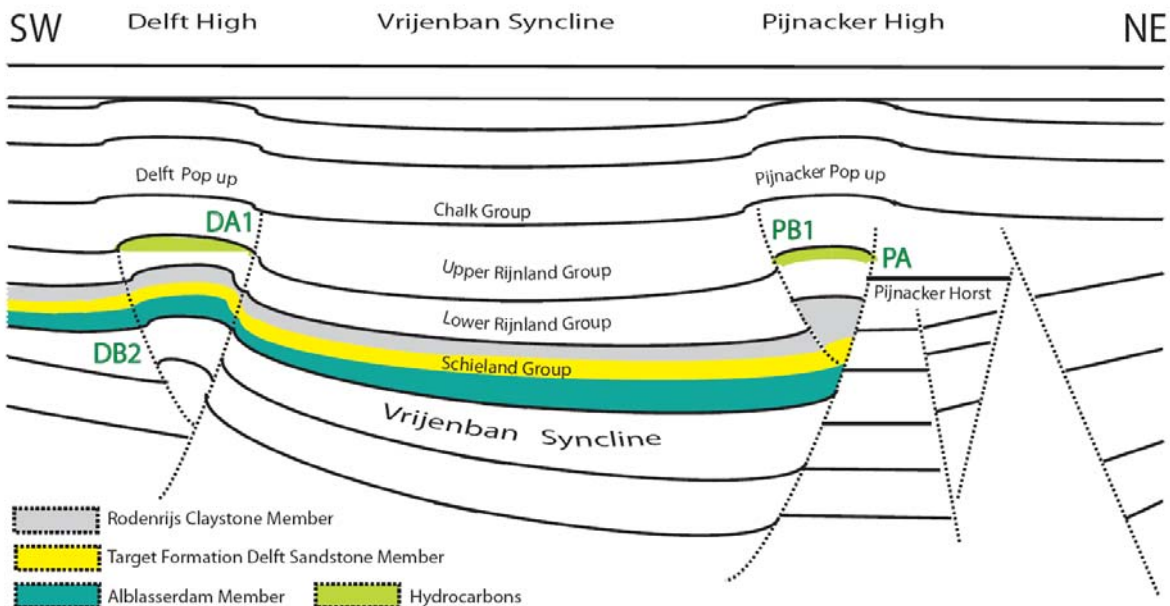


Figure 4-11 Cross section of the Vrijenban area after a 2D reconstruction. The structural setting of the target area Vrijenban is shown as today it can be found on seismics. Major surfaces and fault PA, DA, PB and DB2 are indicated.

4.5. New insights

In the Vrijenban area large thickness differences of deposited sediments can be found related to a syn-tectonic differential faulting. Strong synsedimentary growth movement is the predominate reason of changing depocentres and the large thickness difference of deposited sediments. Growth fault movement occurred during deposition but rarely any topographic relief was present. This is different than previous literature from for example Den Hartog Jager (1996) that described sedimentation in constantly growing pre-existing valleys. The three synsedimentary faults PA, DA and V interacted changing the available accommodation space and depocentres. Therefore the predominant structures in the depositional history of the basin are syn-tectonic differential subsiding large grabens. The thickest sediment deposits can be found in the depocentres in the deepest parts of the basin and towards the synsedimentary growth faults. Thinner sediments deposits can be found on the horst structures and away from the faults and deepest parts of the basin.

The differential fault movement combined with the inversion during the Late Cretaceous created a complex subsurface in the Vrijenban area. The pop-up or flower structures are small compared to the large semi half-grabens where most of the sediment was deposited. This is a large change in perspective as the smaller pup-up structures were always considered the predominant structures of the West Netherlands Basin (De Jager et al., 1996; Van Balen et al., 2000). This could be related to the fact that previous studies were predominant looking at the structures that could form hydrocarbon traps.

Another important feature of the Delft and Pijnacker main boundary faults in the Vrijenban area is their possible sealing capacity as demonstrated by the oil water contact of the Pijnacker oilfield, Moerkapelle oilfield and in similar oilfields in the West Netherlands Basin (Kabel, 1986; Van Balen et al., 2000; Bartlema, 2002). Two way movements along the fault during deposition and inversion would increase the possibility of smearing and sealing of the faults. Also in the core study small sealing faults were found (Figure 4-12). The core and cutting thin sections study showed strong mineralization of small faults by carbonate cement and this could contribute to the sealing capacity of the larger faults (Loerakker, 2009; Drost & Korenromp, 2010). The sealing capacity could cause the effect of compartmentalisation of the subsurface into separate reservoir units. Strong compartmentalisation of the reservoir as found in the Moerkapelle Field could add to the complexity of the reservoir (Kabel, 1986). However no indication of compartmentalization in the Vrijenban target area was found, however the resolution of the seismics could be too low to detect secondary faults, riddle structures related to the fault movement from the exciting faults and other sub seismic faults.

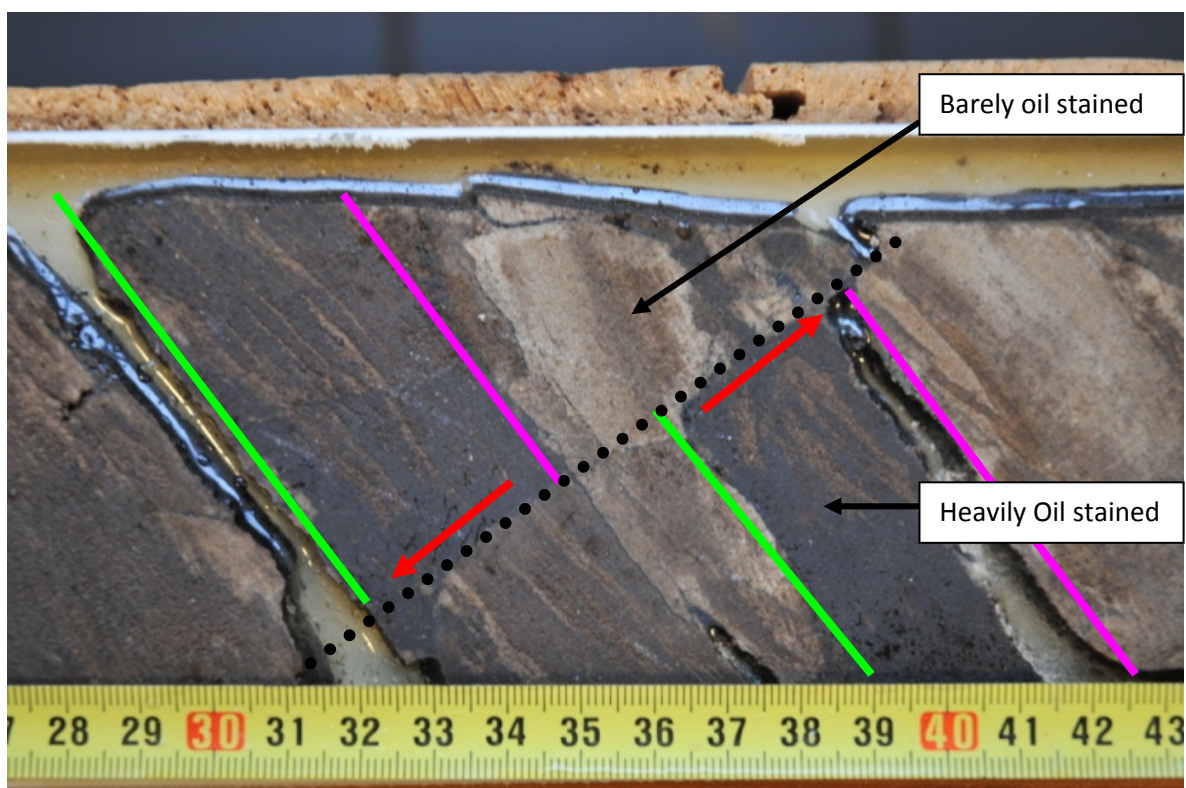


Figure 4-12 Smeared or mineralized sealing fault found in core section 889.25-889.70 of the Well MKP-11. The throw of the fault is 6 cm and the change in oil staining clearly shows the sealing capacity of the small fault.

5. Formations

5.1. Introduction

Three different lithological members can be distinguished as the primary targets of this study; the Alblasserdam Sandstone Member, the Delft Sandstone Member and the Rodenrijs Claystone Member (Table 5-1) (Figure 5-1). The reservoir target of the Delft Geothermal Project and similar projects in the Vrijenban area is the Delft Sandstone Member. A full overview of the predominant groups, target formations and target members is given in paragraph 2.5. Sedimentological descriptions of these formations are made from the available cores and cuttings in combination with literature descriptions. The depositional environment describes the combination of physical, chemical and biological processes under which sediments are deposited. The depositional environments for the three different lithofacies were made and are described with the help of the observations and interpretations.

Zone	Facies name	Depth in Delft-03 (m)	Core Description MKP-11	Depositional environment
SLDNR	Rodenrijs Claystone Member	1650-1780	Clay-stone alternating with interbedded- thin sand to silt stone, coal and lignite layers	Coastal plain, fluvial
SLDND	Delft Sandstone Member	1780-1895	Single and multiple stacked sandstone bodies with intervals of silt- to clay-stone and thin coal layers	Fluvial
SLDNA	Alblasserdam Member	1895-2000+	Clay-stone layers alternating with interbedded- thin to thick sand to siltstone, coal and lignite layers	Floodplain, fluvial

Table 5-1 The three formations of the Schieland Group with their zone nomenclature, depth, descriptions and depositional environment.



Figure 5-1 Representative pictures of the three facies from the MKP-11 well, from left to right; the Alblasserdam Member, the Delft Sandstone Member and the Rodenrijs Claystone Member. The Alblasserdam Member is a laminated interbedded oil-stained sand- and claystone with lignite bands. The Delft Sandstone Member shows an oil saturated friable sandstone (No oil found in the Delft-03 well). The Rodenrijs Claystone Member is organic rich laminated claystone with siderite modules.

5.2. Alblasserdam Member (SLDNA)

The Alblasserdam Member contains the oldest deposits of the Schieland Group in the West Netherlands Basin. The lithofacies is encountered in all the wells that reached beyond upper Jurassic aged formations in the target area Vrijenban. The Alblasserdam Member consists of a succession of light to dark grey, red variegated clay- and siltstones (Van Adrichem Boogaert & Kouwe, 1993-1997). Clay- and siltstone successions go up to several meters and are sometimes interbedded with fine to coarse cemented sands. The sands contain fragmented lignite at the base and thick coal and lignite layers at the top. Thick coarse sandstone bodies are layered with silt- and claystone layers and have a thickness of a few meters. The sorting of the sands in these layers varies from medium to very poor but the sandstone bodies are mostly fining upwards. Lignite fragments are found in the lithofacies as well as red bands of clay and silt. Mm to cm scale lignite or coal laminations and small individual thick coal layers are found in the whole interval and are associated with the grey claystones. The available core sections show extensive mottling of the variegated claystones, although the Alblasserdam Member is hardly ever present in cores (DeVault & Jeremiah, 2002). The Alblasserdam Member has a thickness range of a hundred to several hundreds of meters. In the target area Vrijenban a thickness of at least 100 meters is observed in the Delft-03 well.

The contact between the Alblasserdam Member and the above lying Delft Sandstone Member is a conformable sequence or could be interpreted as a sharp fluvial channel cutting into a floodplain deposit (Figure 5-2). On logs the contact is observed in the core of MKP 11 well and can be seen as a sharp change in the Gamma Ray or Spontaneous Potential logs (Figure 5-3). It is interpreted as a conformably overlain fluvial deposit and therefore it is not expected that the base is a uniform sharp boundary throughout the area. The facies contrast between the Alblasserdam Member and the Delft Sandstone Member is very low as it is a conformable change into a more sand-prone fluvial deposit. This is probably the reason that the contact cannot be confidently interpreted on seismic (Paragraph 4.2) The base of the Alblasserdam Member is formed by the unconformable contact with Altena Group. This contact is found in the Rijswijk 1 well log.

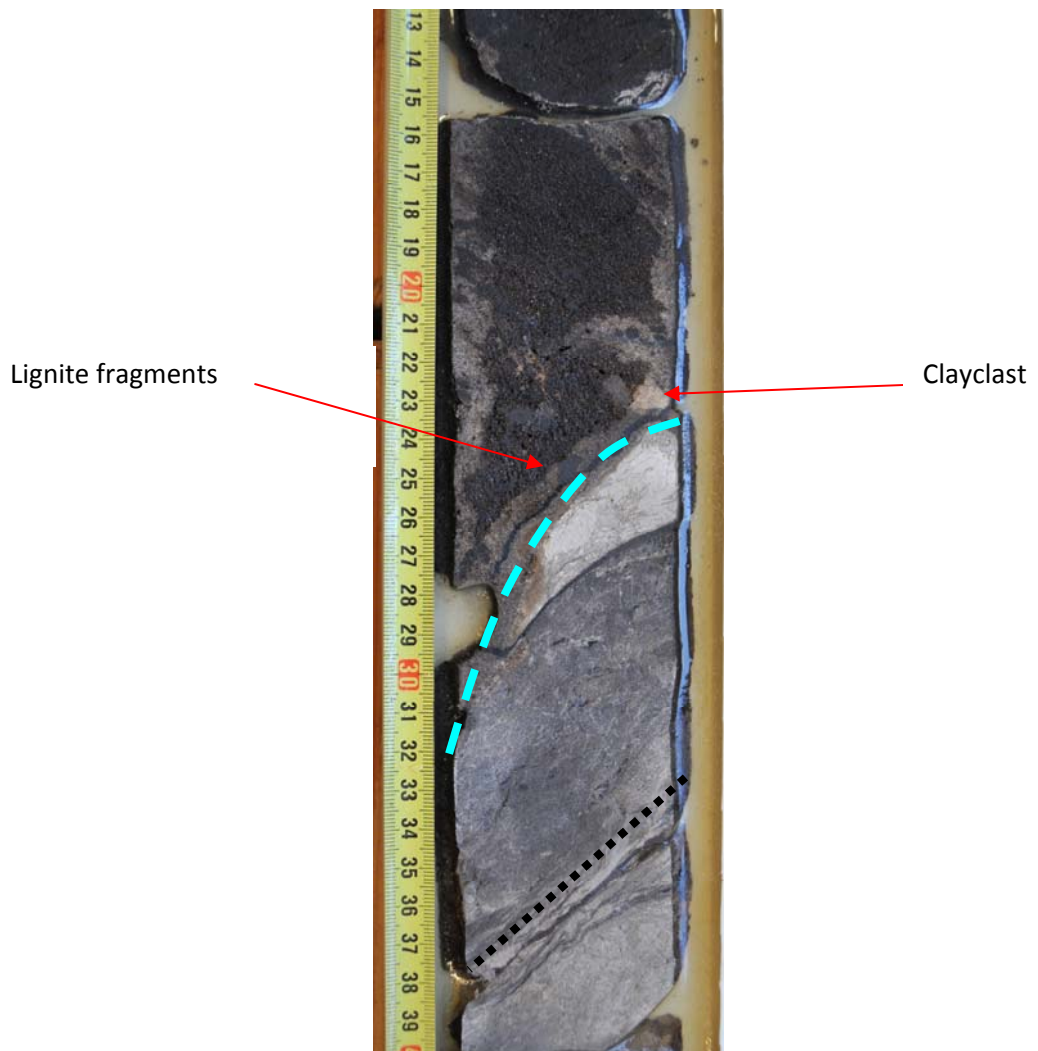


Figure 5-2 The contact between the Alblasserdam Member and the Delft Sandstone Member in the core of the MKP 11 well section (909.50 – 909.95m). The colour change is sharp, in the core above the contact surface clayclasts and lignite shards can be seen in the oil-saturated sandstone. The black dotted line shows the lamination. The contact surface can clearly be interpreted as a cutting surface (Light blue dashed line).

Depositional environment of the Alblasserdam Member

During the syn-rift stage, the West Netherlands Basin is filled with sediment from fluvial systems that came from the southeast and followed the southeast-northwestern trend of the basin (Wiggers, 2009; Van Adrichem Boogaert & Kouwe, 1993-1997). The large thickness changes throughout the Alblasserdam Member are probably related to syn-tectonic deposition caused by movement along local growth faults. The Alblasserdam Member is interpreted as a fluvial to floodplain deposit with sand concentrated in mostly channels and crevasse-splays (Van Adrichem Boogaert & Kouwe, 1993-1997). A high clay content shows that the sediment influx was low during the deposition. Sandstone occurs in sheets, isolated, or stacked channel fills (Wiggers, 2009). Based on the amount of floodplain deposits and the occasional single sandstone bodies, it is interpreted as a single meandering fluvial channel cutting into its own floodplain deposits. The sand and silt in this facies are provided by sedimentary influx from the London Brabant Massif and Rhein Valley Graben (Hancock, 1984). The fact that most of the lignite layers are fragmented indicates that the sediments are reworked. The pink to red beds are interpreted as paleosols that show that the Alblasserdam Member is deposited in a semi-arid climate. The presence of red beds makes palynological age-dating difficult (Den Hartog Jager, 1996). As the Alblasserdam Member is not a main production target of the Delft Geothermal Project the formation is not described in further detail.

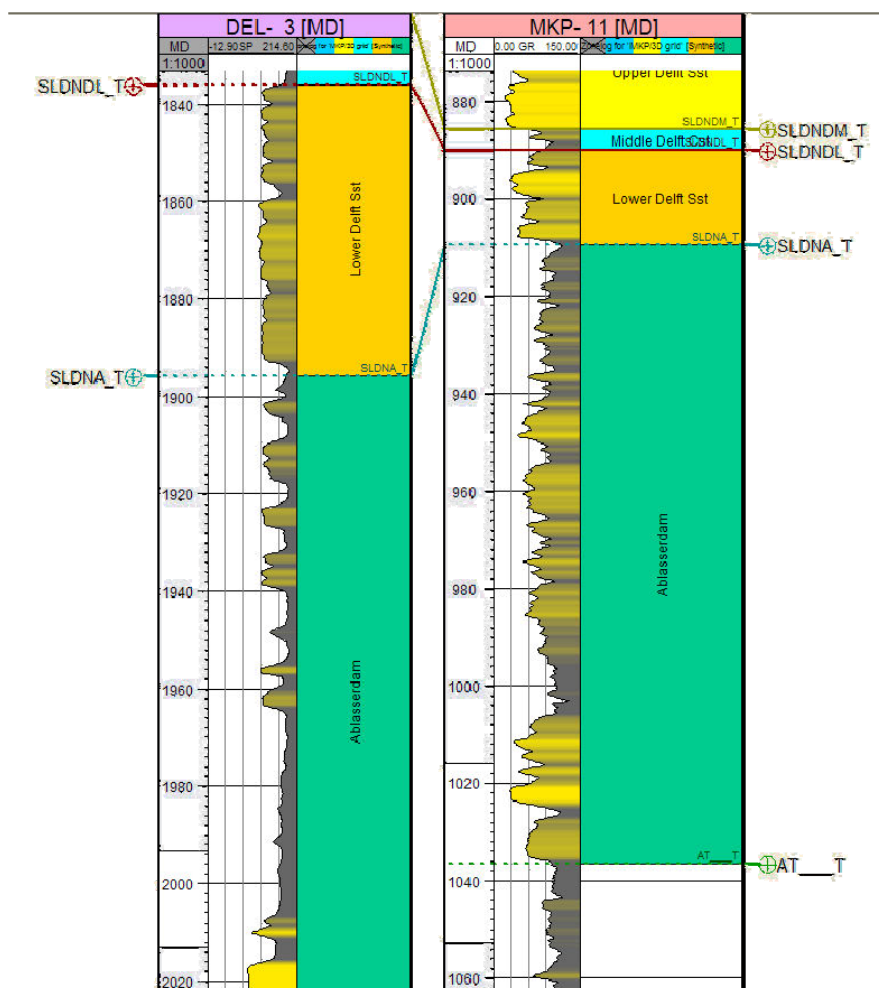


Figure 5-3 The Alblasserdam Member signature in the SP-log of the Delft-03 and on the gamma ray log MKP 11 well. Scale is 1:1000. Wells are in depth along the borehole in meters.

5.3. Delft Sandstone Member (SLDND)

The Delft Sandstone Member is found in all wells in the target area Vrijenban that reach beyond the Rodenrijs Claystone Member with a thickness ranging from at least 60 m up to 115 m. The member is of Valangian age and defined as a light-grey massive sandstone sequence (Wiggers, 2009). The Delft Sandstone Member is layered and consists of fine to coarse sandstones with bands of silt- and claystones. The size of the grains varies over the lithofacies but can overall be seen as fining upwards from coarse sand- to siltstone. The sorting can be medium to poor. Very coarse to large, even gravel size grains and large clayclasts and lignite shards can be found at the base of fining upward sandstone bodies. Multiple and single stacked fining upward sandstone bodies contain clayclasts and lignite particles at the base. In between the sandstone bodies small to medium size silt- and claystone layers interbedded with lignite layers are found. The clay and siltstone layers contain siderite nodules, thin lignite bands and well cemented bands of organic rich dark claystone. The sand is friable in the non cemented parts. Strong mottling can be observed in both the clay- and sandstones. Gradual colour changes that range from dark grey to light grey to even pink occur in the silt- and claystones. Light grey clay can often be found together with hard grounds indications. The Delft Sandstone Member can clearly be distinguished on logs by the low clay content and the fining upward signature (Figure 5-4).

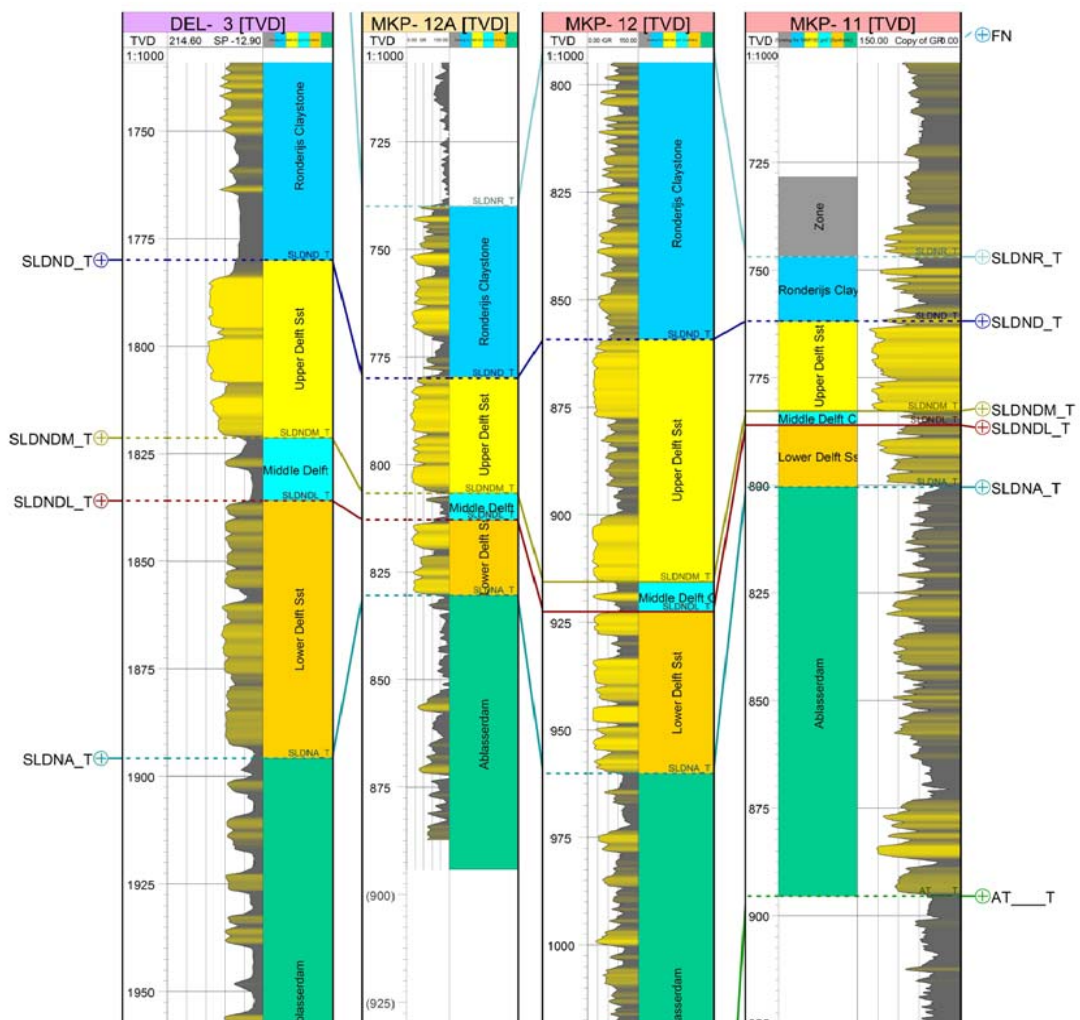


Figure 5-4 Delft Sandstone Member on well logs of the Delft-03 (SP), MKP- 12A, - 12 and MKP-11 with the Upper, Middle, and Lower Delft Sandstone Member. Scale 1:1000 in true vertical depth.

Depositional environment of the Delft Sandstone Member

Based on the amount of fining upwards sandstone bodies and the presence of floodplain deposits, the Delft Sandstone Member is interpreted as a fluvial meandering system or stacked distributary-channel deposit in a lower coastal plain setting (Van Adrichem Boogaert & Kouwe, 1993-1997). This interpretation also takes into account adjacent depositional environments, the lack of marine flora and fauna, the presence of channels sands, in situ lignite beds and paleosoils, cross-bedding and erosional bases (Den Hartog Jager, 1996). The Delft Sandstone Member was deposited during an active phase of rifting by meandering rivers that were flowing through the basin (Wiggers, 2009). The syn-rift deposition of the Delft Sandstone Member is the most probable cause for the thickness changes throughout the Vrijenban area that are observed on seismic data (Paragraph 4.2). The rate of deposition and the total thickness of the Delft Sandstone Member are strongly related to the available accommodation space and the relative base level movement during the active phase of rifting. In the Vrijenban area, deposition of the Delft Sandstone Member was probably controlled by growth fault movement of the Pijnacker boundary fault. The source of the rivers which deposited the fluvial deposits in the Delft Sandstone Member lies towards the southeast and the rivers flowed to the northwest following the main axis of the West Netherlands Basin (Wiggers, 2009). The lack of alluvial fans observed on seismics or encountered in wells in the hanging walls of major faults, suggests that the horst blocks rarely had a large amount of topographic relief from which fans could be shed (DeVault & Jeremiah, 2002).

The Delft Sandstone Member can clearly be divided into three units in all wells used in this study, based on the characteristic signature on well logs (Figure 5-5) and in cores and the development of the sandstone bodies. The division is further supported by the interpreted sand to clay ratio, the net over gross, varying thickness of a single unit, and the amount and presence of lignite and floodplain deposits within a unit. The three subunits of Delft Sandstone Member are 1) The Lower Delft Sandstone Member unit, 2) the Middle Delft Sandstone Member unit, and 3) the Upper Delft Sandstone Member unit.

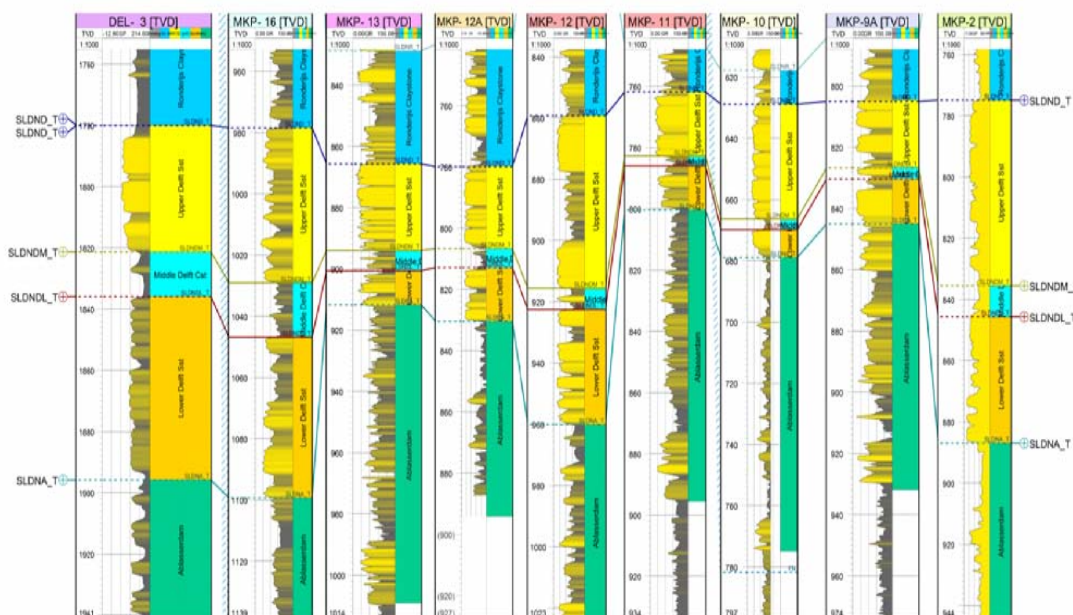


Figure 5-5 The Delft Sandstone Member is divided into three units in the Lower-, Middle- and Upper Delft Sandstone Member on wells Delft-03 and MKP 16, 13, 12A, 12, 11 10, 9A and 2 with the SP or Gamma Ray well log. Scale 1:1000 in true vertical depth.

The Delft Sandstone Member division can be explained by a description of the rate of subsidence and the characteristic effect of the development of the fluvial system related to the created accommodation space (Table 5-2). In the Vrijenban area, fluvial channel style and infill of the basin was primarily controlled by the rate of accommodation space creation, which in turn was controlled by movement along the basin bounding faults. At the contacts between the units no unconformities can be found, however variations in the rates of subsidence and sedimentation in the basin can cause fining- or coarsening-upward sedimentary cycles, with or without internal syn-depositional folds and unconformities (Miall, 1978).

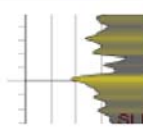
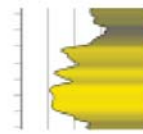
Unit	Gamma-ray signature	Facies description	Depositional architecture
Delft Sandstone Member Upper Unit		Multiple-stacked and laterally-amalgamated fluvial channel sandstone bodies	
Delft Sandstone Member Middle Unit		Interbedded claystone and siltstone deposits with coal layers. Floodplain.	
Delft Sandstone Member Lower Unit		Single fining-upward meandering river sandstone bodies interbedded with claystone and siltstone floodplain deposits.	

Table 5-2 Gamma-ray log signature, facies description and interpreted depositional architecture of the three units in the Delft Sandstone Member.

Unit one, the Lower Delft Sandstone Member

The lower part of the Delft Sandstone Member found in cores and logs show isolated single, well developed sandstone fining-upward sequences, interbedded with floodplain deposits. Based on the amount of floodplain deposits in between the single stacked sandstone bodies, it is interpreted as a well developed relatively stable meandering fluvial channel. The absence of paleosoils and the thick lignite bands show weakly developed but well drained soils. The large differences in thickness (10-60m) that are observed in this unit are attributed to high rates of subsidence due to differential faulting. The well developed loosely stacked meandering fluvial deposits reflect the relatively rapid rates at which accommodation space is created relative to the sediment supply. The well developed channel facies caused a progressive increase in floodplain deposits as the channels became more isolated (Bourquin et al, 2001). Fluvial deposits in an area with rapid increase of accommodation space are characterized by fine-grained flood-basin strata, isolated fluvial sandstones and thin discontinuous lignite. Increased accommodation rates favour high levels of storage of floodplain sediments resulting in isolated channels and weakly developed but well drained soils. The high facies preservation caused by the periods of rapid increase of accommodation space in the Lower Delft Sandstone Member in the Vrijenban target area corresponds with the large thickness variations found in the well and on seismic. The depositional setting of the Lower Delft Sandstone Member can be described as relatively stable meandering fluvial channel and floodplain deposits in a rapidly subsiding basin.

Unit two, the Middle Delft Sandstone Member

The Middle Delft Sandstone Member shows predominantly thin alternating clay- and siltstone bands with thin sandstone deposits and lignite or coal layers. No multiple stacked or full single stacked sandstone bodies are observed, however a single undeveloped fining upward sequence can be found in some wells. The Middle Delft Sandstone Member deposits have a thickness of 3 up to 18 meters with an average of 8 meters as measured in the available data. The clay- and siltstone layers contain lignite bands and siderite nodules. A low net to gross ratio and high clay content can be found in all the well log and core data of the Middle Delft Sandstone Member. Mottling occurs extensively throughout the unit in sandstone, siltstone and claystone layers. The silts and clay are deposited in an area with a low energetic level. After the rapid subsidence of the Lower Delft Sandstone Member, the accommodation increase is slowed and reached its maximum. Periods in between the rapid and slow increase of accommodation space show predominately floodplain deposits, the channels become isolated. During this period, flooding events may be continuous with low fluvial gradient, reduced river discharges and stream power, relating in the depositing of fines, silts and clays (Emery, & Myers, 1996). The dominant fluvial depositional environment gradually changed into a low gradient lower coastal floodplain depositional setting, this interpretation also takes into account adjacent depositional environments. The Middle Delft Sandstone Member consists mostly of sheet like extensive floodplain deposits, deposited during a transitional period after rapid subsidence in the Lower Delft Sandstone Member.

Unit three, the Upper Delft Sandstone Member

The Upper Delft Sandstone Member is found in logs and cores and consists of multiple stacked sandstone bodies with multiple reactivation surfaces and underdeveloped or incomplete fining upward sequences. In cores and on well data the Upper Delft Sandstone Member has a high net to gross ratio compared to the other two units. Very coarse to large, even gravel size grains and large clayclasts and lignite shards can be found at the base of reactivation surfaces and fining upward sequences showing strong reworking of the sediment. There is a lack of floodplain deposits and lignite bands and thin claystone layers show strong colour changes in occurrence with paleosols and hard ground indications. The total thickness of the unit varies less than the other two units based on the well data, indicating far less differential subsidence. The contact between the Upper Delft Sandstone Member and the Middle Delft Sandstone Member can be seen as a sharp contrast in well log data indicating the cutting of fluvial channels into floodplain deposits. Periods of less syn-rift deposition indicate less or no differential subsidence. Period of slow to no subsidence will show a low increase of accommodation space and low facies preservation, this correspond to paleosoil development and/or amalgamated channels (Bourquin et al, 2001). The low rate of accommodation space increase will cause the producing of multi-storey sandstone bodies, floodplain deposits may be prone to reworking by channels or by stripping. The Upper Delft Sandstone Member is therefore interpreted as a more amalgamated meandering fluvial deposit in a setting with a slow rate of accommodation space increase, especially compared to the other two units.

The three units of the Delft Sandstone Member show a relation between the rate of subsidence, the creation of accommodation space and the characteristic depositional style of the fluvial system. First the Lower Delft Sandstone Member was deposited in a rapid subsiding basin with high accommodation space increase. This is followed by low gradient floodplain deposits of the Middle Delft Sandstone Member during a transitional period into the Upper Delft Sandstone Member. Then the rate of accommodation space increase became low and regional subsidence dominated as the amalgamated channels of the Upper Delft Sandstone Member were deposited. The subsidence in the upper unit is followed by decreased active faulting during the deposition of the Rodenrijs Claystone Member in the target area Vrijenban (Wiggers, 2009). This subsidence behaviour during the deposition of the Delft Sandstone Member could be related to a single tectonic pulse in the area during the Late Kimmerian first rifting pulse.

The Delft Sandstone Member is deposited by a meandering fluvial system flowing from southeast to northwest. The fluvial system is expected not to be effected by any topographic highs and therefore could flow freely (Figure 5-6). The rate of subsidence and the increase of accommodation space in the Vrijenban area are controlled by a combination of the regional subsidence and the differential subsidence caused by movement along local faults. The fluvial system was affected by the rate of subsidence and the creation of accommodation space by controlling its fluvial characteristic depositional pattern. The net over gross in a unit is controlled by the fluvial characteristics and its possibility to carry and deposit sands. Because of the differential subsidence caused by local fault movement, creating the strong difference in thickness, the amount of sand deposits within one unit spatially also varies (Figure 5-6).

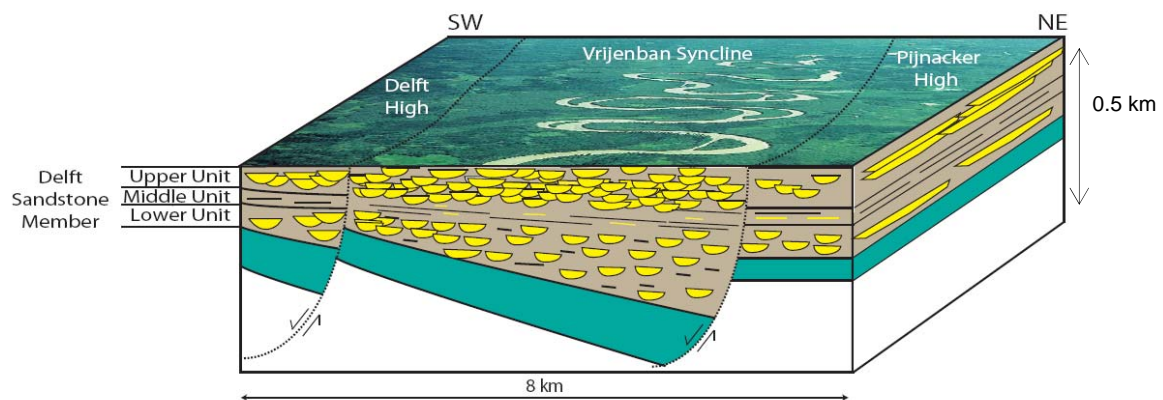


Figure 5-6 The depositional setting of the Delft Sandstone Member with its varying thickness towards the growth fault. It also shows the deposition of sand and floodplain deposits and the isolation or amalgamation of fluvial deposits.

The thickness of the Lower Delft Sandstone Member unit varies strongly because of the strong differential faulting during its deposition. In figure 5.6 the areas with a high accommodation space increase will show a thick Lower Delft Sandstone Member but with more isolated channels resulting in a lower net over gross ratio. The fluvial channels of the meandering system of the Lower Delft Sandstone Member would become more isolated in the areas where accommodation space increase was higher. In areas with a lower increase of accommodation space channels would interact more. The result is a lower net to gross in the thicker depositional centre where more accommodation space increase occurred compared to parts of the basin with a thinner Lower Delft Sandstone Member thickness.

The Upper Delft Sandstone Member units has a more uniform thickness and therefore shows less effect of thickness changes caused by a differential increase of accommodation space in the basin by local fault movement. Areas with a thick Upper Delft Sandstone Member in the depocentres will have a more uniform net over gross.

Areas that are hardly or not affected by local fault moment will show thin deposits of the Upper, Lower and Middle Delft Sandstone Member and more amalgamation. For example the non moving Pijnacker High will be less or not affected by the differential subsidence. The accommodation space increase would be far less and deposits will be thinner and more amalgamated.

Figure 5-6 shows an impression of the depositional environment of the varying thickness of the different Delft Sandstone Member units related to the growth fault. The distribution of sandstone deposits in the different units as found in the wells are related to the rate of subsidence. The depositional characteristics related to subsidence could have a large impact on the reservoir behaviour of the Delft Sandstone Member. The upper and lower parts are with their high net sand a far better target for fluid flow than the Middle Delft Sandstone Member containing silt- and claystones layers. The Middle Delft Sandstone Member could have a strong effect on the connectivity as it could possibly impede pressure and flow from the upper and lower units of the Delft Sandstone Member. The Upper Delft Sandstone Member with a high net to gross and good lateral connectivity created by the amalgamated channels looks the most promising for fluid flow and geothermal production. Dynamic reservoir modelling based on a static architectural reservoir model true to the depositional setting and available data in this study will determine the reservoir behaviour and the effect of heterogeneities on fluid flow related to deposition of the sandstone.

5.4. Rodenrijs Claystone Member (SLDNR)

The Rodenrijs Claystone Member is the youngest deposit in the West Netherlands Basin of the Schieland Group and conformably overlies the Delft Sandstone Member (Van Adrichem Boogaert & Kouwe, 1993-1997). The facies is encountered in all the wells that reached beyond Cretaceous aged formations in the target area. The Rodenrijs Claystone Member is an organic rich silt- and claystone interbedded with sandstone layers and lignite bands. Black to dark grey organic rich clay bands and spots with siderite modules are common in most of the intervals. In the whole interval, rests of rootlets, black organic bands, and black spots are found. Pyrite nodules and siderite crystals are common, as well as grey and red clayclasts. Sharp and gradual colour changes occur and range from dark grey to light grey to pink often associated with chaliche and hard grounds indications (Van Adrichem Boogaert & Kouwe, 1993-1997). The interbedded sandstone layers with lignite particles and clayclasts at the base often show extensive mottling. The Rodenrijs Claystone Member is present in all wells with thicknesses of at least 30 m up to over a 100 m. The Member can clearly be seen in wireline logs for its serrate (saw toothed-shaped) like signature on gamma ray and spontaneous potential logs (Wiggers, 2009) (Figure 5-7). The Rijswijk Member, Member of the Rijnland Group, unconformably overlies the Rodenrijs Claystone Member as a gradual transition from claystone to a large thick sandstone body (Van Adrichem Boogaert & Kouwe, 1993-1997). The contact between the Rodenrijs Claystone Member and the Rijswijk Sandstone Member is not recovered in the available cores but can clearly be found in the logs (Figure 5-7).

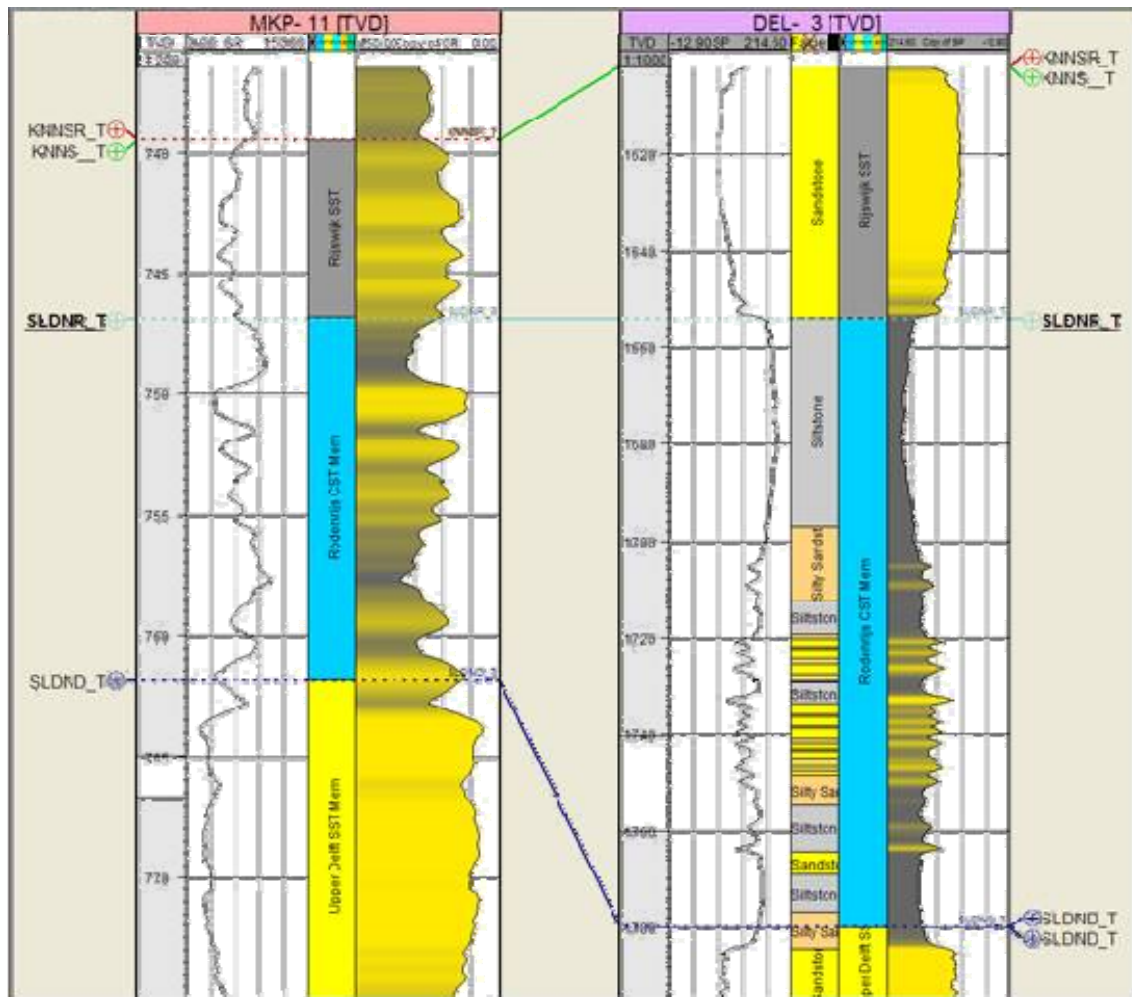


Figure 5-7 The contact between the Rodenrijs Claystone Member and the Rijswijk Member in the MKP 11 and Delft 3 wells. The transitional change from interbedded silt- to claystone to a thick sandstone body marks the contact, the SLDNR_T line. Also is shown the clear serrate like pattern of the Rodenrijs Claystone Member on SP log of the Delft-03. The MKP-11 is given with a scale of 1:200 with true depth in meters with the gamma ray, zone log and mirrored gamma ray. The Delft-03 well is given in scale 1:1000 depth with in meters with the SP log, zone log and mirrored SP log.

Depositional environment of the Rodenrijs Claystone Member.

The Rodenrijs Claystone Member is interpreted as a lower coastal plain to lagoon depositional environment (Van Adrichem Boogaert & Kouwe, 1993-1997). The silt and clay contents are deposited in an area with a low energetic level. Especially the horizontal organic bands and macro rests indicate that plants grew in the area during deposition. Coal bands, the clay composition and the lack of fluvial sand deposits and fossil content indicate a floodplain to near coastal origin. The indicated lower coastal setting is coherent to the broadly accepted interpretation that the Rodenrijs Claystone Member is a transitional facies between the continental fluvial Delft Sandstone Member and the marine system belonging to the transgressive marine sandstone of the Rijswijk Sandstone Member. The Rodenrijs Claystone Member shows synsedimentary thickness differences related syn-rift deposition by local fault movement. This synsedimentary growth is less extensive than found in the Delft Sandstone Member and the Alblasserdam Member. The age assessment is based on sporomorphs as Late Valanginian to Early Hautervian (Van Adrichem Boogaert & Kouwe, 1993-1997). Because the Rodenrijs Claystone Member is not a main production target of the Delft Geothermal Project or this study the formation is not described in further detail.

6. Petrophysics

6.1. Introduction

One of the first steps in building a model is to evaluate the petrophysical log data to determine the properties of the reservoir. Log and core data is studied and petrophysically analyzed, and an evaluation is performed to determine the porosity, density and permeability of the Delft Sandstone Member. The complete list of the available data and used wells and logs can be found in paragraph 3.2. In this chapter, first the core-to-well correlation and the created discrete well log is described in paragraph 6.2. This is followed by the porosity-permeability relationship that is determined from core data in 6.3. Then, in paragraph 6.4, the log analyses determines the porosity and describes the derived horizontal and vertical permeability logs. In paragraph 6.5 the temperature measurements and the thermal gradient of the area are described. The formation fluid properties are described in paragraph 6.6.

6.2. Discrete well log

A discrete facies well log needs to be built to match the well logs with core data. In the core seven types of facies were found; gravel, sandstone, fines, siltstone, coal, lignite, and claystone. The seven types of facies in the core are divided into four discrete facies. The four discrete facies are based on similar, in the core interpreted, lithofacies (Appendix C) (Loerakker 2009).

The “Siltstone” discrete facies represents the siltstones and claystones in the core and well log. The “Coal” discrete facies contains the lignite and coal bands in the core. The discrete facies “Silty Sandstone” is used for representing the very fine sands and interbedded small sandstone with siltstone bands. The “Sandstone” lithofacies log are the fine, medium and coarse sandstones and larger grain sizes. This in total creates four discrete facies representing all lithofacies found in the core (Table 6-1).

Number	Name	Colour	Description
1	Sand	Yellow	Fine to coarse sandstone
2	Silty Sandstone	Orange	Very fine sandstone and silty sandstone
3	Siltstone	Grey	Siltstone and claystone
4	Coal	Black	Coal and/or lignite bands

Table 6-1 the four discrete facies with code, name, colour and description

By linking the petrophysical data to the core log, a correlation between lithofacies and the log responses can be identified. The created correlation is used to identify lithofacies in other non-cored wells. This method created a discrete facies well log for all available wells with sufficient log data. In a similar manner a discrete facies log of the Delft-03 is created in the area. By correlating the “Moerkapelle-11” well to the Delft-03 well through a core study, cutting study and the available log data, a discrete facies log of Delft-03 is created (Figure 6-1). The net to gross ratio of the discrete facies log of Delft-03 is compared to the calculated ratio of the Delft-03, the log data and the performed cutting study (Drost & Korenromp, 2010). This shows a reliable match of the net “sand” over gross based on the well Delft-03 and the derived discrete facies log.

Quality control of this method is performed by comparing the percentage sandstone and fine sandstone facies in each discrete facies well log to the calculated net over gross ratio in the study by Smits (2008). This showed a reliable match of the net over gross based on each Moerkapelle well and the derived discrete facies logs of that particular well. The average percentage “sand” of all discrete facies and the calculated ratio from well log data match the ratios found in the cores.

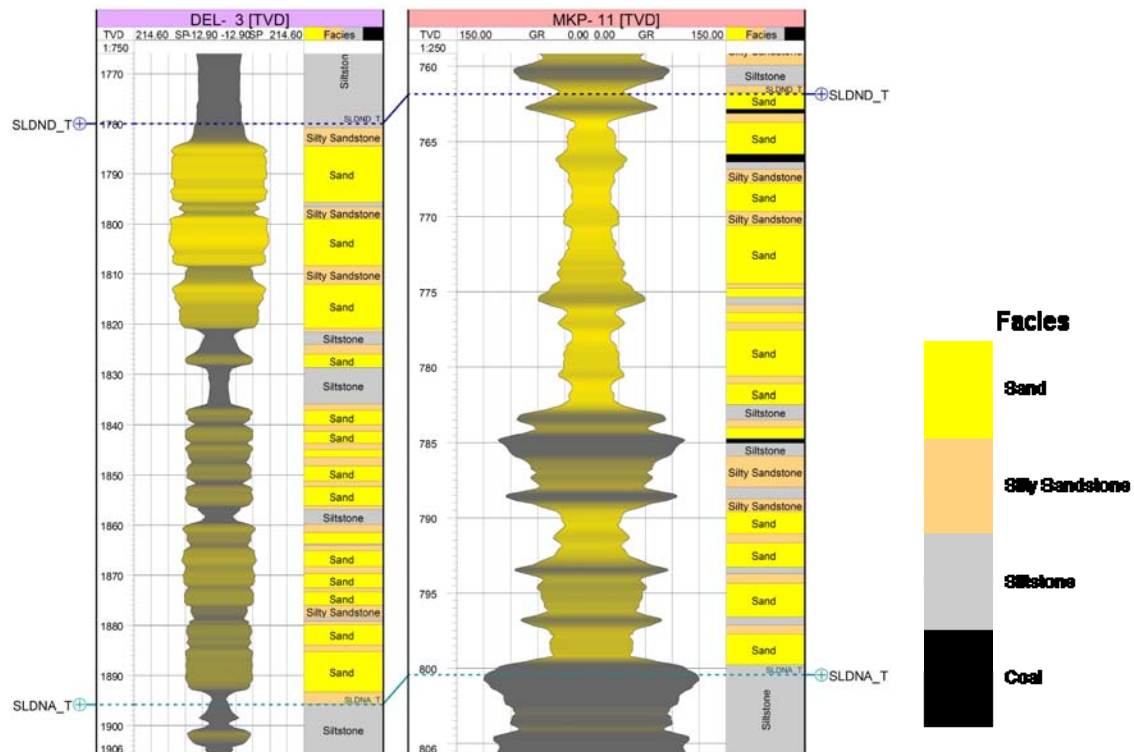


Figure 6-1 The Delft-03 and the MKP-11 wells: mirrored SP-log and discrete facies log for the Delft-03 well and mirrored GR-log, discrete facies log for MKP-11. MKP-11 scale is 1:250, Delft-03 scale is 1:750. Scale is in meters true vertical depth.

6.3. Porosity permeability relationship

Multiple cores of the Delft Sandstone Member have been taken from the Moerkapelle Oilfield twelve kilometres from the target area Delft. The Moerkapelle cores of the Delft Sandstone Member are a reliable analogue in the target area, based on previous studies of the subsurface by Smits (2008), Grobbelen (2009), Drost & Korenromp (2010), and Loerakker (2009). The available porosity and permeability data consists of measurements taken from 3 cores and multiple side wall samples on which porosity and permeability measurements have been performed. The empirical porosity and permeability relationship of the Delft Sandstone Member, the “DAP trendline”, (Equation 6-1) is based on a study by Smits (2008).

$$K = 0.0762e^{35.552\varphi} \pm 12\% \quad K(\text{Darcy}) = \text{Permeability} \quad \varphi = \text{Porosity}$$

Equation 6-1 Permeability porosity equation, “DAP trendline” (Smits, 2008).

The sediment-petrographical analysis of the Delft Sandstone Member by Drost & Korenromp (2010) used a relationship between the grains size distribution and the porosity and permeability of the cuttings found in the Delft-3 well and plugs of the Moerkapelle Oilfield.

The found grain size distribution shows a relationship with the porosity and permeability distribution and the permeability derived from well log. The “Dap trend line” has not been corrected for possible effects of changing of the permeability by relieving the sample of pressure and stress when moved to surface. The measured permeability and porosity at surface is expected to be higher than the real permeability under stress of the subsurface. By correcting the pore perm measurements, a more conservative relationship could be found but with a similar trend. This correction was not performed during this study. The DAP-trend line will be used in the construction of the dynamic flow model.

6.4. Log analyse

All available well and log data is provided by the NAM. A full list of used well log data can be found in Table 6-2. A data quality study is performed by comparing the database log curves with the original recorded log curves. The depth, shape, sample rate, and availability in the Petrel database are checked for each well log curve. The digital Petrel database provided by the NAM, showed to be a reliable data set with all available well data correctly loaded and set to the right depth. The provided porosity log curves were compared to core data and log derived porosity and showed a reliable match. Subsequently the depths of all Delft Sandstone Member markers in all relevant wells were checked. Multiple wells in the database and in Petrel still used the outdated nomenclature of well marker names and group abbreviations. All data in Petrel is updated to the nomenclature of Van Adrichem Boogaert & Kouwe, (1993-1997) (Appendix A). Well deviation paths and well site top locations in the “Rijksdriehoek” coordinate system have been checked to available drilling reports and log heathers and showed no anomalies.

Porosity

The porosities are provided by for each well by the porosity logs shown in green in Table 6-2. The NAM-provided porosities of the Delft Sandstone Member are calculated from the combined available log data. The porosities are predominately derived from a combination of the used neutron density-log and sonic-log and are supported by core data. No spread check of the differences in neutron porosity and density porosity is performed. The porosities have not been weighed or adjusted and are taken from the entire wells section of all wells will available data. An overview of all porosity measurements of the Delft Sandstone Member can be found in Figure 6-2.

Well name	Available Well Logs
DEL-02	RESD, SP
DEL-03	RESM, SP, RESD
PNA-15	DENS, GR, RESD, SH, RESM, NEUT, SON, POR, FLGR, CAL
OLE-01	RESD, RESM, FLGR, SP, CAL, GR
MKP-16	RESM, SZ40, SH, SZ50, NEUT, CAL, POR, SZ70, SZ30, GR, DENS, FLGR, RESD, SON
MKP-14	POR, SH, SZ40, SZ30, RESM, DENS, GR, CAL, NEUT, SON, SZ70, FLGR, SZ50
MKP-13	NEUT, CAL, RESM, POR, GR, SON, DENS, SH, FLGR
MKP-12A	RESM, FLGR, NEUT, POR, RESD, SON, SH, DENS, GR, CAL
MKP-12	RESM, FLGR, NEUT, POR, RESD, SON, SH, DENS, GR, CAL
MKP-11	FLGR, GR, RESM, DENS, SH, CAL, SON, NEUT, RESD, POR
MKP-10	SH, SON, RESM, GR, DENS, NEUT, SZ40, SZ30, SZ70, FLGR, POR, RESD, CAL, SZ50
MKP-9A	CAL, DENS, RESD, SON, SZ40, SZ30, SZ70, SZ50
MKP-2	CAL, RESD, SP

Table 6-2 Table of the available log data per well used in the Petrophysical analyze and evaluation of the Delft Sandstone Member. The full names can be found in the nomenclature (Appendix B), the porosity logs are indicated in green.

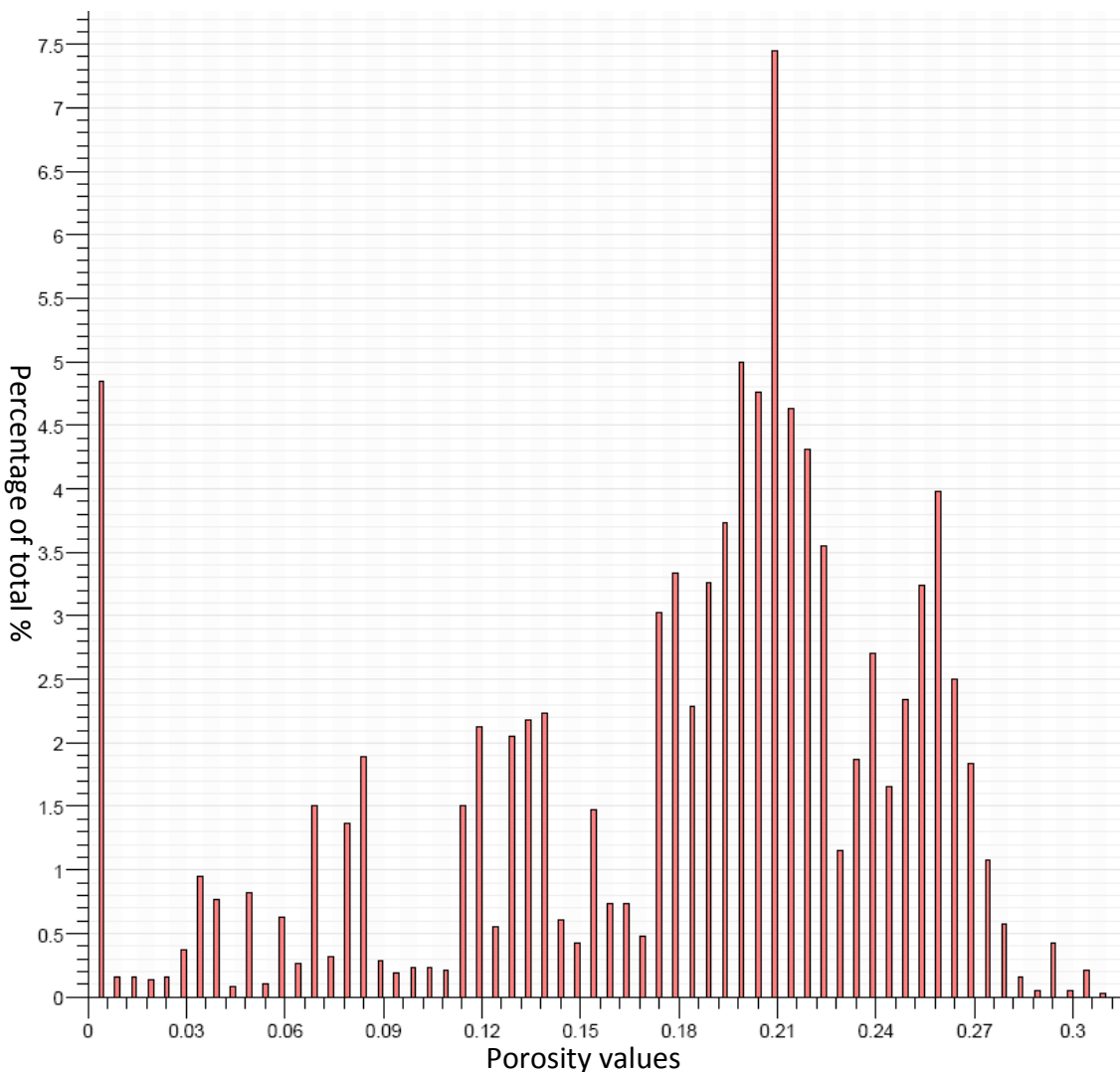


Figure 6-2 Porosity graph of the Delft Sandstone Member from all available well log porosity data points. The horizontal axis shows the porosity and the vertical axis gives the percentage of the total data points.

Horizontal Permeability

From each well in that has a porosity log a permeability log was derived. The permeability log for each data point was calculated using Equation 6-1 and the input values found in the porosity log. For every porosity value a permeability value was calculated. No geostatistics, data analyse or upscaling methods are used. The total number of porosity data points is therefore equal to the amount of permeability data points. An example of a calculated permeability log from a porosity log can be found in Figure 6-3.

Vertical permeability

The Delft Sandstone Member contains layered interbedded sand- and silt-stones. Therefore the Delft Sandstone Member will show a large anisotropy within the permeability. The vertical permeability is therefore different from the horizontal permeability. No vertical permeability measurements or relations are provided of the Delft Sandstone Member, however a relationship was derived using the available permeability data.

The clay- and siltstone layers are most likely to have a large effect on the vertical permeability. Therefore the vertical permeability (K_v) is derived from the Horizontal permeability (K_h) by using the ratio of the average permeability of the discrete siltstone facies versus the average permeability of the discrete sandstone facies. The discrete siltstone facies has an average permeability value of 1 mDarcy with a standard deviation of 3.0 mDarcy. The average permeability of the discrete sandstones facies is 127 milliDarcy with a standard deviation of 123.0 mDarcy. The ratio used for the K_h to K_v ratio is therefore 127:1 with an 8 mDarcy error derived from the standard deviations. From each well in Table 6-2 that has a porosity log and a permeability log and a vertical permeability log was calculated. The vertical permeability log was calculated by using Equation 6-2 and the input values found in the horizontal permeability log for each certain point. An example of a calculated vertical permeability log from a horizontal permeability log can be found in Figure 6-3.

$$K_v = \frac{K_h}{127} \pm 8(mD)$$

Equation 6-2 Vertical permeability (K_v) equation based on the horizontal permeability (K_h).

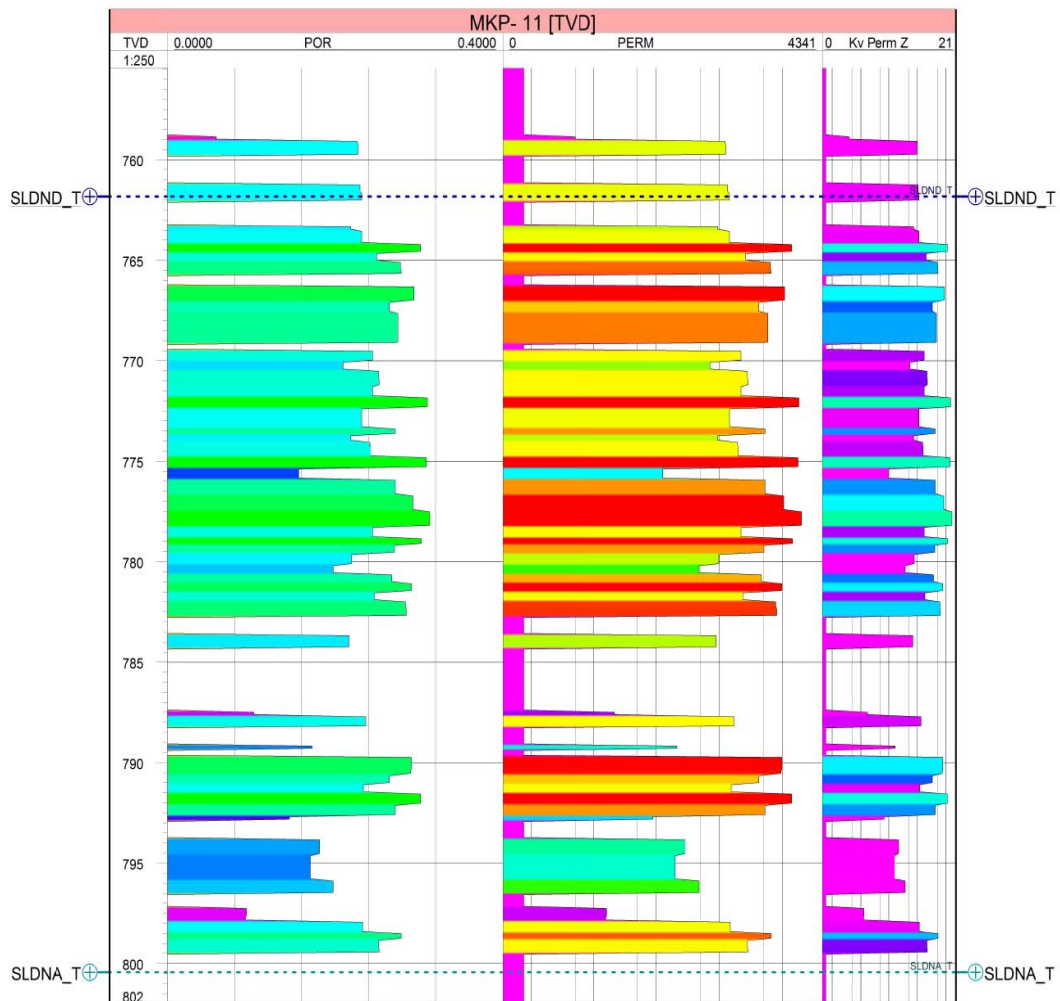


Figure 6-3 Porosity(left) and horizontal Permeability(perm) (centre) and Vertical permeability(K_v Perm Z) (right) Log of the MKP-11 over the Delft Sandstone Member. Depth is in true vertical depth in meters.

6.5. Temperature

For the implementation of geothermal energy production, the formation water temperature is a crucial factor as it determines the energy potential. The formation water temperature is different for each location based on the depth and the local geothermal gradient. The local difference in thermal gradient is caused by the geological variability in space and time (Ramaekers et al, 2006). The temperature at a certain depth is based on a linear depth depended relationship called the geothermal gradient plus an average surface base temperature. The subsurface temperature in target area Vrijenban and the West Netherlands Basin can locally show anomalies but is generally accepted to be a linear relation of about 3 degrees per 100 meters (Grobbelen et al., 2009).

Temperature Equation and maps

To determine the temperature at a certain depth more accurately, a linear thermal gradient based on local well data is used. The thermal gradient is based on multiple corrected formation temperature measurement from local bore hole data (Smits, 2008). Several studies to the thermal gradient near the target area Vrijenban in the West Netherlands Basin have been performed and these are combined in Table 6-3.

(Simmelink et al., 2007)	$T(Z)= 10 + 3.11[Z] \pm 0.01[Z]$	Den Haag
(Grobbelen et al., 2009)	$T(Z)= 10 + 3.10[Z] \pm 0.01[Z]$	Pijnacker
(Smits, 2008)	$T(Z)= 10 + 3.11[Z] \pm 0.01[Z]$	Delft

Table 6-3 Temperature equations and gradients from different studies in the West Netherlands Basin. Left to right: author, equation and target study area. Equation parameters: T is the temperature in degrees Celsius, depth Z is in 100 meters based on True Vertical Depth from NAP.

$$T(Z) = 10.0 + 3.11[Z] \pm 0.015[Z]$$

Equation 6-3 Temperature to depth relationship based on empirical data taken from corrected well bore hole measurements. T in degrees Celsius and Z depth is in 100 meters in the true vertical depth from NAP

The temperature at depth is calculated in this study using Equation 6-3. This is the average geothermal gradient based on the studies of Smits (2008), Grobbelen et al., (2009), and Simmelink et al., (2007).

The temperature of the Delft Sandstone Member in the target area Vrijenban will range from 63.5 to 83.5. Based on Equation 6-3 it is possible to calculate the temperature on the surface map. The calculated temperature maps for the Top Delft Sandstone Member and top Rodenrijs Claystone Member are shown in Figure 6-4 and Figure 6-5. The average temperature over the entire Delft Sandstone Member is 74.4 degrees Celsius. The temperature gradient through the target Delft Sandstone Member can be found in Figure 6-6.

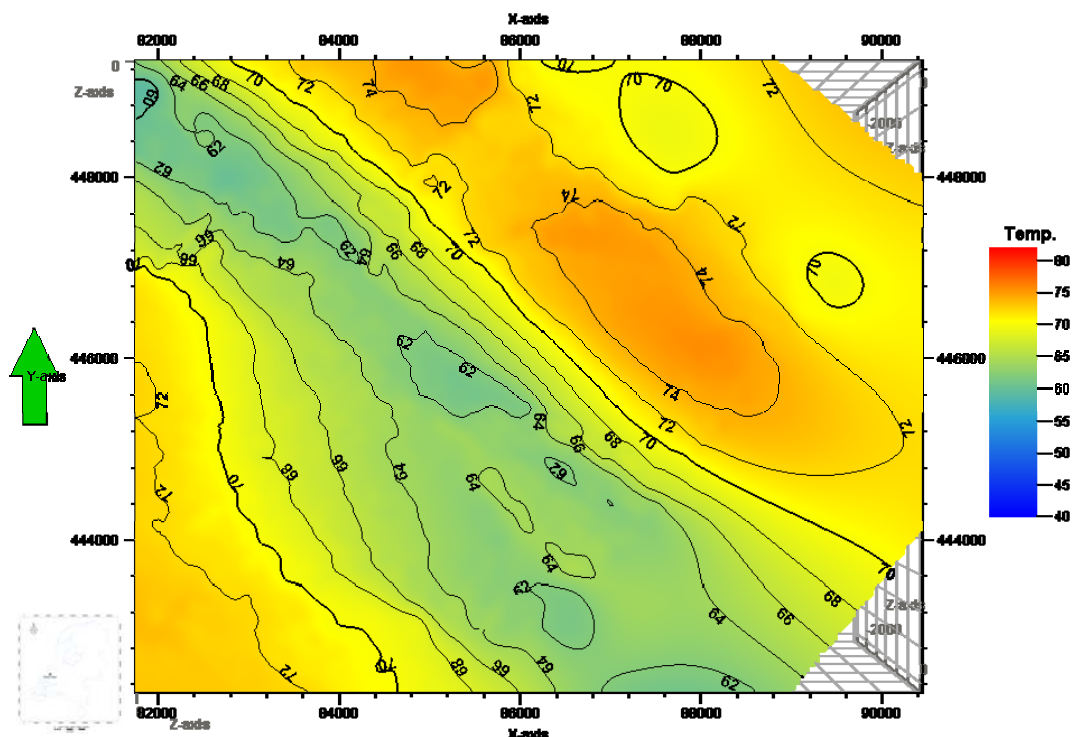


Figure 6-4 Temperature map of the Top Rodenrijs Claystone Member.

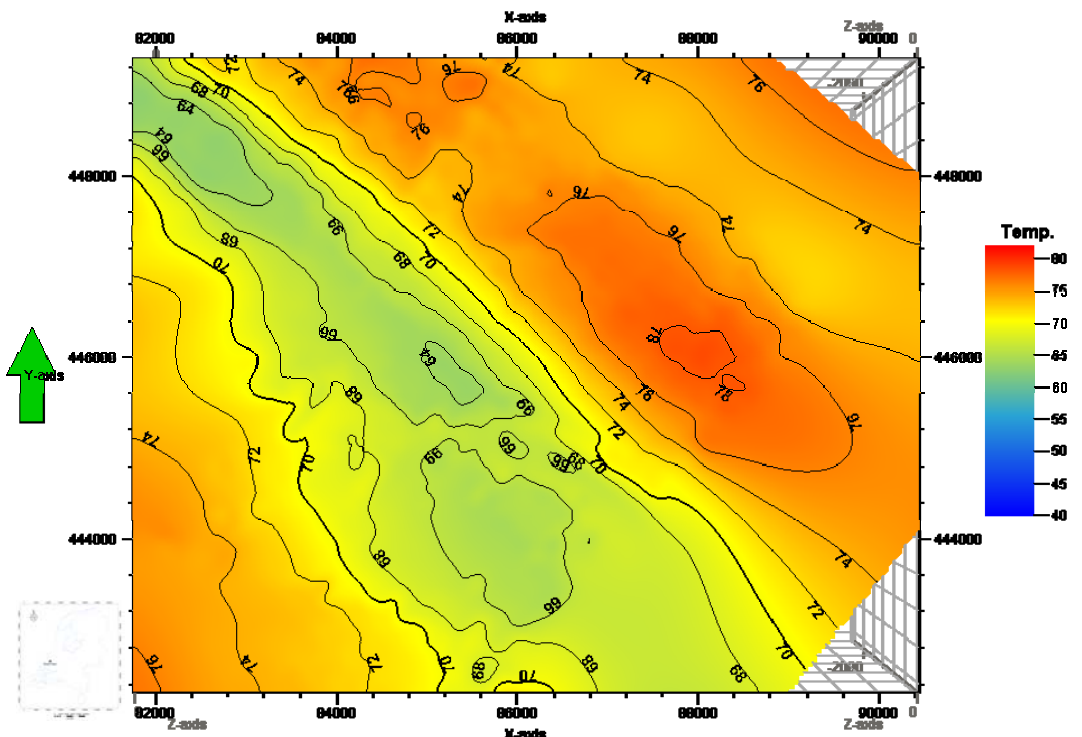


Figure 6-5 Temperature map of the Top Delft Sandstone Member.

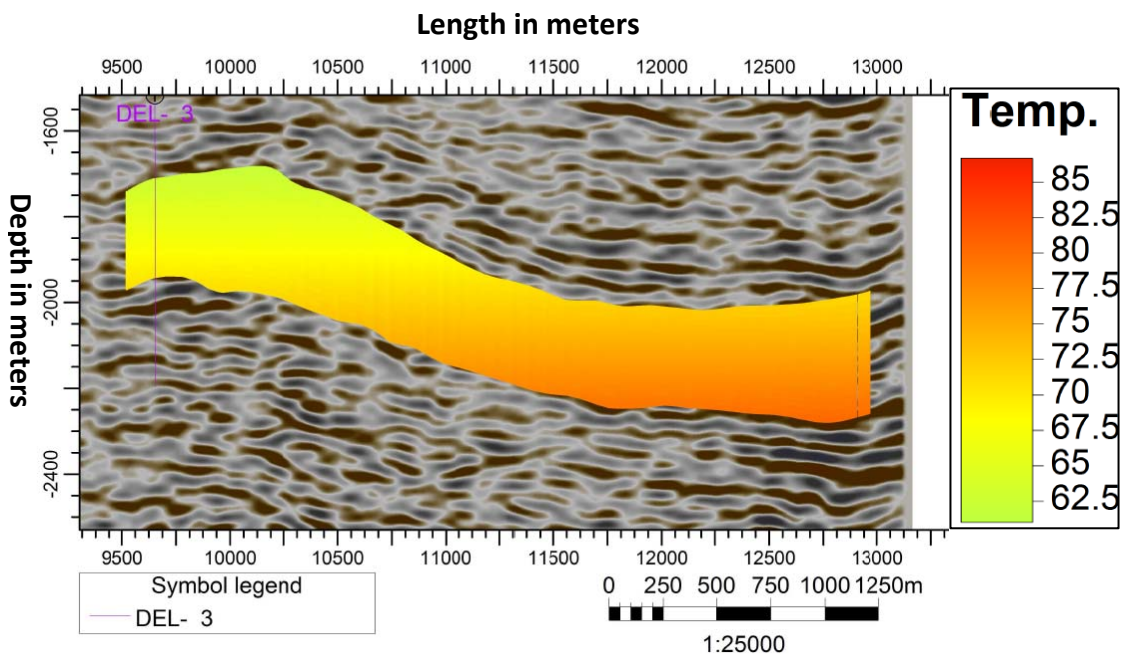


Figure 6-6 Temperature profile of the Delft Sandstone Member with the Delft-03 on seismic inline 2760 (figure 3-7), depth to length ratio to 2:1.

6.6. Formation fluid properties

Multiple oil finds in the West Netherlands Basin show the risks of hydrocarbons in the target area. However, the wells in the Delft High show no evidence of hydrocarbon in the Delft Sandstone Member. Both the log data as well as additional testing of the cuttings from the Delft-03 show no presence of hydrocarbon in the target Delft Sandstone Member (Drost & Korenromp, 2010). The formation fluid or aquifer water of the Delft Sandstone Member in the target area is therefore considered to be a brine.

However other formations in the target area do contain traces of hydrocarbons as found in the Delft-08 well, hence there is still a risk of hydrocarbon presence in the Delft Sandstone Member in the northwestern part of the Vrijenban synclinal structure near the Pijnacker High and Pijnacker oil field. With no wells drilled into the Delft Sandstone Member in this structural high, there is insufficient data to determine the presence of hydrocarbons. Sufficient safety measures should be taken into account whilst drilling for geothermal energy as there is a risk of encountering hydrocarbons.

Formation fluid samples or fluid data from wells in the target area Vrijenban are unavailable. Fluid samples of other nearby wells were studied to determine the fluid properties. A study, performed by Chun (2009), was conducted to further determine the content and properties of the formation fluid. The total number of dissolved substances in the formation fluid gives a salinity of 98,4 mg/L NACL equivalent. The expected salinity, reservoir pressure, and temperature are used to determine the viscosity and density of the formation fluid under reservoir conditions. The viscosity, density, formation volume factor and fluid compressibility are calculated in the dynamic fluid model using the, equations based on Meehan (1980) that are incorporated in Eclipse.

7. Constructing a static model of the Delft Sandstone Member.

To gain more knowledge of the reservoir architecture of the Delft Sandstone Member a static 3D reservoir architecture model (static model) needs to be build of the target area Vrijenban. This static model will be the basis for dynamic flow modelling. In reservoir engineering and flow modelling it has long since been recognized that modelling sedimentary deposits as totally homogeneous bodies, both with regards to sedimentological and structural heterogeneities, is a gross simplification of their potential flow behaviour (Keogh et al., 2007). Building a flow model based on the sedimentary deposits and the available sedimentological data is crucial. To make a static model, Schlumberger's Petrel software was used. This software is designed to assemble oil reservoir data from different sources and build static 3D reservoir architectural models. In this case the program was used to create a static model for the purpose of flow modelling. First an overview of the workflow is given followed by the building of a framework of the static model. Then the grid is populated with facies and the petrophysical properties are added to the static model to give it the flow characteristics. Finally the uncertainties are discussed.

7.1. Work flow

A model was built to show the depositional environment to be used in flow modelling. The work flow used to build the model is as follows (Figure 7-1). First the Vrijenban structural framework and grid is made from the horizons and faults interpreted on seismic data. The grid size is chosen and the boundaries of the model are set. Then the number of zones and layers are determined followed by the upscaling of the well data. This procedure is finalized by populating the created grid with sedimentary bodies using facies modelling in Petrel. The facies modelling, based on the depositional setting of the formation is performed using an object-based modelling tool. To make flow modelling possible, petrophysical properties are conditioned to the facies. The property will define the models flow characteristics this is referred to as the defined static model.

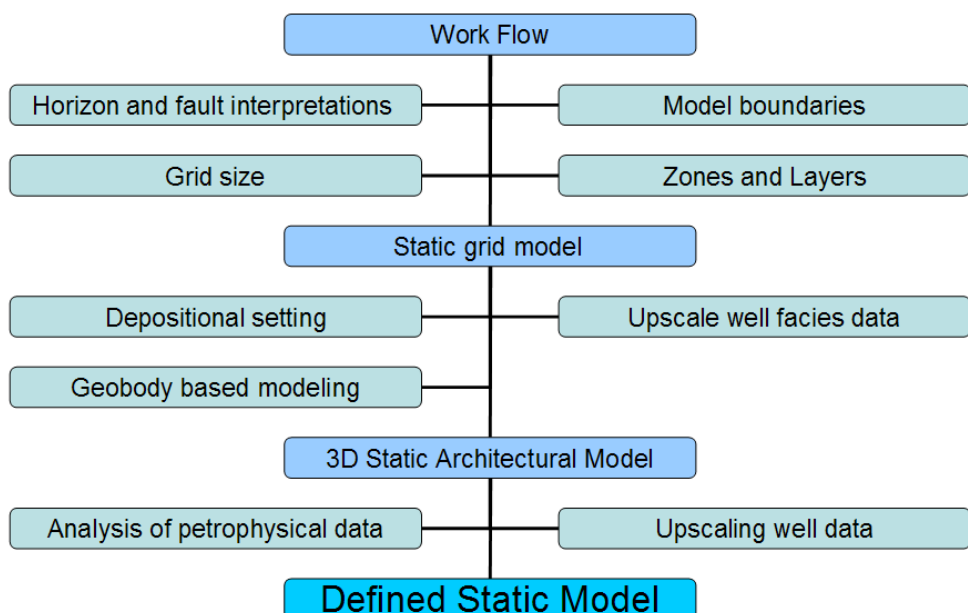


Figure 7-1 Workflow used in this study to build a defined static model for dynamic flow modelling.

7.2. Building a structural framework

To create a static model, a grid is built with set boundaries. To determine the size of the model and the grid, boundaries need to be set based on the dimensions of the subsurface structure and the size of the study area.

Determining the top and base of the model

The top of the static model is the seismic interpretation of the top Rodenrijs Claystone Member tied back to the available wells. The base of the static model is the interpreted Inter Alblasserdam Member surface. The interpreted Top Delft Sandstone Member is modelled as an internal surface in the static model (Figure 7-2). Although the target formation of the geothermal project in the area is the Delft Sandstone Member, the resolution of the seismic data is only adequate to determine the top of the Delft Sandstone Member and not the base of the formation (paragraph 3.1). The static model is based on the boundaries created by the above lying Top Rodenrijs Claystone Member and the below interpreted Inter Alblasserdam Member surface. The vertical height of the structure between the top and the base changes throughout the structure, but is at the Delft-03 well approximately 310 meters thick containing the Rodenrijs Claystone Member, the Delft Sandstone Member and parts of the Alblasserdam Member.

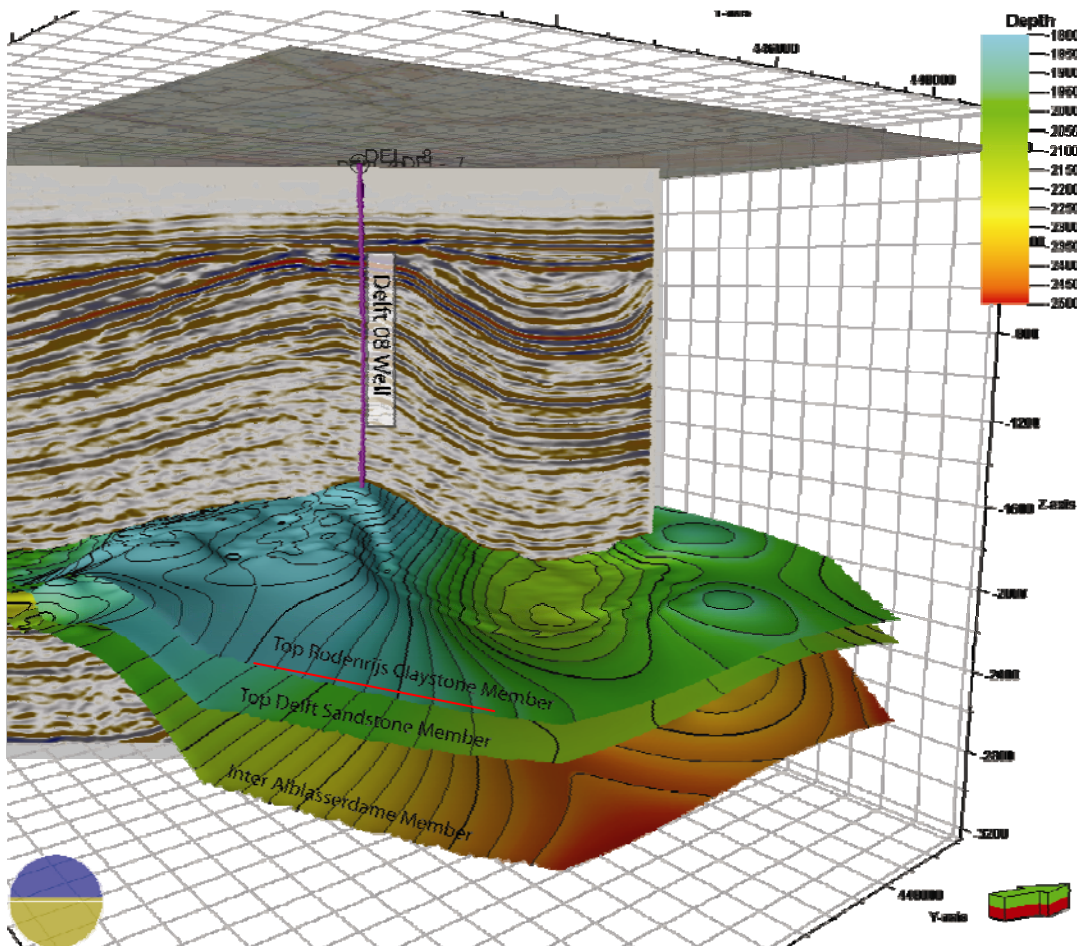


Figure 7-2 3D view showing the top Rodenrijs Claystone Member, the Delft Sandstone Member and the proposed base of the model, the Inter Alblasserdam Member. Depth is in meters, XY to Z ratio is 1:2. Also shown is the Delft-08 Well and seismic inline 2814 of the PSDM data, the location of this inline is shown in Figure 7-3.

Modelling area boundaries

To determine the size and dimension of the static model lateral boundaries need to be set. The Vrijenban synclinal structure is bounded on three sides by three faults. For this reason the lateral boundaries of the static model are also set at these three faults. The structural framework is bounded by the main boundary fault of the Pijnacker High to the northeast. The interpreted 45° degree SSE dipping normal fault at Top Delft Sandstone Member level is the northwest boundary of the structure. The Delft High reverse fault to the southwest is the southwest boundary of the model. Although the synclinal structure continues further to the southeast, it goes beyond the reach of this study and the seismic data (Paragraph 4-2). The boundary towards the southeast is set at the edge of the available seismic data. As the four boundaries are set, a large quadrilateral or trapezium shaped polygon is created (Figure 7-3). No internal faults or subseismic faults have been modelled as there is insufficient data. The main boundary fault of the Delft High is inside the modelled area to keep well data control from the Delft-wells. However it is important to keep in mind that this fault could be sealing.

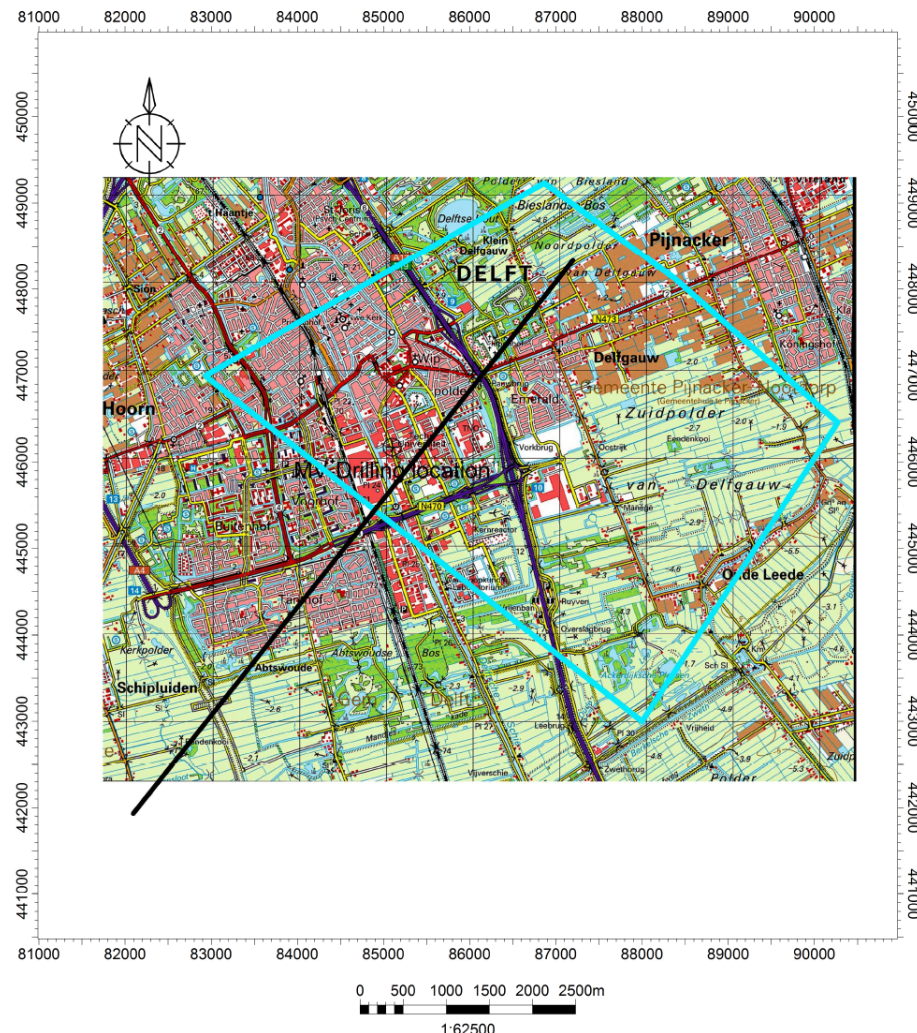


Figure 7-3 Map of the target area with the trapezium shaped polygon used to create the dimensions of the model. The black line is the seismic inline 2814 in PSDM as shown in Figure 7-2.

Building the grid

The structural framework of the static model is a grid that has a chosen grid size in the x, y direction of 50 meters by 50 meters as this is the same size as the bin recording size of the seismic data. For the process of constructing the grid see appendix F. In the horizontal plane the error is two seismic recorded bin sizes or 100 meters. The created grid can be found in Figure 7-4.

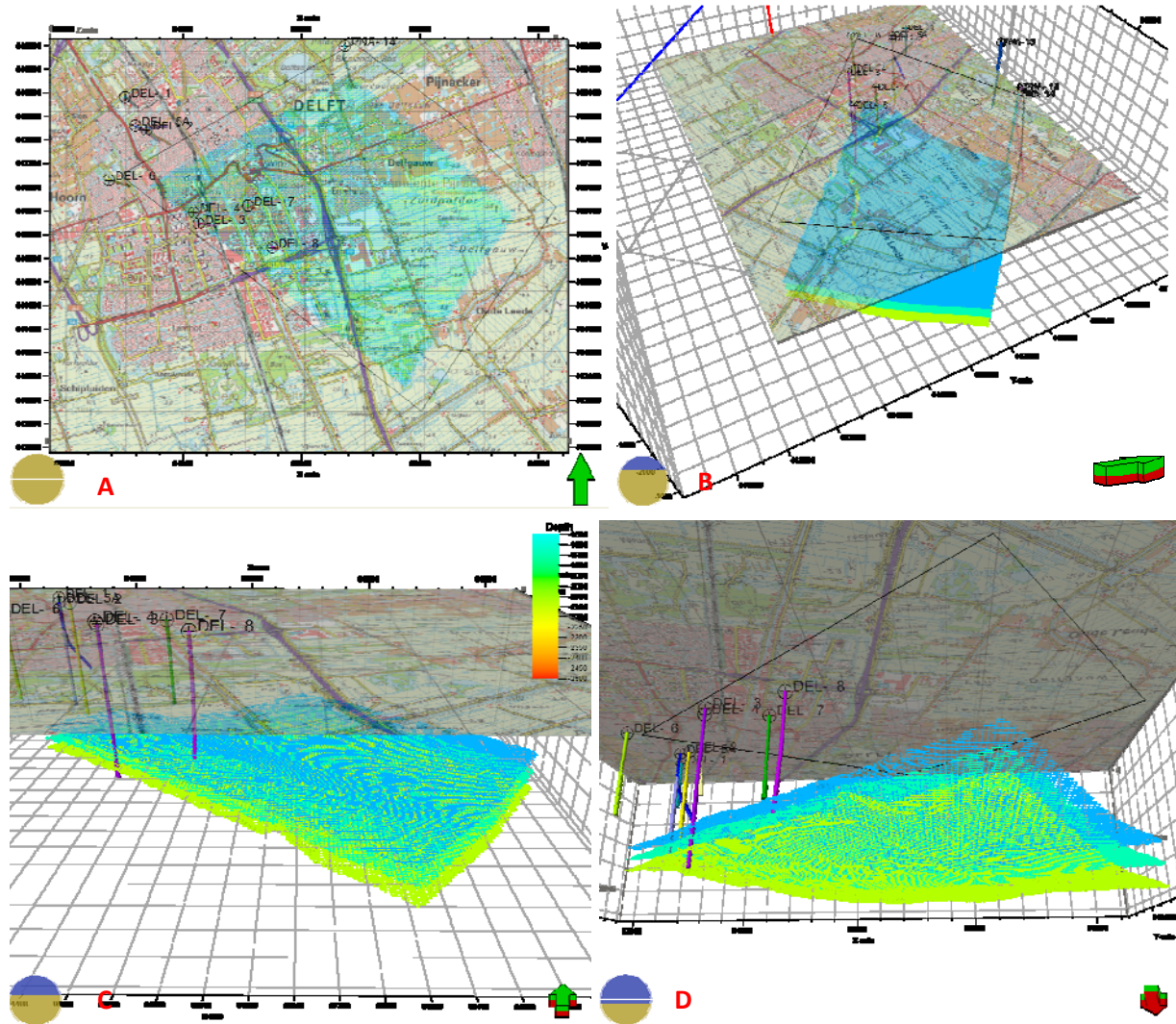


Figure 7-4 A) Map of Delft with the outline of the structure in black. B) Side view of the created coloured grid. C) View from the south of the created grid surfaces. D) View from below on the created model.

Zones

Zones represent the stratigraphic formations and are added to the model to create the horizontal units. Each zone represents a stratigraphic unit in the grid model and is based on the available well data. The zones are determined based on the markers of the Top Rodenrijs Claystone, the Top Upper-, Middle-, and Lower Delft Sandstone Member, the Top Alblasserdam Member and the Inter Alblasserdam Member surface as found in the well. Each zone represents an area between the two tops for example the Rodenrijs Claystone Member zone lies between the Top Rodenrijs Claystone Member and the Top Delft Sandstone Member (Table 7-1) (Figure 7-5).

Zones			
Zone 1	Rodenrijs Claystone Member		SLDNR
Zone 2	Upper Delft Sandstone Member		SLDND U
Zone 3	Middle Delft Sandstone Member		SLDND M
Zone 4	Lower Delft Sandstone Member		SLDND L
Zone 5	Upper Alblasserdam Member		SLDNA

Table 7-1 Zones used to build the model. Each zone represents a stratigraphic unit.

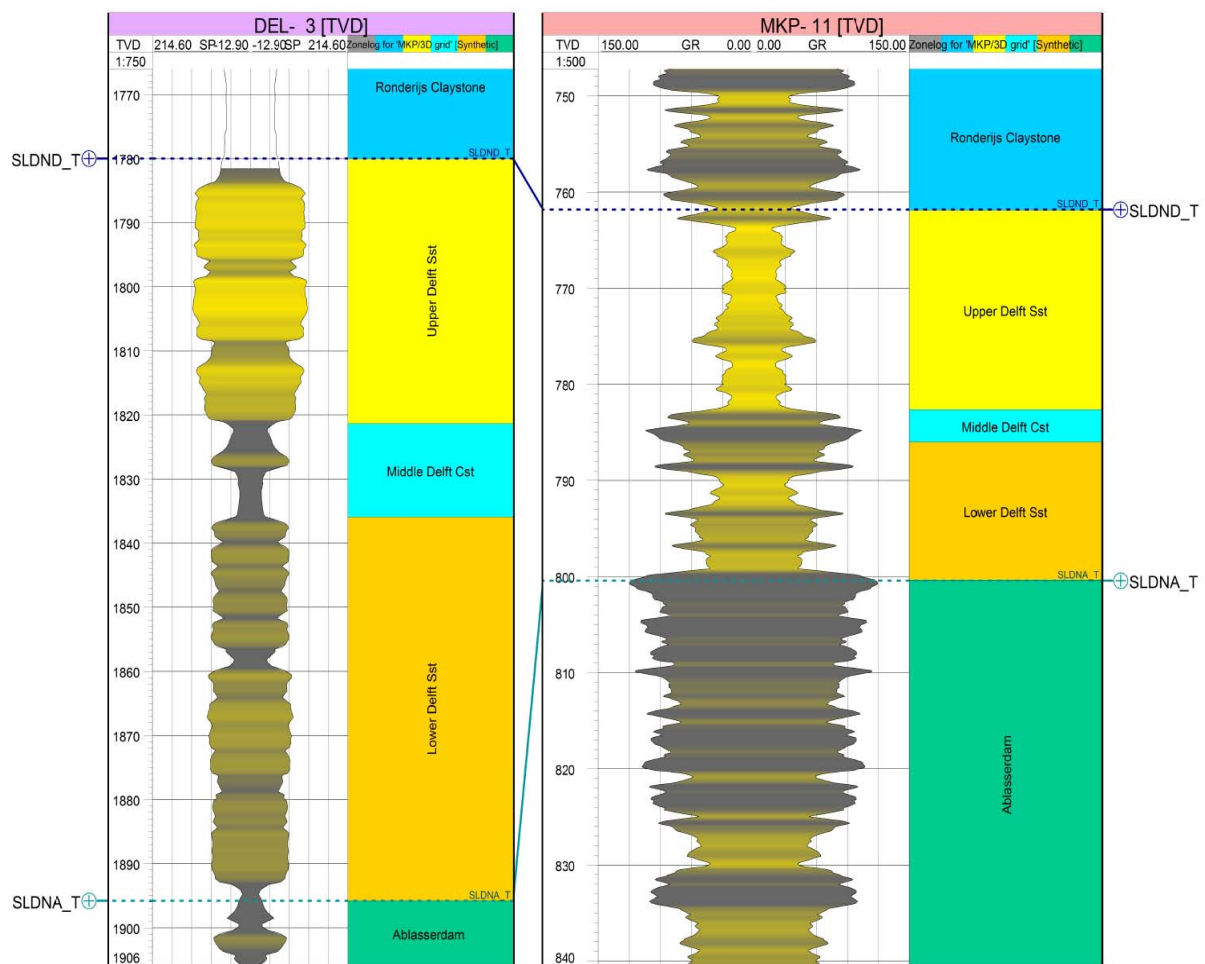


Figure 7-5 The SP log of the Delft-03 well and the Gamma ray log of the MKP-11 well with well tops of the formation and zones used in the model.

The zones from the wells are extrapolated over the entire grid. Normally one would model the thickness of a stratigraphic zone conformably to the interpreted seismic surfaces with the aid of multiple correlated well tops. As there is only one well, the Delft-03 well, within the model area this is not possible, especially when the relative thickness changes throughout the structure created by syn-rift deposition of the formations is to be modelled. Modelling the surfaces as constant or conformably to the well top data would create a model without the syn-sedimentary thickness variation. Therefore an approach is used that upholds the thickness variations throughout the system, as this plays a crucial role in the depositional setting.

The area between the Top Delft Sandstone Member and Inter Alblasserdam Member surface is divided into four zones based on the stratigraphy. These are from base to top respectively, the Alblasserdam Member, the Lower Delft Sandstone Member, the Middle Delft Sandstone Member and the Upper Delft Sandstone Member. As the thickness of each zone is known in the Delft-03 well, a proportional thickness isochore map for each zone is created. This is done by creating a thickness map of the area between the in seismic interpreted surface of the Top Alblasserdam Member and the surface of the Top Delft Sandstone Member. This thickness map is then vertically divided proportionately to the thickness of each zone as found in Delft-03 well. This creates an isochore (thickness) map of each zone. This thickness map honours the varying thickness throughout the total thickness as found in the seismic data proportional to the well data. As the Rodenrijs Claystone Member is not the primary target of this project it is modelled as one zone. It consists of the total area between the Top Rodenrijs Claystone Member on seismics interpreted surface and the Top Delft Sandstone Member interpreted horizon. The method used is not ideal as it only partly takes the different rates of differential subsidence in each single zone into account and the uncertainty in the model is large. The thickness variation of each formation is different and the thickness of each zone is based proportionally on only one well. The resolution of the interpreted surfaces used, creates a possible error of approximately 40 meters. This is a large error when compared to the average thickness of a zone. However as this method does create a proportional thickness variation in the zones representing the syn-depositional thickness differences it is the preferred method. A full description of the process used to create the zones can be found in appendix F (Figure 7-6 and Figure 7-7).

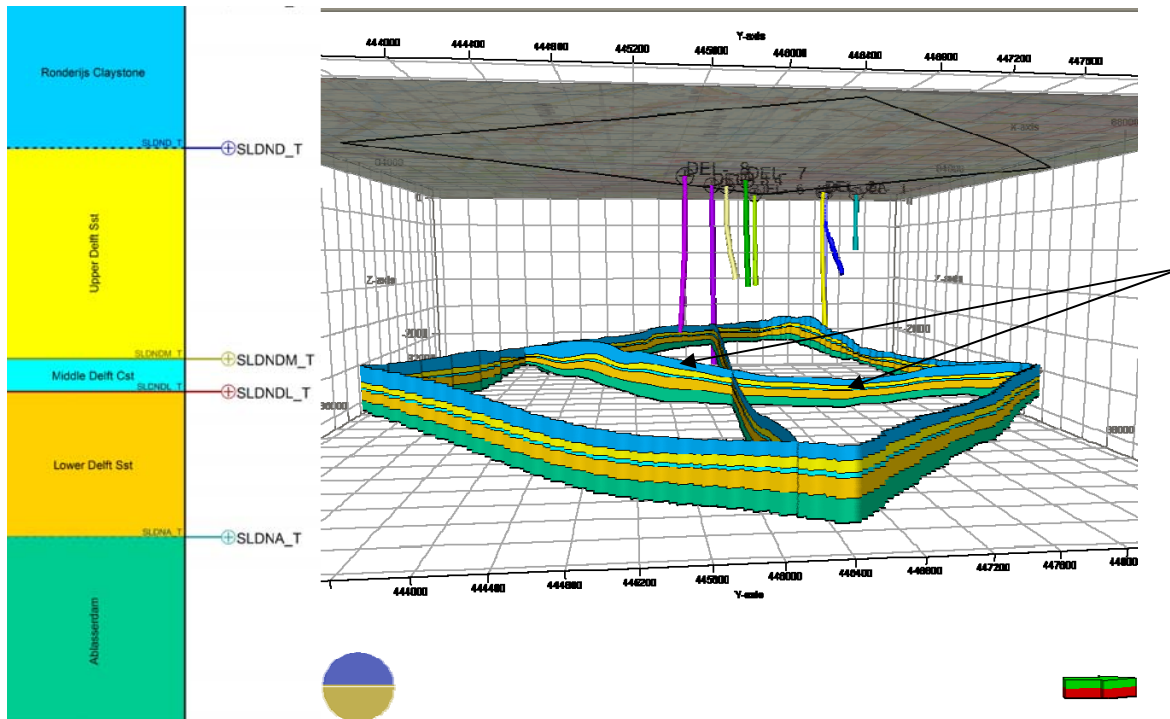


Figure 7-6 A 3D side view from the east of the created model with the zones and the Delft wells. X,Y,Z ratio is 1:1:1 and the scale and depth is in meters. The arrows point to the thickness variation in the zones.

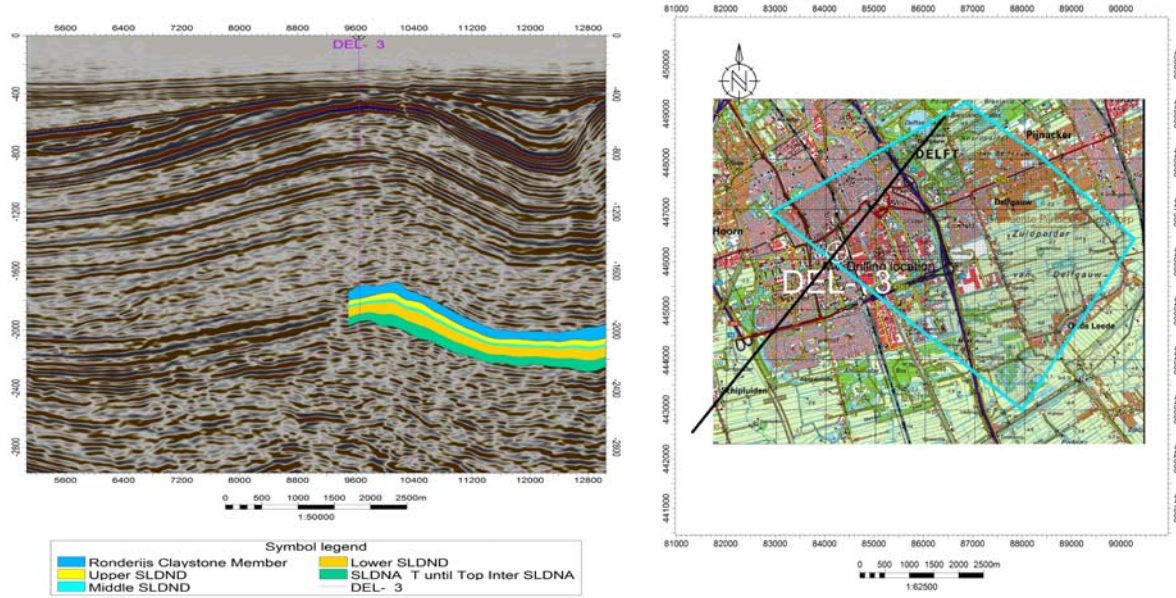


Figure 7-7 A 2D Seismic inline 2765 with the created zones and the Delft-03 well, depth in meters. On the right is the map of Delft showing the inline 2765(black line) and the modelled area (blue).

Layers

Each zone is divided into grid layers because one stratigraphic zone can have different lithofacies. The number of layers is different per zone based on the details that need to be modelled. The Upper, Middle and Lower Delft Sandstone Member zones have been divided into layers based on the thickness of the zones in the Delft- 03 well. The total thickness of the Delft Sandstone Member in Delft-03 well is 115 meters. These 115 m are divided into layers of 5 meters thick at the well location creating 23 layers in the Delft Sandstone Member. The Rodenrijs Claystone Member zone and the Alblasserdam Member zone are not the target of this study and have therefore been divided into 5 layers each (Table 7-2; Figure 7-8). A description of the process used can be found in appendix F.

Layers			
Zone 1	Rodenrijs Claystone Member	SLDNR	5 Layers
Zone 2	Upper Delft Sandstone Member	SLDND U	8 Layers
Zone 3	Middle Delft Sandstone Member	SLDND M	3 Layers
Zone 4	Lower Delft Sandstone Member	SLDND L	12 Layers
Zone 5	Alblasserdam Member	SLDNA	5 Layers

Table 7-2 Layers used to build the model. Each zone is divided into multiple layers.

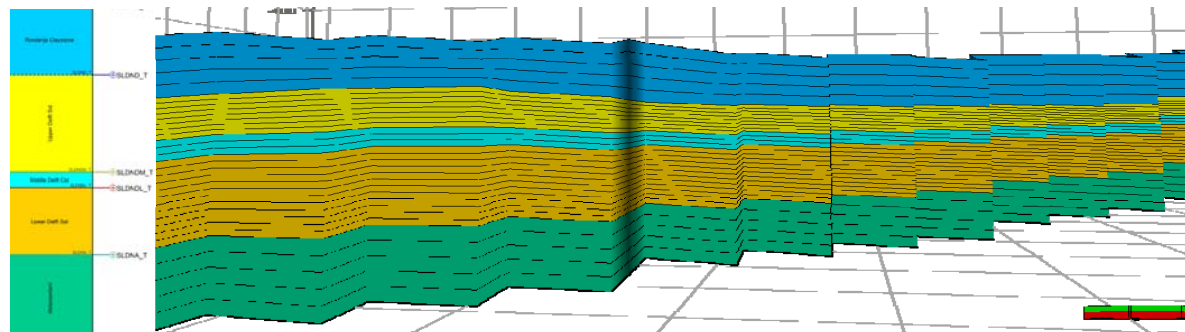


Figure 7-8 Side view from the west of the created layers in the zones of the model.

Because of the lateral thickness variation in the model the average layer thickness changes throughout the model. The layer thickness ranges from 1.5 to 10.5 meters and has an average thickness of 7 meters (Table 7-3). A smaller layer size would be preferable as the average sand body thickness in the well data ranges from 1.5 to 5 meters (Loerakker, 2009). Compared to the horizontal size of 50 by 50 of the meter grid blocks and the vertical error from the seismic resolution of the surfaces of approximately 25 meters, the size and thickness of layers is reasonable. To create smaller layers, more layers would need to be constructed within the grid. The number of grids blocks would rapidly increase and therefore increase the run and modelling time.

Thickness of single layers	Average (m)	Min (m)	Max (m)
Statistics for Upper SLDND	6.04	1.51	9.24
Statistics for Middle SLDND	7.17	2.90	10.17
Statistics for Lower SLDND	7.34	2.98	10.41

Table 7-3 Average, minimum and maximum thickness of layers in the Delft Sandstone Member.

3D grid model discussion

The final created grid model contains 584496 grid blocks. The dimension of the grid is ($n_l \times n_j \times n_k$) $144 \times 123 \times 33$. A single grid block has a horizontal size of 50 by 50 meters and an average vertical height of 7 meters. From base to top it contains 5 zones and 33 layers. The highest point lies at a depth of 1635.7 m and the lowest or deepest point lies at a depth of 2484.5 m. The vertical error per grid cell is based on the seismic resolution and can be up to 50 meters. The horizontal error is a 100 meters based on two bin sizes. This makes the error much larger than the size of the grid cell. The initial grid model is built from only three interpreted seismic horizons, using more interpreted surfaces would be more favourable. This would also improve the zone building method. The syn-depositional thickness differences in the zones are present in the model but it only upholds the variations as found in the interpreted seismic data proportional to the thickness of the zone. It is found in the Moerkapelle oil field that each zone has a different thickness variation. This is not taken into account here but large zones do have a larger variation in the created model. The model could be improved in many of the steps taken to build the model, but that is beyond the scope of this study.

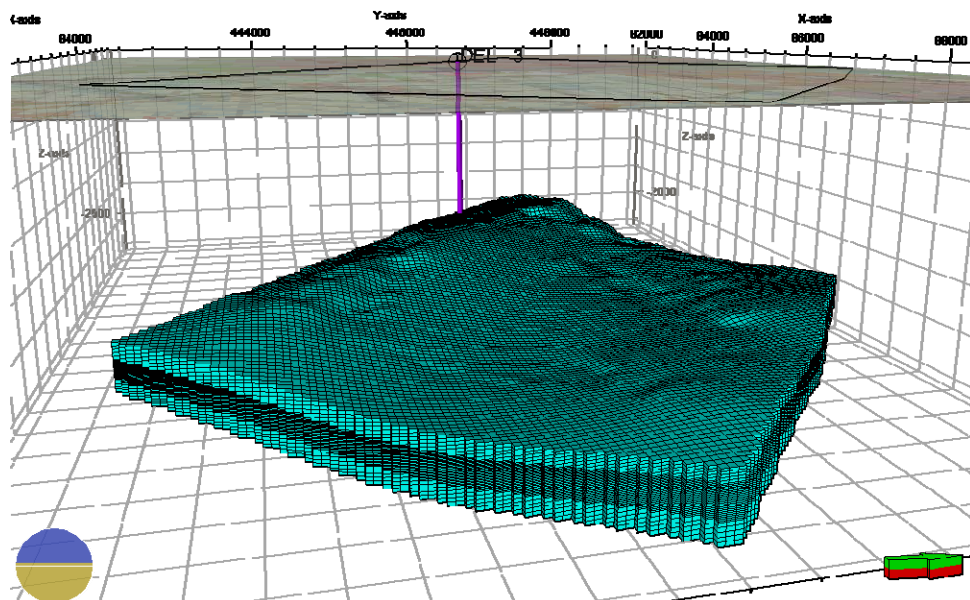


Figure 7-9 Side view from the east of the total created 3D grid structure with the Delft-03 well.

7.3. Facies modelling, populating the grid

Facies modelling is the process of modelling the lithofacies distribution throughout the model. Facies modelling is an important component of geostatistical reservoir characterization and facilitates visualisation of the depositional setting. The depositional setting of the Upper, Middle, and Lower Delft Sandstone Member suggest rules concerning the geometries of the facies and the possible relationships between fluvial characteristics and the well log data. First the wells are upscaled so that the well data fits the layers and zones. The wells were upscaled using the “most of” method, a full description of the process can be found in appendix F. Furthermore a data analysis is performed on the available data followed by Geobody-based modelling, populating the grid.

Facies Modelling

After completing the grid of the static model, which is a framework for the facies model, the next step is to populate the model with lithological properties. For proper facies modelling, knowledge of the spatial distribution of the lithology is necessary. This knowledge is partly derived from the conceptual depositional model and partly from the data. Each zone has different depositional characteristics therefore it is important that each zone is modelled separately. There are different methods to populate the grid with lithofacies and each zone is modelled separately using a specific method. The Delft Sandstone Member is facies modelled using object based modelling. The object based modelling input is knowledge that is partly derived from the depositional setting, such as the direction and size of the meandering channel belt. The channel thickness input of the Delft Sandstone Member is set as found in the cores. A single channel thickness in the Delft Sandstone Member varies from 1.5 to 4.5 meter with an average of 3 meters (Loerakker, 2009). The channel width is derived from the thickness using the general equation developed by Fielding and Crane as stated in Davies et al.(1992). The derived width of the channels varies from 12 meter to 195 meters with an average of 92 meters. As no data is available on the sinuosity of the channels this is set with a wave length of 1500 meters and amplitude of 800 meters, the default settings of Petrel. The flow direction is southeast to northwest similar to the axis of the West Netherlands Basin (Van Adrichem Kouwe & Boogaert, 1993-1997). This is put into the model as an average flow direction of 315 degrees with a normal spreading of 5% or 15 degrees. The generated facies model is then evaluated to check if it represents the depositional setting and the well log data by comparing the sand and shale content to the available data. A full description on the facies modelling process and the different facies can be found in appendix F a summary is given below.

Modelling the Alblasserdam- and Rodenrijs Claystone Member.

The Alblasserdam Member and the Rodenrijs Claystone Member are not the primary target of this study. Therefore these zones have not been modelled in detail. As these members are at the base and top of the structure, they may still interact with the temperature flow during temperature and flow modelling. The Alblasserdam Member and Rodenrijs Claystone Member are therefore modelled using the “assigned value” method. To be able to assign property values to these zones it is chosen to model the Alblasserdam Member and Rodenrijs Claystone Member as massive siltstones. Even though the members contain more than just silt and claystones both zones will be assigned set values for the purpose of heat convection and conduction in the flow modelling part of this study and will not be assigned any fit to purpose properties and flow characteristics.

Modelling the Lower Delft Sandstone Member zone,

The Lower Delft Sandstone Member is modelled by using the object based modelling method. Object based modelling populates a facies model with stochastically generated and distributed objects. The geometrical properties, like size and orientation, can be assigned with a statistical distribution. This method is especially suited for this zone because the zone consists of a single meandering fluvial channel in a background of floodplain deposits. The Lower Delft Sandstone is therefore modelled using object based modelling as a well developed meandering fluvial channel deposit. The geometrical properties of the fluvial channels are known and can be added as input into this modelling process. The exact position of the channels is however not known, except at the one well location in Delft 03 well. The modelling algorithm therefore places the object first at the well location, and fills the rest of the area with randomly placed objects, that honour the data and total percentages. The studied cores and logs combined with literature are used to determine the statistical distribution of the shape, sizes and orientations of the fluvial channels. The results of the object based modelling of the Lower Delft Sandstone Member can be found in Figure 7-10 and Figure 7-11.

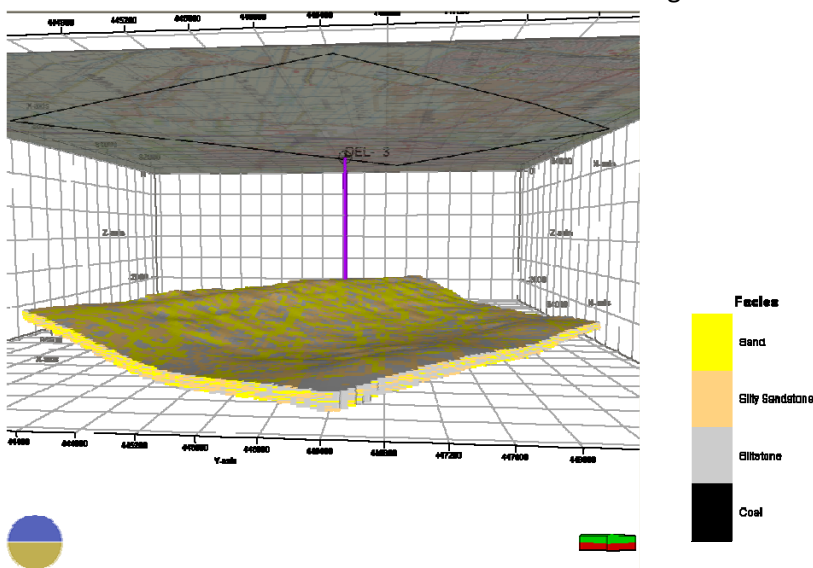


Figure 7-10 Facies model of the Lower Delft Sandstone Member, the single meandering fluvial channels on a background of floodplain deposits with the Delft-03 well. Z is the depth in meters.

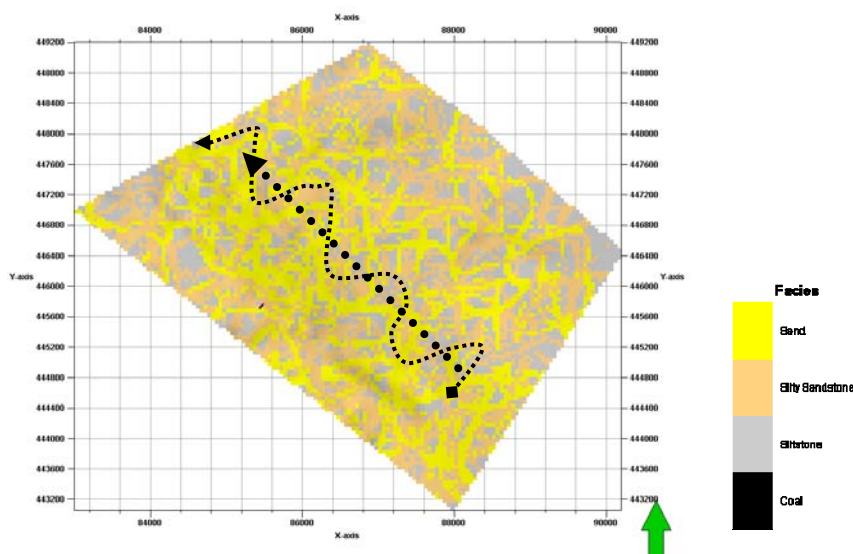


Figure 7-11 Top view of the object based modelled Lower Delft Sandstone Member facies in Petrel. Arrows show the predominant trend line.

Modelling the Middle Delft Sandstone Member zone

The Middle Delft Sandstone Member shows predominantly thin alternating clay- and siltstone bands with thin sandstone deposits and lignite or coal layers. To model this zone the object based modelling method is also used as the facies still contain mostly fluvial deposits. The studied cores and logs combined with literature are used to determine the statistical distribution of the fluvial channels. As the shape, sizes and orientations of the channels are similar to the Lower Delft Sandstone Member deposits the same values for modelling are used here. The result of the modelling is visible in Figure 7-12 and Figure 7-13. The main lithology in this facies is obviously siltstone. Some channels are still populated in this zone, representing an isolated fluvial channel during the deposition of Middle Delft Sandstone Member.

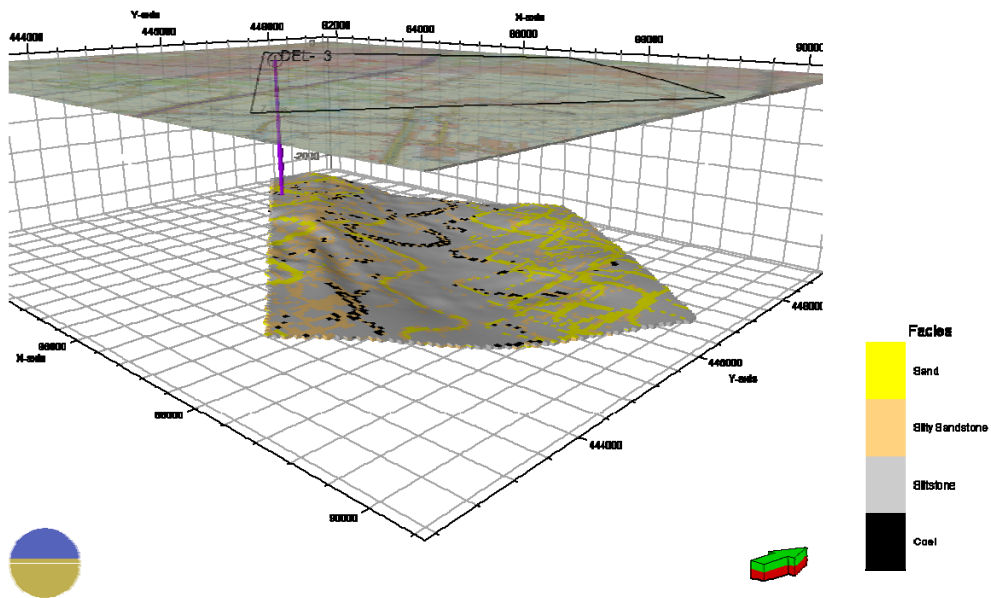


Figure 7-12 Facies model of the Middle Delft Sandstone Member, mostly siltstone deposits with isolated channels and the Delft-03 well. Z is depth in meters.

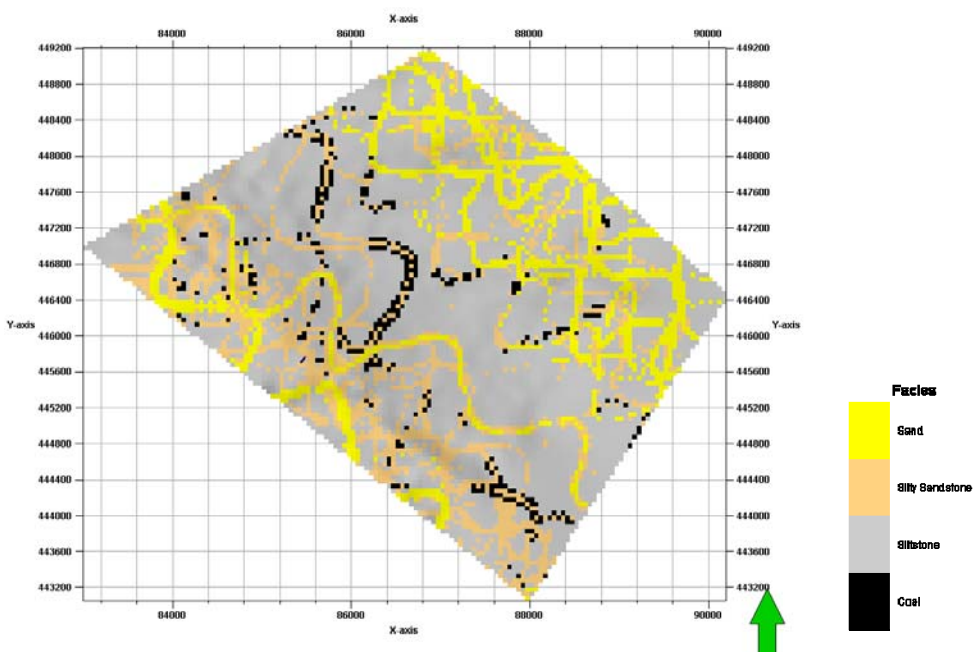


Figure 7-13 Top view of the object based modelled Middle Delft Sandstone Member facies.

Modelling the Upper Delft Sandstone Member zone

To model the Upper Delft Sandstone Member zone the same modelling method as the Lower and Middle Delft Sandstone Member is used. Object based modelling is performed but different parameters are used. The Upper Delft Sandstone Member zone consists of multiple stacked sandstone bodies with almost no floodplain deposits. The geometrical properties of the fluvial channels are similar to that of the Middle and Lower Delft Sandstone Member. The channel thickness and flow direction of the channel belt have the same input values as for the other two members. Only the amount of sandstone and therefore the amount of channels and the background setting are different. The fractions of the lithofacies as found in the log data are honoured. The result of the modelling is visible in Figure 7-14 and Figure 7-15.

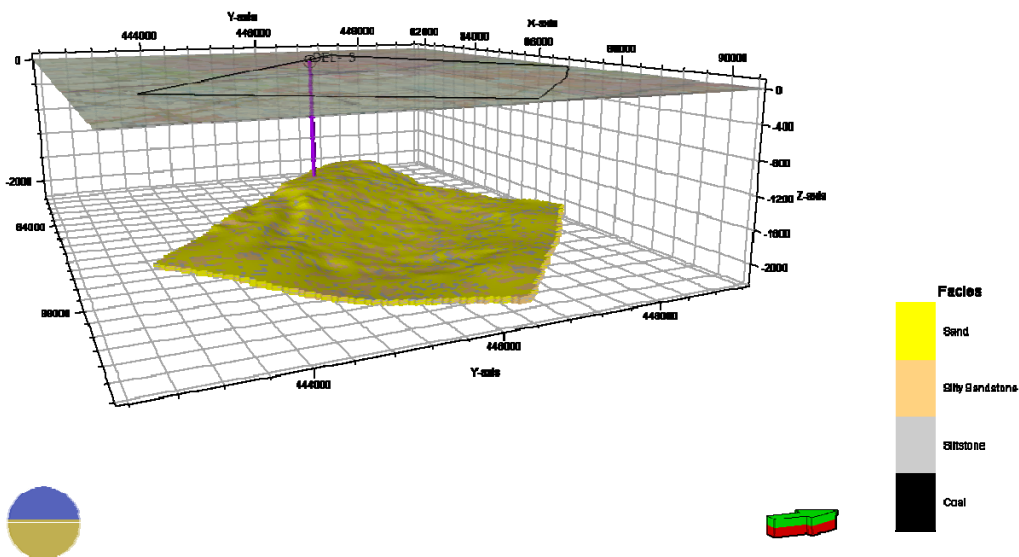


Figure 7-14 Facies model of the Upper Delft Sandstone Member, the multi stacked fluvial channels with the Delft-03 well. Z is depth meters.

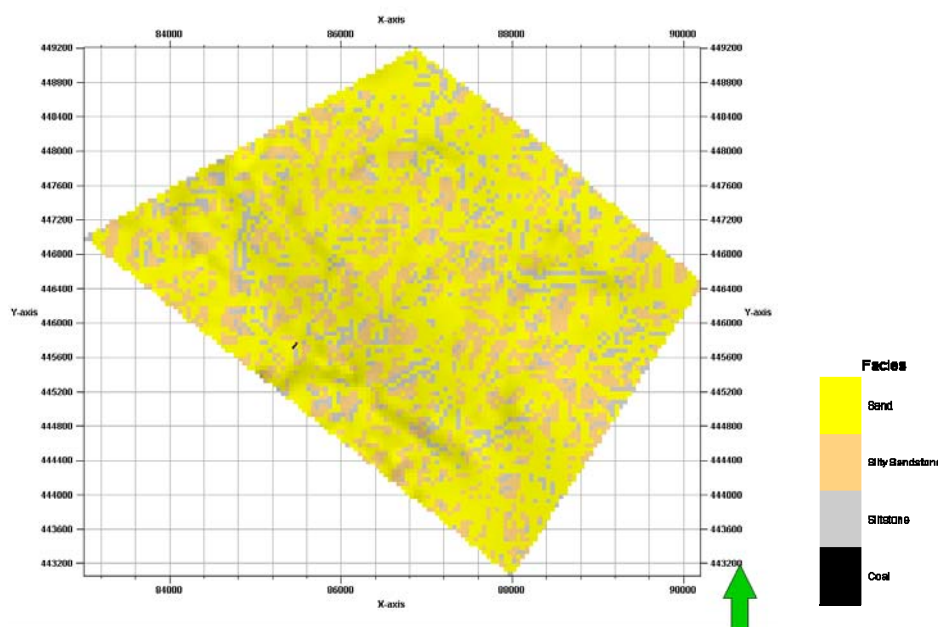


Figure 7-15 Top view of the object based modelled Upper Delft Sandstone Member facies in Petrel.

Facies Discussion

The built facies model represents one realisation of a statically populated 3D grid structure (Figure 7-16). The population gives a 3D insight into the variation and distribution of facies throughout the model. The facies model is based on the depositional setting and the available well data. The only point in the model which is based on real data is in the borehole location of the Delft-03 well. At further distances from this borehole a larger uncertainty exists. This model is based on an object-based modelled fluvial system with input data from the depositional setting and the well log data of the Moerkapelle oilfield. Variations within the lithofacies found in the wells of the Moerkapelle Oilfield were taken into account. The uncertainty caused by the simulation or the interpolation could not be performed due to the lack of data and availability of time. However it can be expected that there is a high level of uncertainty throughout the entire model based on the resolution and amount of available data. The results do however show that with this object based modelling method it is possible to create a structure that upholds both the available data and represent the proposed depositional model. Future modelling of the system with extra wells and additional data should improve the model. It should also be possible to determine the uncertainty and validity of the proposed depositional model. Multiple representations are recommended to gain an understanding of the uncertainty in the model.

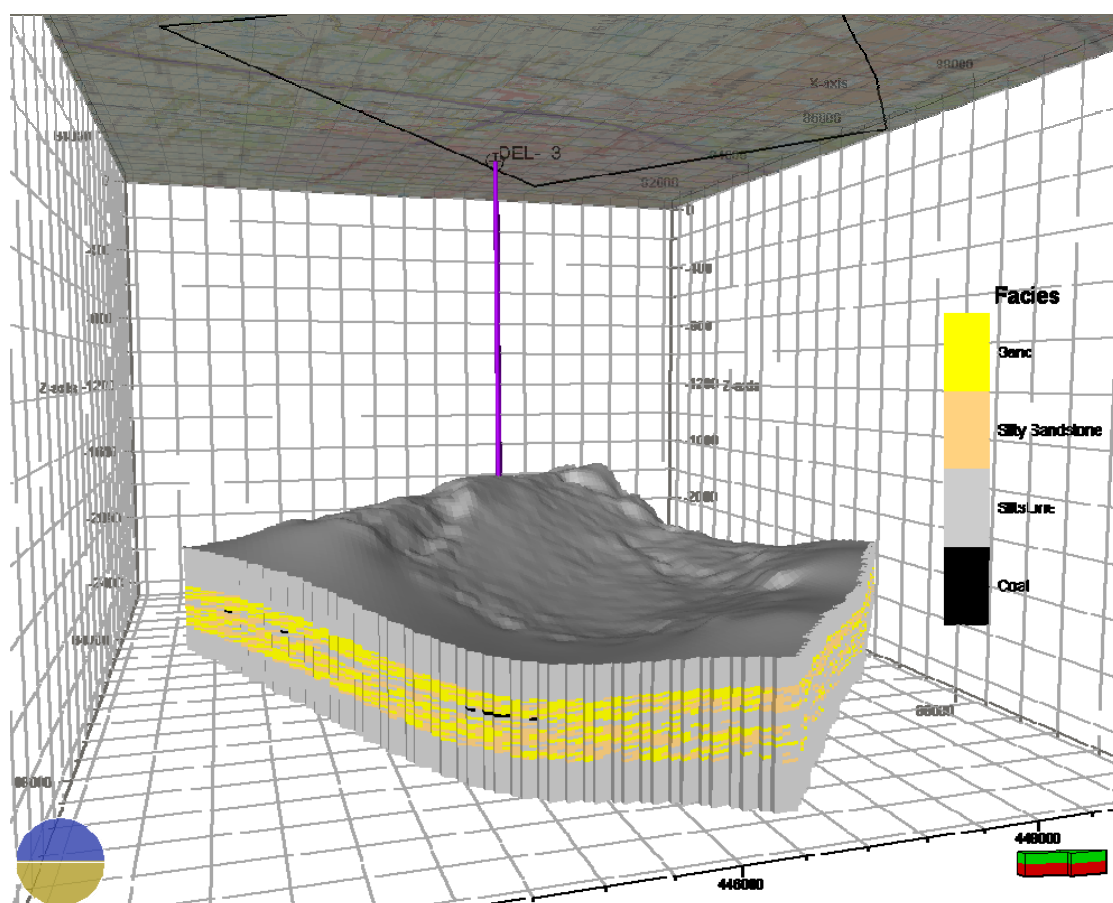


Figure 7-16 3D Side view from the east of the total created facies model with Delft-03 well. The Z to XY ratio is 2:1. So the model is stretched over the Z axis two times.

7.4. Adding the petrophysical properties to the static model

The petrophysical properties are added to the static model to give it its flow characteristics. This is done by conditioning different properties based on well log data to different facies in the model based on the core to well log correlation. As each cell within the static model has a number of defined flow characteristics this will be further referred to as the defined static model. The created defined static model can be used for volume calculations and flow modelling. The petrophysical properties are added to the static model by using Petrel. A full list of the used petrophysical data and equations can be found in chapter 6 including the variation and error margins used.

Upscaling the wells

By upscaling the well information it is possible to fit the data of the wells to the grid size of the model. There are different methods of upscaling. The method used for the porosity upscaling is the “Arithmetic” method. The upscaling method used for the permeability is the “Harmonic” method (Figure 7-17) and are explained in appendix H.

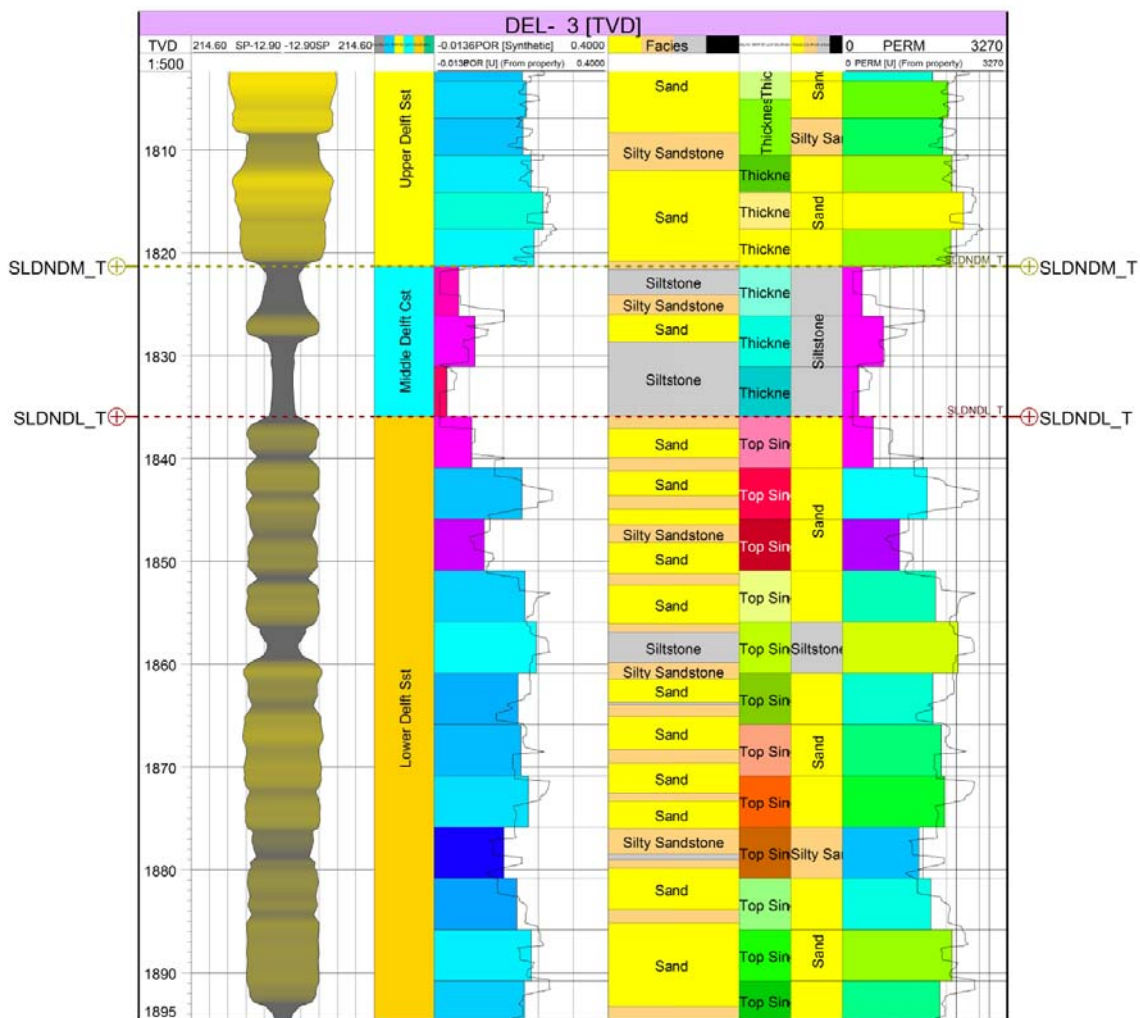


Figure 7-17 The Delft-03 well with the Middle and Lower Delft Sandstone Member with from left to right the Mirrored SP log, the zones, porosity log (line), upscaled porosity log (blocks), facies log, layers of the model, upscaled facies log, horizontal permeability log (line), and the upscaled permeability log (blocks) respectively.

Property based modelling,

The petrophysical properties that are assigned to the static model to create the defined static model are the porosity, the horizontal permeability and the vertical permeability. After upscaling the well log data, the scaled up well data is combined with the static model in Petrel. All cells will be given a petrophysical property value weighed to the facies in that grid cell. The calculation of the property value at each cell in the 3D grid is based on the input well data and the lithofacies in that grid cell. The method used to determine the value for each facies is the Sequential Gaussian Simulation (SGS) (stochastic) method as this honours the well data, the input distributions, variograms and the trends (Petrel 2009). The process of the variogram and distribution used to create local variations, even away from the input data, can be found in appendix F. If no variogram or input data is available from well data the average value for that facies is assigned. Each facies in the upscaled well data matches a number of petrophysical data points. The data combined with its variation is used to determine values for other cell with the same facies of the same formation. The variation within the petrophysical data is used to determine the variation in values for other cells with the same facies. Hence each cell with similar facies will have different values within the variation of the measured or derived petrophysical data. The cells of the Ablasserdam Member and Rodenrijs Claystone Member are not assigned in detail as they are not the target of this study. However by assigning a set value to the entire Ablasserdam Member and Rodenrijs Claystone Member in the static model, the members still receive thermal flow characteristics which can be used in the thermal flow modelling. This is done so that the Ablasserdam Member and Rodenrijs Claystone Member representing the top and base of the static model, can still conduct heat. The created 3D porosity, horizontal and vertical permeability defined static models can be found in Figure 7-18, Figure 7-19 and Figure 7-20.

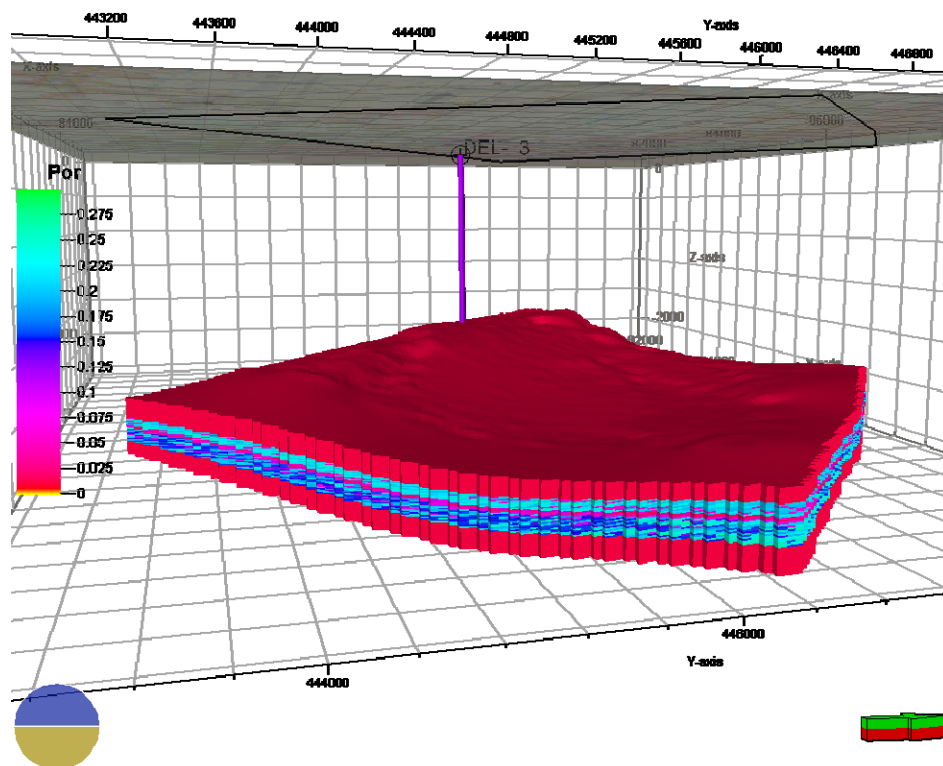


Figure 7-18 The created porosity model with the Delft-03 well. Z is depth in meters.

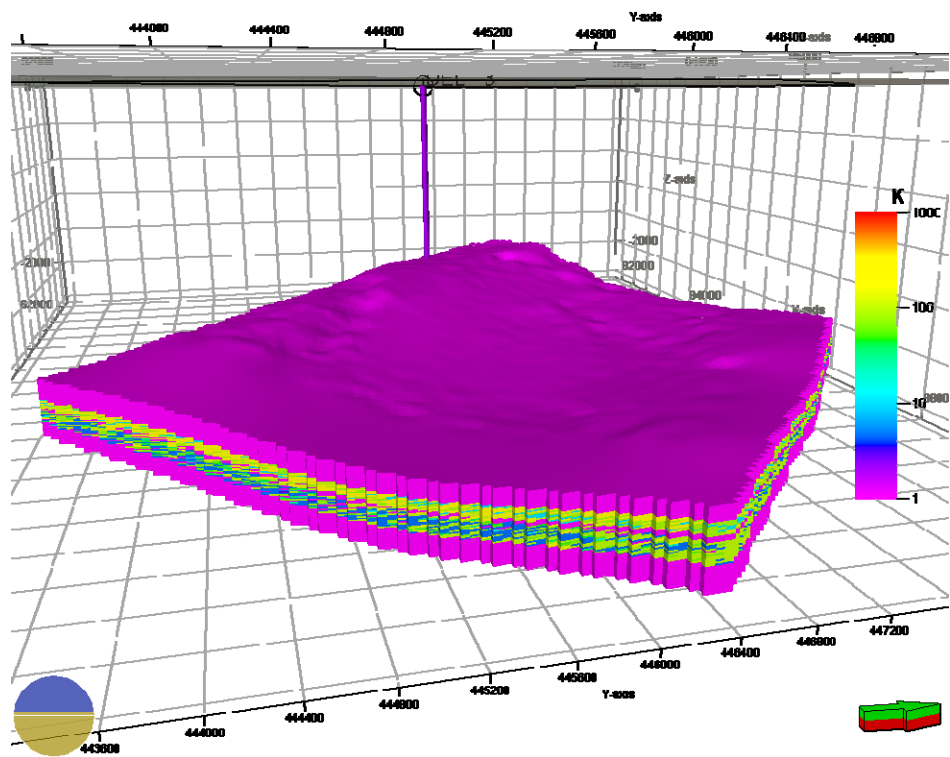


Figure 7-19 The 3D Horizontal permeability with the Delft-03 well. Z is depth in meters.

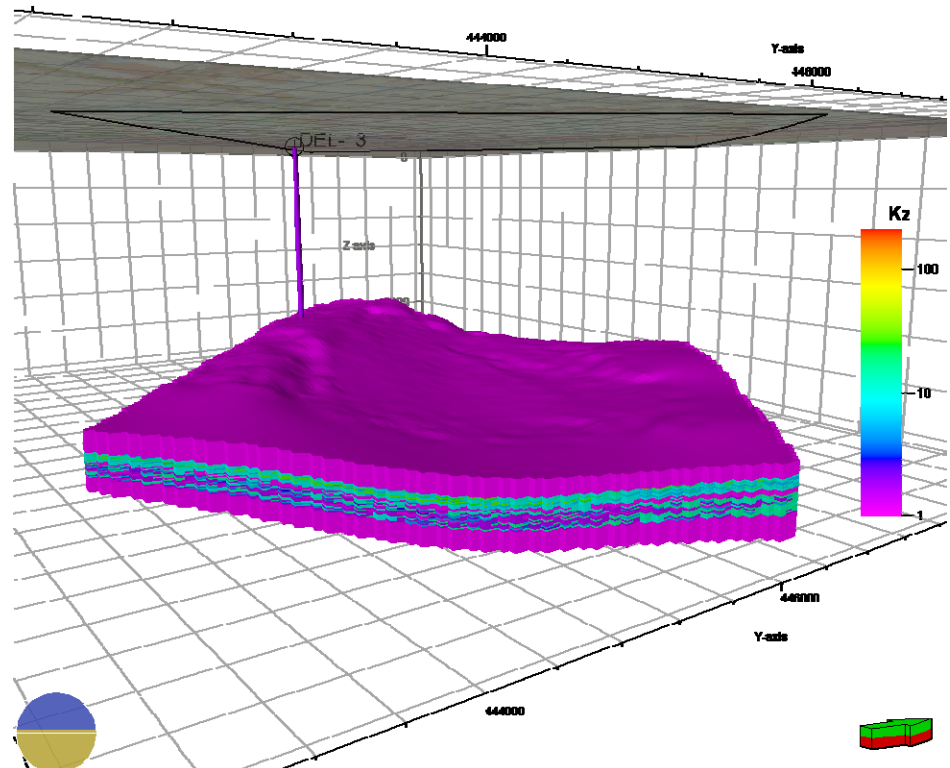


Figure 7-20 The 3D vertical permeability assigned static model with the Delft-03 well. Z depth (m).

The graphs on the next three pages show how a petrophysical property is distributed throughout the cells in comparison with the original distribution of the derived data and derived upscaled data (Figure 7-22, Figure 7-23, and Figure 7-24). Because of lack of time only one realisation could be made of each 3D population of the static model with a property. Multiple realisations would give a better insight in the result of the method used, as this one realisation does not give enough data to do a full uncertainty analysis. The created static model with the flow characteristics defined, can be used for flow modelling and volume calculations. The porosity and permeability have been weighed to the facies (Figure 7-21). The variation of assigned petrophysical values within one facies is based on the distribution found in the well logs. This can clearly be seen in Figure 7-21 picture C by the large colour differences.

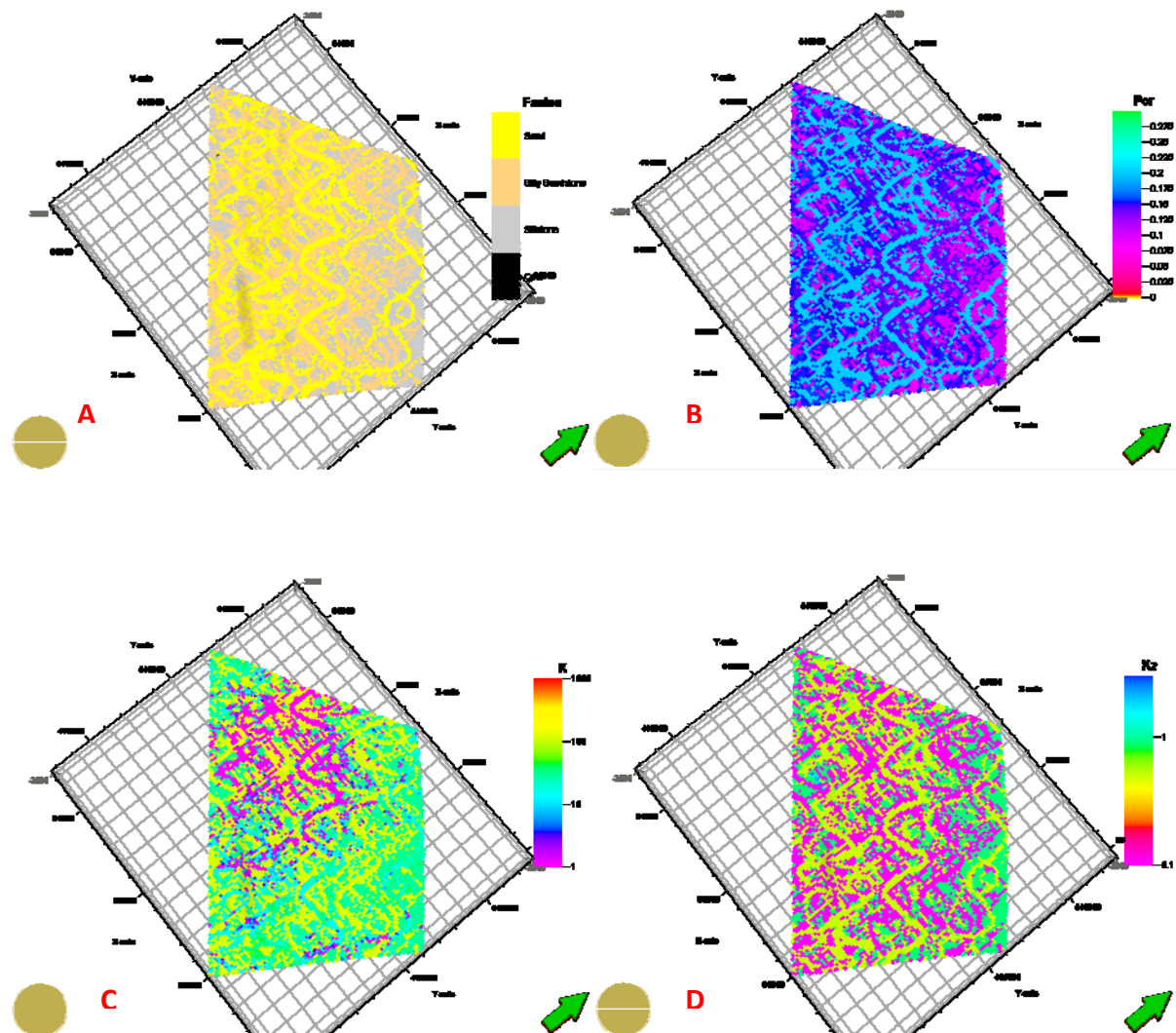


Figure 7-21 An internal layer of the Lower Delft Sandstone Member with A) facies B) porosity C) Horizontal Permeability D) vertical Permeability

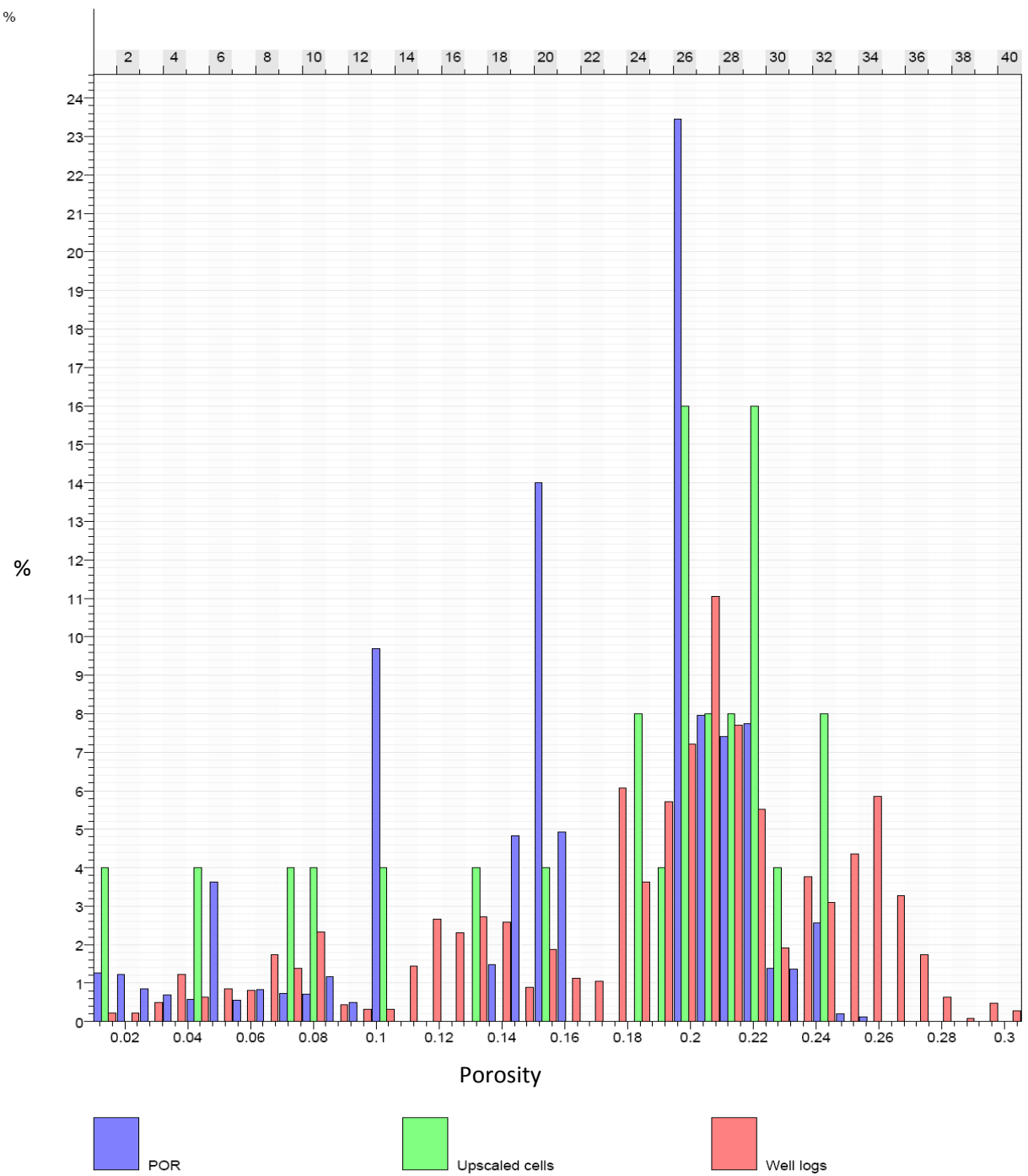


Figure 7-22 Graph showing the distribution in % of the porosity assigned static model (POR), upscaled well logs and the porosity in the well logs.

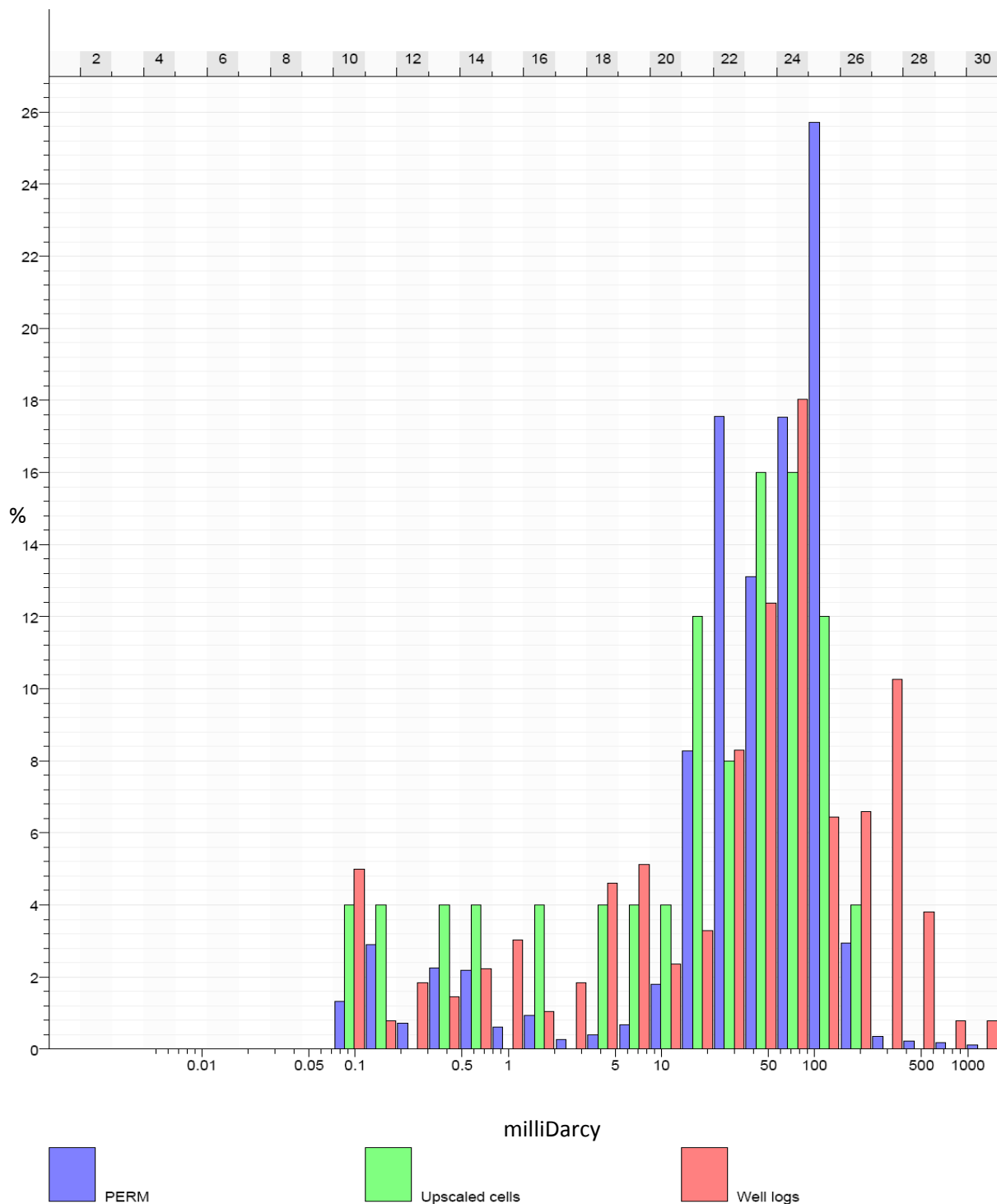


Figure 7-23 Graph showing the distribution in % of the derived horizontal permeability in the assigned static model, upscaled well logs and the permeability derived well logs (Perm). (the MDarcy scale is logarithmic.)

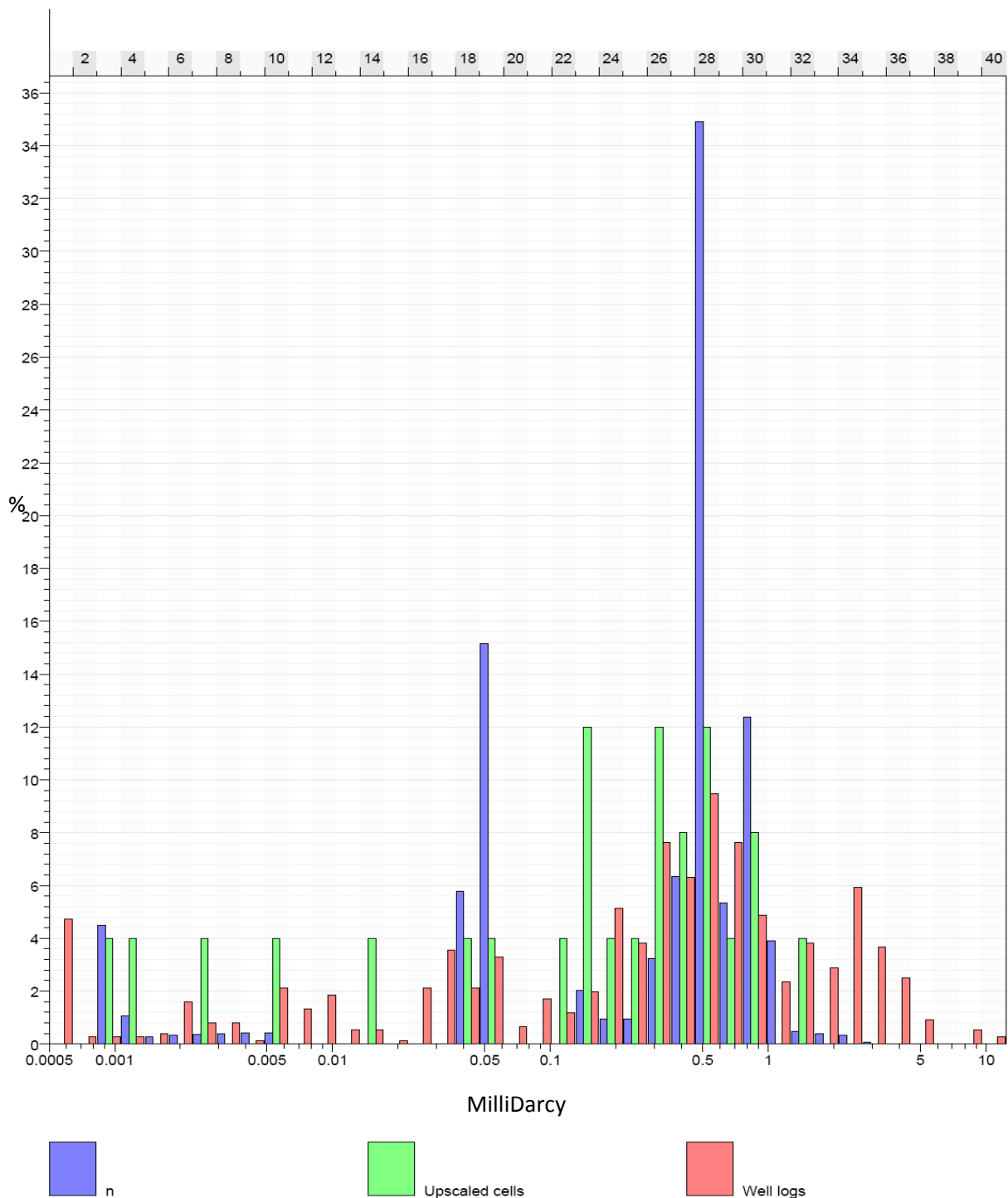


Figure 7-24 Graph showing the distribution in % of the derived vertical permeability in the assigned static model, upscaled well logs and the permeability derived well logs (Perm). (the mDarcy scale is logarithmic.)

8. Dynamic flow and temperature modelling

To determine the effect of heterogeneities on the fluid and temperature flow a 3D dynamic flow model needs to be built of the target area Vrijenban. The model will also give insight in the interference of different geothermal systems. Fluid flow modelling is used to create a representation of fluid flow behaviour in a reservoir. To build a temperature and flow model, Schlumberger's Eclipse and Petrel software are used. Both software packages have been designed for the oil industry. In this case both programs are used to do flow modelling in the static model with defined flow characteristics of the Vrijenban Target area. First an overview of the workflow is given followed by the volume calculations and the building of a fluid flow model. Then a temperature model is created to determine the effect of temperature and fluid flow by geothermal systems. Finally the results and uncertainties are discussed.

8.1. Work flow

The work flow used to build the dynamic temperature and fluid flow model consists of three phases. First a volume calculation is performed to determine the size of the defined static model and the amount of pore space. The second phase consists of adding the fluid properties, the rock physics function and the saturation profile to the model. This procedure is finalized by adding and setting up the production and injection wells. Fluid flow behaviour modelling can then be performed in Eclipse 100 determining the fluid flow behaviour and the pressures in the modelled reservoir. After this, the dynamic temperature flow modelling can be created adding to the fluid flow behaviour model a temperature flow model. By building a static 3D temperature profile and simulating temperature flow a dynamic temperature model is created. This is done by adding temperature data to the injection water and running additional temperature flow processes when simulating the flow behaviour. The temperature flow process calculates the effect of thermal convection and conduction (Figure 8-1). The dynamic temperature flow model is now finished and simulations are run to determine the effect of the heterogeneities on temperature flow. This is done by comparing the simulation results with a created homogenous model. Further the effect of the conductivity is studied and discussed.

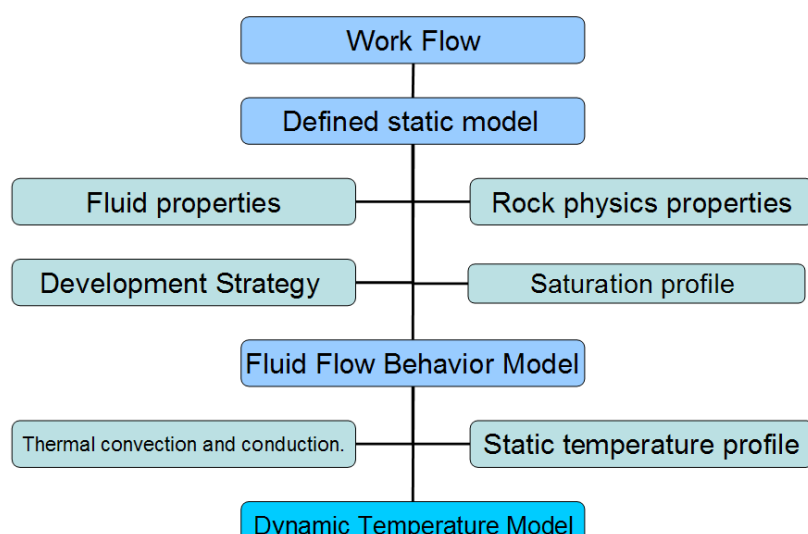


Figure 8-1 Workflow used in this study to build 3D property models for dynamic flow modelling.

8.2. Volume calculation

To determine reservoir dimensions the size and volume needs to be calculated. The bulk and the pore volume are calculated by using Equation 8-1. The input data consists of the created defined static model. The Alblasserdam Member and Rodenrijs Claystone Member are not taken into account and are set as non reservoir. The Net is set for the volume calculation as the discrete “Sandstone” and “Silty sandstone” facies. The calculated bulk volume, net volume and pore volume are shown for each zone and the total reservoir in Table 8-1. The net pore volume can also be visualised in 3D (Figure 8-2).

$$(V_n), \text{Net Volume} = (V_b) \text{ Bulk Volume} * (N/G) \text{ Net over Gross}$$

$$(V_p), \text{Pore Volume} = (V_n) \text{ Net Volume} * (\phi) \text{ Porosity}$$

Equation 8-1 The equations used to calculate the Net Volume and the Pore Volume.

Case	Bulk volume	Net volume	Pore volume
Zones	[*10 ⁶ m ³]	[*10 ⁶ m ³]	[*10 ⁶ m ³]
Rodenrijs Claystone Member	1993	0	0
Upper SLDND	1069	933	200
Middle SLDND	476	175	30
Lower SLDND	1947	1520	241
Alblasserdam Member	2084	0	0
Total	7569	2628	470

Table 8-1 The calculated bulk, net and pore volume of one modelled realisation of the Delft Sandstone Member.

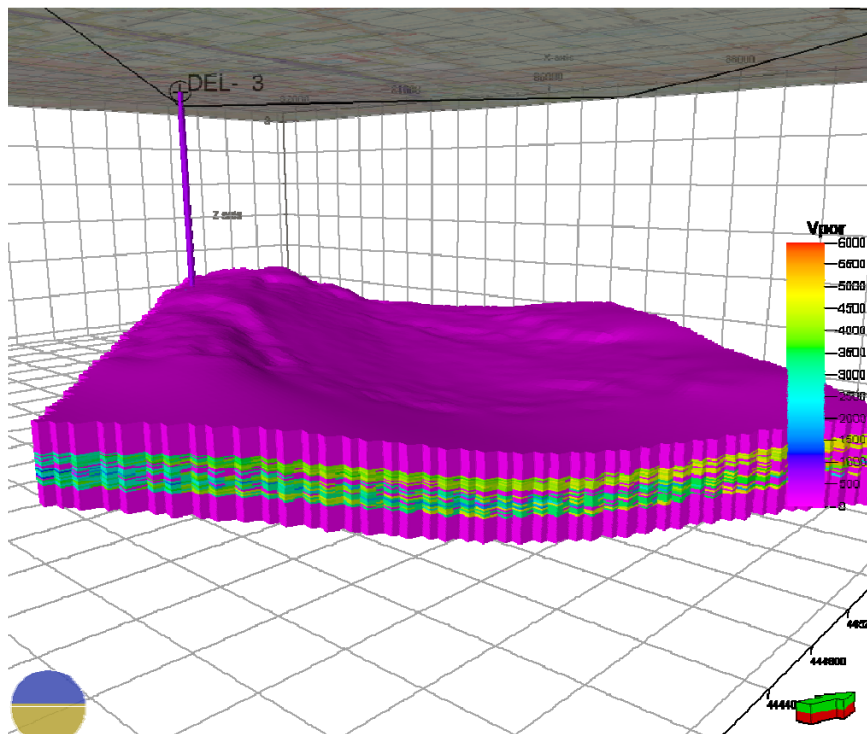


Figure 8-2 Visualised 3D model of the pore volume, the colours represent the pore volume in m³.

8.3. Fluid flow modelling

By fluid flow modelling it is possible to create a representation of fluid flow behaviour. For example a flow case or flow simulation case that models the flow behaviour between two wells in the created defined static model. Defining a simulation case consists of specifying the input properties and selecting predefined initial conditions. By adding a fluid model, rock physics functions, and a development strategy a simulation can be performed. The simulator used in this study is Eclipse 100 2007.1 running from the Petrel 2009.1 interface. The initial input data consist of the porosity model and the horizontal and vertical permeability models see paragraph 7.4. Three functions are added into the model. The Rock Compaction function is created with the “Rock physics” method to represent the effect of the formation rock during flow simulation. It calculates the effect of compaction and adjusts the porosity accordingly. Further the relative drainage curve is added as a saturation curve, representing the water saturation. Finally the “black oil function” is imported which adds the formation fluid properties, the initial pressure in the model, and the amount of phases to the simulation case. The input data and the process of the rock compaction function, formation and fluid properties can be found in Appendix G. Now the reservoir is set and a development strategy is needed to determine the simulation time, the pressure and the amount of fluid flow in the model.

Development strategy, a geothermal doublet, the wells

Development strategies are used to determine which wells will produce or inject and at what rates and pressures the wells will flow. The strategy also determines the flow time simulated in the case. It is possible to apply a constraint to a group of wells, or different values of constraint to individual wells. The development strategy is imported into the model using the “Make development strategy” simulation tool in Petrel. The input data consists of the amount of production and injection wells and the well parameters. Other input consists of the constraints of the wells and the duration in time of the simulation case and can be found in appendix G.

The common design of a geothermal system in the West Netherlands Basin is a so called a geothermal doublet. A geothermal doublet contains one injection and one production well. The hot water is produced from the production well and then cooled down and re-injected using an injection well. This means that the outflow of the production wells equals the inflow of the injection well. The distance between the injection and production wells is set at 1500 meters. The design is further determined by the life time and the total heat production of a system. A geothermal doublet is designed to produce and inject an average 3600 cubic meters of formation fluid per day for 30 years with a maximum pressure difference of 35 bar (DAP, 2008; Grobbelen et al., 2009; Smits, 2008).

In the target area, three parties intend to drill one geothermal doublet each. Therefore in the simulation case, three injection wells and three production wells are simulated. Each production well will be open for a period of 30 years as this is the life expectancy of each system. The wells will produce or inject 3600 cubic meters per day if not constrained by reservoir pressure through well restrictions. The pressure constraints used in the simulation is maximum 35 bar pressure difference over the injection and production well at the initial bottom hole pressure (Grobbelen et al., 2009). The three doublets are named doublet A, B, and C respectively. Doublet A will start producing and injecting at the start of the simulation. Doublet B will start producing and injecting a year after doublet A has started. Doublet C will start in the third year of simulation, two years after doublet A and one year after doublet B has started (Table 8-2).

Doublet	Type	Coordinate		Start Date	End Date	Initial rate m3/day	
name	of well	X	Y			Production	Injection
A	Production	88417	447205	1-6-2010	1-6-2040	3600	
A	Injection	87387	448244	1-6-2010	1-6-2040		3600
B	Production	87750	445700	1-6-2011	1-6-2040	3600	
B	Injection	89164	445922	1-6-2011	1-6-2040		3600
C	Production	86500	446850	1-6-2012	1-6-2040	3600	
C	Injection	85100	446175	1-6-2012	1-6-2040		3600

Table 8-2 Doublet names, the well names, the type of well, locations, the start and end date and the simulated rate of production and injection of all 6 wells in the Vrijenban area.

During the simulation case all wells will be vertical wells and the well are simulated to be open hole over the entire Delft Sandstone Member. Therefore the depth in the well and the thickness vary per well as it encounters the Delft Sandstone Member at a different location. Each well is placed so it encounters a complete sequence of Upper, Middle, and Lower Delft Sandstone Member (Figure 8-3). Each doublet will be constrained to inject the same amount of formation fluid that is produced by using a group control in the simulation.

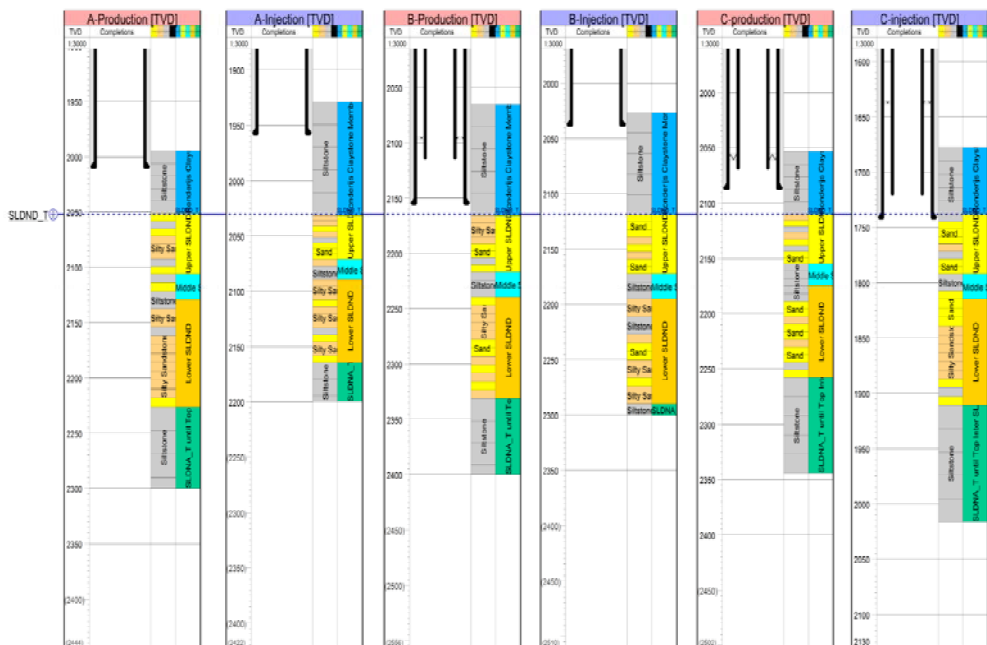


Figure 8-3 Cross panel showing the A,B and C injection and production wells with the model facies found in the well and the zones representing the formation members. The black lines are a schematic representation of the well.

The 3 doublets (6 wells) are placed throughout the reservoir with each pair representing a theoretical doublet. Not one of the locations represents a designed doublet by one of the parties. Each doublet has a distance of 1500 meters between the injection and production well. No two doublets are placed within a closer range of 1500 meters of each other (Figure 8-4 and Figure 8-5). An overview of the created development strategy can be found in appendix G.

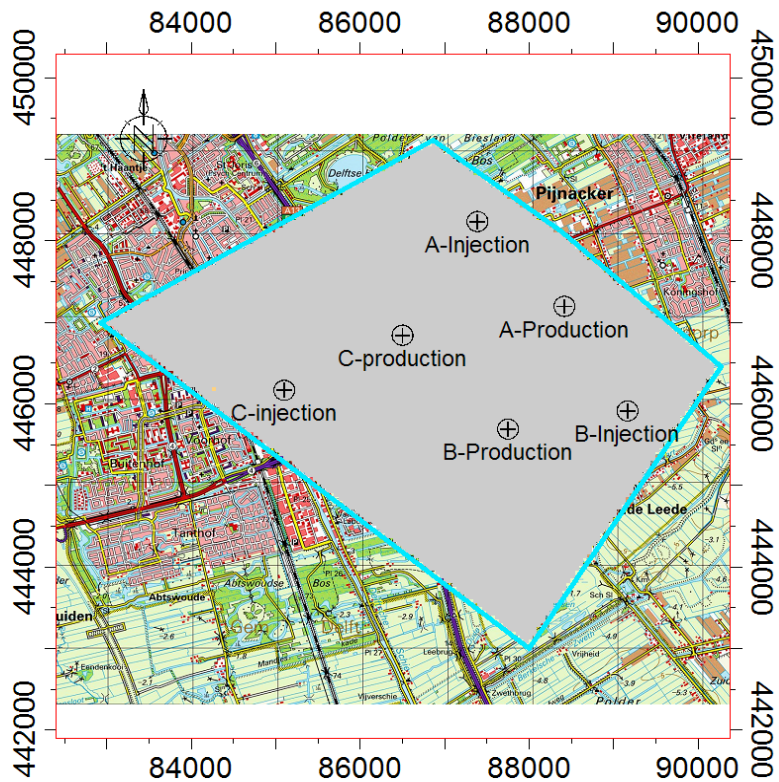


Figure 8-4 Map of Delft and the well locations in the model scale 1:50000.

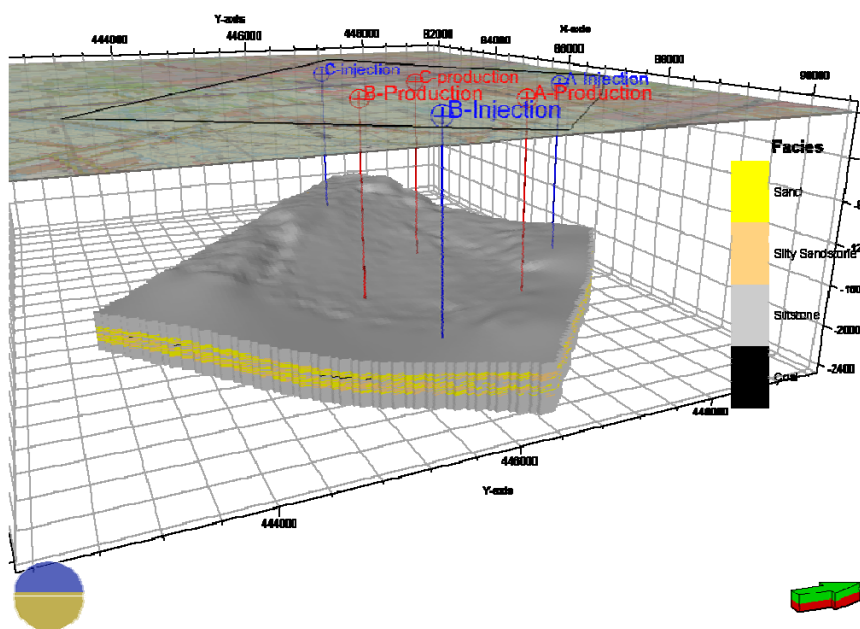


Figure 8-5 A 3D view from the southeast of the facies model with the 6 vertical wells.

Flow behaviour simulations

To determine the effect of interference in the reservoir of different doublets, a simulation case of the flow behaviour in the reservoir model is needed. All the input parameters are now set and the flow simulation are performed in Eclipse 100 version 2007.1. Eclipse 300 is a numerical simulator and uses the “fully implicit” method to determine the numerical solutions of the radial Darcy flow equation and flow simulations. The flow models are based on a black oil model (Eclipse, 2007). No aquifer or, aquifer support is modelled or used during the simulation. All sides of the model are closed so no flow goes in or out at boundaries of the model. The output data and results consist of the flow rates and total volume of production and injection of each well, doublet and the field. Furthermore the pressures are calculated throughout the field and in the wells. The results of one simulation case with all the input presented in this chapter in shown in Figure 8-6 and Figure 8-7.

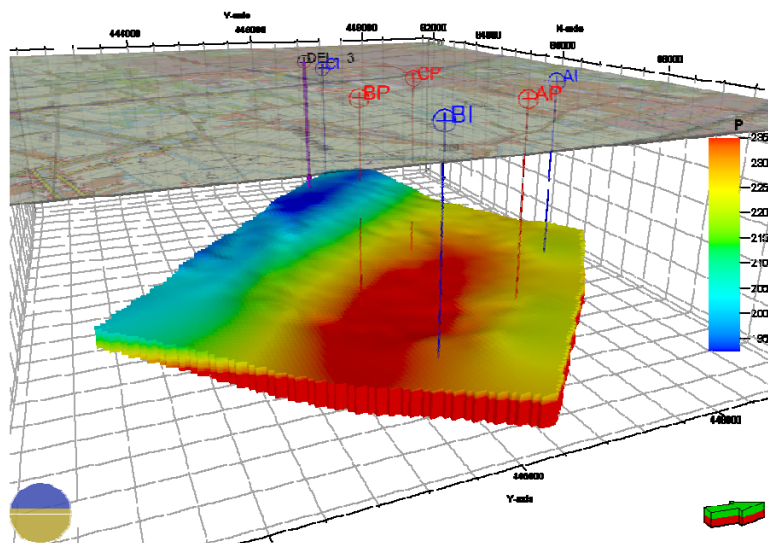


Figure 8-6 3D view from east of the pressure in the Middle and Lower Delft Sandstone Member and Alblasserdam Member at the start of simulation, T = 01-01-2010.

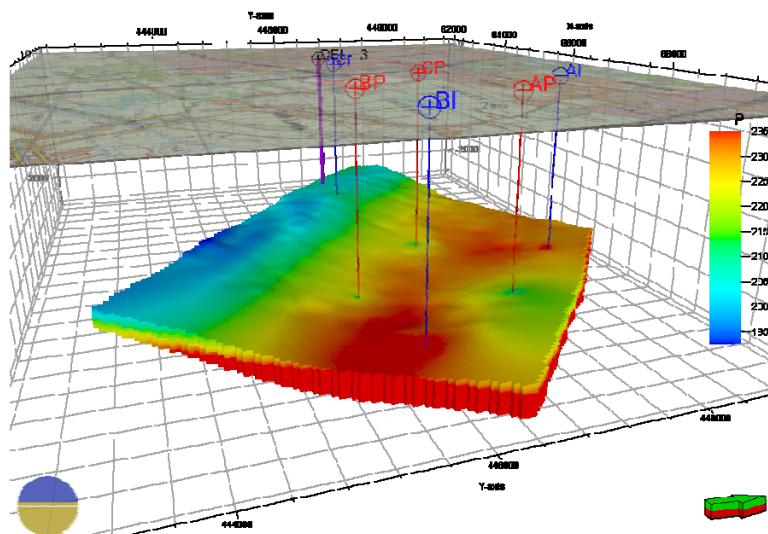


Figure 8-7 3D view from east of the pressure in the Middle and Lower Delft Sandstone Member and Alblasserdam Member. After 5 years of running the simulation case with 3 doublets at full production, T = 01-01-2015.

8.4. Flow behaviour simulation results

The results of the simulation case run show that none of the three doublets A, B, and C, reach their target production and injection rates. The injection rates are far lower than the set 3600 cubic meters per day as the injection wells are constrained by the bottom hole pressure. The injection wells are constrained during simulation at the bottom hole pressure by a set value of 35 bar higher than the initial reservoir pressure in the well (Figure 8-8).

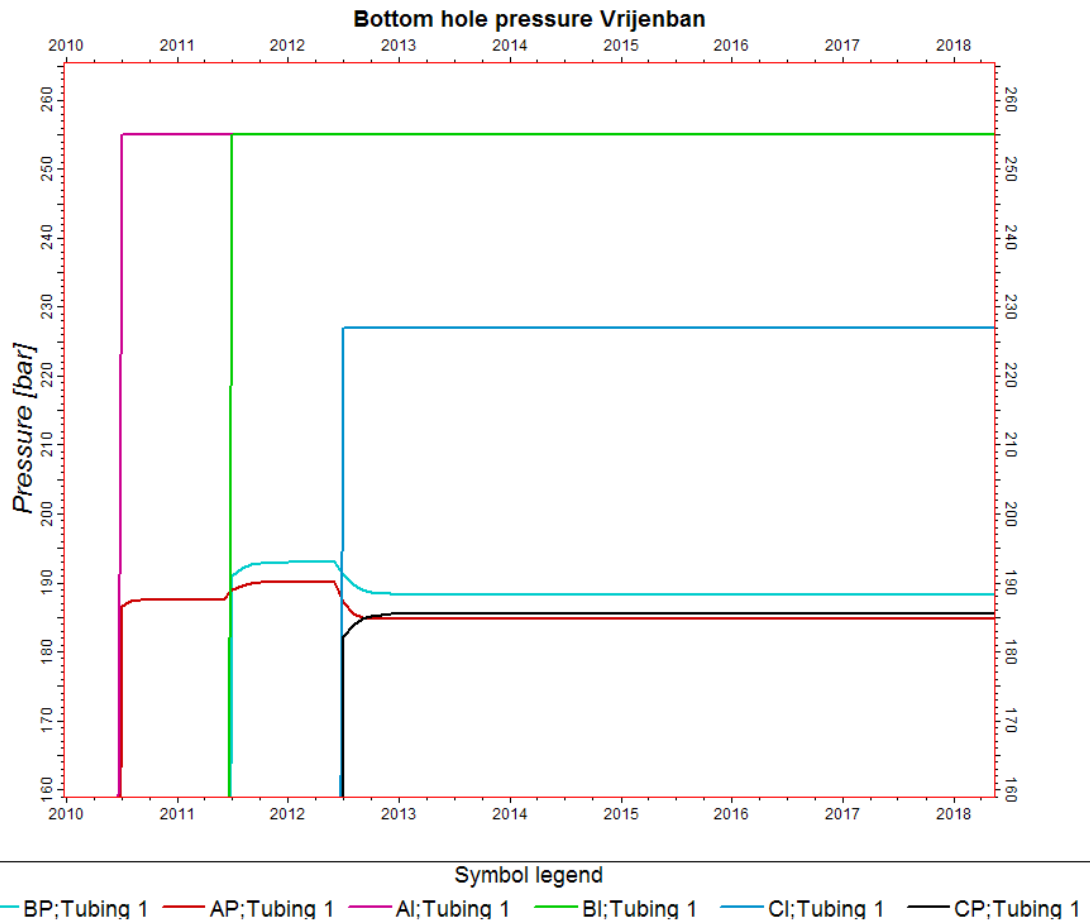


Figure 8-8 Bottom Hole Pressures of the A, B, and C I=injection and P=production wells.

This is related to the design of a geothermal doublet. The amount of water that can be injected based on a Darcy equation is related to the set permeability- and pressure difference between the reservoir and the well. The bottom hole pressure increases when water is injected if the permeability or thickness of the injection zone is not large enough. During simulation the injection wells reach the maximum bottom hole pressure and are constrained. As a result of this pressure constraint the flow rate is adjusted to the maximum injection rate possible at the pressure difference in the reservoir (Figure 8-9).

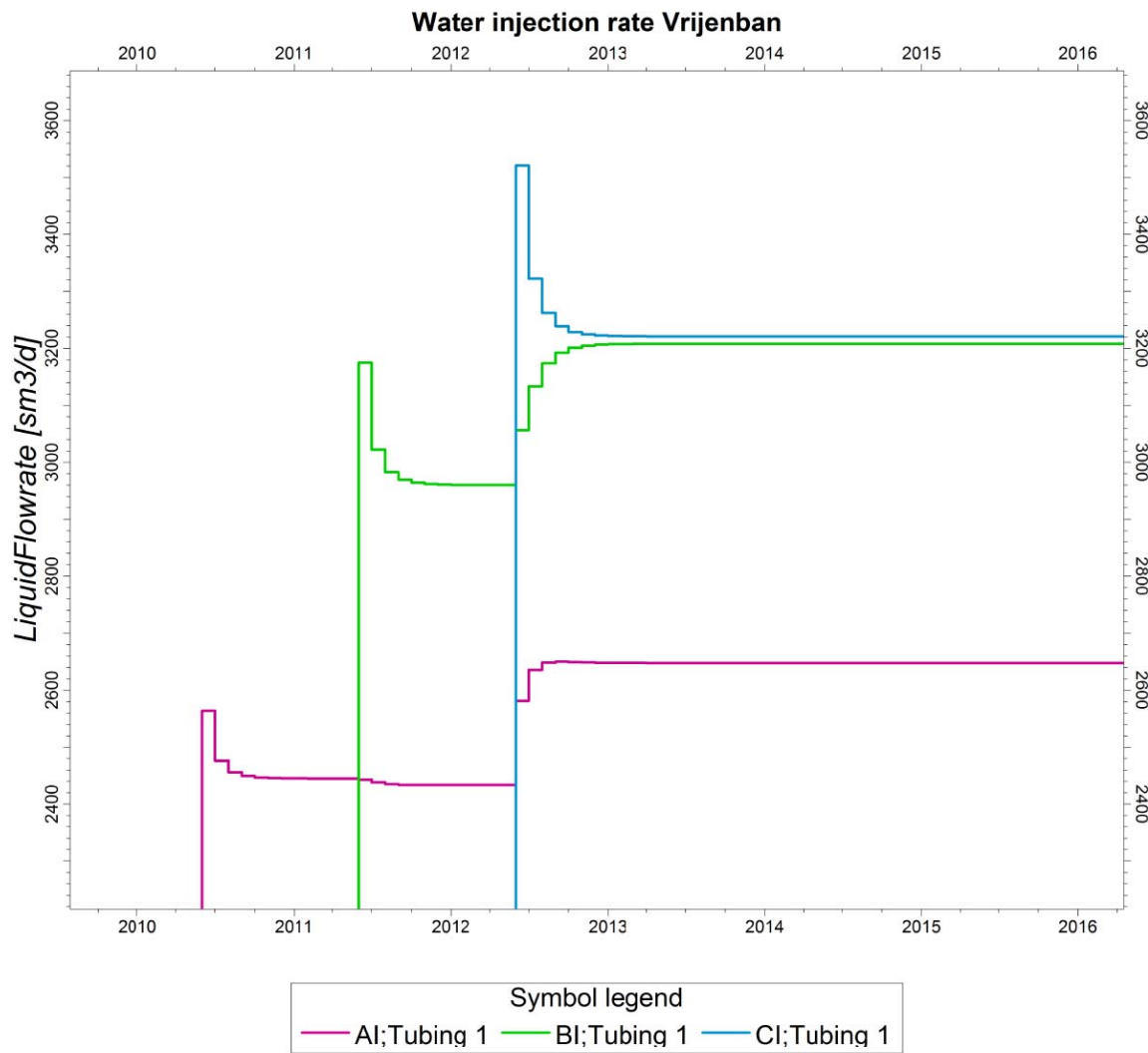


Figure 8-9 Injection in the A, B and C injection wells. The high peaks at the start represent the flow rates before the pressure constraints are reached.

The production rates were set as 3600 cubic meters per day but the doublet produced far less (Figure 8-10). In the simulation case the production wells are constrained by the amount of fluid that is injected as in a geothermal doublet the production well is connected to the injection well. The lower production rates are caused by the constraint that the injection well cannot inject more produced water. All three doublets do show large differences in the production and injection rates. This is caused by the created variation in thickness and permeability in the static model. As only one realisation of the defined static model is used the uncertainty of the flow rate cannot be calculated. But previous work has been done on calculating productivity variation of the Delft Sandstone Member from petrophysical well data (Smits, 2008; Grobbelen et al., 2009). The results of production data of this study are within the probability of the productivity of the Delft Sandstone Member.

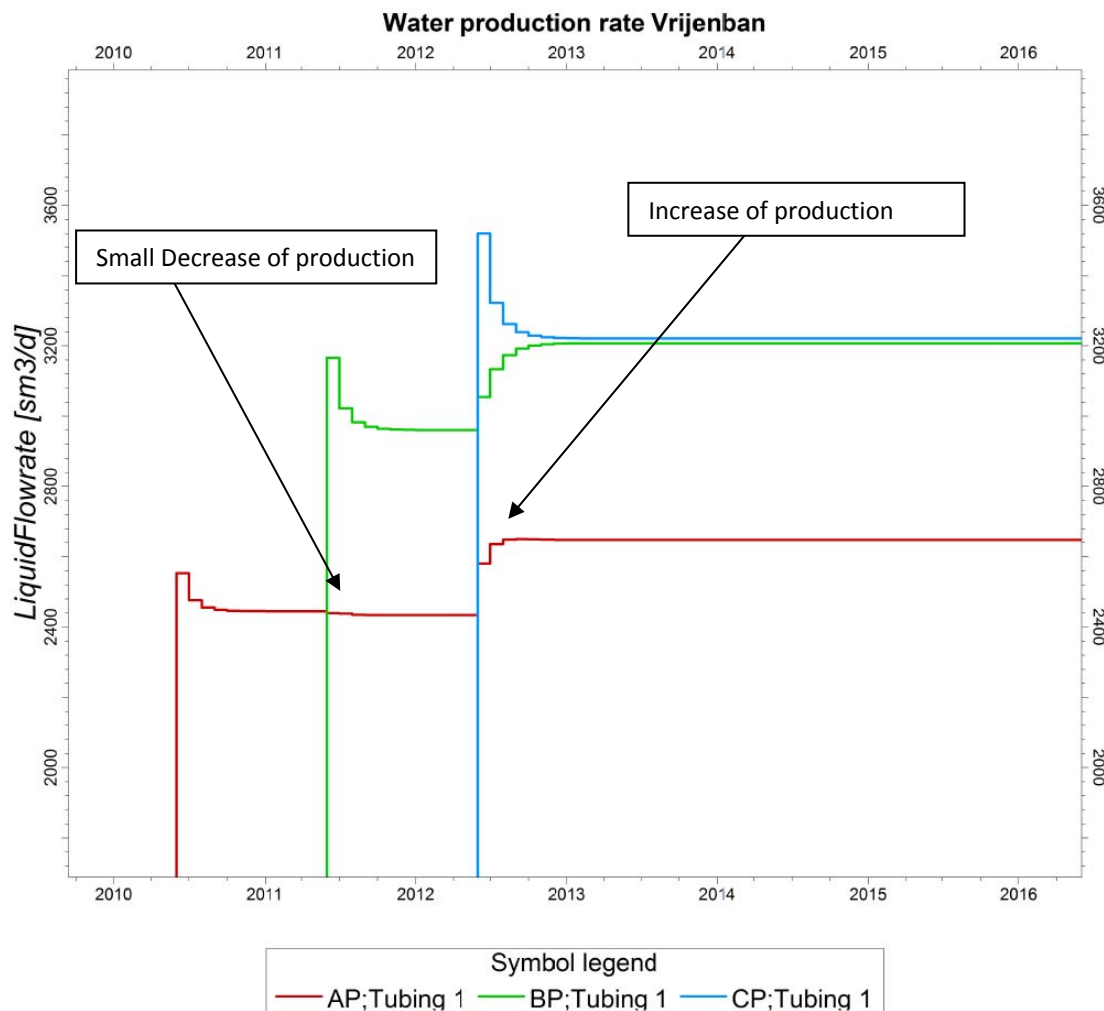


Figure 8-10 Production from A, B and C production wells.

One of the key targets of this study was to determine the presence of interaction and interference of flow from geothermal doublets in one reservoir. The results clearly show that pressure interference occurs between doublets. When studying the production rate curve of injection well A it shows the negative and positive impact of interference (Figure 8-10). The rate of production is the rate on injection. The rate of injection of injection well A is declines after doublet B has started production and injection. This is caused by pressure interference from doublet B, raising the pressure at well A and constraining the injection volume at doublet A. Doublet B has therefore in this simulation a negative impact on the production and injection of Doublet A. The rate of injection of Doublet A and Doublet B increase rapidly at the moment Doublet C start production and injection. This is caused by the production well of doublet C that creates a lower reservoir pressure at the injection wells of doublet A and B increasing the injectivity.

8.5. Heat flow modelling

To determine the effect of heterogeneities on temperature flow a temperature flow simulation can be performed in a therefore adapted defined static model. The temperature option in Eclipse enables the option to simulate temperature effects, for example the injection of cold water into a hot reservoir. The major effect of temperature changes in the vicinity of a cold water injection well is cooling the formation. In addition, changes in the reservoir temperature will possibly change the temperature of the produced formation fluid in time. The “Temperature” option in ECLIPSE 100 is an energy conservation equation. This equation is solved at each converged time step, and the grid block temperatures are updated. The new temperatures are then used to calculate the rock and water properties for the subsequent time step. In the simulation case, the rock and all fluids in a grid block are assumed to be at the same temperature. To start temperature modelling a static temperature profile of the reservoir needs to be created. A temperature model is created by multiplying the depth of a cell to the thermal gradient equation as stated in paragraph 6.5. The results of this shown in Figure 8-11.

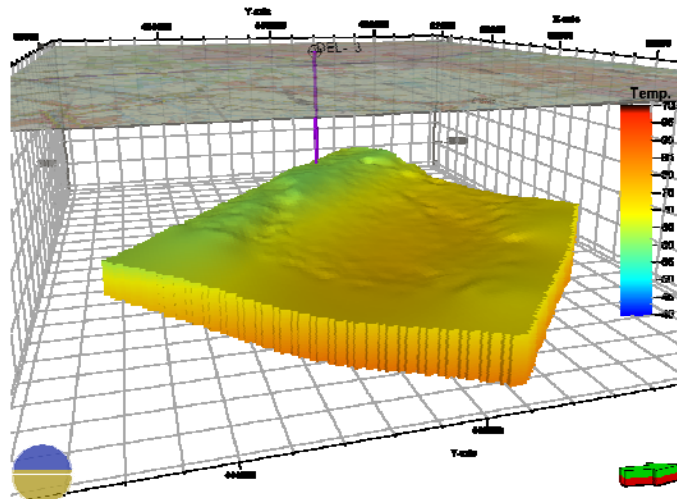


Figure 8-11 3D side view of the static temperature model at the start of the simulation. The temperature of each cell is the calculated by the thermal gradient times the average depth of the cell block.

The temperature option is added to the Eclipse program to allow the modelling of the temperature and the effects of cold water injection. The input consists of the thermal properties, the heat capacity of the rock and the fluids, and the injection temperatures which are set per well. The fluid specific heat is added as a function of the temperature. The energy conservation equation in Eclipse calculates both the thermal convection and the thermal conduction. For this the thermal conductivity of the rock is added. During the simulation it is set that no heat loss to and from areas outside the reservoir model can occur. The expected heat losses at the four sides of the model will not be significant as it is not a large surface. However the heat flow from top and base is considered significant and therefore important. To model the effect of the above and below lying formations on temperature flow the reservoir model is extended by including the Rodenrijs Claystone Member and the Albllasserdam Member. Thermal influx from the core of the earth is not taken into account but could be added in future studies. The radiation of heat is also not taken into account because it will have a minimal effect (Smits, 2008).

The temperature of the injection water

A geothermal system will by utilising the heat from the produced formation fluid by cooling it down. How far it will cooled down will depend on the operator of the system, the heat demand at surface, the season of the year and on the temperature of the produced formation fluid. The cooled down water can have a temperature ranging from 20 to 80 degrees Celsius. In the design phase of a doublet and in the economics of a geothermal system the most commonly used (re)injection temperature is 30 degrees (DAP, 2008). The three injection wells will therefore inject 30 degrees Celsius water (Table 8-3).

Well Name	Injection temperature degrees (Celsius)
A Injection well (AI)	30
B Injection well (BI)	30
C Injection well (CI)	30

Table 8-3 Injection temperatures for well A, B, and C.

Rock specific heat

The rock specific heat defines the specific heat capacity. The specific heat capacity is the rock volume specific heat of the rock as a function of the temperature. The function consists of a table with the rock specific heat and the temperature. The specific heat input data is set as that of a dry sandstone at 20 and 90 degrees Celsius (Lake, 1989) (Table 8-4).

Temperature	Rock Specific heat	Rock Specific heat
Degrees (Celsius)	kJ/rm ³ .°K	kJ/Kg.°K
20	2260	0.999
90	2410	1.142

Table 8-4 Thermal conductivity of the formation rock input in Eclipse.

Fluid specific heat data

Fluid specific heat data defines the specific heat of the formation fluid as a function of the temperature. The fluid specific heat also depends on the formation fluid salinity. Table 8-5 is adapted from Mijnlief et al. (2009) by using the salinity of 94.8 mg/L NaCl Equivalent as input data (Chun, 2009).

Temperature	Heat capacity
Degrees (Celsius)	kJ/kg.°C
1	3.67
80	3.74
100	3.75

Table 8-5 Thermal conductivity formation fluid input in Eclipse.

Thermal conduction

The energy conservation equation is based on thermal convection and thermal conduction. The thermal conduction is simulated optional in the model. The simulation models the thermal conduction of heat in the model. By turning the thermal conduction simulation on and off, the effect of the thermal conduction can be visualized by comparing the results. The thermal conduction input consists of populating a grid with a specific thermal conductivity for the saturated reservoir rock. To keep the simulation simple one value is set for the thermal conductivity of the rock. The thermal conductivity of the saturated reservoir rock is set at 2.5 (J/s-m-K) (Lake, 1989). However in future studies it is possible to create a 3D thermal conductivity model that weighs the thermal conductivity values on the created facies model. The effect of thermal conduction will be shown in the results.

Temperature modelling

The energy conservation equation for thermal energy has been added to the defined static model and flow simulations are run. The output of the simulation case contains the production water temperature, the injection water temperature, the average reservoir temperature and a 3D visualisation of the temperature in each grid cell at each time step in the simulation (Figure 8-12). The viscosity of the formation water does change with temperature but this is not simulated. Den Boer (2008) showed that the change in viscosity of the formation water and the effect on flow is minimal and can be neglected. However in future studies it is possible to take viscosity changes into account.

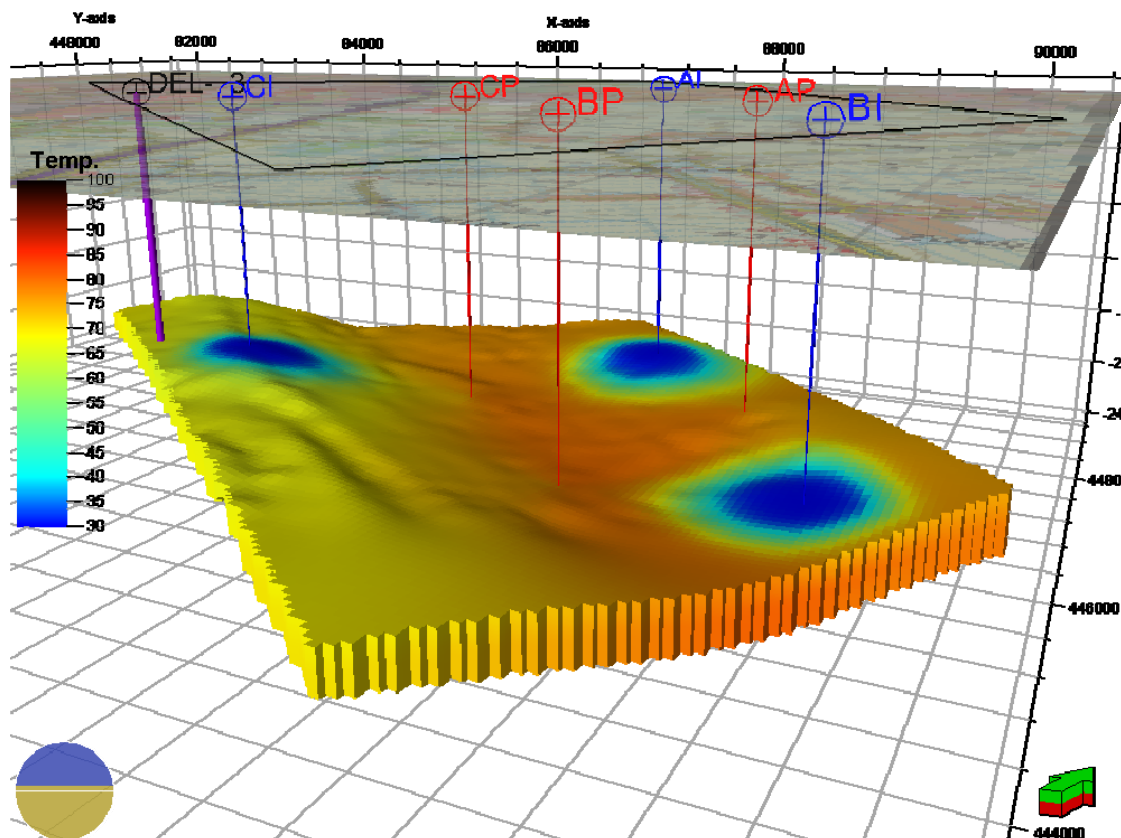


Figure 8-12 3D View showing temperature flow from production wells to injection wells after 30 years viewing the Top Delft Sandstone Member.

Results of temperature modelling

The results of the simulation show the temperature profile over time of the injection and production wells. The injection temperature stays constant at 30 degrees Celsius while the production temperature varies in time per well (Figure 8-13). The results of the simulation case show that all three doublets A, B, and C produce water above 73 degrees Celsius during the 30 years of production (Figure 8-13). No considerable cooling occurs and there is no sign of a considerate breakthrough of cold water. The production temperature does however change gradually in time. This is caused by the production of hotter or colder water flowing towards the well. For example the production temperature of production well A increases as hot water from the deeper part of the reservoir flows towards the well (Figure 8-14). All three wells see a slow cooling of the production temperature as the reservoir temperature drops because of cold water injection. The production temperature however does not drop below the 73 degrees which is needed to economically sustain a geothermal doublet (DAP, 2008). The difference between the production and injection temperature over 30 years stays above the 40 degrees Celsius, enough to economically sustain the three doublets (DAP, 2008). From this data it is possible to calculate the energy production of each well but this is not performed as it goes beyond the reach of this study.

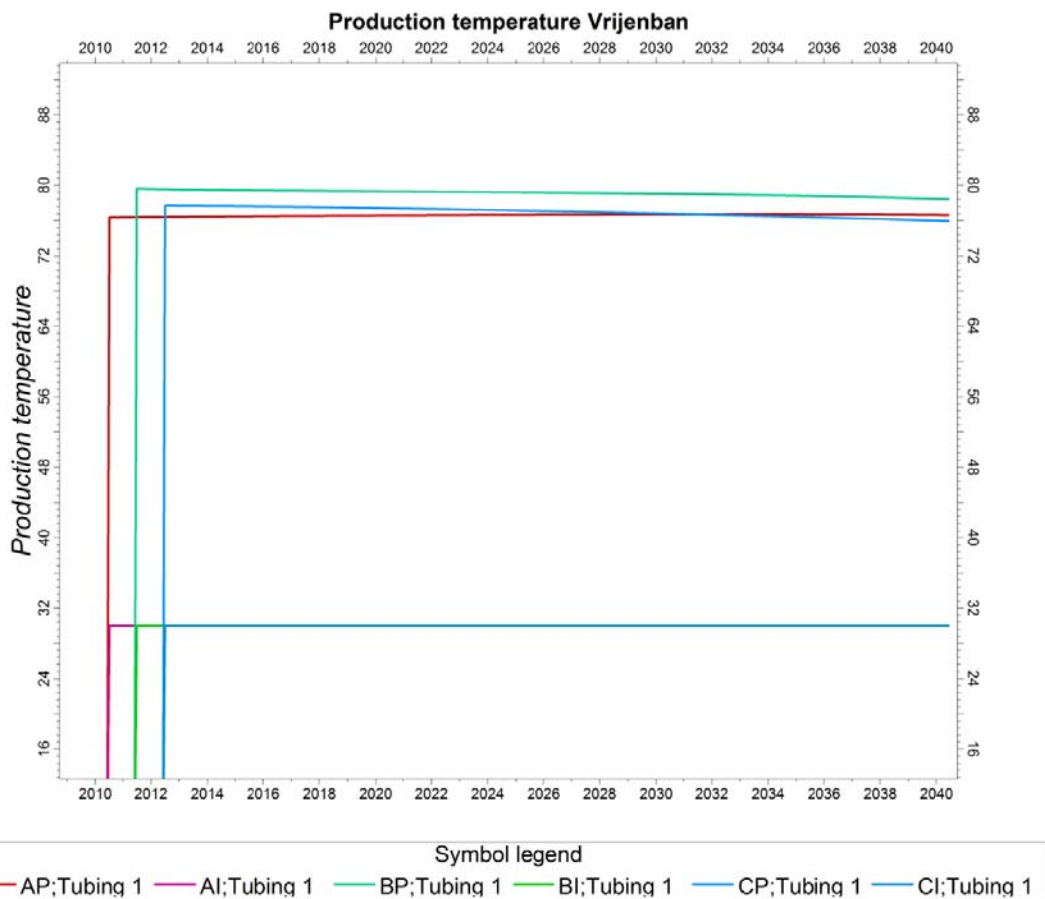


Figure 8-13 The production and injection temperature in degrees Celsius of fluids produced and injected by wells A, B, and C over time in years.

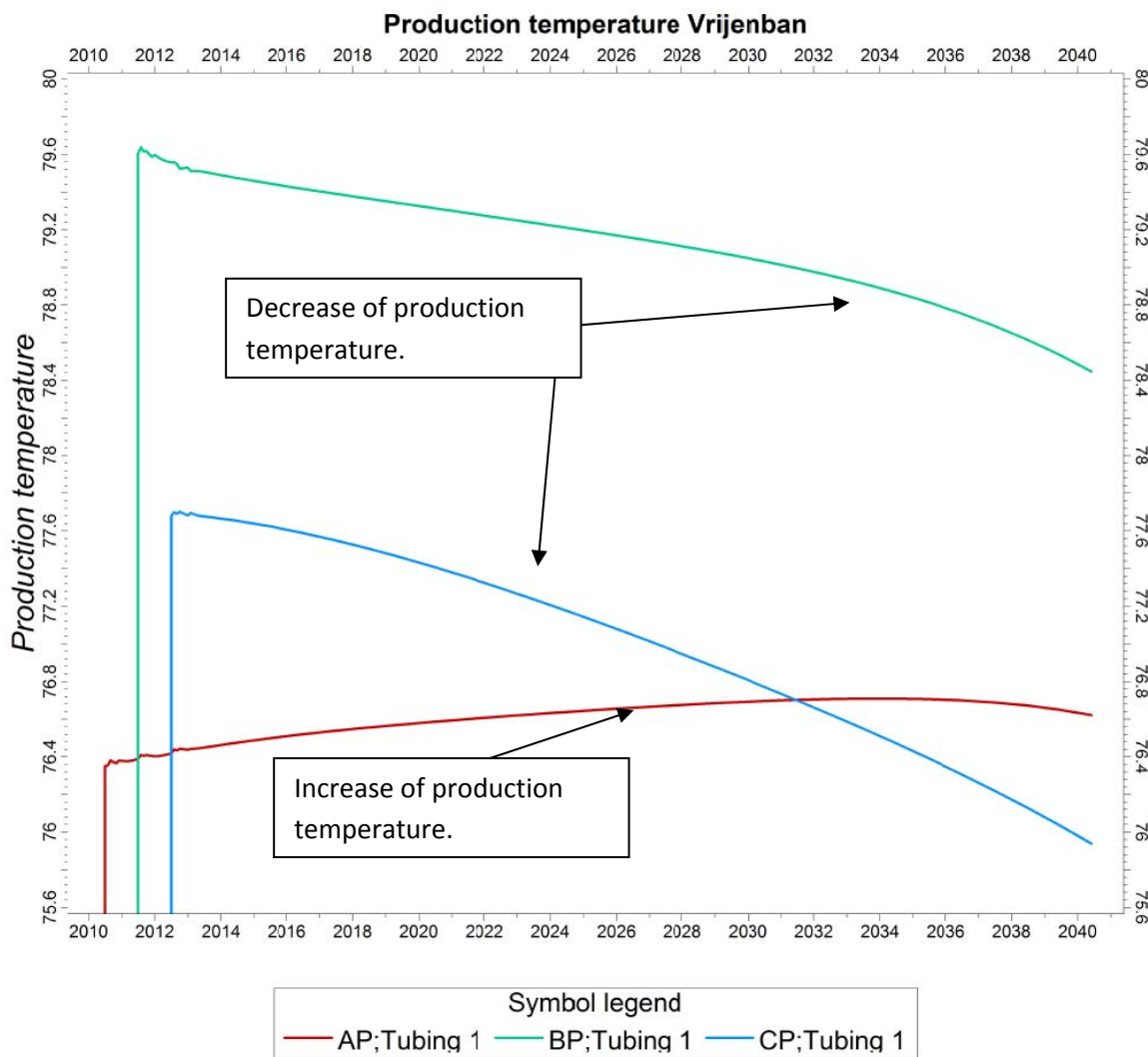


Figure 8-14 The production temperature in degrees Celsius of fluids produced by wells A, B, and C over time in years. Y scale starts at 72 degrees Celsius.

The 3D temperature output model of the simulation case shows the movement of thermal flow in the reservoir over time. This creates the possibility to see what the effects are of the injection of cold water into the reservoir. In Figure 8-15 a top view is given of the Upper Delft Sandstone Member after 30 years of production. This shows the temperature in the reservoir and the change of the reservoir temperature caused by the injection of cold water. The simulation shows that no cold front breakthrough occurs within the first 30 years of production. The reservoir however is considerably cooled around the injection wells. It can be concluded that no signs of temperature breakthrough of the doublets to other doublets occur in the simulation. When studying this in detail (Figure 8-16) a droplet shaped form is created between a production and injection well. As the production well creates a pressure difference a flow is started from the injection well towards the production well. This shape is similar to that found in previous work performed by Mijnlief & Van Wees, (2009), Smits (2008) and (Figure 8-18) Den Boer (2008).

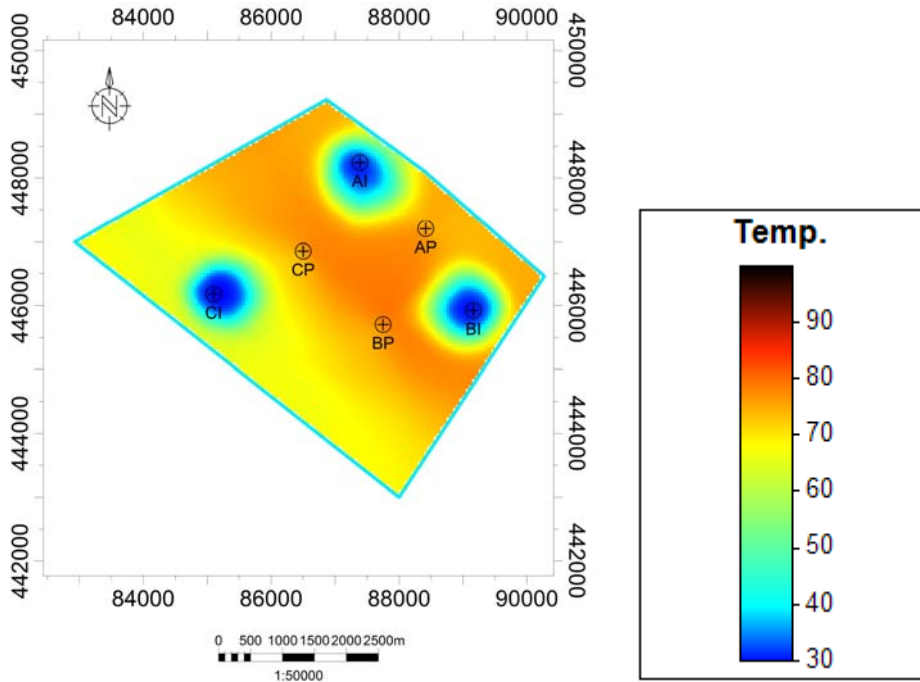


Figure 8-15 Overview showing the temperature flow from injections well to the production wells after 30 years in the Upper Delft Sandstone Member.

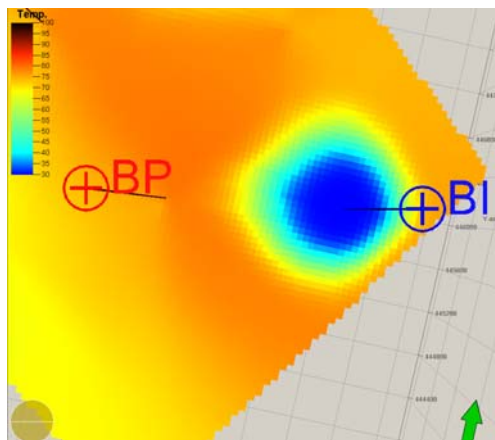


Figure 8-16 Top view showing temperature flow from injection well BI blue to production well BP (red) after 30 years in the Upper Delft Sandstone Member.

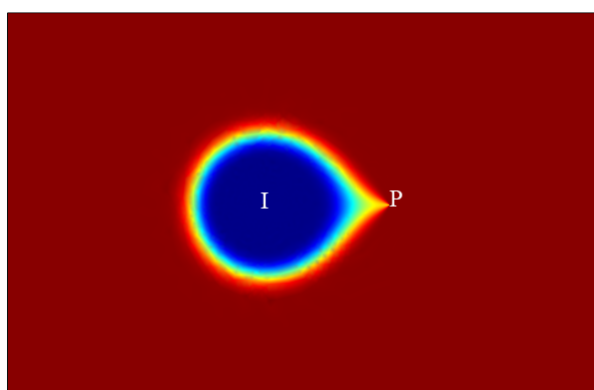


Figure 8-17 Top view showing temperature flow from injection to production (Den Boer, 2008)

The key target of this study was to determine the effect of heterogeneities on the temperature changes and fluid flow. The results show that high permeability layers do create flow paths for cold water to flow through. For example the Upper Delft Sandstone Member has a considerable higher permeability to the Middle and Lower Delft Sandstone Member. In Figure 8-18 it can clearly be seen that in the higher permeable Upper Delft Sandstone Member the cold water front has moved faster than in the other formation members. However the thermal conductivity of the formations has a large effect on the cold water front in the reservoir. To confidently determine the effect of the heterogeneities, a better understanding is needed of the effect of thermal conductivity of the temperature flow. Also a further comparison of a heterogeneous reservoir with a homogeneous reservoir gives a better understanding of the effect of heterogeneities on temperature flow.

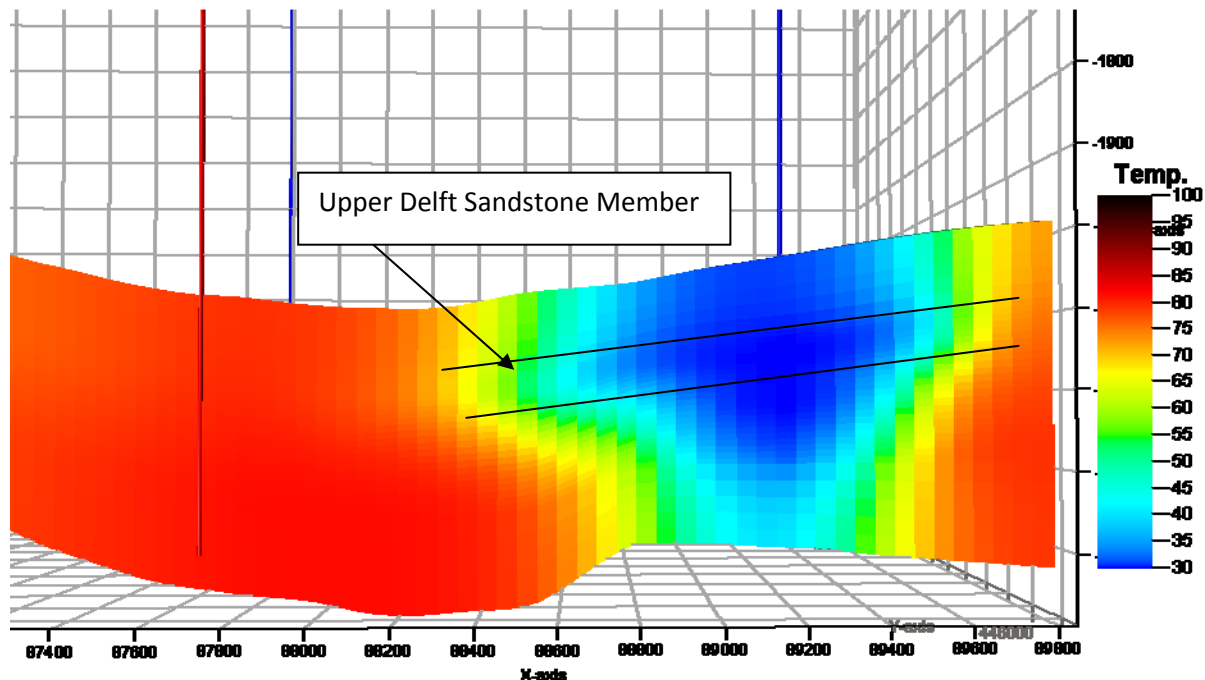


Figure 8-18 Cross section showing temperature flow from injection well PI (Blue well) to production well BP (Red Well) after 30 years, Z:X ratio 2:1. (see also Figure 8-16)

8.6. Homogeneous versus Heterogeneous static model

To determine the effect of the heterogeneities it is imperative to compare the temperature and fluid flow behaviour simulation of a defined static homogeneous reservoir model with that of the above discussed defined static heterogeneous reservoir model. A homogeneous define static reservoir was created of the Delft Sandstone Member in target area of Vrijenban. The input values consist of the average values of the heterogeneous reservoirs. In Table 8-6 the input data can be found.

Values Homogeneous	Input Value	Unit
Porosity	0,16	-
Horizontal Perm	35	mDarcy
Vertical Perm	0,4	mDarcy

Table 8-6 Porosity, horizontal and vertical permeability input for the static homogeneous model.

A defined static homogeneous model was created by populating the Delft Sandstone Member in the static model with a constant porosity, vertical and horizontal permeability. The created 3D homogeneous model has the same structural static model boundaries, static temperature profile and injection temperatures as the heterogeneous reservoir. All flow and rock function parameters are equal and no changes were made to the development strategy of the field. So the defined homogeneous static model is a twin to the defined heterogeneous static model apart from the porosity and permeability flow characteristics defined to the cell blocks of the Delft Sandstone Member. Figure 8-19 shows the created porosity, vertical- and horizontal permeability 3D defined static homogeneous model. The flow characteristics of the Rodenrijs Claystone Member and the Alblasserdam Member were not changed.

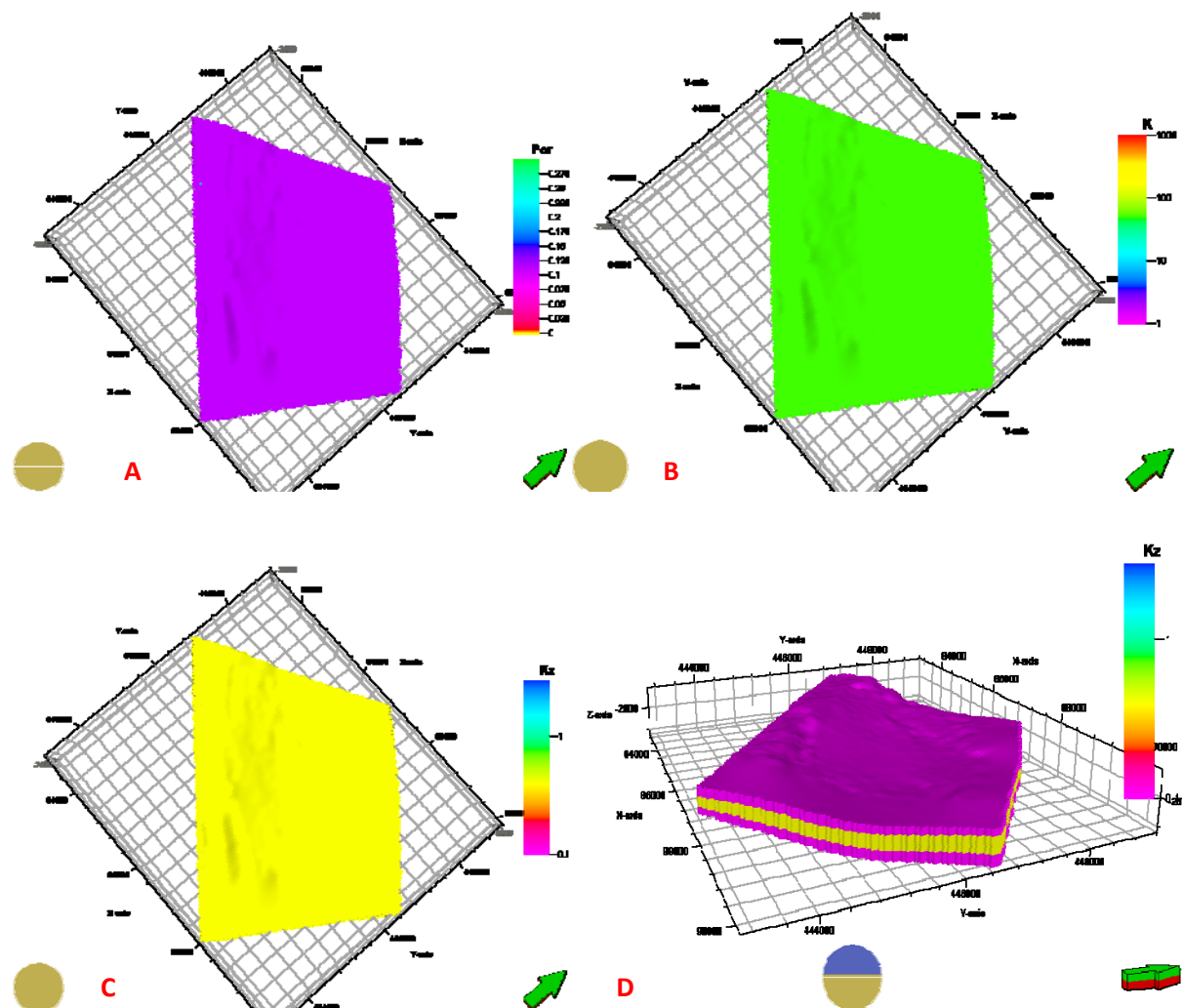


Figure 8-19 Top view of the Delft Sandstone Member in the 3D homogeneous model, A) Porosity, B) Horizontal Permeability, C) Vertical Permeability, D) 3D side view of the homogeneous static model with the Rodenrijs Claystone Member and the Alblasserdam Member.

Flow rate results of the homogeneous reservoir

Similar to the simulation of flow behaviour in a defined static 3d architectural reservoir model a simulation was run in the homogeneous static model. The two simulation cases are referred to as the homogeneous simulation case and the heterogeneous simulation case. The results of the simulation case run in the homogeneous static model show that none of the three doublets A, B, and C, reached their target production rates. The injection rates are lower than the set 3600 cubic meters per day as the injection wells are constrained by the bottom hole pressure. The group constraint per doublet prevents more production than injection. In the simulation case the production wells are constrained by the amount of fluid that is injected as in a geothermal doublet. The production well is connected to injection well. All three wells do show large differences in the production rates (Figure 8-20). This is caused by the created variation in thickness and depth in the static homogeneous model in the wells. The results of production data of this homogeneous simulation are within the probability of the productivity of the Delft Sandstone Member from petrophysical well data (Smits, 2008; Grobbelen et al., 2009).

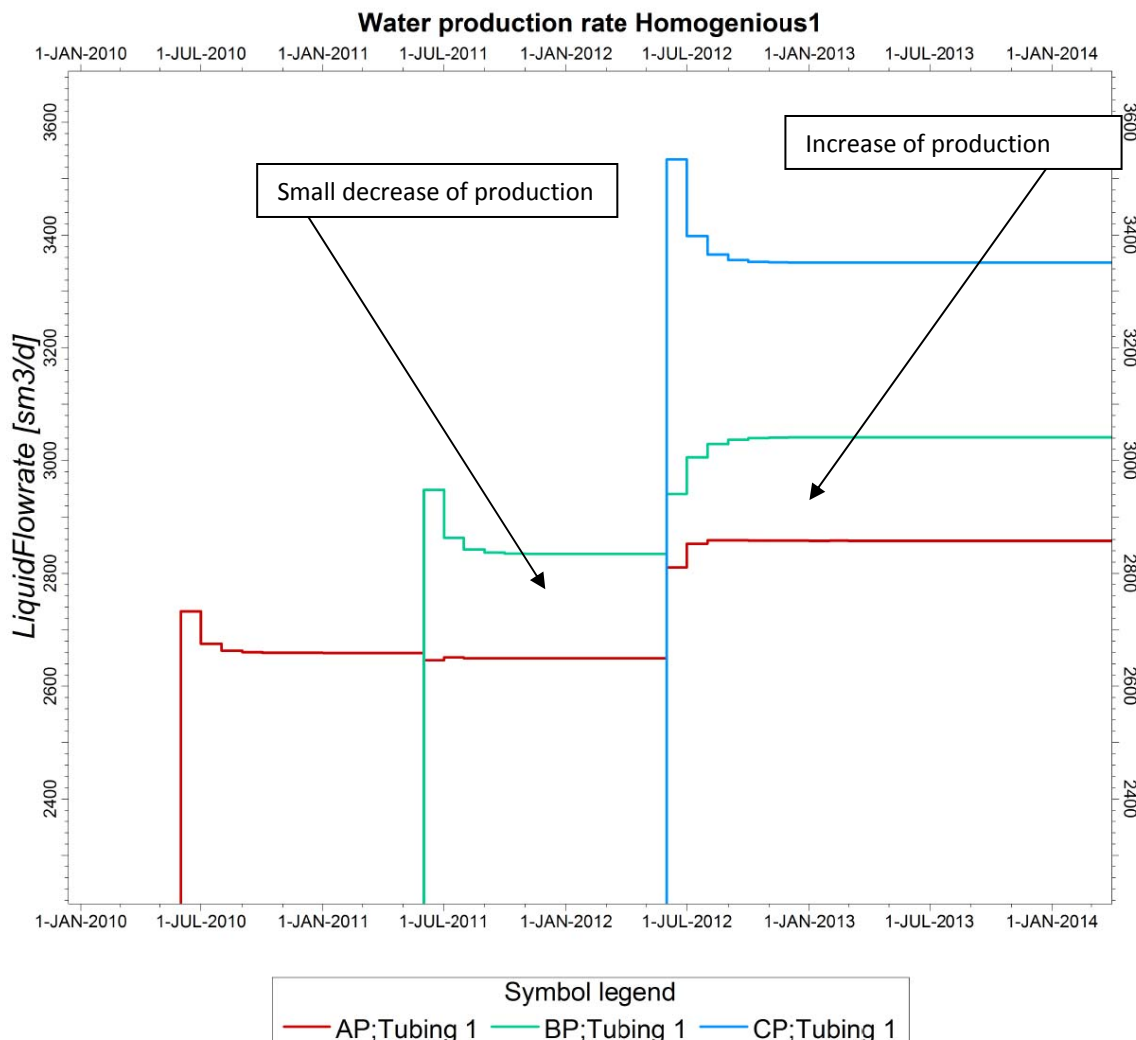


Figure 8-20 Production from A, B and C production wells in simulation case called “homogenous1”.

When comparing the flow behaviour result from the two simulation cases it can bee seen that the flow behaviour is similar (Figure 8-21). The flow injection rates of one doublet is within a similar range in both models but does vary slightly in amount. Doublet A shows the lowest injection rate in both simulation cases and doublet C the highest (Figure 8-21). As the thickness and structural boundaries in the two simulation cases has not been changed, the wells placed in the thickest part will still show the highest flow rates compared to wells in a thinner reservoir section. Smits (2008) showed that the thickness of the formation has a large impact on determining the flow rate from a well. However as can been from the flow rate from a well in the homogeneous simulation case it can be both higher or lower than in the heterogeneous simulation case (Figure 8-21). This is caused by the flow characteristics given by the assigned petrophysical properties around a well. Injection wells in the heterogeneous simulation case with a higher than average porosity and permeability will have a higher flow rate. Injection wells encountering lower than average flow characteristics than found in the homogeneous simulation case will have a lower flow rate.

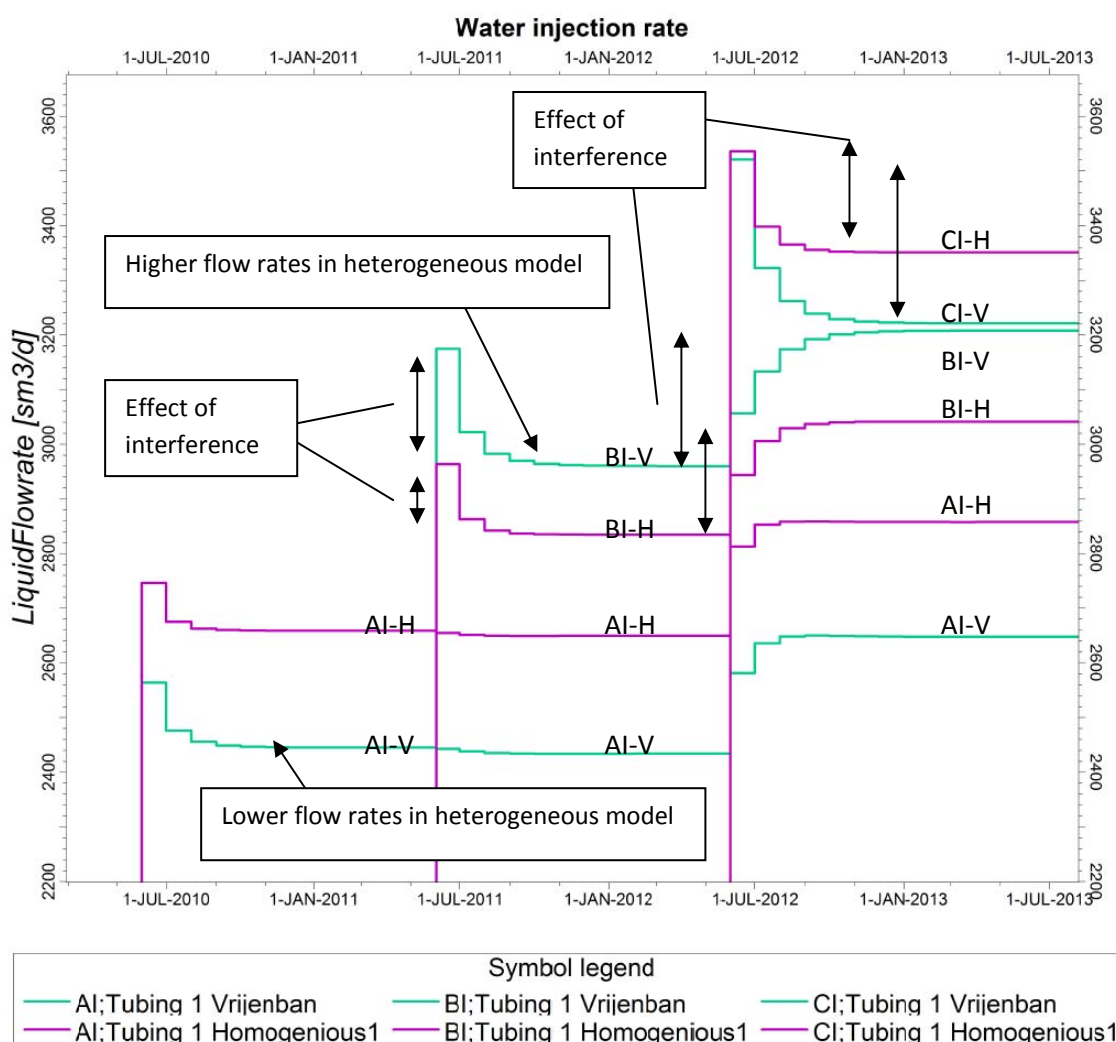


Figure 8-21 Production from A, B and C production wells in both the heterogeneous static model called “Vrijenban”(Green) and the homogeneous static model called “Homogenous1” (Purple).

Similar to the heterogeneous simulation case, the homogeneous simulation case shows that pressure interference occurs between doublets affecting the flow rates. Both negative and positive interference is found in the simulation of flow behaviour in a homogeneous static model. The flow rate of one doublet is changed by a change in the reservoir pressure caused by other doublets (Figure 8-21). A large difference is shown in the amount of interference. The flow rate change caused by interference is much larger within a heterogeneous reservoir than in a homogeneous reservoir (Figure 8-21).

The temperature results of homogeneous simulation case

The 3D temperature output model of the homogeneous simulation case temperature shows the movement of thermal flow in the reservoir over time. In Figure 8-22 a top view is given of the Upper Delft Sandstone Member after 30 years of production in the homogeneous defined static model. The simulation shows no cold front breakthrough occurs within the first 30 years of production. The reservoir however is considerably cooled around the injection wells. It can be concluded that no signs of temperature breakthrough of the doublets to other doublets occur in the simulation. When studying this in detail (Figure 8-23) a droplet shaped form is created between a production and injection. As the production well creates a pressure difference flow is started from the injection well towards the production well. This shape is similar to that found in previous work performed by Mijnlief & Van Wees, (2009), Den Boer (2008) and Smits (2008) who also studied thermal flow in a homogeneous static reservoir models.

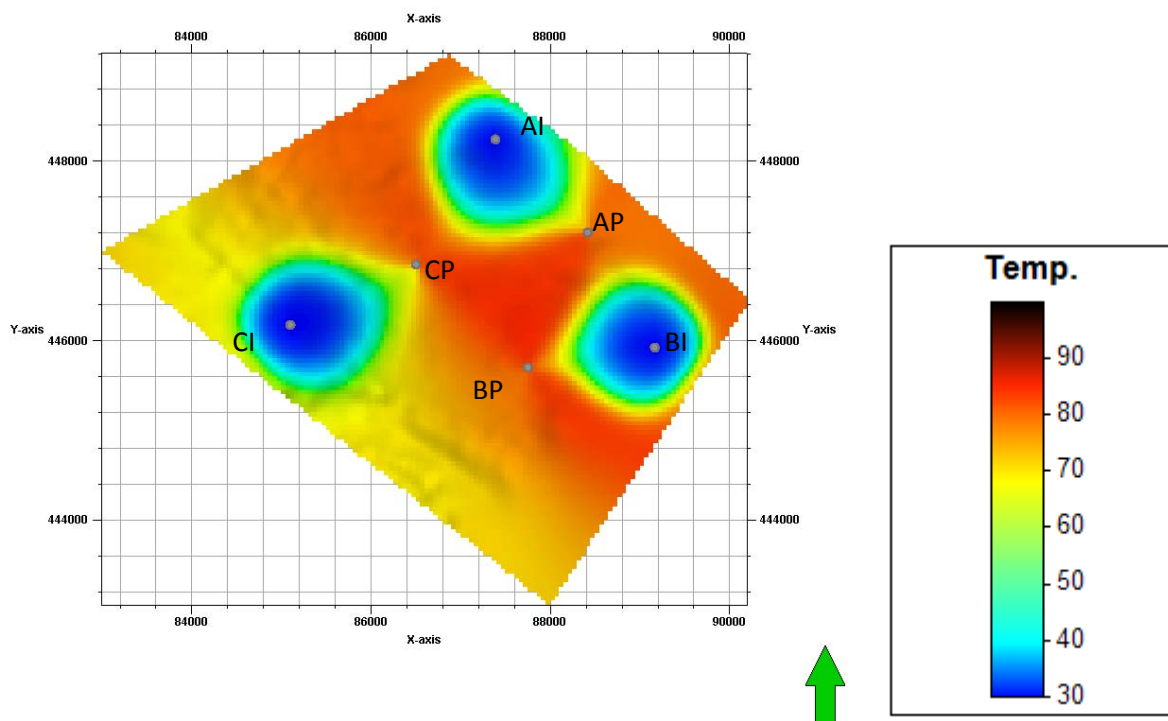


Figure 8-22 Overview showing temperature flow from production wells to the injections well after 30 years in a homogeneous reservoir in the Upper Delft Sandstone Member.

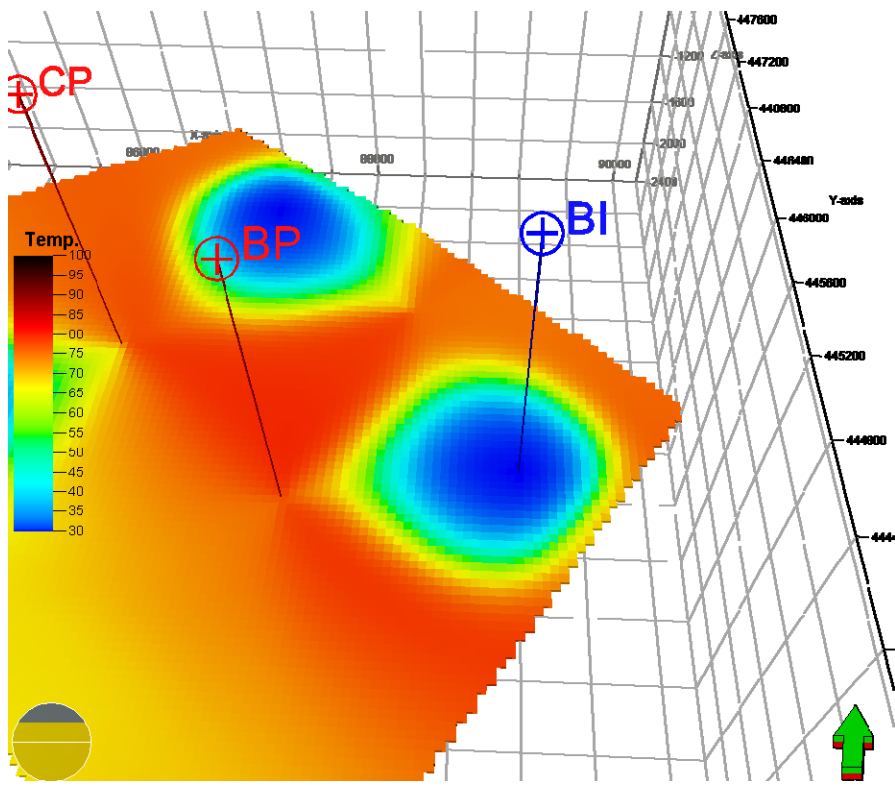


Figure 8-23 Top view showing temperature flow from injection well PI blue to production well BP red after 30 years in a homogeneous reservoir. Model is flattened and shows the Upper Delft Sandstone Member.

The key target of simulating flow in a homogeneous defined static reservoir was to determine the effect of heterogeneities on the temperature changes and fluid flow. In the Homogeneous reservoir simulation shows no signs of flow paths as the heterogeneous model did. In Figure 8-24 no temperature streak is found.

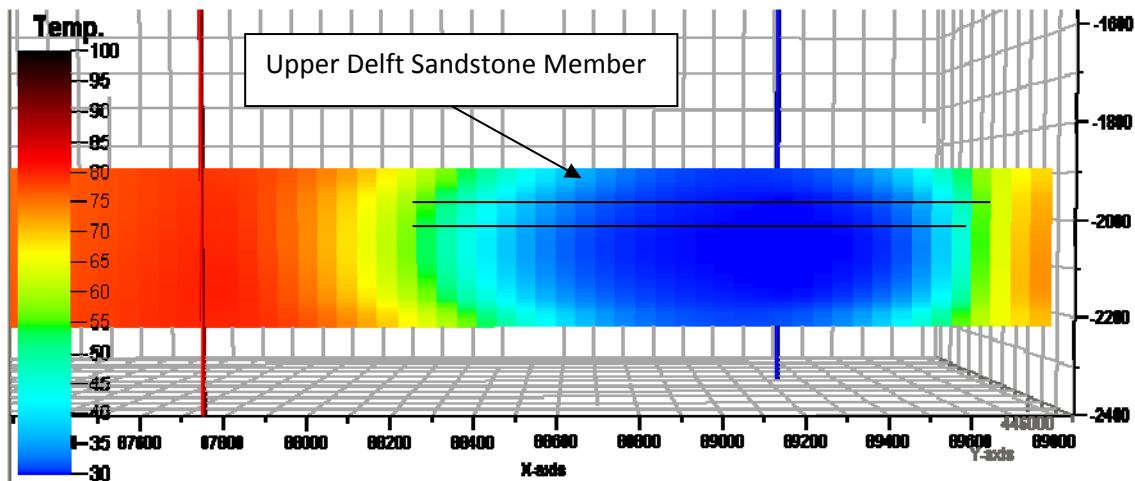


Figure 8-24 Cross section showing temperature flow from injection well PI (Blue well) to production well BP (Red Well) after 30 years, model is flattened in this visualisation.

The comparison of a heterogeneous reservoir with a homogeneous reservoir temperature output gives a better understanding of the effect of heterogeneities on temperature flow (Figure 8-25). The difference in the production temperature per well over time in both simulation cases shows that the average temperature production from a heterogeneous simulation case is higher over time.

One has to take into account that the flow rates of the two simulation cases are different as this will have a large effect on the amount of cold water injection and thus the reservoir temperature. A colder production temperature because of faster breakthrough of cold water through high permeability streaks in the heterogeneous reservoir simulation did not occur. A possible cause that the temperature is higher in a heterogeneous simulation case than the homogeneous simulation case is that water that flows through high permeable streaks will interact more with the reservoir rock. This effect is caused by thermal conductivity from the surrounding reservoir rock to the formation fluid. To determine this effect of thermal conductivity, it should be studied in more detail. However the results show that heterogeneities have a positive effect on heat flow from geothermal point of view as it is sustaining a higher production temperature over time.

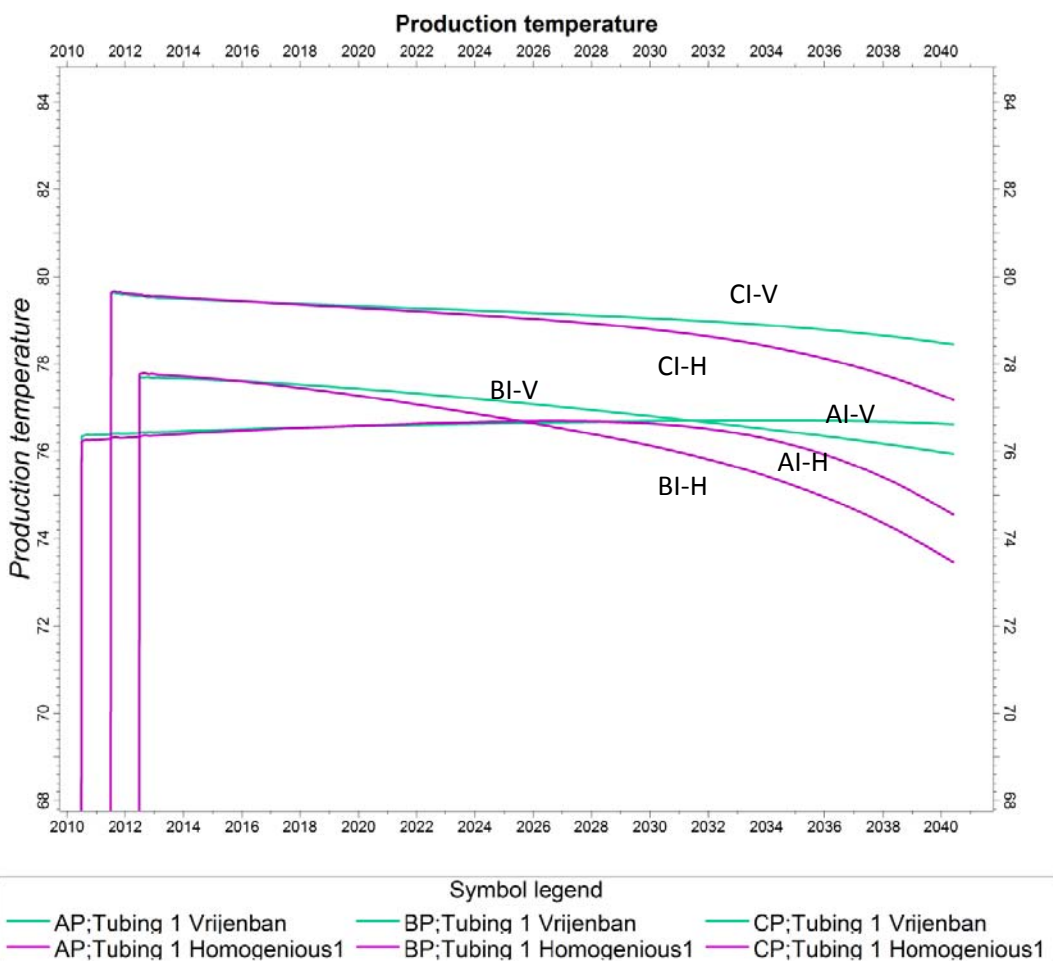


Figure 8-25 The production temperature in degrees Celsius of fluids produced by wells A, B, and C over time in years in both the heterogeneous static model called “V=Vrijenban”(Green) and the homogeneous static model called “H=Homogenous1” (Purple). Y scale starts at 68 degrees Celsius.

8.7. Effect of thermal conductivity

To determine the effect of thermal conductivity in a heterogeneous reservoir a simulation of the temperature and flow behaviour in a defined static heterogeneous architectural reservoir model is performed. By removing the thermal conductivity effect from the energy conservation equation used in the simulation, a reservoir simulation is performed with no thermal conductivity. The defined static architectural model built in paragraph 7.4 is used with no further changes. Thermal conductivity is the process of conduction of heat. In appendix H the thermal conduction equation can be found. Heat convection and interaction of injection fluid with the formation water still occurs.

The 3D temperature output model of the heterogeneous simulation case with no thermal conductivity shows the movement of thermal flow in the reservoir over time. The flow of cold water flows through the high permeable zones (Figure 8-26). In Figure 8-27 a top view is given of the Upper Delft Sandstone Member after 30 years of production in a heterogeneous defined static model without thermal conductivity. The shape is completely different as to that found in the simulation case with thermal conductivity. (Figure 8-28) The simulation clearly shows the cold water front within the defined high permeable zones after 30 years of production at the top of the Lower Delft Sandstone Member. The reservoir however is considerably cooled around the high permeability streaks flowing from the injection wells. No droplet shaped form is created between a production and injection. Cold water breakthrough can clearly be seen between the wells of all three doublets, see arrows in Figure 8-27. Also temperature interference between doublet occurs as cold injection water from one doublet flow to another doublet. When comparing Figure 8-27 with Figure 8-28 it can clearly be seen that the effect of thermal conductivity has a large effect on heating up the cold water front and preventing thermal breakthrough.

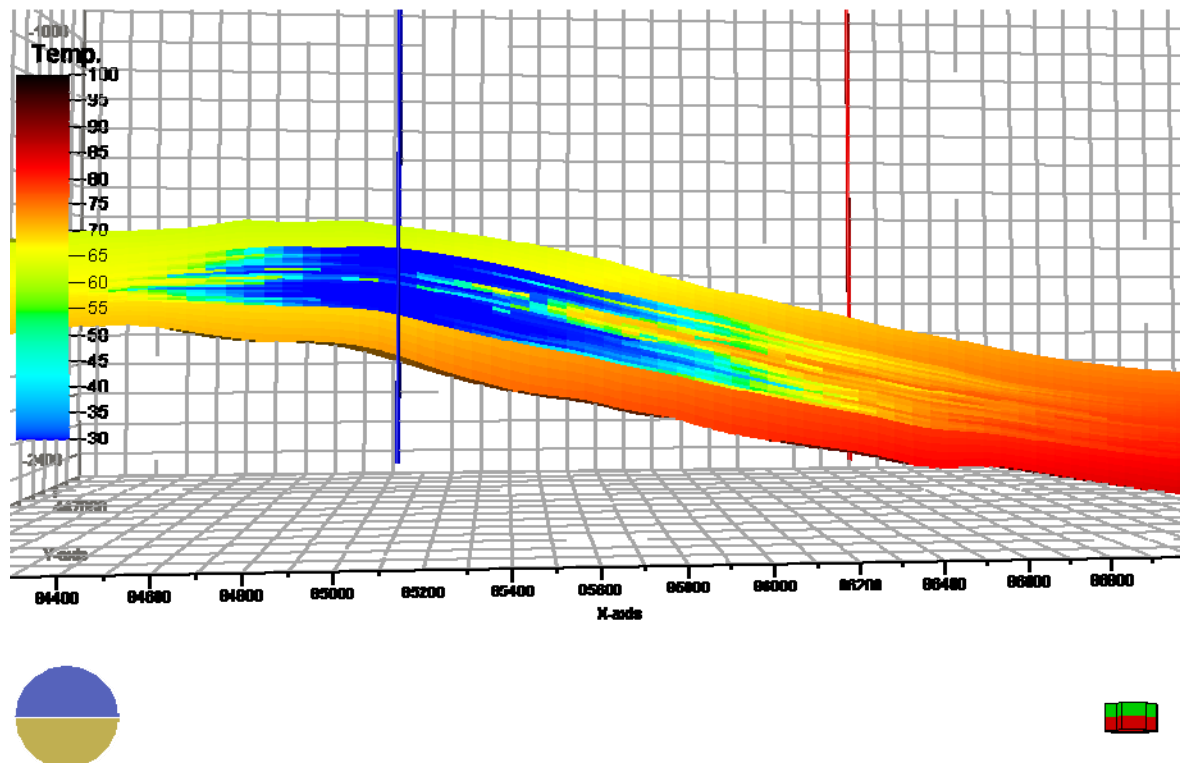


Figure 8-26 Cross section showing temperature flow from injection well CI (blue well) to production well CP (red well) after 30 years.

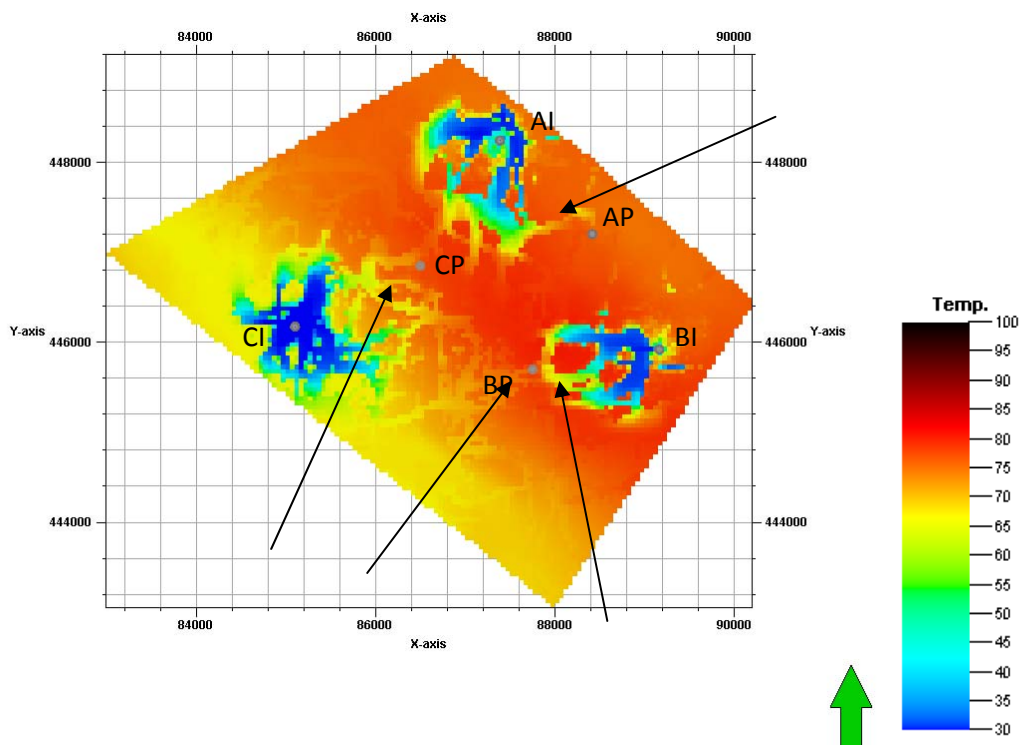


Figure 8-27 Overview showing temperature flow from the injections well to the production wells after 30 years in a heterogeneous reservoir simulation case with no thermal conductivity at the top of the Lower Delft Sandstone Member. Arrows show cold water breakthrough.

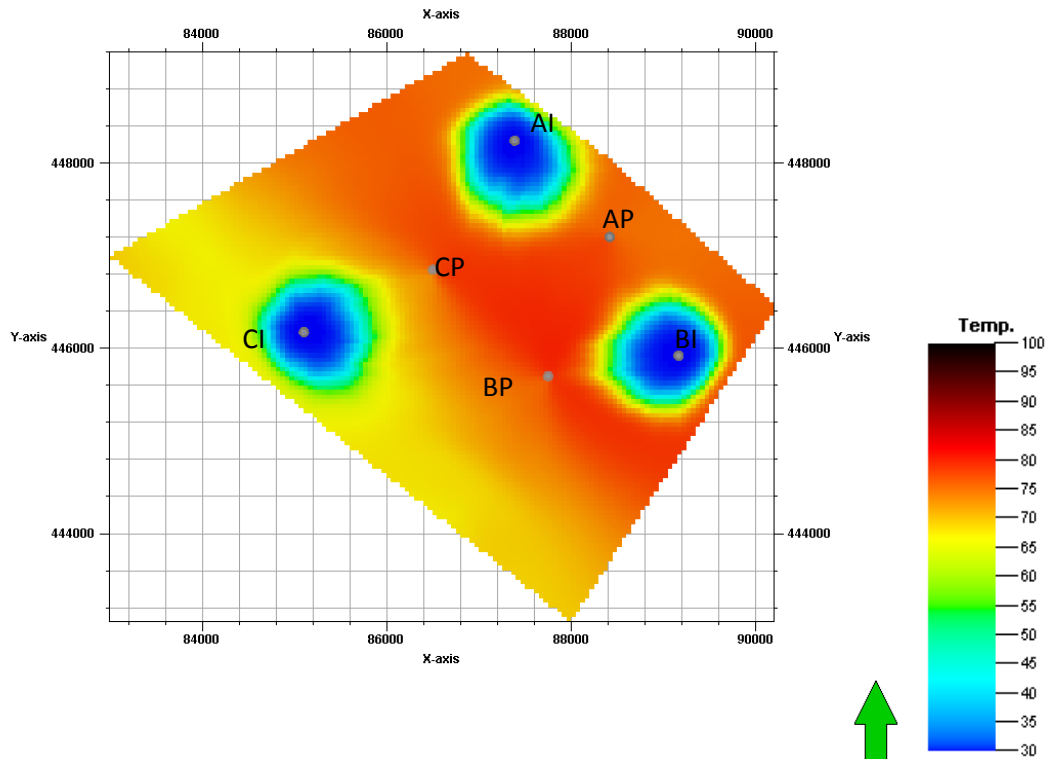


Figure 8-28 Overview showing temperature flow from the injections wells to production wells after 30 years in a heterogeneous reservoir simulation case with thermal conductivity at the top of the Lower Delft Sandstone Member.

When comparing the production temperatures from the simulation cases with and without thermal conductivity in the energy conservation equation during simulation, large difference are found. The production temperature of the well in the simulation case with no thermal conductivity is colder and is cooling down fast (Figure 8-29). As the produced formation water is not heated up by the surrounding formation rock, by thermal conductivity, thermal breakthrough occurs through high permeability zones. It can be seen from Figure 8-27 that cold water breakthrough from other injection well will create a colder production temperature. Thermal conductivity has a large impact on thermal flow and slows the thermal breakthrough through high permeability zones by heating the cold injection water. This considerably prevents cold water breakthrough within a doublet as well as between different doublets and slows the effect of temperature interference within 30 years of simulation.

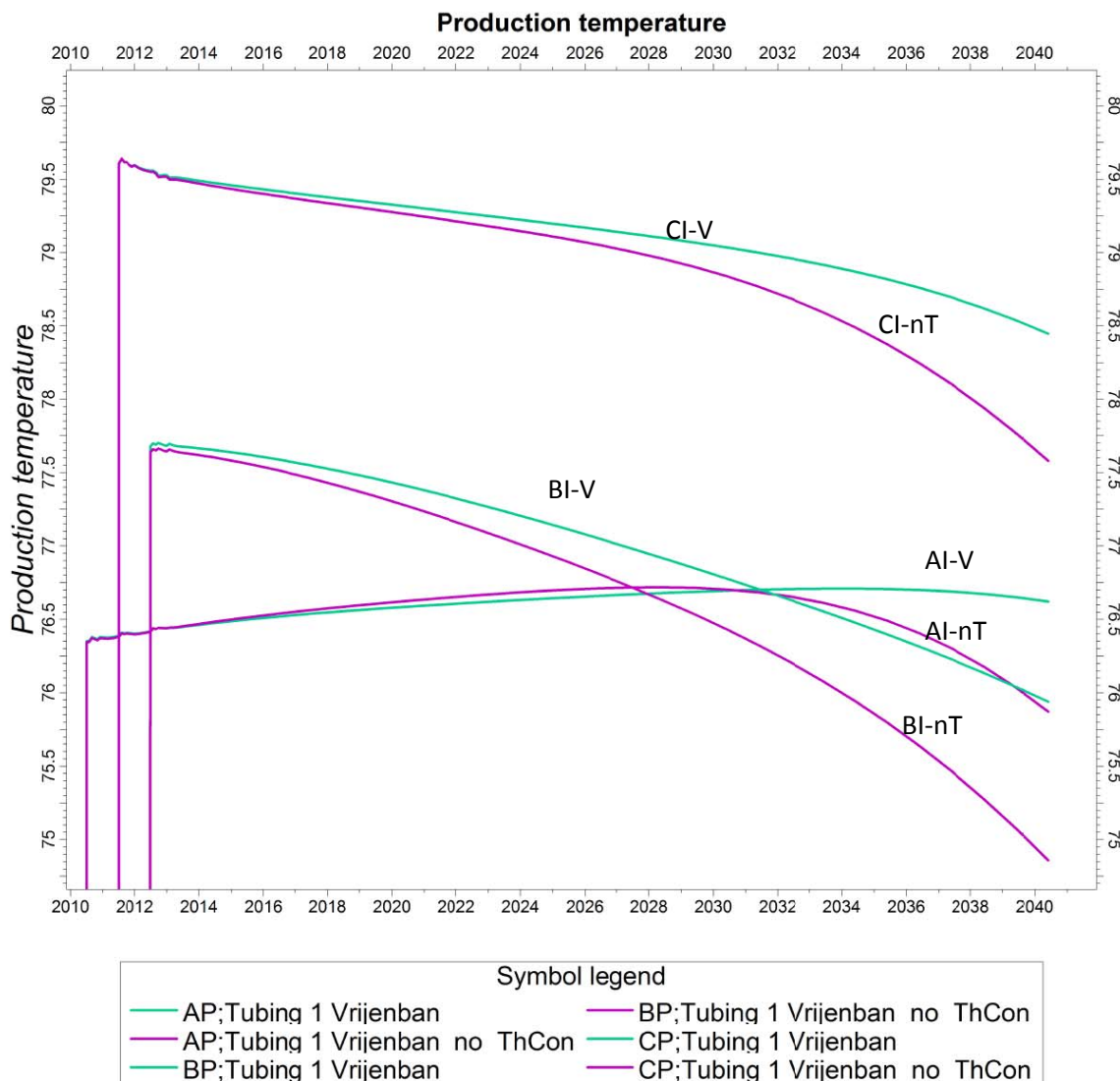


Figure 8-29 The production temperature in degrees Celsius of fluids produced by wells A, B, and C over time in years in a heterogeneous static model both with thermal conductivity called “V=Vrijenban”(Green) as without thermal conductivity called “nT=Vrijenban no ThCon” (Purple). Y scale starts at 74,5 degrees Celsius.

New insight

In both simulation cases of temperature flow and fluid flow behaviour in a heterogeneous and homogeneous static model it can be seen that the cooling of the reservoir goes beyond the top and base of the Delft Sandstone Member. The temperature is lowered beyond the modelled Rodenrijs Claystone Member in both simulation cases. The Rodenrijs Claystone Member was modelled as a 0.01 porosity and with a 0 mD horizontal and vertical permeability. As there is no fluid flow during simulation in the Rodenrijs Claystone Member, the heat flow can only be described by a cooling process through thermal conductivity. The Rijswijk Sandstone Member above the Rodenrijs Claystone Member will also be cooled giving new insights in the idea that multiple systems could work in different layers. Temperature interference of different geothermal systems in different geological formations above and below each other with not enough distance apart will show temperature interference. It also shows that not enough over- and under- burden was created in the static model and used during temperature simulation. Because of this the effect of heat flow from top and base on the temperature flow between the wells has not been fully taken into account during simulation. However this can be taken into account in future simulations.

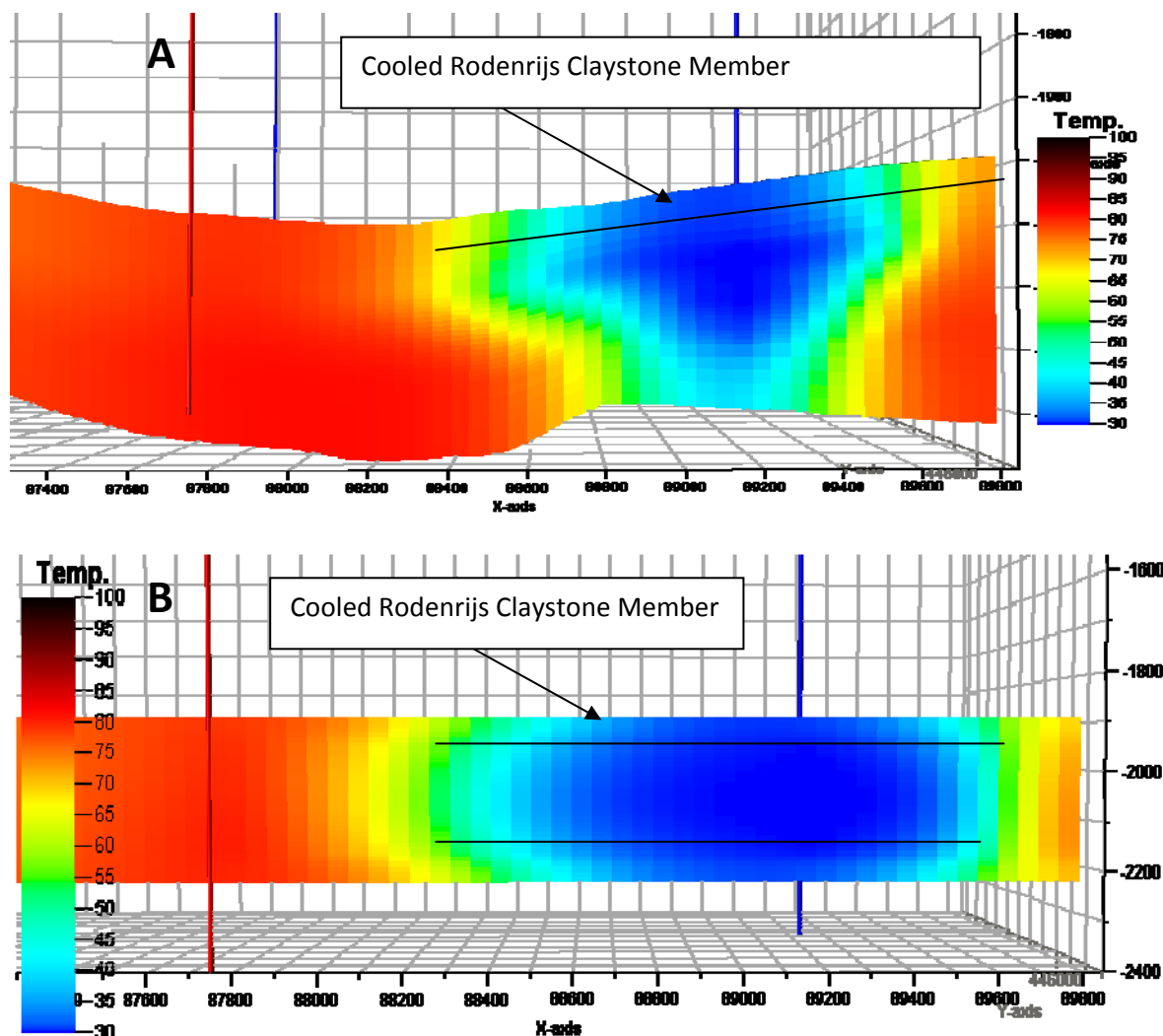


Figure 8-30 Cross section showing temperature flow from injection well PI (Blue well) to production well BP (Red Well) after 30 years. The Rodenrijs Claystone Member is cooled down in both cases. A is in heterogeneous static reservoir model and has Z:X ratio 1:2. Figure B is homogeneous static reservoir model and has been flattened.

9. Conclusion and recommendations.

The objectives of this study are: (1) to show the effect of heterogeneities in the subsurface on interaction and interference of flow on closely placed geothermal systems; (2) to gain a better understanding of the geological setting and the heterogeneities and the depositional setting of the primary target Delft Sandstone Member; and (3) to build a subsurface dynamic reservoir model with which optimal well performance and placement can be assessed. A large amount of smaller results and conclusions can be found throughout the report. Based on the performed work and the results the following major conclusions can be drawn about the subsurface architecture, the tectonics, and depositional environments that played a role during the sedimentation of the Delft Sandstone Member. Furthermore the conclusions about the heterogeneities of the Delft Sandstone Member and their effect on temperature and flow behaviour in a three dimensional flow characterised static architectural reservoir model during flow simulations are presented.

9.1. Conclusions

This study gives new insights and a better and detailed understanding of the reservoir architecture of the Delft Sandstone Member. It shows that the Vrijenban Syncline is the predominant structure in the Delft subsurface. From the palinspastic reconstruction a better understanding of the basin evolution and the effect on deposition of sediment gives new insights into the depositional settings and thickness differences of the Delft Sandstone Member. The sediments of the Delft Sandstone Member have been deposited by a meandering fluvial system in three different depositional settings, controlled by syn-tectonic movement. The Delft Sandstone Member can therefore be divided into three members: The Lower Delft Sandstone Member that contains single fining upward meandering river sandstone bodies interbedded with claystone and siltstone floodplain deposits, a Middle Delft Sandstone Member that contains interbedded claystone and siltstone floodplain deposits with coals layers and an Upper Delft Sandstone Member that contains multi-stacked and laterally amalgamated fluvial channel sandstone bodies. The depositional environment depends on multiple factors in which the accommodation space increase is the most important. The depositional characteristics related to subsidence could have a large impact on the reservoir behaviour of the Delft Sandstone Member. The upper and lower parts are with their high net sand a far better target for fluid flow than the Middle Delft Sandstone Member containing silt- and claystones layers. The Middle Delft Sandstone Member might have a strong effect on the connectivity as it might possibly impede pressure and flow from the upper and lower units of the Delft Sandstone Member. The Upper Delft Sandstone Member with a high net to gross and good lateral connectivity looks the most promising for fluid flow and geothermal production. Lateral and vertical connectivity between the different Delft Sandstone Members is expected to be poor, which makes this Delft Sandstone Member a risky target for geothermal energy production.

The 3D static architectural reservoir model built, visualizes the 3D spatial distribution of the sediments based on core, cuttings and well log data combined with the depositional setting of the Delft Sandstone Member. The facies modelling was performed with object based modelling for the Lower, Middle and Upper Delft Sandstone Member, based on sedimentary properties and trends observed in the data.

The created 3D static architectural reservoir model represents the subsurface architecture of the study area according to the available data and literature. By adding flow characteristics from petrophysical properties a base is created for flow behaviour modelling. The results do however show that with this object based modelling method it is possible to create a structure that upholds both the available data and represent the proposed depositional model.

By modelling the flow behaviour in the static reservoir model the flow rates of a single geothermal system and the pressure interference of the different geothermal systems were determined and quantified. From the flow simulations of the Delft Sandstone Member no evidence is found that it is likely that the economic production rate for geothermal system in the area cannot be achieved. Although the results of production data of this study are within the probability of the productivity of the Delft Sandstone Member, they are on the low side. Different geothermal systems closely placed within one reservoir will have pressure interference that will considerably affect the production and injection volumes. By comparing flow simulation in a homogeneous static reservoir model with the created 3D static architectural reservoir model it is shown that interference is much larger than previously expected. Different geothermal systems in one reservoir will communicate in the reservoir creating both positive and negative effects on flow that are large enough to improve or badly affect the economics of a project.

From a dynamic reservoir flow model it is possible to determine the effects of heterogeneities on heat and fluid flow in the reservoir. Simulations were run of a multi well configuration determining the effect of interference and field performance. The effects of heterogeneities on temperature flow are minimal. The heat flux from the reservoir rock through thermal conductivity cools down the formation and heats up the formation water. This results in increasing the temperature in the cold front considerably and minimizes the possibility of cold water breakthrough. The results of the simulation case run show that all three geothermal systems produce water above 75 degrees Celsius during the 30 years of production. No large amount of cooling occurs and there is no sign of a considerable breakthrough of cold water from the injection well. The production temperature does however change gradually in time and cools slightly. It can therefore be concluded that multiple geothermal systems can be placed in one reservoir and sustain economic production temperatures for over 30 years if the distance between the systems is large enough. However the interference between geothermal systems through the reservoir pressure could increase or decrease the flow rate of an individual geothermal system. This could then affect the productivity and temperature and elongate, shorten or even impede the life time of a geothermal system. Temperature and flow behaviour simulation were also performed in a homogeneous static model to compare the results with the heterogeneous static model. The results of comparing the two simulations show that heterogeneities have a positive effect on heat flow by sustaining a higher production temperature over time. From the temperature heat flow reservoir simulations it is also possible to determine the effects of heat flow from the top and base of the reservoir. This shows that temperature interference between above and below lying formations is considerable and should be taken into account when planning multiple geothermal systems in subsurface levels, situated above and below each other.

9.2. Recommendations

This research forms a base to show the effects of heterogeneities on the interaction and interference of flow on closely placed geothermal systems in the Delft Sandstone Member. Improvements can be made to verify certain parameters, to reduce uncertainties and improve modelling results. The following recommendations are made to ensure and provide the foundation for a true rollout of geothermal systems through the western parts of the Netherlands

The results in this study are depended on the availability, the quality, processing and resolution of the provided data. The available seismic data has al low resolution at target depth as it is not processed for the Delft Sandstone Member. By reprocessing the data it is possible to improve the resolution and determine the thickness and exact depth of the Top and Base of the Delft Sandstone Member. Also it would improve the possibility to find more faults, fractured or cemented areas or determine the possibility of compartmentalisation and or hydrocarbons in the reservoir.

More extensive cutting and core studies could create a better grip on the spatial values and trends of the fluvial channels that deposited the Delft Sandstone Member. With this better understanding of thickness, width, sinuosity and the variation and distribution of the meandering system that deposited the Delft Sandstone Member could be achieved. Additionally the cuttings of the Delft-02 well that only drilled the Upper Delft Sandstone Member could be studied. Extended research on the grain size distribution of the Delft Sandstone Member in core and cuttings can confirm or give more insight in the depositional environment. The mineralogical content of DELFT-03 has been studied in detail, it was however performed only on a fraction of the total amount of cuttings of the Delft Sandstone Member interval. It is possible to do a new analysis that taken into account all grains from an interval instead of a fraction. Also the cutting and core studies showed that the Delft Sandstone Member is still partly friable and sand production must be accounted for and the necessary measures in the completion design should be taken.

There is little knowledge of cementation and mineralization of the Delft Sandstone Member. SEM photos of cuttings and core data may give insight in diagenesis, the grain contacts, cementation and deformations of the grains of the Delft Sandstone Member. XRD/XRF analysis of the Delft Sandstone Member could give information on the dominance of some atoms and therefore on the mineralogical content additional to the optical examination. Cementation and the possible sealing effects of faults and cemented fractures could strongly impede geothermal production.

There was no trace of bitumen in the Delft Sandstone Member but a hydrocarbon risk still exists in the area. The Rijswijk Member does contain oil and lies above the Delft Sandstone Member. Therefore, it is most likely that the oil migrated through the Delft Sandstone Member. A study to the migration path of the oil in the Rijswijk Member could clarify and give new insights into the movement of the basin, especially when combined with the performed palinspastic reconstruction.

More formation fluid samples need to be studied as the possibilities of geothermal clogging is still a under estimated risk. By taking formation fluids from the subsurface of the Delft from newly drilled wells planned in 2010, the knowledge and data density of formation fluid properties and mineral content could be improved. By studying this data it will be possible to get a better understating of mineralization and the maintenance and stimulation of geothermal wells as well as specific heat properties of the formation fluid.

All wells used in this study were drilled on the structural highs. Additional data from the newly drilled wells in the lows could confirm the presented depositional environment of the Delft Sandstone Member. Also it could improve the reliability of the seismic interpretation and the depth and thickness of the formation in the Vrijenban syncline. It will further give additional insight in the petrophysical properties and reduce uncertainties of the Delft Sandstone Member in the lows.

A palinspastic reconstruction was performed on 2D sections, this could be improved by performing the invert movement in three dimensions using the available 3D seismics. This could give more insight and the knowledge of the basin evolution, and the accommodation space creation, sedimentation and the thicknesses differences of the Delft Sandstone Member.

By studying the information presented in this study about the formations in Delft subsurface it is possible to determine the effect of sea level changes during the time of deposition. A sequence stratigraphy study can now be performed giving a better insight in deposition of the target formations and determine if trends are local or regional.

The available petrophysical data and the derived trends could be improved, for example the, porosity- permeability relationship from core data has not been corrected for surface expansion. Additional studies into the petrophysical well log data could lower the amount of uncertainties of the flow characteristics of the Delft Sandstone Member.

Multiple representations are recommended to gain an understanding of the uncertainty in the model. During the building of the 3D static architectural reservoir model several modelling steps could be greatly improved. By modelling smaller layers and more grid cells the resolution could be increased of the static model. Through drilling of new wells and/or additional data acquisition and by incorporating this new data into the model it would be possible to greatly increase the reliability of the 3D static architectural reservoir model.

Only one flow behaviour simulation was performed, by running multiple simulations and additional Monte Carlo analysis of the results better probability curve for the estimation of the production rate would be created. An uncertainty study into the petrophysical data combined with the 3D flow characterised grids and the flow behaviour simulation results could quantify the error and improve the flow and pressure interference predictions.

Enhancing more realism in the simulations and in the created models could greatly improve the reliability of the results. This can be done by adding; slanted or deviated wells, the skin factors and well completions and taking into account possible formation damage. By adding seasonal flow rate fluctuations and injection temperatures fluctuations from existing wells history matching will become an option.

To improve the simulations of the temperature flow more over- and under-burden should be modelled. Also by including the viscosity changes through difference of formation fluid temperature the possibility of the effect of viscosity depended undershooting of colder water could be assessed in a heterogeneous reservoir. Within the simulation performed for this study no heat source from the earth's crust or interior is implemented. This could potentially lead to slightly higher production temperatures over time.

The designed 3D temperature grid is based on the linear thermal gradient measured in wells. But to verify the temperature gradient, a thermodynamic model of the subsurface could be made. With the heat flux of the crust and heat capacities of the different formations, it could predict the temperature in the subsurface more accurately and explain the local differences found in the regional well data.

In the simulations, the heat capacity is assumed to be independent of the facies. However, in reality the heat capacity does depend on facies. A 3D thermal capacity characterised facies grid could be built and used in temperature flow simulation in Eclipse, enhancing the true effect of heterogeneities making the results more realistic and accurate.

The temperature flow simulations were performed based on flow in porous media and thermodynamic theories and equations. Comparing the results in more detail to theoretical modelling and literature studies will support the result of this study and possibly suggest improvements.

The temperature and flow rate results from the simulations could be used for net thermal energy and economics calculations. This could determine the amounts of thermal watts a geothermal system produces and determine if the system is economically sustainable. In combination with an uncertainty analysis this could assess the economic success of a proposed geothermal system.

The temperature flow behaviour simulations can now be used to find the optimal well placement and determine the positive and negative effect on pressure performance per well in multiple well configurations. The results of this study can be a base case for further research as it can form a benchmark for future local and regional geothermal studies.

10. References,

- Bartlema, H., 2002: "3-D Geological modelling and a SAGD production forecast of the Moerkapelle Field" (volume 1), MSc Thesis, Delft University of Technology, Delft, the Netherlands.
- Berendsen, H.J.A. 2004: "Inleiding", In: Berendsen, Fysische geografie van Nederland; De vorming van het land. p. 1-14
- Bourquin, S., Rigollet, C., Bourges P., 2001: "High-resolution sequence stratigraphy of an alluvial fan environment: fluvial reservoir implications - Example of the Chaunoy Sandstones (Triassic, France)", at AAPG Search and Discovery Article #90906©2001 AAPG Annual Convention, Denver, Colorado
- Cacace, M., Bayer, U., Marotta, A.M., 2008: "Late Cretaceous-Early Tertiary tectonic evolution of the Central European Basin System (CEBS): Constraints from numerical modelling," In Tectonophysics 470 (2009) 105-128
- Chun, N., 2009: "Geochemische watersamenstelling van de Berkel Zandsteen", BSc Thesis, Delft University of Technology, Delft, the Netherlands.
- DAP, 2008: "Voorontwerp", Business case of the Delft Geothermal Project.
- Davies, D.K., Williams, B.P.J., and Vessel, R.K., 1992: "Models for Meandering and Braided Fluvial Reservoirs With Examples From the Travis Peak Formation", East Texas, SPE 24692, presented at the Annual Technical conference and Exhibition, October 4-7, 1992.
- De Jager, J., 2007: "Geological development", In: Wong, Th. E., Batjes, D.A.J. & De Jager, J., Geology of the Netherlands, Royal Netherlands Academy of Arts and Sciences, p. 5-26
- De Jager, J., Doyle, M.A., Grantham, P.J., and Mabillard, J.E., 1996: "Hydrocarbon habitat of the West Netherlands Basin", In H.E. Rondeel, D.A.J. Batjes, and W.H. Nieuwenhuijs, eds., Geology of gas and oil under the Netherlands: Dordrecht, Kluwer Academic Publishers, p. 191-209.
- Den Boer, C.A., 2008: "Doublet spacing in the "Delft Aardwarmte Project""", BSc Thesis, Delft University of Technology, Delft, the Netherlands.
- Den Hartog Jager, D.G., 1996: "Fluviomarine sequences in the Lower Cretaceous of the West Netherlands Basin: correlation and seismic expression", In: Rondeel, et al. (eds), Geology of gas and oil under the Netherlands, Kluwer Academic Publishers, p. 229-241.
- DeVault, B. and Jeremiah, J., 2002: "Tectonostratigraphy of the Nieuwerkerk Formation (Delfland subgroup), West Netherlands Basin." AAPG Bulletin, v. 86, no 10, p 1679-1707.
- Drost G.I.A., & Korenromp M.H.A., 2010: "Sediment petrographical analyse of the Delft Sandstone", BSc Thesis, Delft University of Technology, Delft, the Netherlands.
- Dufour, C., 2009: "De Ontwikkeling van Aardwarmteonderzoeken projecten t.b.v. Aardwarmtewinning in Nederland in de periode 1974 -1985", Seminar: Geschiedenis van aardwarmte in Nederland. (2009).

Emery, D. & Myers, K.J., 1996: "Fluvial systems" In Sequence Stratigraphy, London, Blackwell Science Ltd., p.113.

Geluk, M., 1999: "Late Permian (Zechstein) rifting in the Netherlands: models and implications for petroleum geology", In: Petroleum Geoscience, Geological Society, London, 5: p. 189-199

Gilding, D.T.G., 2009: "Casus: Geothermie ingepast in het energie klimaat beleid: Het DAP Project.", Seminar: Geschiedenis van aardwarmte in Nederland. (2009).

Grobbelen, J., Van Driel, W.W., De Coo, J.C.M., 2009: "Aardwarmte Pijnacker", Geologisch onderzoek Ammerlaan Grond- & Hydrocultuur, Panterra Rapport G746 (2009).

Hancock, J.M., 1984: "Cretaceous", In: Glennie, K.W. (eds), Introduction to the Petroleum Geology of the North Sea, Blackwell Scientific Publications, p 133-150

Haq, B.U. et al., 1987: "Chronology of Fluctuating Sea Levels Since the Triassic", In: Science, 235: p. 1156-1167

Heederik, J.P., 2009: "Geothermisch onderzoek Asten en ontwikkelingen tot 2000", Seminar: Geschiedenis van aardwarmte in Nederland. (2009).

Herngreen, C.F.W. & Wong, Th. E., 2007: "Cretaceous", In: Wong, Th. E., Batjes, D.A.J. & De Jager, J., Geology of the Netherlands, Royal Netherlands Academy of Arts and Sciences, p. 127-150

Kabel, A.B.E.T., 1986: "Production geological review of the Moerkappelle structure", Nederlandse Aardolie Maatschappij, Assen, The Netherlands, PE Report Nr. 281

Keogh, K.J., Martinus, A.W., Osland, R., 2007: "The development of fluvial stochastic modelling in Norwegian oil industry: A historical review, subsurface implementation and future directions", In: Sedimentary geology, 202: p. 249-268.

Lake, L.W., 1989: "Fractional Flow in Thermal Displacements Enhanced Oil Recovery", In: Enhanced Oil Recovery, Sec 11-3: p. 461

Loerakker, M., 2009: "Combining the geological information from a core with its logs to increase knowledge about the heterogeneity of the Delft sandstone formation", BSc Thesis, Delft University of Technology, Delft, the Netherlands.

Meehan, D.N., 1980: "Improved Oil PVT Property Correlations", In: Oil and Gas Journal, 78(43): p 64-71

Miall, A.D., 1978: "Tectonic setting and syndepositional deformation of molasse and other nonmarine-paralic sedimentary basins.", Canadian Journal of Earth Sciences, 15: p. 1613-1632.

Mijnlief, H. Obdam, A., Kronimus, A., Van Wees, J.D., Van Hooff, J., 2009: "Rapportagevereisten geologische evaluatie aardwarmte project.", TNO-Rapport 2009-01133.

NLOG, 2010: "interactive Oil and Gas map of the Netherlands", On www.Nlog.nl visited at 24th of March 2010.

Scotese, C.R. Gahagan, L.M., Larson, R.L.P., 1987: "Plate tectonic reconstructions of the cretaceous and Cenozoic ocean basins", In: Tectonophysics, 155 (1988): p. 27-48

Smits, P.F., 2008: "Construction of an integrated reservoir model using the Moerkapelle field for geothermal development of the Delft sandstone", MSc Thesis, Delft University of Technology, Delft, the Netherlands.

Simmelink, H.J., Van de Weijer, V., Ramaekers. J., 2007: "Geologisch locatie-specifiek onderzoek voor het business plan geothermie Den Haag Zuid West", TNO-Rapport 2007-UR1118/B.

Ramaekers, J., Geel, K., Lokhorst, A., Simmelink, H.J., 2006: "Nader onderzoek naar mogelijkheden van Aardwarmtewinning voor de vleestomaatkwekerij van Fa A&G van den Bosch BV te Bleiswijk" TNO-rapport 2006-U-R0016/B

TNO, 2010: "Aardwarmte in Nederland vergunningensituatie op 1 mei 2010". TNO Bouw en Ondergrond 3 editie (2010), <http://www.nlog.nl/nl/home/geothermy.html>

Van Adrichem Boogaert, H.A. & Kouwe, W.F.P., 1993-1997: "Stratigraphic nomenclature of the Netherlands, revision and update by RGD and NOGEPA", In: Mededelingen Rijks Geologische Dienst (RGD), nr 50.

Van Balen, R.T., , Van Bergen, F., De Leeuw, C., Pagnier, H., Simmelink, E., Van Wees, J.-D., Verweij, H., 1999: "Modelling the hydrocarbon generation and migration in the West Netherlands Basin, The Netherlands". In: Netherlands Journal of Geosciences ,79 (2000): p. 29-44.

Van Balen, R.T., Van Bergen, F., De Leeuw, C., Pagnier, H., Simmelink, E., Van Wees, J.-D., Verweij, H., 2000: "Modelling the evolution of hydrocarbon systems of the inverted West Netherlands Basin, The Netherlands", In: Journal of Geochemical exploration, 69-70 (2000): p. 685-688.

Verweij, J.M. & Simmelink, H.J. 2001: "Geodynamic and hydrodynamic evolution of the Broard Fourteens Basin (Netherlands) in relation to its petroleum systems", In: Marine and Petroleum Geology, Elsevier, 19 (2002): p. 339-359

Van Eldert, J., 2008: "The layers and their properties inside the Delft sandstone formation", BSc Thesis, Delft University of Technology, Delft, the Netherlands.

Van Wijhe, D.H., 1987: "Structural evolution of inverted basins in the Dutch offshore", In Tectonophysics, 137 (1987): p. 171-219

Vis, G.-J., Van Gessel, S.F., Mijnlieff, H.F., Pluymakers, M.P.D., Hettelaar, J.M.M., Stegers D.P.M. 2010: "Lower Cretaceous Rijnland Group aquifers in the West Netherlands Basin: suitability for geothermal Energy", TNO-034-UT-2009-02410

Wiggers, C.J.I., 2009: "The Delft Sandstone in the West Netherlands Basin", BSc Thesis, Applied Earth Sciences, Delft University of Technology, Delft, the Netherlands.

Wong, Th. E., 2007: "Jurassic", In: Wong, Th. E., Batjes, D.A.J. & De Jager, J., Geology of the Netherlands, Royal Netherlands Academy of Arts and Sciences, p. 107-125.

A. Appendix Formation and group abbreviations.

B. Appendix Nomenclature and abbreviations

C. Appendix Moerkapelle core log

D. Appendix List of wells

E. Appendix Palinspastic reconstruction

F. Appendix 3D static architectural reservoir modelling processes

G. Appendix Temperature and flow simulation processes

H. Appendix Additional Equations

A. Appendix Formation and group abbreviations.

B. Appendix Nomenclature and abbreviations

C. Appendix Moerkapelle core log

D. Appendix List of wells

E. Appendix Palinspastic reconstruction

F. Appendix 3D static architectural reservoir modelling processes

G. Appendix Temperature and flow simulation processes

H. Appendix Additional Equations

A. Appendix Formation and Group abbreviations

Below is a list of abbreviations used in well logs and in literature about the West Netherlands Basin. A comparison of the new and old litho stratigraphic nomenclature for the Netherlands can be found in Van Adrichem Boogaert & Kouwe (1993-1997).

Abbreviation	Group	Subgroup	Formation	Member
NU	North Sea Group	Upper		
NS	North Sea Group			
NM	North Sea Group	Middle		
NMRF	North Sea Group	Middle	Rupel Formation	
NMRFC	North Sea Group	Middle	Rupel Formation	Rupel Clay Member
NMRFS	North Sea Group	Middle	Rupel Formation	Berg (Sand) Member
NL	North Sea Group	Lower		
NLLF	North Sea Group	Lower	Landen Formation	
NLFF	North Sea Group	Lower	Dongen Formation	
NLLFC	North Sea Group	Lower	Landen Formation	Landen Clay Member
NLFFY	North Sea Group	Lower	Dongen Formation	Ieper Member
NLFFB	North Sea Group	Lower	Dongen Formation	Asse Member
NLFFS	North Sea Group	Lower	Dongen Formation	
NLFFT	North Sea Group	Lower	Dongen Formation	Basal Dongen Tuffite Member
NLFFD	North Sea Group	Lower	Dongen Formation	Basal Dongen Sand Member
KU	Cretaceous			
CK	Chalk Group			
CKGR	Chalk Group		Ommelanden Formation	
CKGRL	Chalk Group	Lower	Ommelanden Formation	
CKTX	Chalk Group		Texel Formation	
CKTXP	Chalk Group		Texel Formation	Plenus Marl Member
CKTXM	Chalk Group		Texel Formation	Texel Marl Member
CKTXG	Chalk Group		Texel Formation	Texel Greensand Member
KNGL	Rijnland Group		Holland Formation	
JW	Jurassic			
KN	Rijnland Group			
KNGLU	Rijnland Group	Upper	Holland Formation	Holland Marl Member
KNGLM	Rijnland Group		Holland Formation	Holland Claystone Member
KNGLG	Rijnland Group		Holland Formation	Holland Greensand Member
KNGLL	Rijnland Group	Lower	Holland Formation	Holland Marl Member
KNN	Rijnland Group		Vlieland Subgroup	
KNNSL	Rijnland Group		Vlieland Subgroup	De Lier Member
KNNCU	Rijnland Group		Vlieland Subgroup	Eemhaven Member
KNNCA	Rijnland Group		Vlieland Subgroup	IJsselmonde Claystone Member
KNNC	Rijnland Group		Vlieland Subgroup	Vlieland Claystone Formation
KNNSY	Rijnland Group		Vlieland Subgroup	IJsselmonde Sandstone Member
KNNSB	Rijnland Group		Vlieland Subgroup	Berkel Sandstone Member
KNNS	Rijnland Group		Vlieland Subgroup	Vlieland Sandstone Formation
KNNSC	Rijnland Group		Vlieland Subgroup	Berkel Sand-Claystone Member
KNNSR	Rijnland Group		Vlieland Subgroup	Rijswijk Member
SL	Schieland Group			
SLD	Schieland Group		Delfland Subgroup	
SLDN	Schieland Group		Delfland Subgroup	Nieuwekerk Formation
SLDNR	Schieland Group		Delfland Subgroup	Rodenrijs Claystone Member
SLDND	Schieland Group		Delfland Subgroup	Delft Sandstone Member
SLDNA	Schieland Group		Delfland Subgroup	Alblasserdam Member

AT	Altena Group			
ATWD	Altena Group		Werkendam Formation	
ATBRL	Altena Group	Lower	Brabant Formation	Brabant Marl Member
ATBR	Altena Group		Brabant Formation	Brabant Limestone Member
ATBR1	Altena Group	Lower	Brabant Formation	Brabant Limestone Member
ATWDU	Altena Group	Upper	Werkendam Formation	Werkendam Member
ATWDM	Altena Group	Middle	Werkendam Formation	Werkendam Member
ATWDL	Altena Group	Lower	Werkendam Formation	Werkendam Member
ATPO	Altena Group		Posidonian Shale Formation	
ATAL	Altena Group		Aalburg Formation	
ATTRT	Altena Group		Sleen Formation	
TR			Triassic	
RN	Germanic Trias Group			
RNKP	Germanic Trias Group		Keuper Formation	
ZE	Zechstein Group			
DC	Limburg Group			
FR	Fault			Reversed
FN	Fault			Normal
TD	Total Depth			

Table A-A-1 Formation and Group abbreviations based on Van Adrichem Boogaert & Kouwe (1993-1997).

B. Appendix Nomenclature and abbreviations

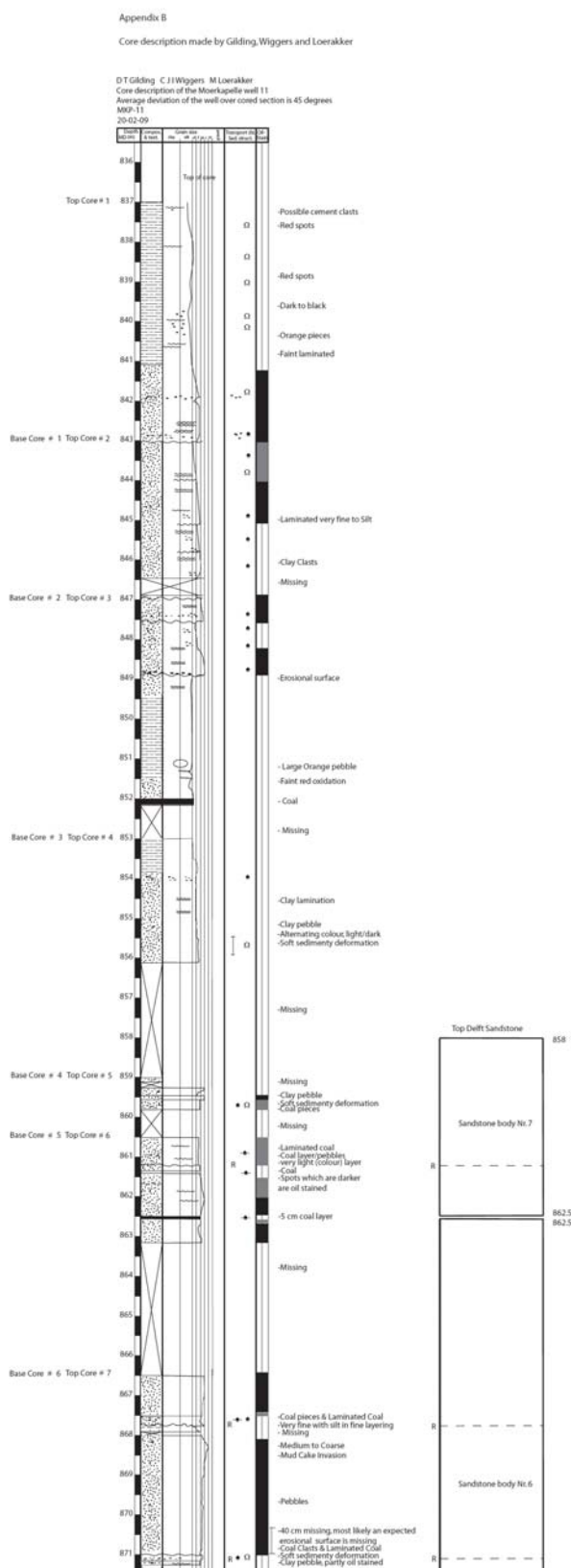
See below the table for a list of abbreviations used in this report

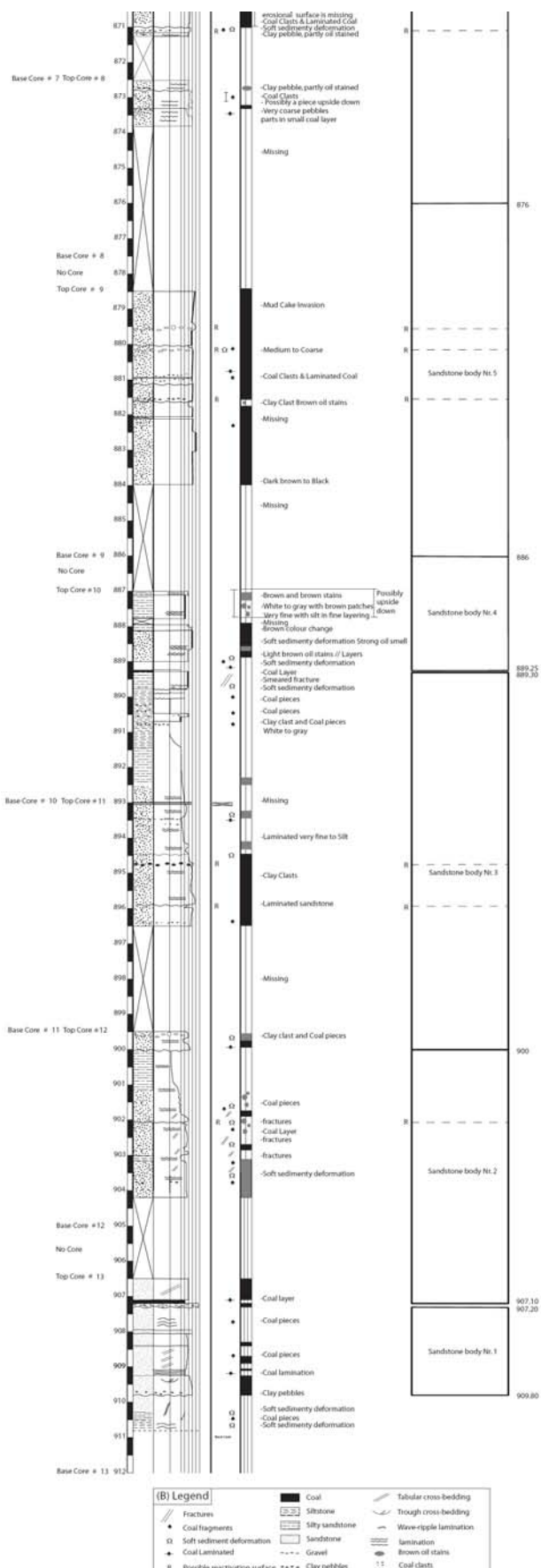
κ	thermal diffusivity	[m ² /day]
ϕ_D	porosity from density log	[-]
ϕ_e	effective porosity	[-]
ϕ_N	porosity from neutron log	[-]
ΔP	pressure difference	[Pa]
μ_w	viscosity of water	[Pa * s]
C_{pr}	rock specific heat	[J/kg °C]
C_{pw}	water specific heat	[J/kg °C]
C_{sh}	shale conductivity	[mmho/m]
C_t	conductivity log reading	[mmho/m]
C_w	water conductivity	[mmho/m]
h	reservoir thickness	[m]
k	permeability	[m ²]
K	thermal conductivity	[J/ m day °C]
L	characteristic length	[m]
m	cementation factor	[-]
n	saturation exponent	[-]
N_{PeT}	thermal Peclet number	[-]
Q_w or q	water production rate	[m ³ /s]
R	reservoir radius	[m]
R_o	log reading in 100 % water bearing section	[Ohm * m]
R_{sh}	shale resistivity	[Ohm * m]
R_t	resistivity log reading	[Ohm * m]
R_w	water resistivity	[Ohm * m]
r_w	well radius	[m]
S_w	water saturation	[-]
t	time	[day]
T	temperature	[°C]
u_w	Darcy water velocity	[m ³ /day]
V_{cl}	corrected clay volume (fraction)	[-]
v_i	velocity of the water from injection well	[m/day]
v_p	velocity of the water from production well	[m/day]
V_{sh}	shale volume (fraction)	[-]
v_T	velocity of the thermal front	[m/day]
v_w	velocity of water	[m/day]
ρ_{cl}	clay density	[kg/m ³]
ρ_{fluid}	borehole fluid density	[kg/m ³]
ρ_m / matrix	matrix density	[kg/m ³]
ρ_w	water density	[kg/m ³]

Table B-1 List of symbols used in this paper

DAP	Delft Aardwarmte Project Delft Geothermal Project
PSDM	Pre-stacked depth migrated
WNB	West Netherlands Basin
TVD	True Vertical Depth
NAP	Normaal Amsterdams Peil
MD	Measured Depth
TWT	Two Way Travel
EGS	Enhanced Geothermal Systems
VDB	Van Den Bosch (well location name)
MKP	Van Den Bosch (well location name)
HAG	Den Haag (well location name)
LIR	De Lier (well location name)
PNA	Pijnacker (well location name)
POR	Porosity
RESD,	Deep Resistivity
SP	Spontaneous Potential
RESM	Micro Resistivity
DENS,	Density
GR,	Gamma ray
SH,	Shale
NEUT,	Neutron Density
SON,	Sonic
FLGR,	FL Gamma ray
CAL	Calliper
SZ40, SZ50, SZ70, SZ30,	Sonic (number is hertz)
SON	Sonic tool

C. Appendix Moerkapelle core log





D. Appendix List of wells

	Name	Surface X	Surface Y	KB	TD (TVDSS)	TD (MD)
1	BLE- 1	96265.14916	447999.419	-2.68	892.3504028	890
2	BRK- 24	91363.25914	440987.0627	2.88	1286.824341	1482
3	DEL- 1	83005.44897	448319.2189	2.5	762.5	765
4	DEL- 2	83366.03898	447765.0392	2.55	1841.394409	1845
5	DEL- 3	84248.21901	446176.2901	4.06	2195.852295	2200
6	DEL- 4	84163.789	446368.48	4.43	1145.295288	1160
7	DEL- 5	83181.45898	447839.4892	4.93	1684.002808	1689
8	DEL- 5A	83181.45898	447839.4892	4.93	1095.070068	1193
9	DEL- 6	82734.95898	446916.2597	4.23	1266.406738	1271
10	DEL- 7	85076.47902	446482.6699	4.35	1197.20459	1202
11	DEL- 8	85486.65903	445770.5103	4.56	1695.690063	1703
12	HAG- 1	77113.45886	452159.3668	4.19	2124.52124	2129
13	HAG- 2	76208.86881	455164.9051	11.59	2644.101807	2661
14	KDZ- 2	71041.59875	454390.0856	34.3	2446.646973	2482
15	KDZ- 2A	71041.59875	454390.0856	34.3	3736.973389	3775
16	LED- 1	87795.079	453565.746	1.01	1865.536743	1867
17	LED- 3	88666.79899	456780.4841	1.11	1168.652588	1170
18	LIR- 45	75133.58889	444646.9509	7.61	3892.008545	3915
19	LOD- 1	78824.73888	451796.157	1.02	1516.108398	1518
20	MKP- 1	98895.39918	451350.1271	-0.33	1430.629517	1460
21	MKP- 10	98032.34916	451844.5169	0.53	1120.331787	1260
22	MKP- 11	98034.42916	451849.0568	0.58	989.2907104	1165
23	MKP- 12	98038.34916	451858.1068	2.4	1154.147095	1225
24	MKP- 12A	98038.34916	451858.1068	2.4	891.7918701	910
25	MKP- 13	99685.2092	449825.848	2.38	1101.46936	1327
26	MKP- 14	97442.97915	452342.8866	2.45	2687.648682	2820
27	MKP- 15	97403.55915	452374.1266	2.57	1050.222046	1170
28	MKP- 16	96268.58913	452703.3964	2.4	1467.784302	1525
29	MKP-2	100483.53	449086.26	-1.89	1401.597259	1400
30	MKP-3	98581.02	450635.41	-0.07	1214.859201	1215
31	MKP-9	98849.14	450942.98	-0.35	878.3973966	900
32	MKP-9A	98849.14	450942.98	-0.35	1093.972995	1160
33	MON- 2	71825.0088	449956.1981	9.22	2966.199463	3030
34	MON- 2A	71825.0088	449956.1981	9.22	2978.135498	3034
35	MON- 3	72591.13881	450070.028	11.42	3010.199463	3191
36	MSG- 1	62089.47872	444653.6811	13.58	3369.251953	4260
37	OLE- 1	87222.43907	443812.4913	2.52	1865.092285	1868
38	PNA- 13	86517.07901	449433.3883	1.4	2413.907715	2500
39	PNA- 14	86711.28902	449186.2584	2.31	1856.286865	1910
40	PNA- 15	84680.76898	450094.5379	2.22	1896.053711	1900
41	RTD- 1	90846.37919	432582.1269	11.97	3050.89917	3305
42	RTD- 1A	90846.37919	432582.1269	12.01	1682.226196	2000
43	RWK- 1	81064.78894	449085.7585	5.02	2566.617676	2575
44	RWK- 2	81027.27894	449147.2685	3.34	1558.549316	1562
45	RWK- 4	80809.33893	449715.0682	4.49	2025.162476	2031

46	RWK- 6	81057.03894	448695.4287	3.85	1775.459229	1780
47	RWK- 8	80848.74894	449086.7285	4.46	1541.275757	1546
48	RWK- 13	81897.98895	449062.7885	3.25	1624.833862	1636
49	RWK- 17	80776.91893	449434.5883	4.15	1554.82019	1560
50	RWK- 18	80846.22894	449091.5285	4.85	615.0024414	650
51	RWK- 18A	80846.22894	449091.5285	4.85	1522.862427	1847
52	SCL- 1	82103.34898	445585.8004	1.79	1465.039429	1467
53	WAS- 23	84837.18892	458389.7632	4.62	2085.563721	2093
54	WAS- 23A	84837.18892	458389.7632	4.62	1324.521973	1330
55	WAS- 23B	84837.18892	458389.7632	4.62	3112.689941	3149
56	ZOM- 2	92646.03906	454797.8252	0.77	1682.165894	1684
57	ZOM- 2A	92646.03906	454797.8252	0.77	1083.510376	1100

Table D-1 List of wells available used in the study for the writing of this paper.

E. Appendix Palinspastic reconstruction

A two dimensional palinspastic reconstruction of target area Vrijenban was performed to get a better understanding of the structural geology and the basin evolution. By reconstructing the major surfaces and back convolution of deposits, it is possible to get a better understanding where, how and how much accommodation space is created. Furthermore it gives insight into how the target area was formed and the deposition of the sediments, took place.

Geological reconstruction uses a scientific flattening method, available geological data, deductive reasoning and their interrelationships to acquire knowledge to the events that may have led up to the geological complex structures that are found under the target area Vrijenban. It can determine what exactly happened at a specific moment in geological time.

Specific incident reconstruction of faulting and rifting, deals with the tectonic components as subsidence and uplift and the effect of compression en extensional forces. Depositional reconstruction looks at deposition, erosion, etc. It is important to reconstruct a geological site because if one has no knowledge as to what took place and how it took place, they lack the ability to figure out what the depositional setting was during deposition of a single formation. Geological 2D reconstruction helps interpret physical movement. It is an aid to help formulate a hypothesis and arrive at a conclusion about what major structures are, the movement along faults and the amount of deposition, subsidence and movement.

By approximating all major formation boundaries to be horizontally flat at deposition, all structures formed by faulting and rifting, and taking possible erosion into account, it is possible to make a reconstruction of the major tectonic events that led to the creation of a geological structure.

For this study multiple 2D interpreted sections of seismic data were loaded into a program called 3D Move.

An overview of the 2D reconstructed sections can be found in the figure below. From each of the section the major surfaces and some good reflectors were interpreted. Then major tectonic events where unscrambled by flattening surfaces and un-raffling the movement caused by tectonic events in geological history. This flattening step was performed for three surfaces showing in reverse the amount and type of movement that happened during or after the deposition of the interpreted boundary.

Workflow

The process of reconstruction a 2d seismic section.

Several 2d seismic profiles were chosen and scaled from the Pre Stacked Depth Migrated seismic. Each 2D slices contains at least one well for depth control. A top map of the slices is shown in the figure below.

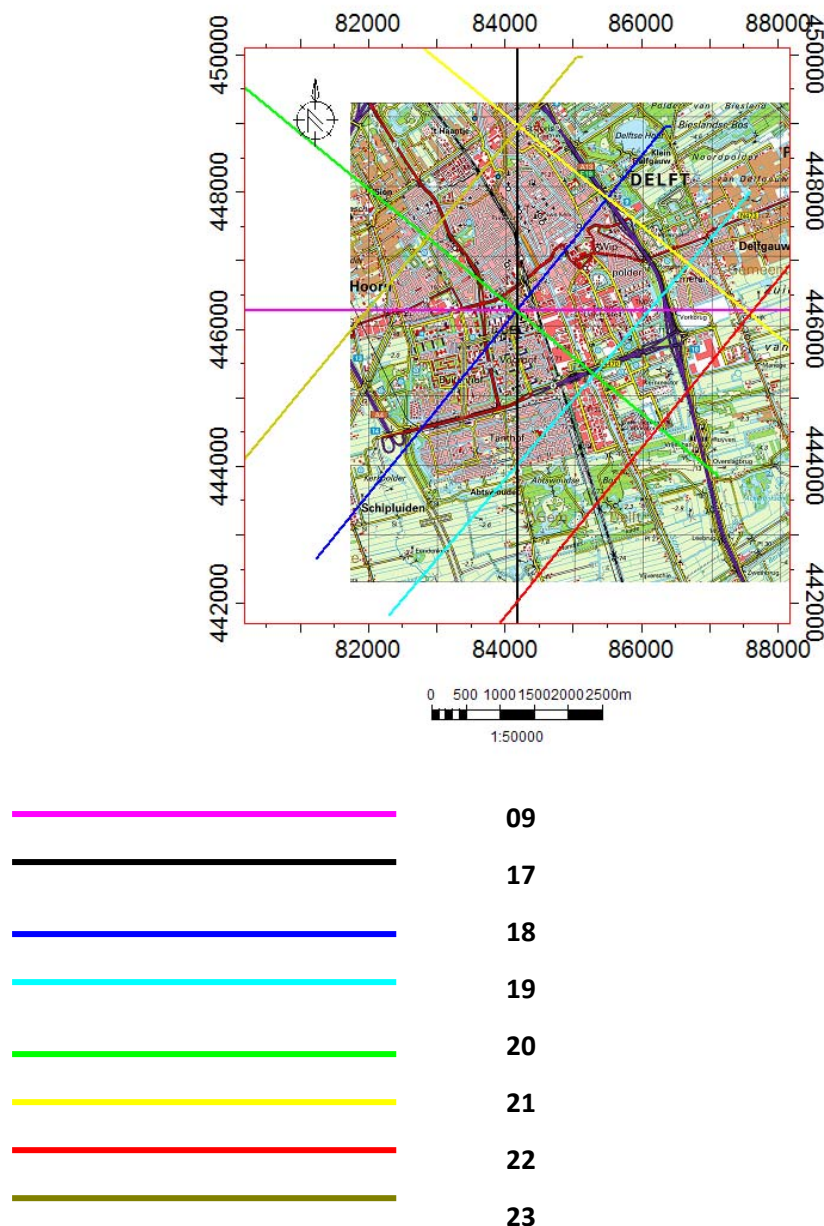


Figure E-1 Map of Delft with the seismic profiles that have been 2D palinspastic reconstructed.

The pictures were loaded into a reconstructing software called 3D Move; the seismic sections were loaded and scaled with the z in true vertical depth.

The north sea unconformity, Top Chalk, top Texel marl and Top Schieland group where interpreted and loaded as surface lines. Also two or three good reflectors below the Top Schieland Group were interpreted as base mark to show the predominant structures below the Schieland Group. The major faults were interpreted and loaded.

Although possibly none of the chosen boundaries are deposited horizontal but for the purpose of this study they are modelled as such. Therefore every continuous interpreted “top” surface was approximated as a horizontal flat boundary surface. Possible detachment, on laps, valley fills, erosion, reworking of sediment or deposition on non flat surfaces were neglected when flattening a single surface. Large structural infill’s and erosion of large parts of formations can still be interpreted and these surface are not flattened.

Faults were loaded as a break in a single horizontal surface. Movement of layers around faults during the 2d reconstruction is possible along the fault when flattening higher surfaces. If a surface was flattened still containing a fault, the horizontal layers were connected and fitted accordingly to the flattening depth.

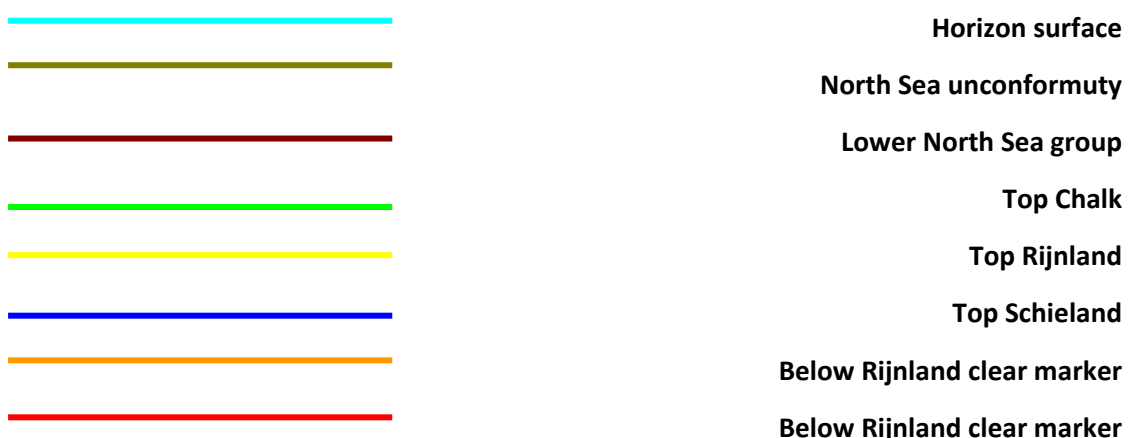


Figure E-2 Colours used and represented in the 2D palinspastic reconstructed.

Profile 09

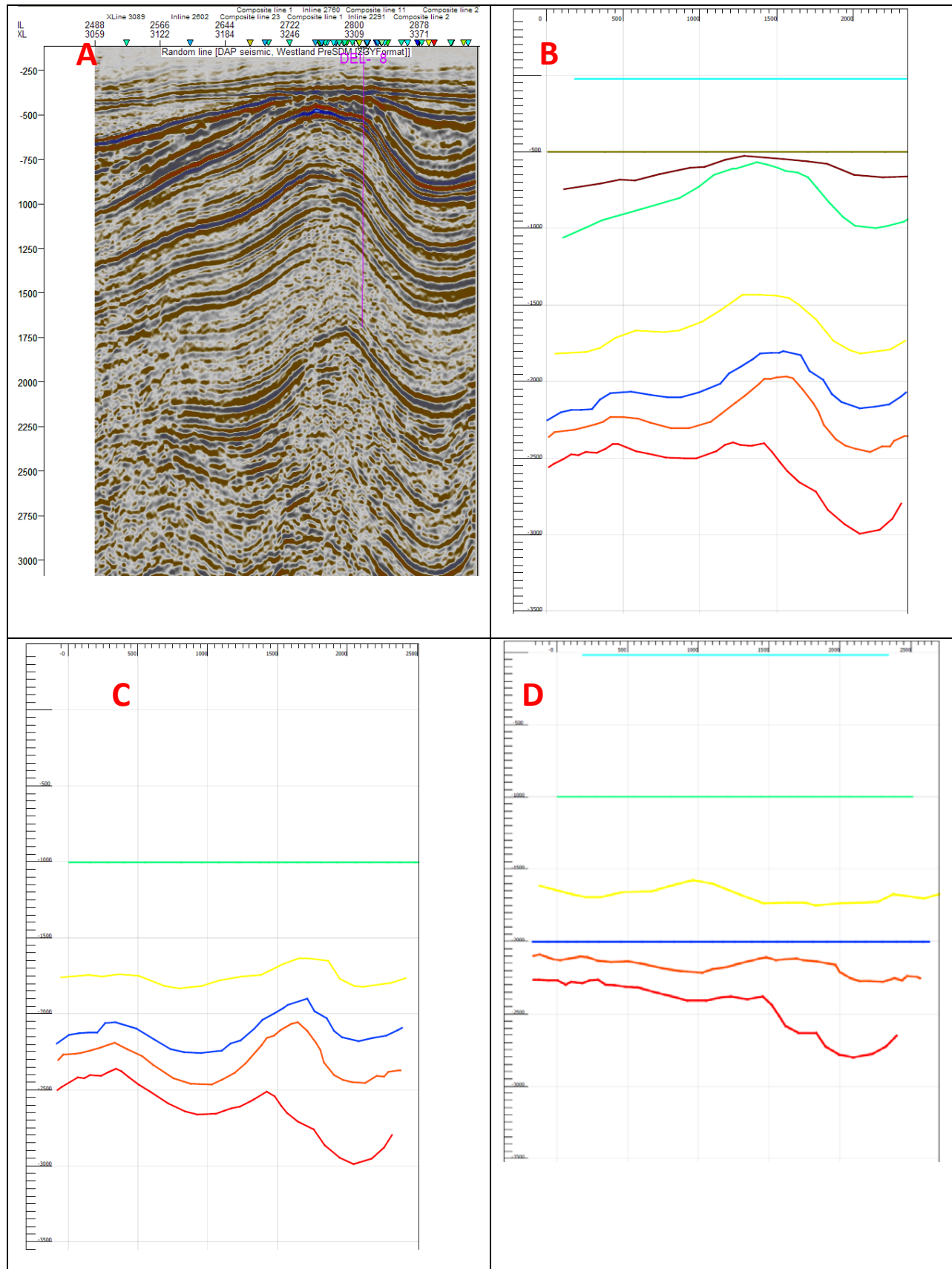


Table E-1 A) Image scaled interpreted surfaces. B) Flattened Top North sea unconformity
C) Flattened Top Chalk Group D) Flattened Top Scheiland Group

Profile 17

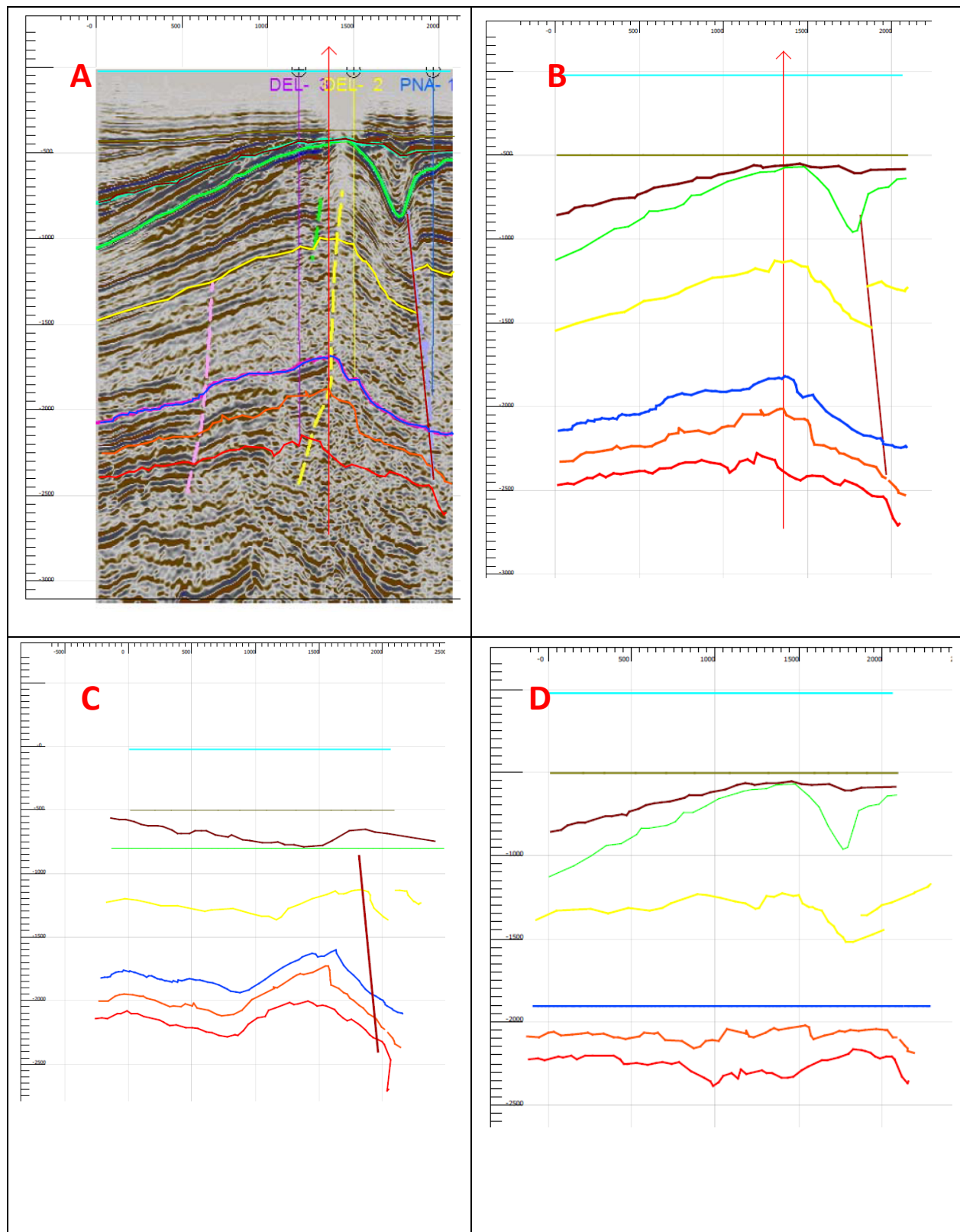


Table E-2 A) Image scaled interpreted surfaces. B) Flattened Top North sea unconformity
C) Flattened Top Chalk Group D) Flattened Top Scheiland Group

Profile 18

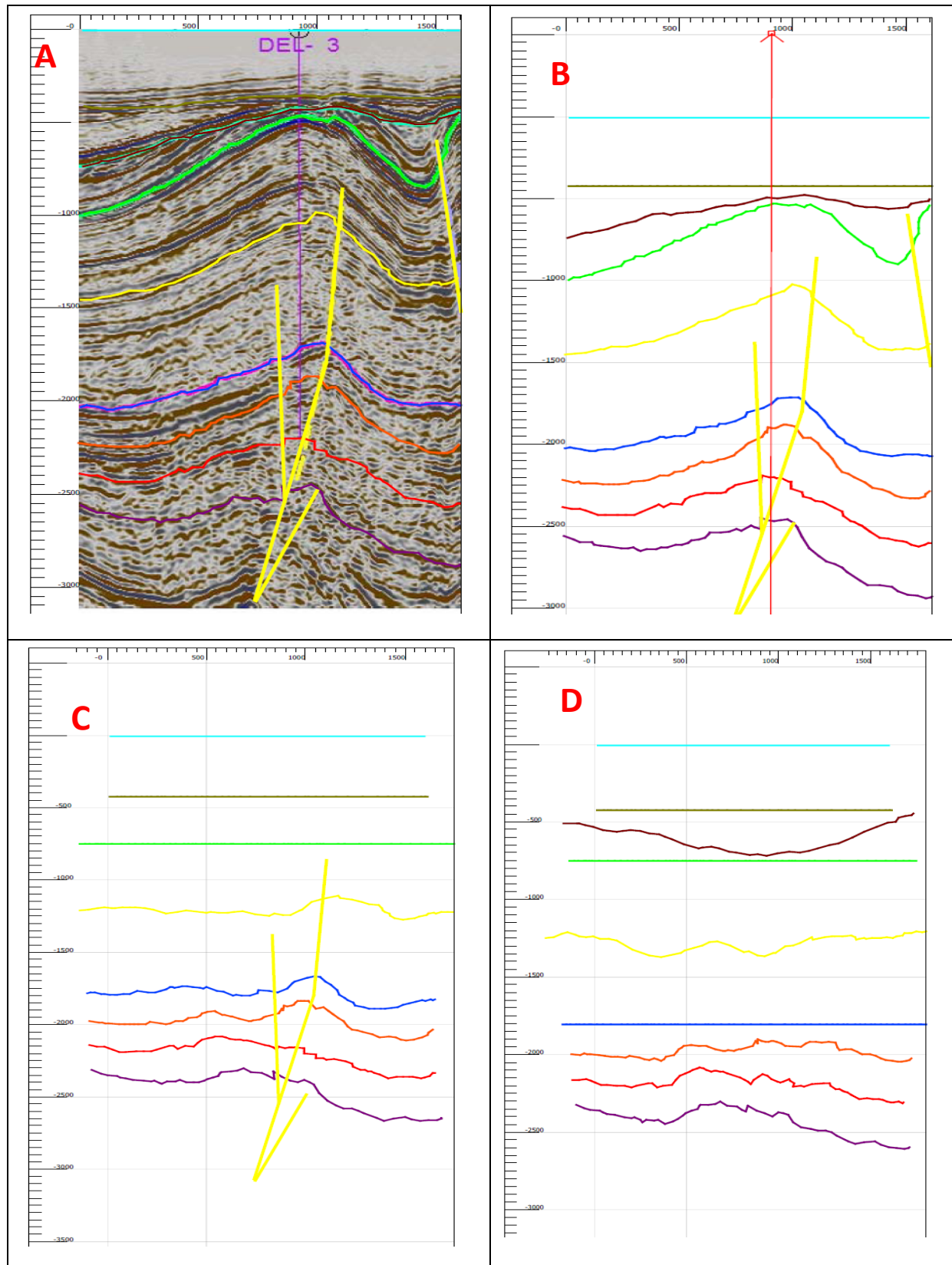


Table E-3 A) Image scaled interpreted surfaces. B) Flattened Top North sea unconformity C) Flattened Top Chalk Group D) Flattened Top Scheiland Group

Profile 19

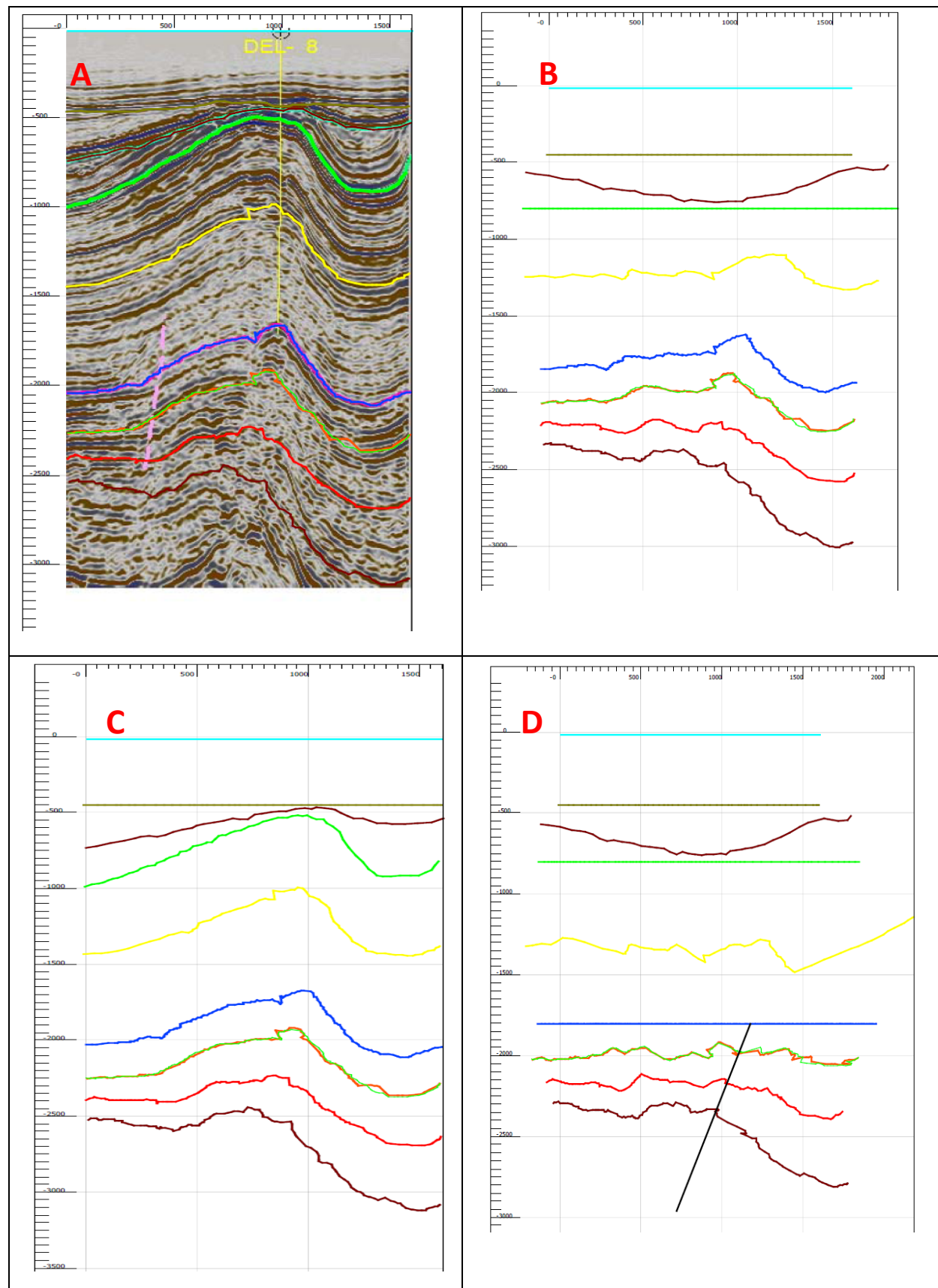


Table E-4 A) Image scaled interpreted surfaces. B) Flattened Top North sea unconformity C) Flattened Top Chalk Group D) Flattened Top Scheiland Group

Profile 20

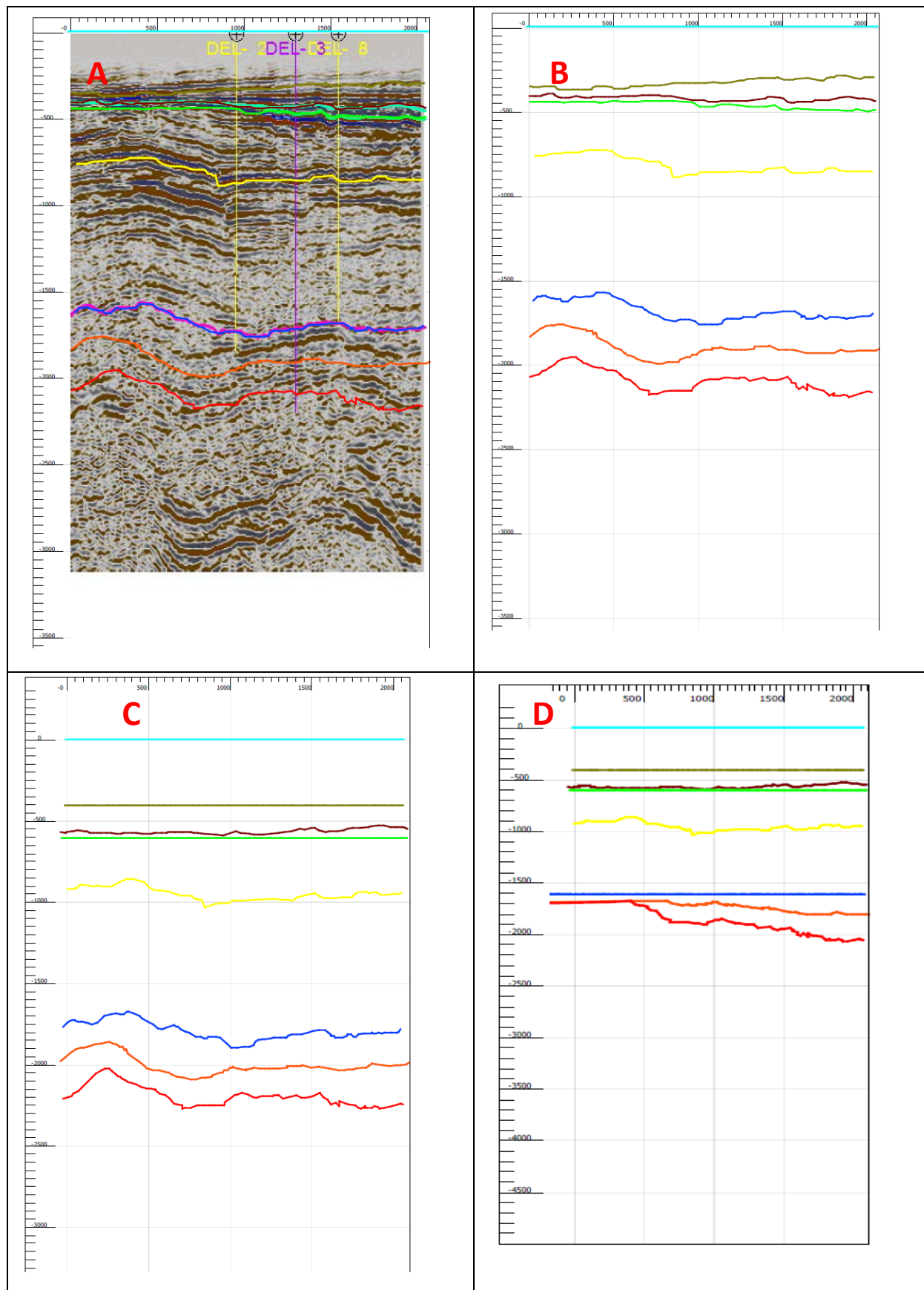


Table E-5 A) Image scaled interpreted surfaces. B) Flattened Top North sea unconformity C) Flattened Top Chalk Group D) Flattened Top Scheiland Group

Profile 21

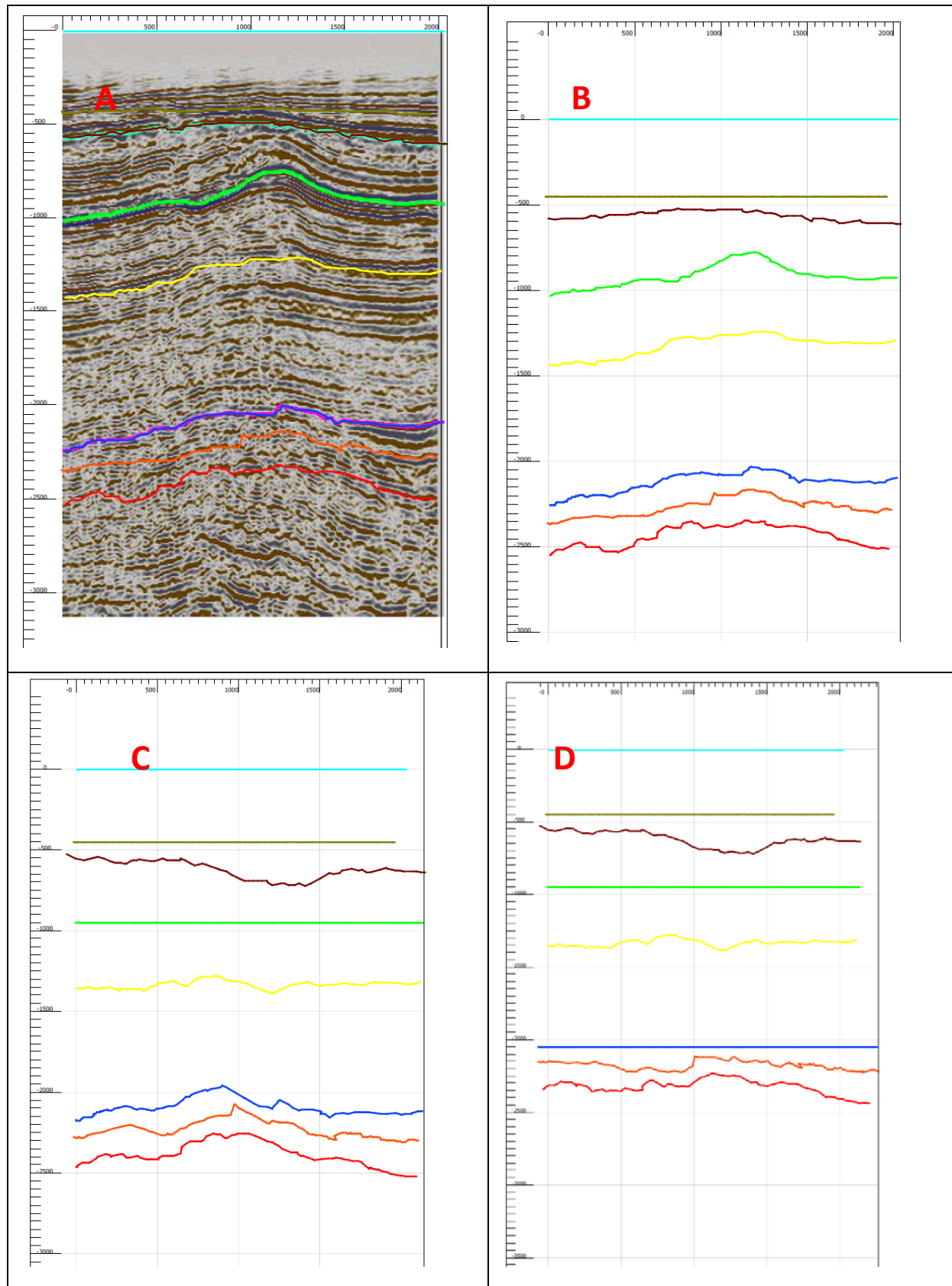


Table E-6
 A) Image scaled interpreted surfaces.
 B) Flattened Top North sea unconformity
 C) Flattened Top Chalk Group
 D) Flattened Top Scheiland Group

Profile 22

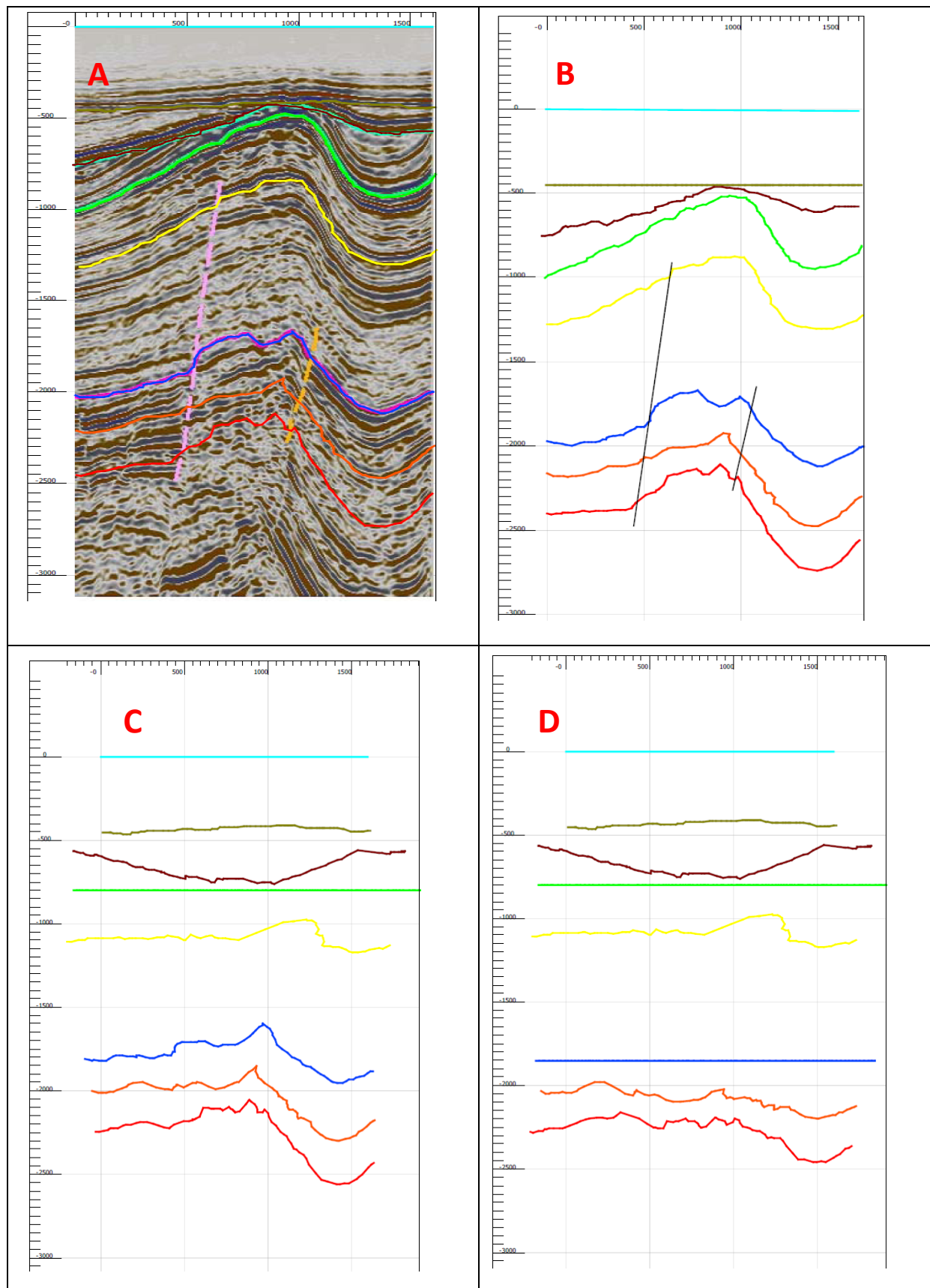


Table E-7
A) Image scaled interpreted surfaces.
B) Flattened Top North sea unconformity
C) Flattened Top Chalk Group
D) Flattened Top Scheiland Group

Profile 23

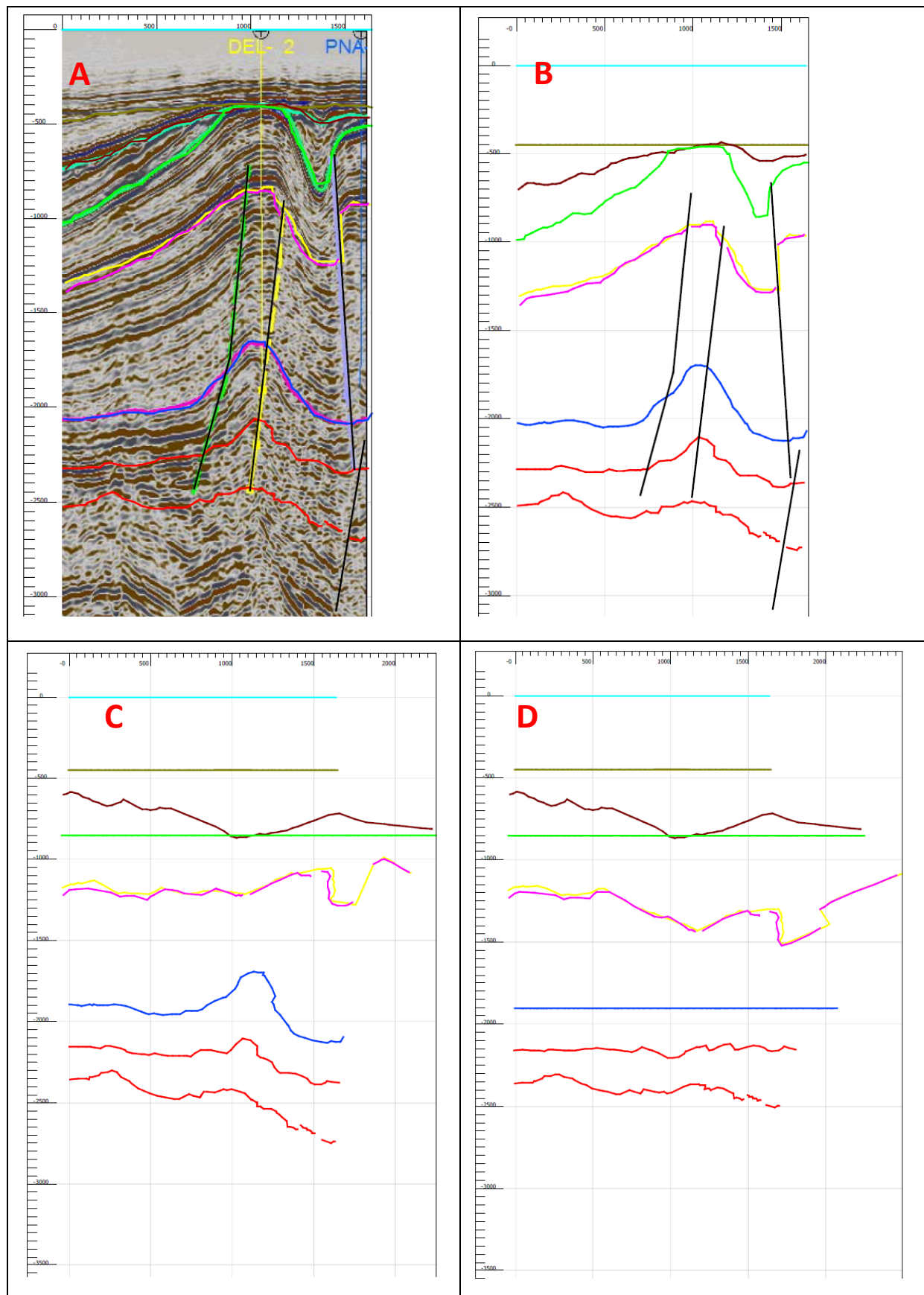


Table E-8
A) Image scaled interpreted surfaces.
B) Flattened Top North sea unconformity
C) Flattened Top Chalk Group
D) Flattened Top Scheiland Group

To gain a better view of the entire basin another southwest – northeast section was also reconstructed.

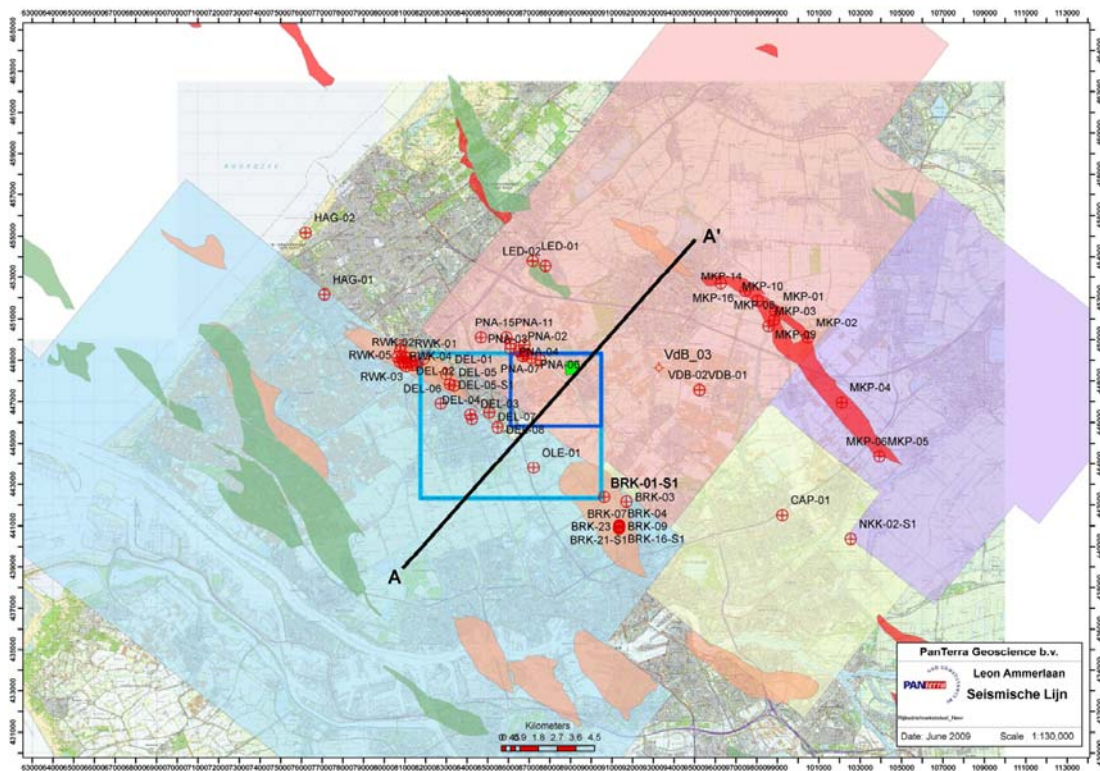


Figure E-3 Map showing the SW-NE section over the entire area.

Profile SW-NE

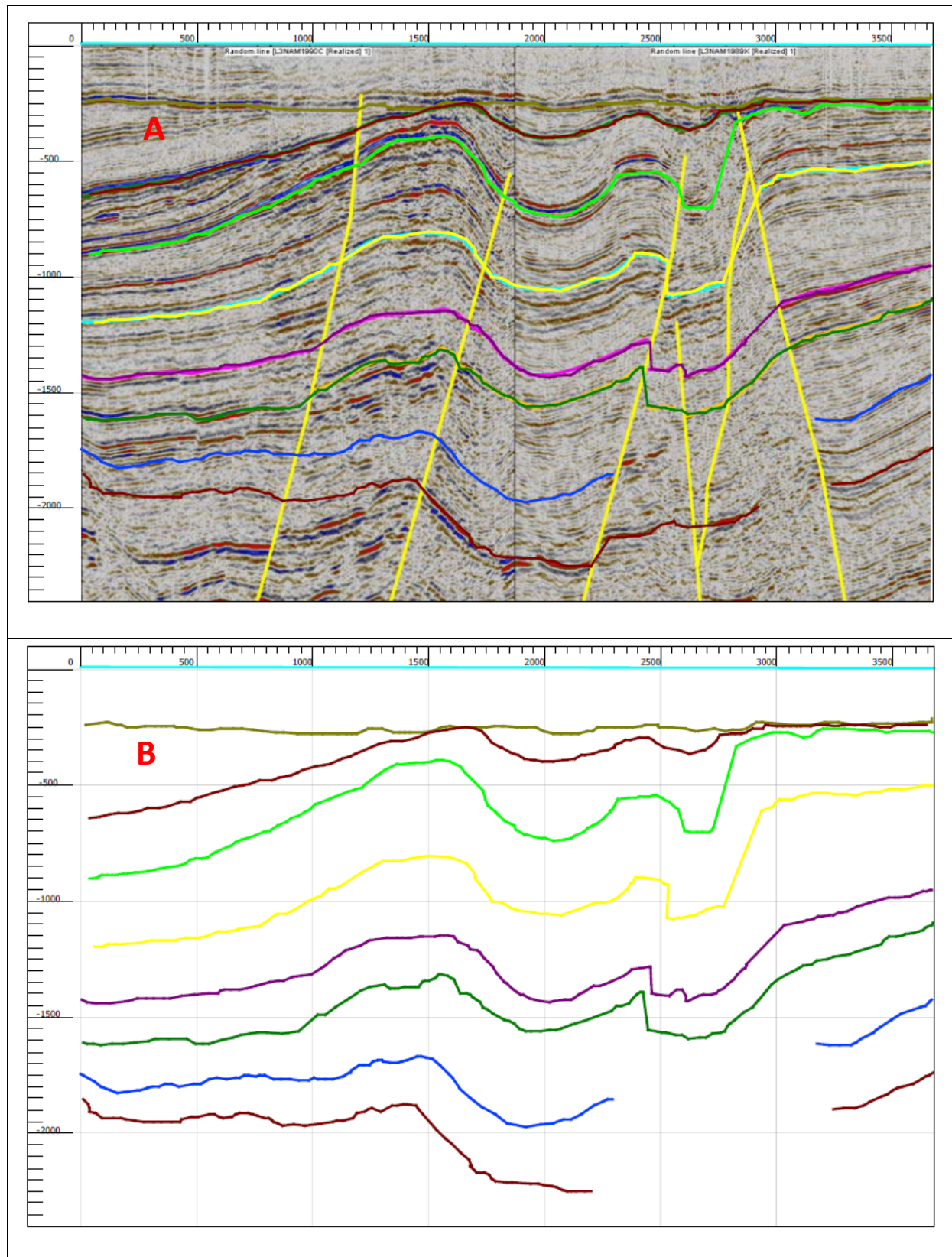


Table E-9 A) Image scaled interpreted surfaces. B) Lines without image

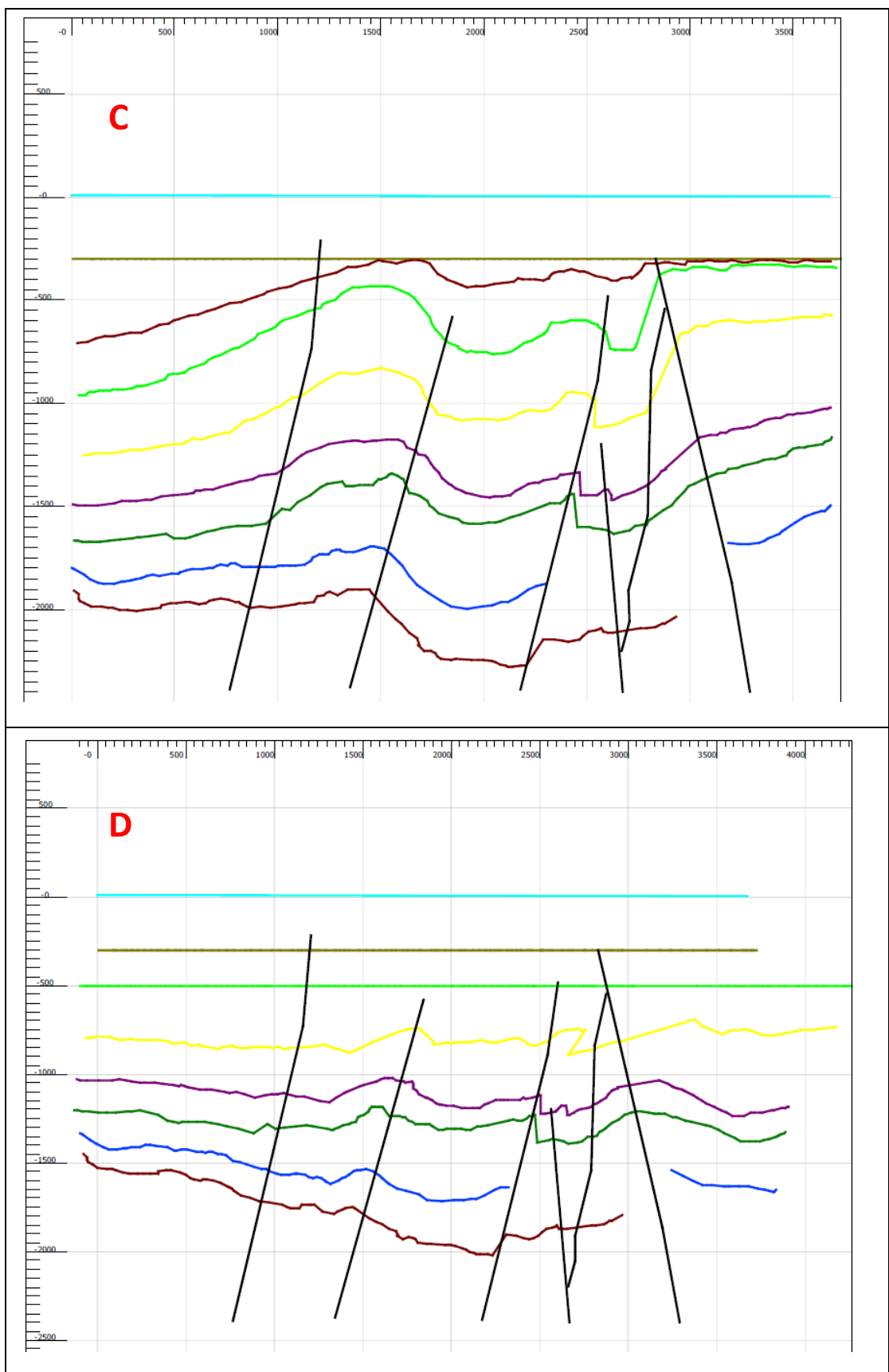


Table E-10 C) Flattened Top North Sea unconformity D) Flattened Top Chalk Group

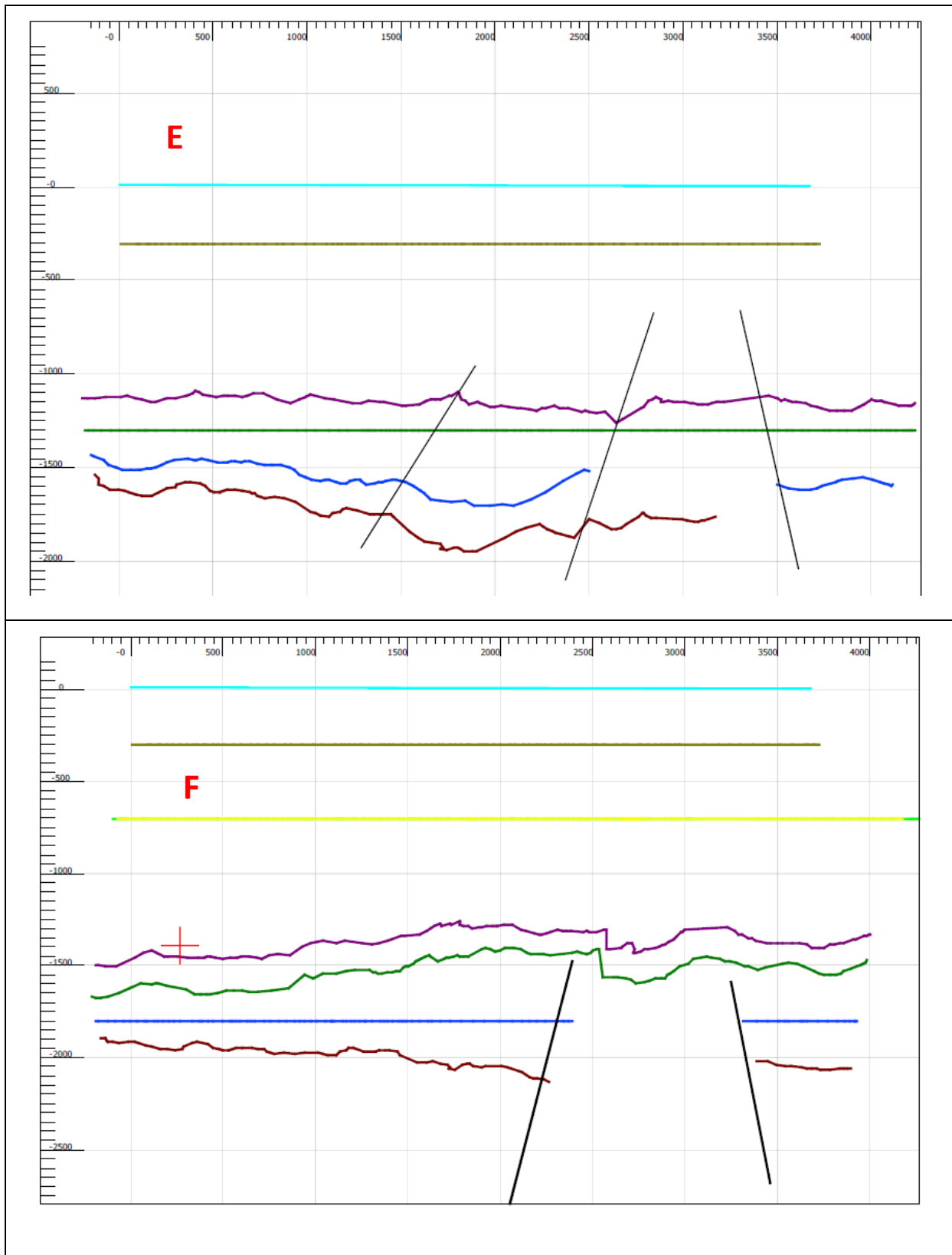


Table E-11 E) Flattened Top Scheiland Group 3 faults F) Flattened Top Scheiland Group 2 faults

Results and points of concern

The 2D reconstruction shows clearly that there were 4 tectonic phases, the first and second creating a syn rift tectonic growth fault during the deposition of Rodenrijs Claystone member and the formation directly above and below and, a second phase where reactivation took place along the predominant main bounding faults creating popup structures. These phases could have happened continuous with two large pulses or as two separate phases. During the inversion of the structures the popup structures were created and erosion took place because of the uplift. After the erosion and uplift through inversion, a third phase took place where further subsidence continued, deposition on top of the current predominant structures until this day.

The reconstruction does not go beyond the growth faults created during the pre-rift stage as phase one. It is expected from literature that prior tectonic activity and deposition has occurred before this first phase that is not accounted for in the 2D reconstruction study.

The main 2D movement in the 2D reconstruction could also be containing a strike slip component that is not visible. Therefore caution has to be taken in the interpretation and a 3D construction is advisable in further studies.

The results were imported into Petrel. A description of the basin evolution can be found in chapter 4.

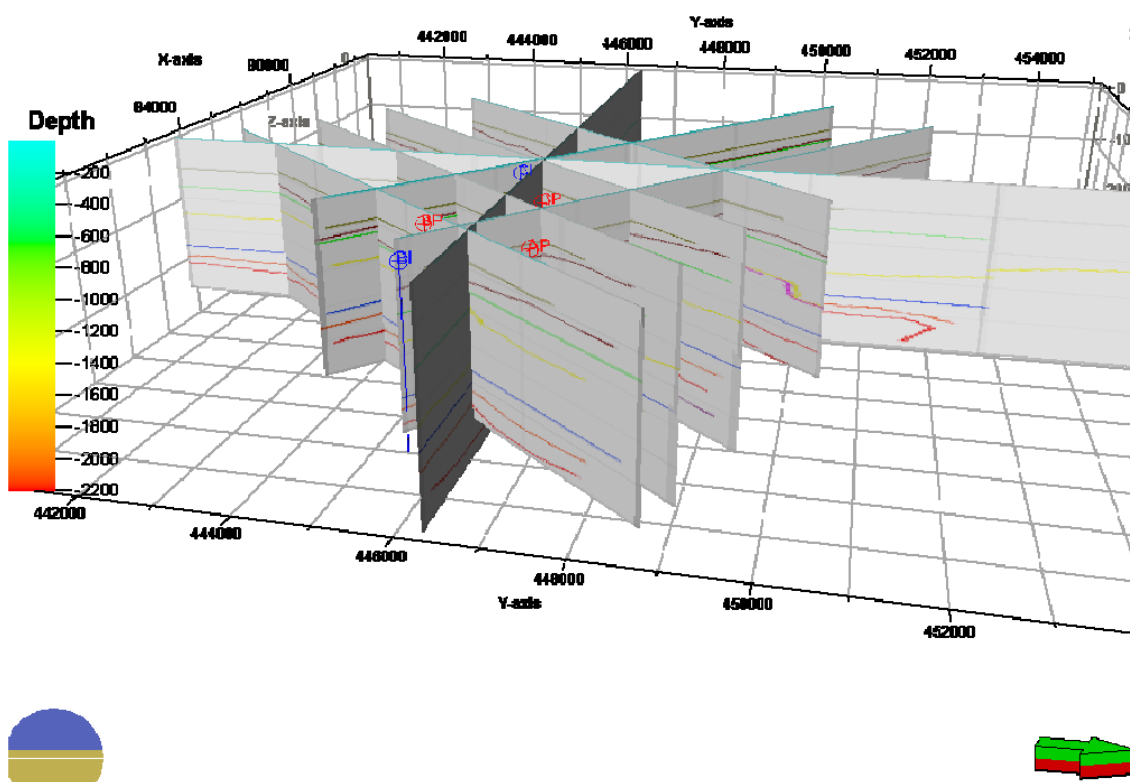


Figure E-4 3D view from east showing the palinspastic reconstruction of the basin.

F. Appendix 3D static architectural reservoir modelling processes

Building the grid

The grid is needed as a structural frame to populate the grid cells with properties. The grid is created using the “make simple grid” building utility tool in Petrel[®] (Figure F-1). The input data consist of the vertical boundaries in a polygon, the surfaces of the Top Rodenrijs Claystone Member, Top Delft Sandstone Member and the Inter Alblasserdam Member and the chosen grid size. The chosen grid size in the x, y direction is 50 meters by 50 meter as this is the same size as the bin recording size of the seismic data.

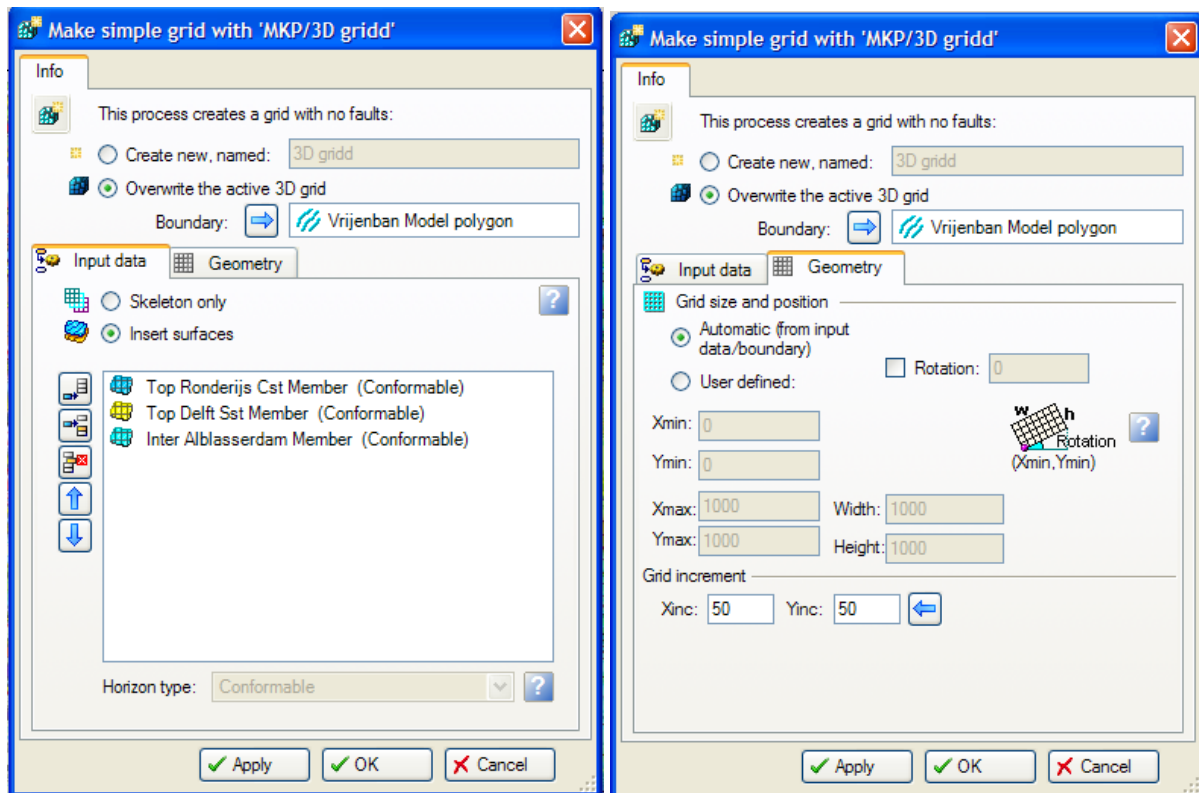


Figure F-1 The used “Make simple grid” windows with the input data and values.

Zones

The zones are built into the model using the “Make zone” structural modelling tool in Petrel[®], Using the “Isochore” input type (Figure F-2). In this method the relative thickness of a zone, throughout the model, is based on isochores thickness maps. The input data consists of the grid, the surfaces of the Top Rodenrijs Claystone Member, Top Delft Sandstone Member and the Inter Alblasserdam Member marker surface and the well tops and stratigraphic thicknesses from the Delft-03 well.

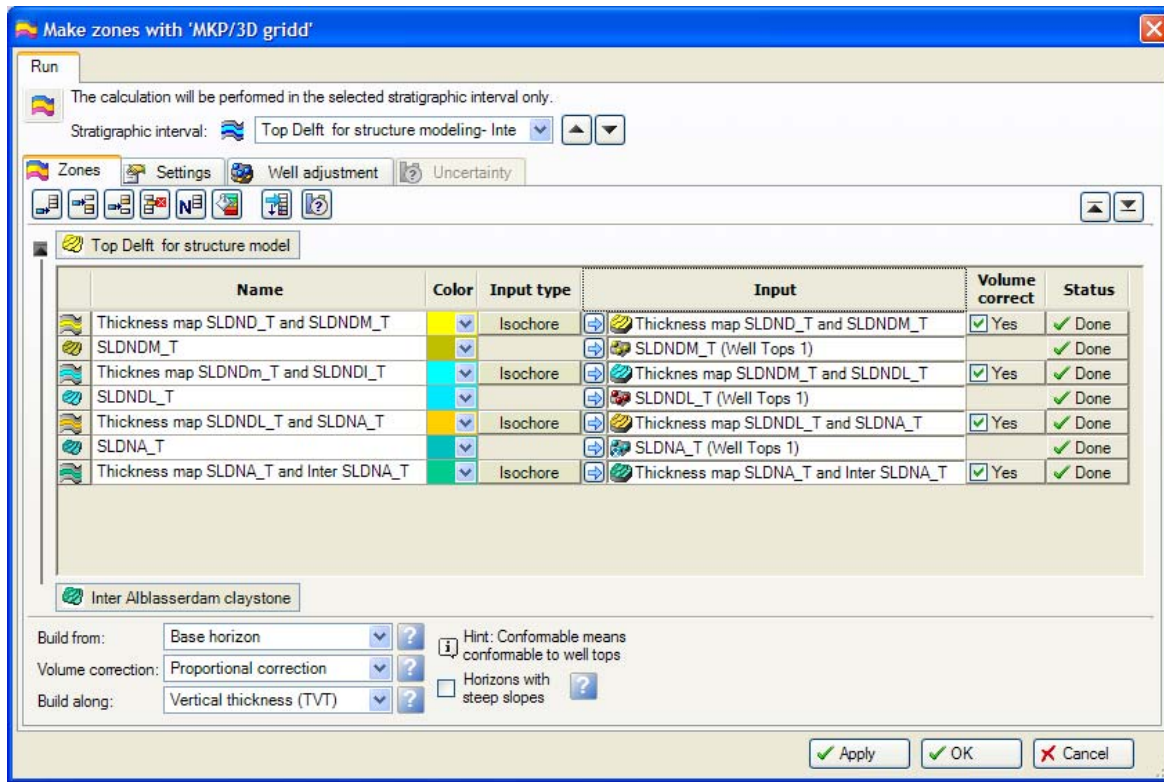


Figure F-2. The “Make zone” tool with the isochore input type and input data.

Layers

Each zone is divided into grid layers because one stratigraphic zone can have different lithofacies. For each zone a number of layers will be needed to be set so that the grid can represent the layered lithofacies. The layering of the zone is performed by using the “layering” structural modelling tool in Petrel® (Figure F-3).

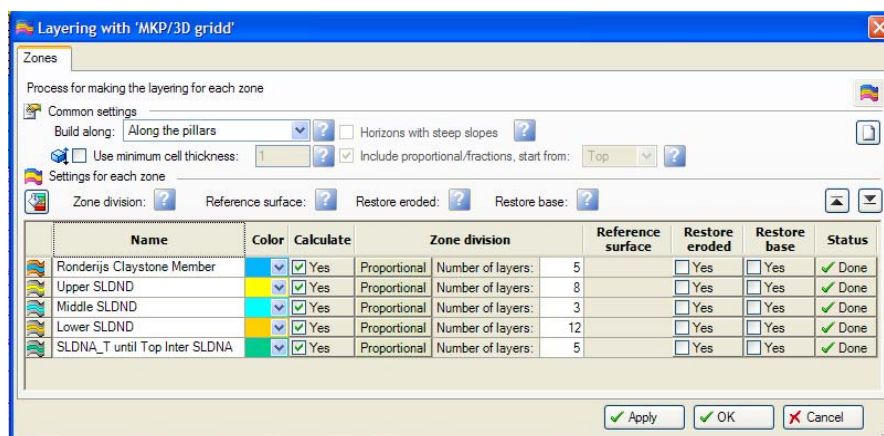


Figure F-3. The “layering” tool with the number of created layers per zone.

The input data consists of the created grid model including the created zones and the chosen number of layers per zone. The number of layers is different per zone based on the details that need to be modelled. The Upper, Middle and Lower Delft Sandstone Member zones have been divided into layers based on the thickness of the zones in the Delft-03 well. The total thickness of the Delft Sandstone Member in the Delft-03 well is 115 meters. The total thickness is divided into layers of 5 meters, creating 23 layers in the Delft Sandstone Member. The Rodenrijs Claystone Member zone

and the Alblasserdam Member zone are not the target of this study and have therefore been divided into 5 layers each (Table F-1) (Figure F-4).

Layers				
Zone 1	Rodenrijs Claystone Member	SLDNR	5 Layers	
Zone 2	Upper Delft Sandstone Member	SLDND U	8 Layers	
Zone 3	Middle Delft Sandstone Member	SLDND M	3 Layers	
Zone 4	Lower Delft Sandstone Member	SLDND L	12 Layers	
Zone 5	Alblasserdam Member	SLDNA	5 Layers	

Table F-1 Layers used to build the model. Each zone is divided into multiple layers.

3D grid model

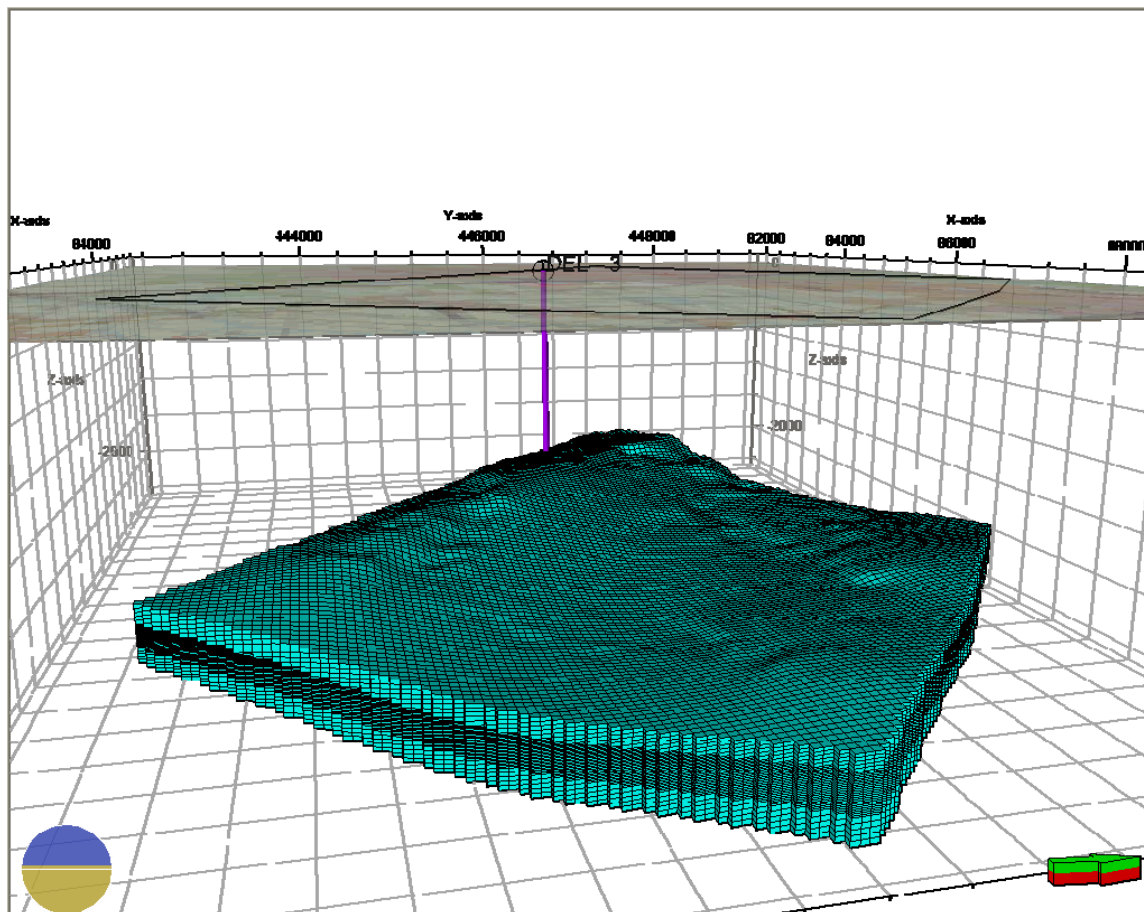


Figure F-4 Side view from the east of the total created 3D grid structure with the Delft-03 well.

Upscaling the wells,

By upscaling the wells it is possible to fit the data of the wells to the grid size of the model. Upscaling is a process that matches the resolution of the well data to that of the model. Well and core data have a far higher resolution compared to the layer thickness in the model. By upscaling the resolution of the well it is changed, using a mathematical or statistical approach to the layer size. The upscaling of the discrete facies well log data is performed by using the “scale up well logs” property modelling tool in Petrel® (Figure F-5). The input data consist of the layered grid model and the discrete facies logs of the Delft wells 1 to 8 and the Moerkappelle wells 1 to 16. There are different methods of upscaling. Options are however constrained, for the facies log is a discrete log so statistical options are not preferred. The method used in this study is the “Most of” method. The “Most of” method will select the discrete value which is most represented in the log for each particular cell. This method is chosen as each cell represents the most found facies in that cell and therefore the most dominant depositional mechanisms. A better option would be not to upscale the well log and use infinite cells and layers.

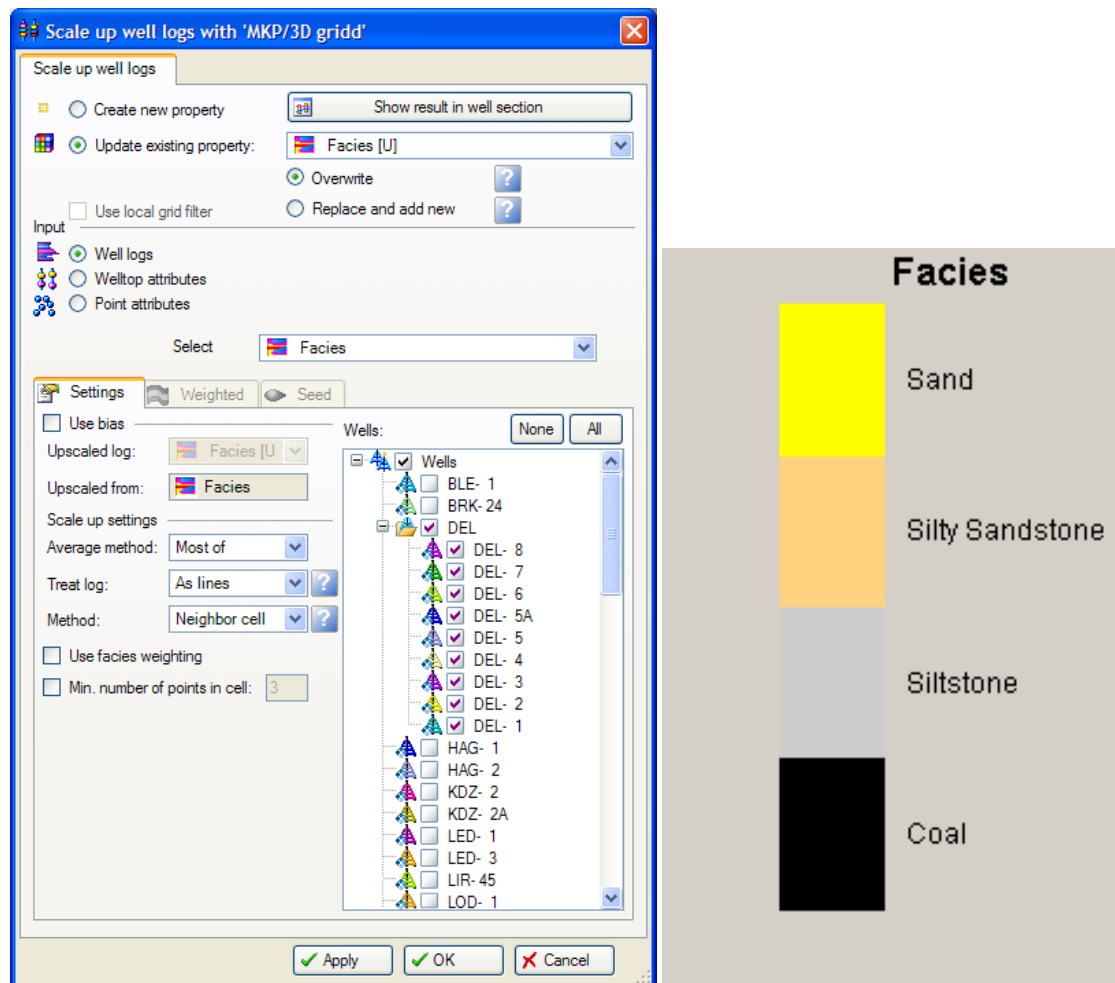


Figure F-5 The “Scale up well logs” tool with settings and wells used. On the left the discrete facies input is shown.

Facies Modelling

After completing the structural model, which is a framework for the facies model, the next step is to populate the model with lithological properties. For proper facies modelling, knowledge of the spatial distribution of the lithology is necessary. This knowledge is partly derived from the conceptual depositional model and partly from the data itself. The facies modelling, creating a 3D model of distribution of the discreet facies, is performed by using the “Facies modelling” property modelling tool in Petrel[®] (Figure F-6, Figure F-7, Figure F-8, and Figure F-9). Facies modelling methods can be done by using either deterministic or stochastic methods. Deterministic facies modelling have the disadvantage that with little data the result is too continuous and does not represent the natural variation created by sedimentological processes. Therefore modelling was done with stochastic modelling methods. These methods use a random seed, which means that every outcome will be slightly different, even with the same input data. Each zone was deposited in a different depositional environment. Therefore it is important that each zone is modelled separately. There are different methods to populate the grid with lithofacies and each zone is modelled separately using a specific method (Table F-2).

Zone	Name	Modelling Method	Seed
Zone 1	Rodenrijs Claystone Member	Assigned Value	
Zone 2	Upper Delft Sandstone Member	Object modelling (stochastic)	10000
Zone 3	Middle Delft Sandstone Member	Object modelling (stochastic)	10000
Zone 4	Lower Delft Sandstone Member	Object modelling (stochastic)	10000
Zone 5	Alblasserdam Member	Assigned Value	

Table F-2 Methods used in modelling the zones with the used seed number.

Modelling the Alblasserdam- and Rodenrijs Claystone Member.

The Alblasserdam Member and the Rodenrijs Claystone Member are not the primary target of this study. Therefore these zones have not been modelled in detail. As these members are at the base and top of the structure, they may still interact with the temperature flow during temperature and flow modelling. The Alblasserdam Member and Rodenrijs Claystone Member are therefore modelled using the “assigned value” method. To be able to assign property values to these zones it is chosen to model the Alblasserdam Member and Rodenrijs Claystone Member as massive siltstones (Figure F-6). Although the members contain more than just silt and claystones both zones will be assigned set values for the purpose of heat convection and conduction in the flow modelling part of this study and will not be assigned any siltstone properties.

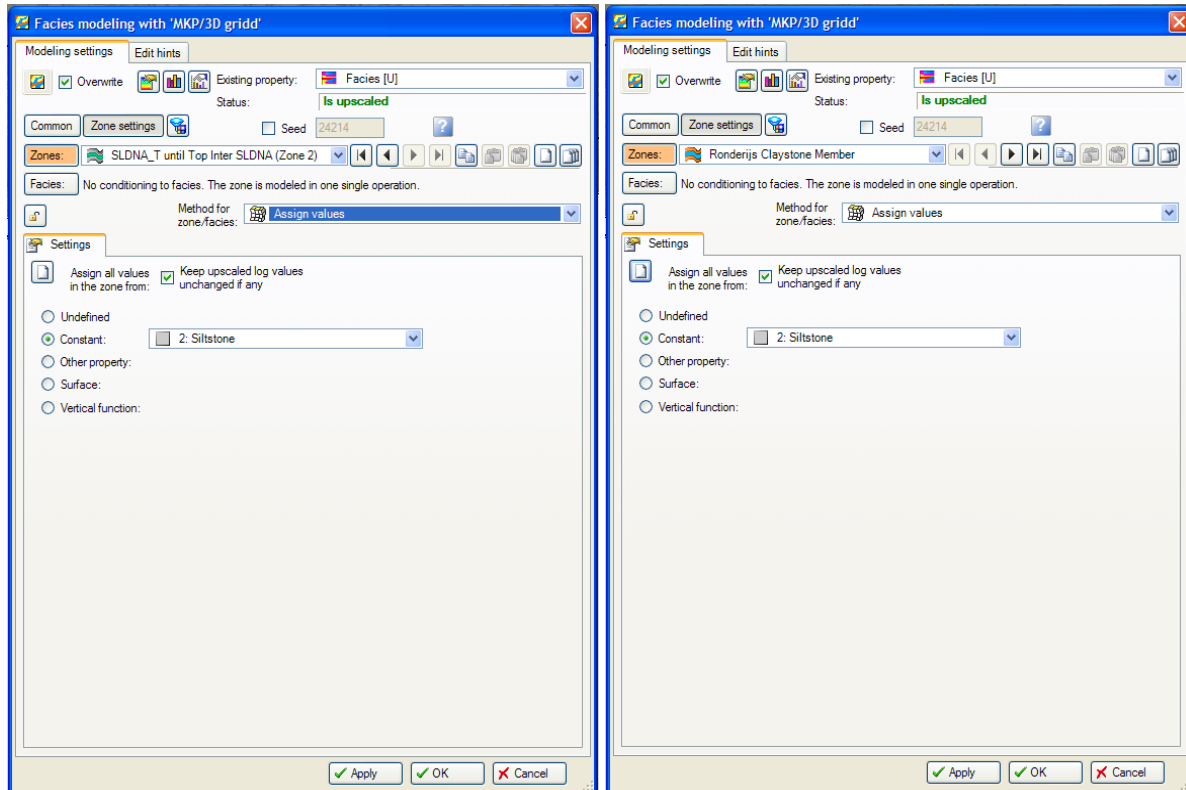


Figure F-6 The “Facies modelling” tool with the settings used to model the Alblasserdam Member (right) and the Rodenrijs Claystone Member.

Modelling the Lower Delft Sandstone Member zone,

The Lower Delft Sandstone Member is modelled by using the object based modelling method. Object based modelling populates a facies model with stochastically generated and distributed objects. The geometrical properties, like size and orientation, can be assigned with a statistical distribution. This method is especially suited for this zone because the zone consists of a single meandering fluvial channels and the background of floodplain deposits. The Lower Delft Sandstone is therefore modelled using object based modelling as a well developed meandering fluvial channel deposit. The geometrical properties of the fluvial channels are known and can be added as input into this modelling process. The exact position of the channels is however not known, except at the one well location in Delft 03 well. The modelling algorithm therefore places the object first at the well location, and fills the rest of the area with randomly placed objects, that honour the data and total percentages. The studied cores and logs combined with literature are used to determine the statistical distribution of the shape, sizes and orientations of the fluvial channels. The input of the object based modelling method is the fraction of fluvial channels containing mostly sandstone channels and channels containing mostly silty-sandstone. The background is set as siltstone representing the floodplain deposits (Figure F-7).

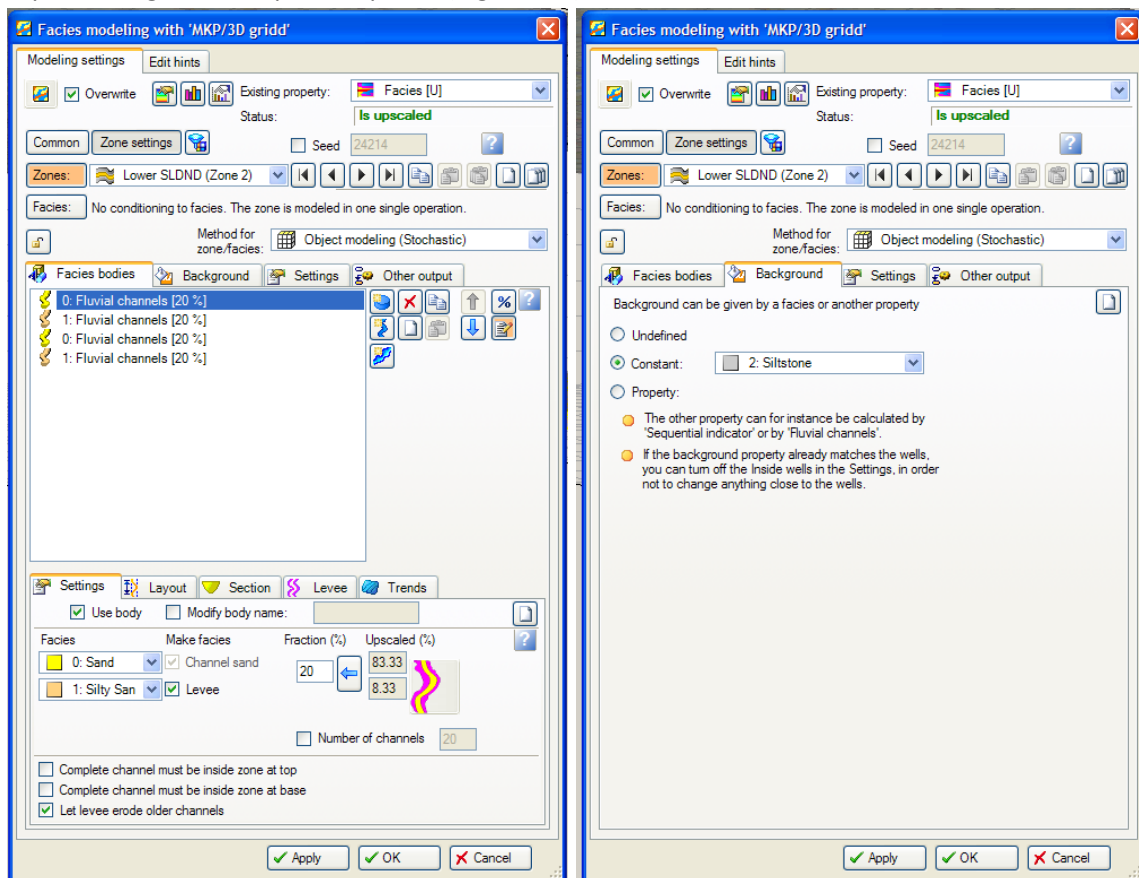


Figure F-7 The “Facies Modelling” tool with the settings used to model the Lower Delft Sandstone Member.

Modelling the Middle Delft Sandstone Member Zone

The Middle Delft Sandstone Member shows predominantly thin alternating clay- and siltstone bands with thin sandstone deposits and lignite or coal layers. To model this zone the object based modelling method is also used as the facies still contain mostly fluvial deposits. The studied cores and logs combined with literature are used to determine the statistical distribution of the fluvial channels. As the shape, sizes and orientations of the channels are similar to the Lower Delft Sandstone Member deposits “Object based modelling” is used here as well. The input of the method contains mostly channels with silty-sandstone and floodplains with silt and coal (Figure F-8). This represents the meandering fluvial channel with lower fluvial gradients, reduced river discharges and stream power, resulting in the deposition of fines. The background is set as siltstone representing the floodplain deposits (Figure F-8). The main lithology in this facies is obviously siltstone. Some channels are still populated in this zone, representing an isolated fluvial channel during the deposition of Middle Delft Sandstone Member.

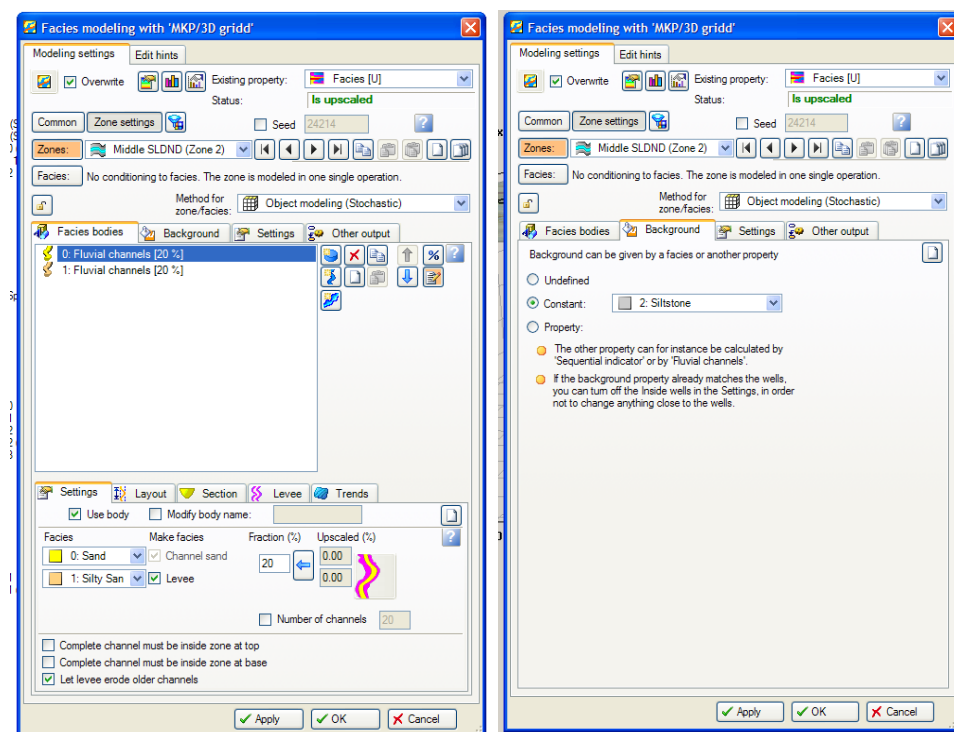


Figure F-8 The “Facies Modelling” tool with the settings used to model the Middle Delft Sandstone Member.

Modeling the Upper Delft Sandstone Member zone

To model the Upper Delft Sandstone Member zone the same modelling method as the Lower and Middle Delft Sandstone Member is used. Object based modelling is performed but then different parameters are used. The Upper Delft Sandstone Member zone consists of multiple stacked sandstone bodies with almost no floodplain deposits. The geometrical properties of the fluvial channels are similar to that of the Middle and Lower Delft Sandstone Member. The channel thickness and flow direction of the channel belt have the same input values as for the other two members. Only the amount of sandstone and therefore the amount of channels and the background setting are different. As there is a lack of flood plain deposits the background is set as a silty sandstone (Figure F-9). The fractions of the lithofacies as found in the log data are honoured.

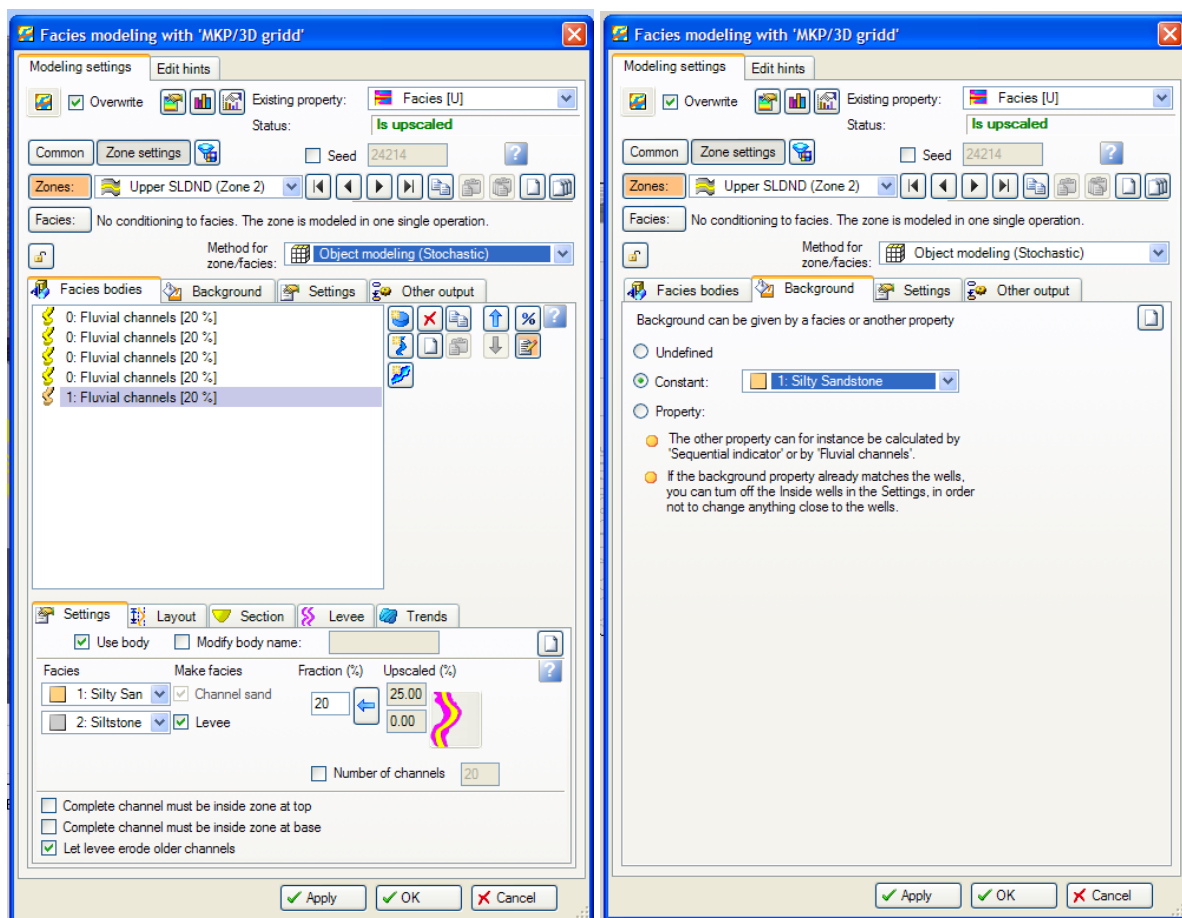


Figure F-9 The “Facies Modelling” tool with the settings used to model the Upper Delft Sandstone Member.

Flow characteristics

The property model is built using the “Property modelling” tool in Petrel. The input data consist of the upscaled property logs and the facies model (Figure F-10). In the property modelling each cell block receives a property value in this study the porosity. The horizontal- and vertical permeability properties are modelled. After upscaling the well logs the scaled up logs are combined with the facies model performing the petrophysical modelling. All cells will be given a value related to the facies in that grid cell. The calculation of the property value at each cell in the 3D grid is based on the input well data and the lithofacies in that grid cell. The method used to determine the value for each facies is the Sequential Gaussian Simulation (SGS) (stochastic) method as this honours the well data, the input distributions, variograms and the trends. The variogram and distribution are used to create local variations, even away from the input data. If no variogram or input data is available from well data the average value for that facies is assigned. As a stochastic simulation is used, the result is dependent upon the input and a seed number.

The properties of the Abllasserdam Member and Rodenrijs Claystone Member are not modelled in detail as they are not the target of this study. However by assigning a set value to the entire Abllasserdam Member and Rodenrijs Claystone Member they still can be used in the thermal flow modelling as the base and top to conduct heat.

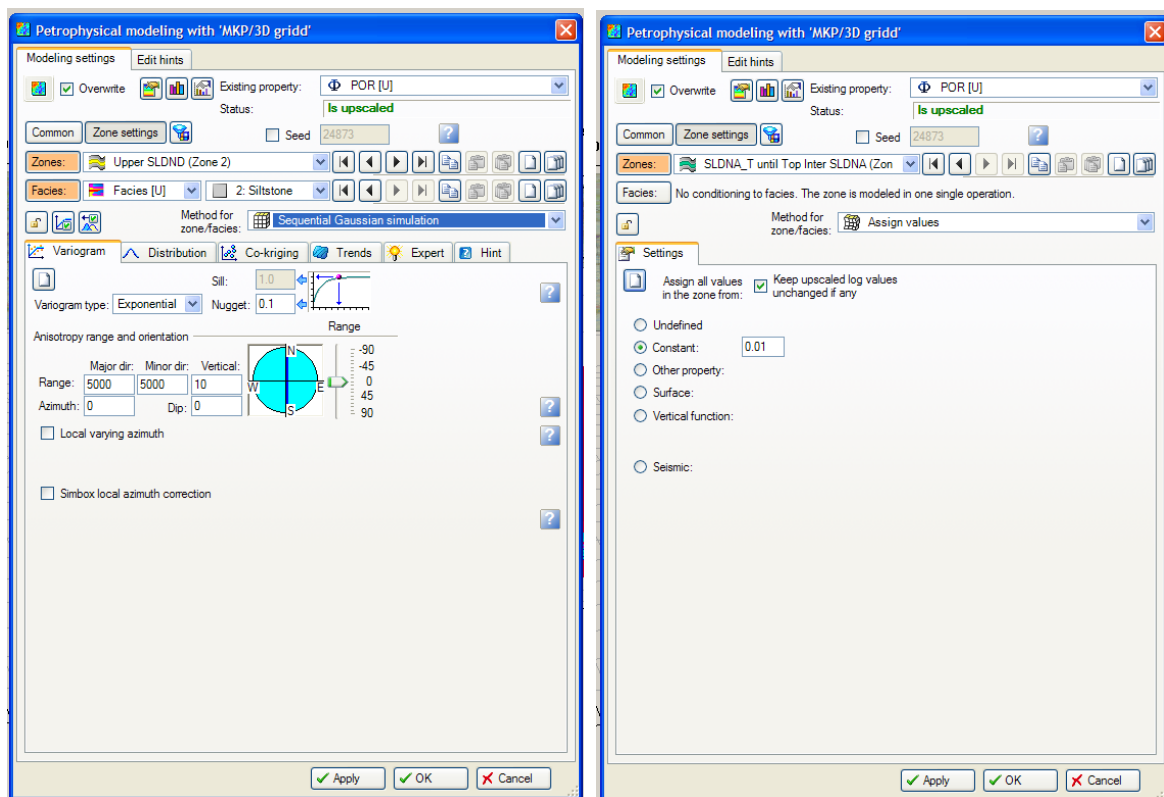


Figure F-10 The “Petrophysical modelling” tool with the settings used for modelling the porosity. On the left to the facies in the model Upper Delft Sandstone Member and on the right the assigned values in the Abllasserdam Member.

G. Appendix Temperature and flow simulation processes

Fluid properties.

The fluid properties need to be imported into the model, this is done by using the “Make Fluid Model” simulation tool in Petrel. The input consists of the salinity of formation fluid, the initial reservoir pressure and its reference depth. The formation fluid is water with a salinity of 98,4 mg/L NaCl equivalent (Chun, 2010). The expected salinity and reservoir temperature and pressure are used to determine the viscosity and density of the formation fluid under reservoir conditions. The viscosity, density, formation volume factor and fluid compressibility are calculated in the dynamic fluid model using the, in Eclipse incorporated, function based on Meehan (1980). As no reservoir pressure data is available and the formation fluid is water, the initial reservoir pressure is derived from the hydrostatic pressure of the formation fluid at 2200 meters depth. The initial reservoir reference pressure is set as 237 bars at 2200 meters depth and its corresponding temperature of 78,2 degrees.

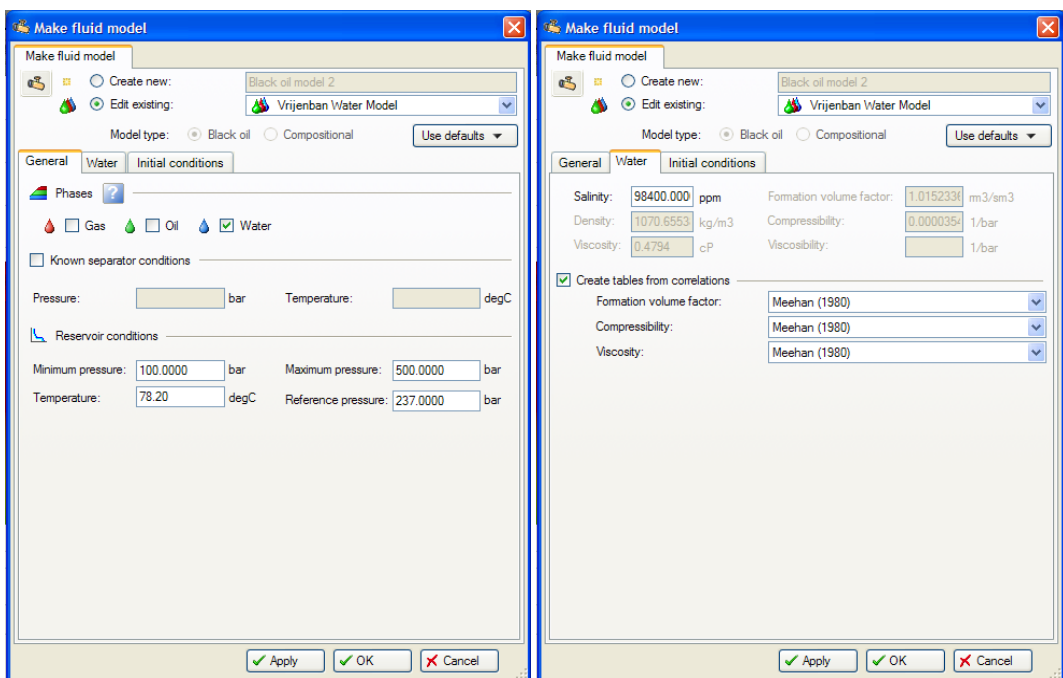


Figure G-1 “Make fluid model” windows with the input setting, data and values.

Rock Physics function

The Rock physic function is used in the simulation to represents the physics of the rock and the interaction between the rock and the formation fluids. The “make rock physics” process in petrel is used to create functions that represent the physics of the rock enabling the creation of rock compaction functions. Functions are tables showing pore volume multipliers versus pressure, or a single rock compressibility value used by the simulator to calculate the pore volume change. Creating rock compaction functions also creates a transmissibility multiplier versus pressure curves. The input data consist of the rock physics properties and the porosity model. The core and cutting data showed that the Delft Sandstone Member is partly friable but strongly compacted. As no knowledge is available of the rock physics of the Abllasserdam Member, Delft Sandstone Member or the Rodenrijs Claystone Member the default settings of the consolidated sandstone are therefore used.

Saturation function

Petrel includes functions of saturation or pressure used in simulation that represent the physics of the fluids, and the interaction between rock and fluids. The “Make fluid model” process with the “Make rock physics function” creates the functions that represent the formation fluids enabling the creation of saturation functions. Saturation functions are tables showing relative permeability and capillary pressure versus saturation. These tables are used to calculate; the initial saturation for each phase in each cell, the initial transition zone saturation of each phase and the fluid mobility used to solve the flow equations. Creating saturation functions is done by using “The Make fluid model” process, it also generates the curves for gas-oil and water-oil capillary pressure versus saturation. As the model does not run without the function and the function does not run with one phase only, the input values consist of both the oil and water phase. As no further information is known about the formation fluid properties the default setting are used for a “Sandstone” reservoir as this will apply typical values for a sandstone reservoir. As only the water phase is present in the reservoir the simulation is run with the reservoir fully saturated with only water (Figure G-2). The saturation function will therefore only determine the capillary forces during simulation.

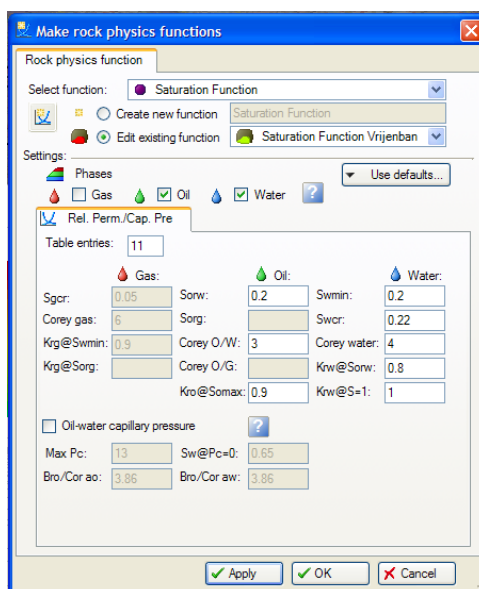


Figure G-2 “Make rock physics functions” window building the saturation function with the input setting, data and values.

The Development strategy (Figure G-3)

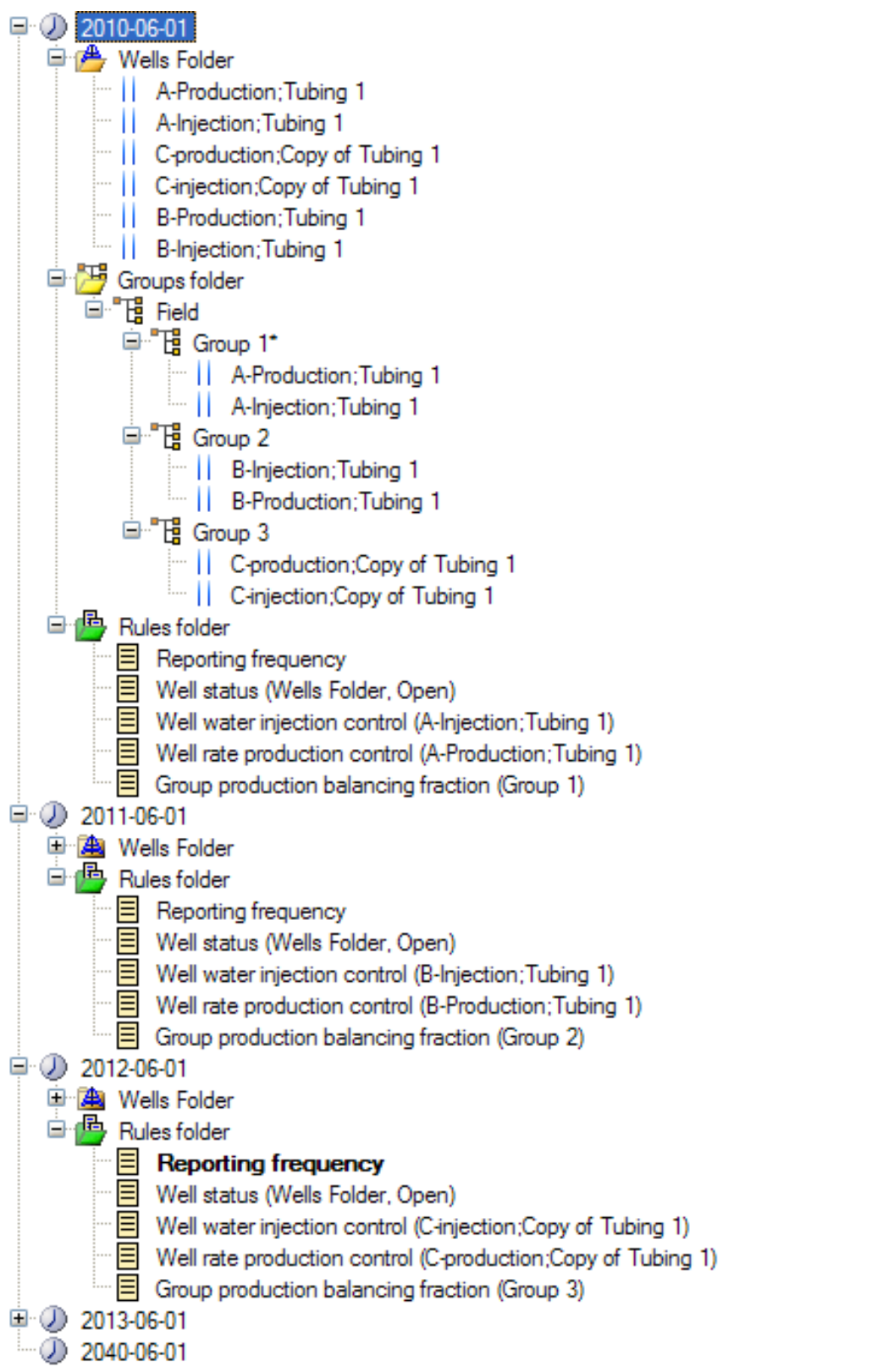


Figure G-3 The development strategy used in the flow simulation.

Input values in Eclipse

The temperature of the injection water

A geothermal system will by utilising the heat from the produced formation fluid by cooling it down. How far it will cool down will depend on the operator of the system, the heat demand at surface, the season of the year and on the temperature of the produced formation fluid. The cooled down water can have a temperature ranging from 20 to 80 degrees Celsius. In the design phase of doublet and in the economics of a geothermal system the most commonly used (re)injection temperature is 30 degrees (DAP, 2008). The three injection wells will therefore inject 30 degrees Celsius water

Well Name	Injection temperature
	Degrees (Celsius)
AI A Injection well	30
BI B Injection well	30
BI C Injection well	30

Rock specific heat

The rock specific heat defines the specific heat capacity. The specific heat capacity is the rock volume specific heat of the rock as a function of temperature. The function consists of a table with the rock specific heat and the temperature. The specific heat input data is set as that of a dry sandstone at 20 and 90 degrees Celsius (Lake, 1989)

SPECROCK

The corresponding volume specific heat of rock.

UNITS: kJ/rm³.°C (METRIC), btu/rft³.°F (FIELD),

J/rcm³.°C (LAB).

Sand 0,999 (Kj/kg-K) * 2.270 kg/m³ = 2,267 KJ/m³-K

Coarse sand 1,249 (Kj/kg-K) * 2.080 kg/m³ = 2,597 KJ/m³-K

Silty Sand 1,142 (Kj/kg-K) * 2.110 kg/m³ = 2,410 KJ/m³-K

Fluid specific heat data

Fluid specific heat data defines the specific heats of the formation fluid as a function of the temperature. The fluid specific heat also depends on the formation fluid salinity. The table below is adapted from Mijnlief et al. (2009) by using the salinity of 94.8 mg/L NaCl Equivalent as input data (Chun, 2009).

Temperature	Thermal conductivity
Degrees (Celsius)	kJ/kg.°C
1	3.67
80	3.74
100	3.75

SPECHEAT

The corresponding water specific heat.

- UNITS: kJ/kg.°C (METRIC), btu/lbm.°F (FIELD),
J/g.°C (LAB).

Thermal conduction

The energy conservation equation is based on thermal convection and thermal conduction. The thermal conduction is simulated optional in the model. The simulation models the thermal conduction of heat in the model. By turning the thermal conduction simulation on and off, the effect of the thermal conduction can be visualized by comparing the results. The thermal conduction input consists of populating a grid with a specific thermal conductivity for the rock. To keep the simulation simple one value is set for the thermal conductivity of the rock. The thermal conductivity of the rock is set at 2.5 (J/s-m-K) (Lake, 1989). However in future studies it is possible to create a 3D thermal conductivity model that weighs the thermal conductivity values on the created facies model. The effect of thermal conduction will be shown in the results.

THCONR

The keyword should be followed by one non-negative real number for every grid block in the current input box, specifying the rock thermal conductivities. The data must be terminated by a slash (/).

- UNITS: kJ/m/day/°C, (METRIC), btu/ft/day/°F (FIELD),
J/cm/hr/°C (LAB), kJ/m/day/°K (PVT-M).

$$2.6 \text{ (j/s-m-K)} * 3600 * 24 / 1000 = 224,69$$

Temperature in eclips

Rtempvd

Static temperature see paragraph 5.4 Temperature.

RTEMPVD

1600 59.6

1700 62.7

1800 65.8

1900 68.9

2000 72

2100 75.1

2200 78.2

2300 81.3

2400 84.4

2500 87.5

2600 90.6

/

H. Appendix Additional Equations

Arithmetic mean

The arithmetic mean is the "standard" average, often simply called the "mean" and was used in the study to upscale the porosity log.

$$\bar{x} = \frac{1}{n} \cdot \sum_{i=1}^n x_i$$

Equation Arithmetic mean

Typically used for additive properties such as porosity, saturation and net-to-gross. Volume weighting will produce a more appropriate arithmetic mean when input values have variable presence within the resulting cell. (Petrel 2009.1)

Harmonic mean

The harmonic mean is an average which is useful for sets of numbers which are defined in relation to some unit, in this study used to upscale the permeability.

$$\bar{x} = n \cdot \left(\sum_{i=1}^n \frac{1}{x_i} \right)^{-1}$$

Equation Harmonic mean

The harmonic mean works well with log normal distributions. It is used for permeability because it is sensitive to lower values. The method is not defined for negative values. In other words the permeability k_v is the "harmonic" average of the permeability's in each layer. We put "harmonic" between quote signs to indicate that the harmonic average would indeed be obtained if all the layer heights were equal. A varied permeability will be get too high a value using arithmetic mean since it is the lower permeability values which will have the greatest influence on the effective permeability (a chain is only as strong as its weakest link) That why the permeability was up scaled using the Harmonic mean. (Petrel 2009.1)

Radial flow towards wells

Figure 2.1: Radial influx

$$Q = \frac{-2\pi k h(p_R - p_w)}{\mu_o \left(\ln \frac{r_e}{r_w} - \frac{1}{2} \right)} \quad (2-6)$$

Steady state Radial Darcy flow equation (Mattews and Russel, 1967)

Fluid flow and Heat Transfer (Modifies after Chris Den Boer 2009)

Thermal retardation factor

If we assume local thermodynamic equilibrium between rock and fluid because rock grains are sufficiently small and fluid velocities are low, the conservation of energy and mass equation for a single phase fluid can be written in this manner: (Den Boer, 2009)

$$\varphi \frac{\partial \rho_w}{\partial t} + \vec{\nabla} \cdot (\rho_w \vec{u}_w) = 0$$

$$\frac{\partial(\rho_{eq} C_{eq} T)}{\partial t} + \vec{\nabla} \cdot (\rho_w \vec{u}_w C_w T) = \vec{\nabla} \cdot (K_{eq} \vec{\nabla} T)$$



 Temperature Convection Conduction
 Change

where

$$\rho_{eq} C_{eq} = \varphi \rho_w C_w + (1 - \varphi) \rho_r C_r$$

And the combined conductivity is a function of rock and thermal conductivities

$$K_{eq} = K(K_r, \varphi, K_w)$$

If we assume incompressible rock and constant thermal properties of both rock and fluid and neglect conduction as second order effect we can combine equations 1 and 2 to get an equation that describes the velocity of the thermal front in porous media, (Den Boer, 2009)

$$\frac{\partial T}{\partial t} + \frac{u_w}{\varphi} \left(\frac{\varphi \rho_w C_w}{(1 - \varphi) \rho_r C_r + \varphi \rho_w C_w} \right) \vec{\nabla} T = 0$$

The following equation describes the velocity of the thermal front is retarded relative to the fluid velocity :

$$\frac{v_T}{u_w / \varphi} = \frac{v_T}{v_w} = \left(\frac{\varphi \rho_w C_w}{(1 - \varphi) \rho_r C_r + \varphi \rho_w C_w} \right) = R_T < 1$$

Here RT is the thermal retardation factor. So the thermal front velocity is the fluid velocity times the factor RT.

References

- Chun, N., 2009: "Geochemische watersamenstelling van de Berkel Zandsteen", BSc Thesis, Delft University of Technology, Delft, the Netherlands.
- DAP, 2008: "Voorontwerp", Business case of the Delft Geothermal Project.
- Den Boer, C.A., 2008: "Doublet spacing in the "Delft Aardwarmte Project""", BSc Thesis, Delft University of Technology, Delft, the Netherlands.
- Matthews, C.S. and Russell, D.G. 1967: "Pressure Buildup and Flow Tests in Wells", In SPE Monograph vol.1, Henry L. Doherty series SPE of AIME, N.Y. 1967
- Meehan, D.N., 1980: "Improved Oil PVT Property Correlations", In: Oil and Gas Journal, 78(43): p 64-71
- Lake, L.W., 1989: "Fractional Flow in Thermal Displacements Enhanced Oil Recovery", In: Enhanced Oil Recovery, Sec 11-3: p. 461
- Van Adrichem Boogaert, H.A. & Kouwe, W.F.P., 1993-1997: "Stratigraphic nomenclature of the Netherlands, revision and update by RGD and NOGEPA", In: Mededelingen Rijks Geologische Dienst (RGD), nr 50.